



**International Committee for Future Accelerators**

Sponsored by the Particles and Fields Commission of IUPAP

# **Beam Dynamics Newsletter**

**No. 33**

**Issue Editors:  
K. Ohmi and M. Furman**

**Editor in Chief:  
W. Chou**

**April 2004**



## CONTENTS

<b>1</b>	<b>FOREWORD.....</b>	<b>9</b>
<b>1.1</b>	<b>FROM THE CHAIRMAN .....</b>	<b>9</b>
	1.1.1 Changes in the Panel .....	9
	1.1.2 Panel activities in 2004:.....	9
	1.1.3 ICFA and the Linear Collider.....	10
	1.1.4 Other issues .....	10
<b>1.2</b>	<b>FROM THE EDITORS .....</b>	<b>11</b>
<b>1.3</b>	<b>ICFA STATEMENT ON LINEAR COLLIDERS .....</b>	<b>11</b>
<b>2</b>	<b>ELECTRON CLOUD EFFECTS IN ACCELERATORS.....</b>	<b>14</b>
<b>2.1</b>	<b>ELECTRON CLOUD BUILD UP IN MACHINES WITH SHORT BUNCHES .....</b>	<b>14</b>
	2.1.1 Introduction .....	14
	2.1.2 Primary Electrons .....	14
	2.1.3 Beam-Induced Multipacting.....	16
	2.1.4 Secondary Emission Yield .....	18
	2.1.5 Saturation.....	20
	2.1.6 Cloud Decay and Electron Survival .....	20
	2.1.7 Remedies .....	21
	2.1.8 References .....	23
<b>2.2</b>	<b>COUPLED-BUNCH INSTABILITY CAUSED BY ELECTRON CLOUD .....</b>	<b>24</b>
	2.2.1 Introduction .....	24
	2.2.2 Characterization of Coupled-Bunch Instability from bunch oscillations .....	25
	2.2.3 References .....	29
<b>2.3</b>	<b>SINGLE BUNCH INSTABILITIES INDUCED BY ELECTRON CLOUD IN SHORT POSITRON/PROTON/ION BUNCHES .....</b>	<b>29</b>
	2.3.1 Introduction .....	30
	2.3.2 Review of the observations and approaches to the problem .....	31
	2.3.3 Simulation codes for single bunch instabilities and applications.....	33
	2.3.4 Peculiarities of the electron cloud wake fields .....	37
	2.3.5 Miscellaneous .....	38
	2.3.6 Acknowledgements .....	42
	2.3.7 References .....	42
<b>2.4</b>	<b>MEASURING THE PROPERTIES OF THE ELECTRON CLOUD AT THE ADVANCED PHOTON SOURCE.....</b>	<b>43</b>
	2.4.1 Experimental results .....	44
	2.4.2 Beam-cloud interaction and EC amplification .....	45
	2.4.3 Simulations .....	47
	2.4.4 Superconducting undulator (SCU) .....	48
	2.4.5 Summary.....	48

2.4.6	Acknowledgement .....	51
2.4.7	References .....	51
<b>2.5</b>	<b>MEASUREMENT OF ELECTRON CLOUD EFFECTS IN KEKB .....</b>	<b>52</b>
2.5.1	Introduction .....	52
2.5.2	Measurement of electron cloud .....	53
2.5.3	Beam size blow-up .....	54
2.5.4	Transverse coupled bunch instability .....	54
2.5.5	Effect of solenoid .....	54
2.5.6	Effect of wiggler magnets .....	55
2.5.7	Summary .....	55
2.5.8	References .....	56
<b>2.6</b>	<b>MEASUREMENT OF ION EFFECTS IN KEKB .....</b>	<b>58</b>
2.6.1	Introduction .....	58
2.6.2	Experiment of the fast ion instability [1] .....	58
2.6.3	Measurement of transverse coupled bunch instability [5] .....	59
2.6.4	References .....	60
<b>2.7</b>	<b>STUDIES ON ELECTRON CLOUD INSTABILITY IN THE BEPC .....</b>	<b>60</b>
2.7.1	Introduction .....	61
2.7.2	Experimental studies .....	61
2.7.3	Simulation studies .....	62
2.7.4	The potential methods to cure ECI issued from studies .....	63
2.7.5	References .....	64
<b>2.8</b>	<b>ELECTRON CLOUD EFFECT IN THE LINEAR COLLIDERS .....</b>	<b>64</b>
2.8.1	Introduction .....	65
2.8.2	Generation of the cloud .....	65
2.8.3	Thresholds for the development of the cloud: SEY Thresholds .....	66
2.8.4	Head-Tail single-bunch and coupled bunch instabilities .....	67
2.8.5	Remedies for the electron-cloud build-up .....	68
2.8.6	Miscellaneous discussions .....	69
2.8.7	Acknowledgments .....	69
2.8.8	References .....	69
<b>2.9</b>	<b>ELECTRON-CLOUD BUILD-UP IN HADRON MACHINES .....</b>	<b>70</b>
2.9.1	Introduction .....	70
2.9.2	Primary sources of electrons and secondary electron emission .....	71
2.9.3	Electron-cloud formation and dissipation .....	72
2.9.4	Acknowledgments .....	75
2.9.5	References .....	75
<b>2.10</b>	<b>THEORY OF ELECTRON CLOUD INSTABILITY IN HIGH INTENSITY PROTON MACHINES .....</b>	<b>77</b>
2.10.1	Introduction .....	77
2.10.2	Review of Data from the PSR [6-9] .....	77
2.10.3	Coasting Beam Theory .....	78
2.10.4	Bunched Beam Theory .....	79

2.10.5	Nonlinear Space Charge .....	80
2.10.6	Other effects .....	81
2.10.7	Conclusions .....	82
2.10.8	References .....	82
<b>2.11</b>	<b>MEASUREMENTS OF ELECTRON CLOUD EFFECTS AT PSR* .....</b>	<b>83</b>
2.11.1	Abstract .....	83
2.11.2	Introduction .....	83
2.11.3	Recent studies on electron-cloud buildup .....	89
2.11.4	Some unresolved issues.....	97
2.11.5	Electron bursts.....	98
2.11.6	Beam response to weak kick.....	102
2.11.7	Summary and Conclusions.....	104
2.11.8	Proposals for future work.....	105
2.11.9	Acknowledgements.....	106
2.11.10	Appendix: PSR Layout.....	106
2.11.11	References.....	107
<b>2.12</b>	<b>ELECTRON CLOUD IN THE SNS ACCUMULATOR RING.....</b>	<b>107</b>
2.12.1	Introduction .....	107
2.12.2	Multipacting mechanism .....	108
2.12.3	Important parameters related to multipacting .....	108
2.12.4	Multipacting inside dipole and quadrupole magnetic fields .....	110
2.12.5	Electron cloud clearing with solenoids and electrodes .....	111
2.12.6	References .....	112
<b>2.13</b>	<b>ELECTRON CLOUD STUDIES IN J-PARC AND KEK-PS .....</b>	<b>114</b>
2.13.1	Introduction .....	114
2.13.2	Simulation studies .....	114
2.13.3	Experiments at the KEK 12 GeV Proton Synchrotron (KEK-PS).....	116
2.13.4	Conclusion.....	119
2.13.5	References .....	119
<b>2.14</b>	<b>RHIC TWO STREAM EFFECTS .....</b>	<b>120</b>
2.14.1	Introduction .....	120
2.14.2	Injection pressure rise.....	120
2.14.3	Transition pressure rise .....	121
2.14.4	Scenario of 360 bunches in eRHIC .....	122
2.14.5	References .....	123
<b>2.15</b>	<b>VACUUM LIMITATIONS DUE TO ELECTRON CLOUDS DURING THE RELATIVISTIC HEAVY ION COLLIDER RUN-4.....</b>	<b>124</b>
2.15.1	Introduction .....	124
2.15.2	Beam current limitations .....	124
2.15.3	Experimental background limitations .....	126
2.15.4	Summary .....	127
2.15.5	Acknowledgements .....	128
2.15.6	References .....	128

<b>2.16</b>	<b>ELECTRON CLOUD OBSERVATIONS AT RHIC .....</b>	<b>128</b>
2.16.1	Introduction .....	128
2.16.2	Experimental results .....	130
2.16.3	Electron Cloud in the Interaction Regions .....	131
2.16.4	Possible cures .....	134
2.16.5	Conclusion .....	135
2.16.6	Acknowledgements .....	136
2.16.7	References .....	136
<b>2.17</b>	<b>MEASUREMENT OF ELECTRON CLOUD EFFECTS IN SPS .....</b>	<b>137</b>
2.17.1	Introduction – SPS and LHC Issues .....	137
2.17.2	Set up description - Specific results .....	139
2.17.3	Beam related effects .....	142
2.17.4	Room temperature observations .....	144
2.17.5	Observations at cryogenic temperatures .....	144
2.17.6	Epilogue: Open questions – Actions required .....	146
2.17.7	Acknowledgements .....	147
2.17.8	References .....	147
<b>2.18</b>	<b>ELECTRON-CLOUD EFFECTS IN THE LHC .....</b>	<b>150</b>
2.18.1	Introduction .....	150
2.18.2	Experiments in the LHC Injectors .....	150
2.18.3	Concerns for the LHC .....	151
2.18.4	Countermeasures .....	153
2.18.5	Uncertainties .....	154
2.18.6	References .....	155
<b>3</b>	<b>ADVANCED AND NOVEL ACCELERATORS .....</b>	<b>157</b>
<b>3.1</b>	<b>ACTIVITY AT KEK-ATF .....</b>	<b>157</b>
3.1.1	Outline of ATF at KEK .....	157
3.1.2	Emittance measurements at the EXT .....	158
3.1.3	Beam tuning in the DR .....	158
3.1.4	Future plans .....	159
3.1.5	References .....	160
<b>3.2</b>	<b>LASER-ACCELERATOR RESEARCH ACTIVITY AT AIST .....</b>	<b>161</b>
3.2.1	Research .....	162
3.2.2	Experimental setup .....	162
3.2.3	Publications .....	163
<b>3.3</b>	<b>RESEARCH ACTIVITY AT NUCLEAR ENGINEERING RESEARCH LABORATORY, UNIVERSITY OF TOKYO .....</b>	<b>165</b>
3.3.1	Experimental verification of new bunch compression, velocity bunching .....	165
3.3.2	Compact hard X-ray source based on X-band LINAC for medical use .....	166
3.3.3	Electron acceleration via interaction between ultra-short intense laser pulse and gas jet .....	168
3.3.4	Laser plasma ion generation .....	169
3.3.5	Time-resolved X-ray diffraction .....	169

3.3.6 Plasma simulation.....	169
3.3.7 References .....	170
3.3.8 Publications .....	171
<b>3.4 ACTIVITY AT HIROSHIMA UNIVERSITY .....</b>	<b>173</b>
3.4.1 Space-Charge-Dominated Beam Physics .....	173
3.4.2 Phase Transition of Ion Beams.....	174
3.4.3 Study of Compact Accelerators.....	175
3.4.4 Laser-Matter Interactions .....	176
3.4.5 References .....	177
<b>3.5 PROGRAM OF THE PARTICLE BEAM PHYSICS LABORATORY (PBPL) .....</b>	<b>178</b>
3.5.1 Some of the highlights of recent research include: .....	179
3.5.2 Contact information:.....	181
3.5.3 Publications .....	183
<b>3.6 LASER GUIDING FOR HIGH ENERGY PLASMA ACCELERATORS.....</b>	<b>185</b>
3.6.1 Introduction .....	185
3.6.2 Laser wakefield in a capillary tube: model and numerical simulations ...	186
3.6.3 Laser guiding in a capillary tube: experimental results.....	189
3.6.4 Conclusion.....	190
3.6.5 Acknowledgements .....	191
3.6.6 References .....	191
<b>3.7 COMPUTATIONAL ACCELERATOR PHYSICS AT TECH-X CORPORATION.....</b>	<b>192</b>
3.7.1 Beam and plasma simulation codes VORPAL and OOPIC .....	192
3.7.2 Field-induced tunneling ionization.....	192
3.7.3 Simulating LWFA channels, in support of l'OASIS experiments .....	193
3.7.4 Simulating high-power laser-pulses in overdense plasmas .....	194
3.7.5 Simulating positron-driven PWFA experiments .....	194
3.7.6 Simulating electron cooling physics at relativistic energies for RHIC .....	195
3.7.7 Simulating electron emission from structures and related physics.....	195
3.7.8 Particle tracking.....	195
3.7.9 Acknowledgements .....	196
3.7.10 References .....	196
<b>4 RECENT DOCTORAL THESES .....</b>	<b>198</b>
<b>4.1 ANALYTICAL AND NUMERICAL STUDIES OF STOCHASTIC EFFECTS IN BEAM DYNAMICS.....</b>	<b>198</b>
<b>5 WORKSHOP AND CONFERENCE REPORTS .....</b>	<b>199</b>
<b>5.1 13<sup>TH</sup> ICFA BEAM DYNAMICS MINI-WORKSHOP ON BEAM INDUCED PRESSURE RISW IN RINGS.....</b>	<b>199</b>
5.1.1 Summary of Pressure Rise Workshop.....	199
5.1.2 Report of the Working Group on Electron Cloud Effects .....	203
5.1.3 Electron and ion desorption working group summary .....	211

<b>5.2</b>	<b>31<sup>ST</sup> ICFA ADVANCED BEAM DYNAMICS WORKSHOP ON ELECTRON-CLOUD EFFECTS “E-CLOUD04”</b> .....	<b>215</b>
5.2.1	E-CLOUD04 Workshop (Napa, California, April 19-23, 2004). .....	215
<b>6</b>	<b>FORTHCOMING BEAM DYNAMICS EVENTS</b> .....	<b>217</b>
<b>6.1</b>	<b>ICFA ADVANCED BEAM DYNAMICS WORKSHOPS</b> .....	<b>217</b>
6.1.1	32nd ICFA Advanced Beam Dynamics Workshop on Energy Recovering Linacs, "ERL2004" .....	217
6.1.2	33rd ICFA Advanced Beam Dynamics Workshop on High Intensity and High Brightness Hadron Beams "HB2004" .....	217
<b>7</b>	<b>ANNOUNCEMENTS OF THE BEAM DYNAMICS PANEL</b> .....	<b>218</b>
<b>7.1</b>	<b>ICFA BEAM DYNAMICS NEWSLETTER</b> .....	<b>218</b>
7.1.1	Aim of the Newsletter .....	218
7.1.2	Categories of Articles .....	218
7.1.3	How to Prepare a Manuscript .....	219
7.1.4	Distribution .....	219
7.1.5	Regular Correspondents .....	220
<b>7.2</b>	<b>ICFA BEAM DYNAMICS PANEL MEMBERS</b> .....	<b>221</b>

# 1 Foreword

## 1.1 From the Chairman

Weiren Chou, Fermilab  
mail to: [chou@fnal.gov](mailto:chou@fnal.gov)

### 1.1.1 Changes in the Panel

At the February 2004 meeting in Paris, ICFA approved five new Panel members: Yoshiharu Mori (KEK), Ingo Hofmann (GSI), Miguel Furman (LBNL), In Soo Ko (POSTECH) and Rainer Wanzenberg (DESY). These are well-known physicists in the global accelerator community. Please join me to welcome them on board. Yoshi replaced me as the new Chair of the ICFA Working Group on High Intensity and High Brightness Hadron Beams. Rainer replaced Helmut Mais to take over the responsibility of printing and distributing the ICFA BD Newsletter in Europe and Africa.

John Jowett (CERN) and Helmut Mais (DESY) resigned from the panel. John did excellent service as the Panel Chair in the past several years. Helmut made great contributions to the panel, in particular for his work on the Newsletter. On behalf of the Panel, I'd like to give them my sincere and heartfelt thanks.

The Panel now has 19 members, who are listed at the end of this Newsletter. The membership is well balanced among three regions: 6 from Asia, 6 from Europe and 7 from North America.

The Panel also has 4 working groups, with each chaired by a Panel member:

- Future Light Sources (Chair: K-J. Kim)
- High Luminosity e+e- Colliders (Chair: C. Biscari)
- High Intensity and High Brightness Hadron Beams (Chair: Y. Mori)
- Remote Experiments in Accelerator Physics (Chair: D. Rice)

For technical reasons the Panel's web site has moved to a new address:

<http://www-bd.fnal.gov/icfabd/>

It has links to the main ICFA web site as well as to the sites of the 4 working groups. Ernie Malamud, a retired senior physicist from Fermilab, serves as the web master.

### 1.1.2 Panel activities in 2004:

It is planned to publish three issues of the ICFA BD Newsletter this year: No. 33 (this issue, editors K. Ohmi and M. Furman), No. 34 (August, editor D. Rice) and No. 35 (December, editor C. Biscari).

Also scheduled are three ICFA Advanced Beam Dynamics Workshops (ABDW): the 31<sup>st</sup> titled *ECLLOUD04* (April 19-23 in Napa, California, U.S.A., chaired by M. Furman), the 32<sup>nd</sup> titled *ERL2004* (October 10-14, JLab, Virginia, U.S.A., co-chaired by S. Chattopadhyay and L.

Merminga), and the 33<sup>rd</sup> titled *HB2004* (October 18-22, Bensheim, Germany, co-chaired by I. Hofmann and J-M. Lagniel).

Each working group also plans to have one or more ICFA mini-workshops. These mini-workshops have proved to be effective and productive, because they are well focused, easy to organize and the publication of formal proceedings is not required.

In addition to these activities, the Panel is working on a new project: the compilation of a new Accelerator Catalogue. The existing one was published more than a decade ago and needs to be updated. The new one will be published both in paper copy and online. The following five Panel members have agreed to take lead responsibilities on this project:

- e+e- Colliders – C. Biscari (LNF-INFN)
- Light sources (including FELs) – K-J. Kim (ANL)
- Ion accelerators – I. Hofmann (GSI)
- Cyclotrons and FFAGs – Y. Mori (KEK)
- Proton machines – W. Chou (Fermilab)

We have also invited J.-F. Ostiguy (Fermilab) to be the technical adviser for this project. The scheduled completion date is January 2005.

### 1.1.3 ICFA and the Linear Collider

In February 2004, ICFA issued a Second Statement on Linear Colliders, which is included in this issue (Section 1.3). In the present Linear Collider organization structure, ICFA is the governing body and oversees the work of the International Linear Collider Steering Committee (ILCSC). This will remain the case until a group of governments establish an oversight board to take over the leadership from ICFA. On the ICFA main web page:

[http://www.fnal.gov/directorate/icfa/icfa\\_home.html](http://www.fnal.gov/directorate/icfa/icfa_home.html)

you can find all the important documents regarding Linear Colliders.

### 1.1.4 Other issues

At the February ICFA meeting, attended by about fifteen lab directors in addition to the ICFA members and Panel Chairs, there was a discussion about how to support panel activities, such as attending ICFA meetings and workshops, organizing the workshops, and printing and distributing the Newsletter. There was general agreement that the lab directors should recognize the importance of support for these activities and give favourable consideration to requests to participate in these activities by their staff members.

There have been a number of complaints on the visa problems experienced by foreign visitors to the U.S. In particular, ICFA workshop organizers often find it difficult to have invited speakers from China or Russia if the workshop takes place in the U.S. Although this is a problem for more than just accelerator scientists, ICFA has taken steps to address this issue in conjunction with the American Physical Society (APS) and other science organizations. The problems have been reported to the White House Office of Science and Technology Policy (OSTP). It is our hope that the present U.S. visa policy will be changed soon and international collaboration in science and technology between the U.S. and other countries can return back to normal.

## 1.2 From the Editors

Kazuhito Ohmi, [KEK](#) mail to: [kazuhito.ohmi@kek.jp](mailto:kazuhito.ohmi@kek.jp)

Miguel Furman, [LBNL](#) mail to: [mafurman@lbl.gov](mailto:mafurman@lbl.gov)

In this issue of the ICFA Beam Dynamics Newsletter, we have a special section (Section 2) dedicated to electron cloud effects in accelerators. Electron cloud effects were first studied in proton rings. Ion trapping and fast ion instability came later. Photoelectron emission due to synchrotron radiation became an important issue in positron rings during the past 10 years or so. Secondary electrons and multipactoring became important with increasing beam intensities. In the present concept of the electron cloud, many electrons are produced at the chamber wall and are widely distributed inside the chamber. Recently, electron cloud studies returned to proton rings. By now, many studies have been done in many types of accelerators, namely in positron storage rings (B-factories and damping rings of the LC's), high intensity neutron sources (PSR, SNS and J-PARC), and high-energy hadron machines (RHIC and LHC). The electron cloud causes various types of instabilities and other undesirable phenomena. There are still many aspects to be studied on electron cloud effects. We hope, as editors, that this issue helps readers understand electron cloud effects and their importance.

Section 3 of this Newsletter contains a number of well written articles contributed by the ICFA Advanced and Novel Accelerators Panel. (Another set of articles from that Panel were published in the last issue, No. 32.)

We want to thank Ms. Sawabe, the KEK accelerator physics group secretary, for her help in editing this Newsletter.

## 1.3 ICFA Statement on Linear Colliders

ICFA  
13 February 2004

ICFA welcomes the January 2004 Organisation for Economic Co-operation and Development (OECD) Ministerial Statement on International Cooperation on Large Accelerator-based Projects in High-Energy Physics, which “acknowledged the importance of ensuring access to large-scale research infrastructure and the importance of the long-term vitality of high-energy physics. They noted the worldwide consensus of the scientific community, which has chosen an electron-positron linear collider as the next accelerator-based facility to complement and expand on the discoveries that are likely to emerge from the Large Hadron Collider currently being built at CERN. They agreed that the planning and implementation of such a large, multi-year project should be carried out on a global basis, and should involve consultations among not just scientists, but also representatives of science funding agencies from interested countries. Accordingly, Ministers endorsed the statement prepared by the OECD Global Science Forum Consultative Group on High-Energy Physics (see Appendix).”

## ***Background***

In 1999 ICFA issued a statement on Linear Colliders, noting that scientific panels charged with studying future directions for particle physics in Europe, Japan, and the United States have concluded that there would be compelling and unique scientific opportunities at a linear electron-positron collider in the TeV energy range. Such a facility is a necessary complement to the LHC hadron collider now under construction at CERN.

As a consequence, at that time ICFA recommended continued vigorous pursuit of the accelerator research and development on a linear collider in the TeV energy range, with the goal of having designs complete with reliable cost estimates within a few years.

### ***Since 1999 major progress has been made in several key areas:***

**Science:** In 2001-2002, the three regional organizations of the HEP community (ACFA in Asia, HEPAP in North America, and ECFA in Europe) have reached the common conclusion that the next accelerator should be an electron-positron linear collider with an initial centre-of-mass energy around 500 Giga-electronvolts (GeV), later upgradable to higher energies, and that it should be built and operated in parallel with the Large Hadron Collider under construction at CERN. In January 2004, the ECFA, ACFA and HEPAP Chairs, in communications to the ICFA Chair, reaffirmed their community's priorities as formulated in 2001-2002. In addition, the scientific case has recently been published in a tri-regionally based consensus paper 'Understanding Matter, Space and Time'. So far, this document has been signed by more than 2000 physicists from the world-wide community of high-energy physicists. These developments provide clear evidence of the ongoing widespread support for the near-term construction of a linear collider.

**Technology:** In February 2001 ICFA requested the International Linear Collider Technical Review Committee (ILC-TRC) to assess the current technical status of electron-positron linear collider designs in the various regions. The ILC-TRC concluded that, based on the progress in both major technologies, a linear collider could be built in the next few years. As a consequence ICFA established a process to select one technology, in order to focus the world-wide efforts, and in fall of 2003 set up an International Technology Recommendation Panel which was charged to provide its recommendation before the end of 2004.

**Organisation:** In 2002 ICFA set up an International Linear Collider Steering Group (ILCSC) which is charged to engage in explaining the intrinsic scientific and technological importance of the project; to engage in defining the scientific roadmap, the scope and primary parameters for machine and detector; to monitor the machine R&D activities and make recommendations on the coordination and sharing of R&D tasks as appropriate; and to identify models of the organizational structure, based on international partnerships, adequate for constructing the LC facility. The ILCSC is supported by steering groups in the three regions, each with a mandate strongly allied with the ILCSC.

At present the ILCSC is preparing a recommendation on how best to establish an international design group that can start the machine design as soon after the technology decision as is possible.

ICFA reaffirms its conviction that the highest priority for a new machine for particle physics is a linear electron-positron collider with an initial energy of 500 GeV, extendible up to about 1 TeV, with a significant period of concurrent running with the LHC.

\* \* \* \* \*

## Appendix

### **The January 2004 OECD Ministerial Statement on International Co-operation on Large Accelerator-based Projects in High-Energy Physics**

Ministers expressed their appreciation for the work of the OECD Global Science Forum Consultative Group on High-Energy Physics. They welcomed the report from the Group and commended the clarity and world-wide consensus they found amongst the high-energy physics community in developing the Roadmap for future large accelerator-based facilities.

In particular, the Ministers note several important points that were articulated in the report:

- A roadmap that identifies four interdependent priorities for global high energy physics (HEP) facilities
  - i)* the exploitation of current frontier facilities until contribution of these machines is surpassed,
  - ii)* completion and full exploitation of the Large Hadron Collider at CERN,
  - iii)* preparing for the development of a next-generation electron-positron collider, and
  - iv)* the continued support for appropriate R&D into novel accelerator designs.
- The need to have large, next-generation facilities funded, designed, built, and operated as global scale collaborations with contribution from all countries that wish to participate.
- The need for strong international R&D collaboration and studies of the organisational, legal, financial, and administrative issues required to realize the next major accelerator facility on the Consultative Group's Roadmap, a next generation electron-positron collider with a significant period of concurrent running with the LHC.
- The need to continue to educate, attract and train young people in the fields of high-energy physics, astrophysics and cosmology in the face of the increasingly competitive environment where all areas of science, industry and commerce are seeking to capture the imagination of the most creative minds.

Ministers agreed that, given the complexity and long lead times for decision making of major international projects, it is important that consultations continue within the scientific communities and, when it becomes appropriate, within interested governmental communities in order to maximise the advantages offered by global collaboration.

## 2 Electron cloud effects in accelerators

### 2.1 Electron Cloud Build Up in Machines with Short Bunches

F. Zimmermann  
 mail to: [frank.zimmermann@cern.ch](mailto:frank.zimmermann@cern.ch)  
[CERN, AB Department, ABP Group](#)  
 1211 Geneva 23 , Switzerland

G. Rumolo, GSI, Germany; K. Ohmi, KEK, Japan

#### 2.1.1 Introduction

The term ‘electron cloud’ refers to an accumulation of electrons inside an accelerator beam pipe which is sufficiently strong to affect the accelerator operation, e.g., by causing beam loss, emittance growth, increase in the vacuum pressure, or degradation of the beam diagnostics. Primary electrons are generated by a number of processes. Their number can be rapidly amplified by a beam-induced multipacting mechanism, which involves acceleration of electrons in the beam field and secondary emission following their impact on the chamber wall. In this brief review, we first describe the primary generation mechanisms. We then discuss the multipacting process, secondary emission, equilibrium electron densities, and the electron-cloud decay in the gap behind a bunch train. We conclude with a list of possible remedies.

#### 2.1.2 Primary Electrons

Primary electrons are generated during a bunch passage either, on the wall, as photo-electrons from synchrotron radiation (mainly for positron or electron beams) and as secondary electrons generated by beam loss (especially for ion beams) or, inside the beam volume, by ionization of the residual gas. The energy gain of primary electrons in the beam potential depends on whether the electrons are generated at the wall or inside the beam.

The number of electrons created per unit length by synchrotron radiation or by beam loss during one bunch passage can become comparable to the average line density of beam particles, in which case these processes alone can give rise to appreciable amounts of electrons.

The rate of photoemission may be estimated as follows. The number of synchrotron-radiation photons emitted in a dipole per unit length and per beam particle is  $dN_\gamma/ds \approx 5\alpha\gamma/(2\sqrt{3}\rho)$ , where  $\gamma$  denotes the Lorentz factor and  $\alpha$  the fine-structure constant. The rate of photoelectron production is the product of the photo-electron yield  $Y_\gamma$  and the photoemission rate,

$$\frac{dN_{e\gamma}}{ds} \approx Y_\gamma \frac{dN_\gamma}{ds} \approx Y_\gamma \frac{5}{2\sqrt{3}} \frac{1}{\rho} \alpha\gamma, \quad (1)$$

where the photo-electron yield depends on the photon energy. For many materials, the yield  $Y_\gamma$  may be approximated as a constant, of the order of 0.1, over a fairly large energy range, e.g., between a few eV and a few 10s of keV.

The azimuthal distribution of absorbed photons around the chamber wall and, thus, the launch positions of the emitted primary photo-electrons depend on the reflective properties of the chamber wall. If the probability of photon reflection is high, the reflected photons can illuminate the entire chamber wall. Photo-electrons are emitted from all the places where the synchrotron-radiation photons are ultimately absorbed. Thus, inside bending magnets a low photon reflectivity is desirable, since the magnetic field confines the photo-electrons emitted at the outer side of the chamber, which is the primary impact point of synchrotron radiation, to the vicinity of the wall.

We can take the LHC as an example to illustrate the considerations that enter into the modeling of photo-electrons. To control the position of the photo-emission, the reflectivity of the LHC arc beam pipe is reduced by impressing a ‘sawtooth’ pattern on the chamber wall (more accurately on the beam screen that forms the inner part of the chamber and serves to protect the cold bore of the magnets from synchrotron radiation) [1]. The sawtooth pattern makes the photons impact perpendicularly to the local surface, which has the effect of substantially lowering the photon reflectivity. For the LHC sawtooth chamber the measured residual reflection is not uniform in all directions, but it is approximately described by a  $\cos^2 \phi$  or  $\cos^3 \phi$  distribution, where  $\phi$  denotes the angle of the reflected photon direction with respect to the horizontal plane [2]. The reflection for the LHC chamber is mainly diffuse. Specular backward reflection from the sawtooth chamber was measured to be negligible, of the order of some percent of the (already few) reflected photons [3].

The first simulation of an electron-cloud build up for short bunches was written by K. Ohmi. It served to explain coupled-bunch instabilities observed with positron beams at the KEK photon factory [4]. Ohmi’s pioneering study considered only photo-emission at the chamber wall as a source of electrons, though a little later he extended his code PEI to include secondary emission by lost electrons as well.

Residual-gas ionization by individual charged beam particles occurs with a typical cross section of 1-2 Mbarn for CO and N<sub>2</sub> gases, and a lower cross section of about 0.2 Mbarn for H<sub>2</sub> [5]. These numbers refer to singly charged particles at ultrarelativistic energies. For fully ionized atoms, the cross section increases roughly with the square of the atomic number, i.e., like  $Z^2$ ; it increases by several orders of magnitude towards lower beam energies. If the beam density is sufficiently high, as it will be in certain sections of the next generation of linear colliders or as it has already been for peculiarly short bunches, field ionization by the collective effect of the total bunch charge replaces single-particle ionization as the dominant ionization process [6]. When this happens, the beam completely and instantly ionizes the residual gas in its neighbourhood. Recently field ionization due to a beam was observed experimentally, perhaps for the first time, with a short electron bunch traversing a plasma cell at the end of the SLAC linac [7].

Protons or ions impacting on the wall can generate a large number of electrons, especially if they impinge under a shallow angle, nearly parallel to the surface. Denoting the angle of incidence with respect to the surface normal by  $\theta$ , the secondary-electron yield for ion impact is approximately given by [8]

$$Y_z \approx \Lambda \left( \frac{dE}{dx} \right)_e \cos^{-1} \theta, \quad (2)$$

where  $(dE/dx)_e$  denotes the electronic stopping power and  $\Lambda$  is a ‘magical number’, varying between 5 and 20 mg/(MeV cm<sup>2</sup>) for protons as projectiles. The expression (2) diverges for angles  $\theta$  approaching  $\pi/2$ . Experimentally, it ceases to be valid for angles  $\theta$  larger than about 89.8 degrees [9]. Notice that the stopping power scales roughly as the square of the atomic number divided by the inverse of the atomic mass. The electron generation by beam loss is particularly important for heavy-ion beams in view of their high secondary yield and for collimators where significant beam loss routinely occurs by design.

### 2.1.3 Beam-Induced Multipacting

The primary and most (in)famous mechanism causing a build up of electrons is beam-induced multipacting. Here electrons are accelerated by the electric field of a passing bunch to such high an energy that they produce, on average, more than 1 secondary electron when they again hit the vacuum-chamber wall. The number of secondary electrons depends on the secondary emission yield of the chamber material, which is a function of the primary-electron energy, its angle of incidence, and the chamber history. For a round chamber of radius  $b$  and a short bunch the resonance condition for beam-induced multipacting takes the simple form [10]

$$N_b r_e s_b = b^2, \quad (3)$$

where  $r_e$  denotes the classical electron radius,  $N_b$  the bunch population and  $s_b$  the bunch spacing in units of length. However, condition (3) is far too stringent. Most secondary electrons are low in energy and they stay in the vacuum chamber for a long time after a bunch passage. Therefore, even for bunch spacings much larger than that suggested by the above relation, most of the secondary electrons generated at, or after, the passage of the preceding bunch may not yet be lost when the next bunch arrives and these electrons will be accelerated during its passage, producing a new generation of secondaries. Conversely, for shorter bunch spacing, electrons can interact with several passing bunches, and, also in this case, they may gain sufficient energy to acquire an average secondary yield larger than 1.

Indeed, measured multipacting thresholds reveal that (3) is oversimplified. At the CERN SPS the multipacting thresholds for bunch spacings of 5 ns, 25 ns, and 50 ns were experimentally found to be at bunch populations of about  $8 \times 10^9$ ,  $5 \times 10^{10}$  and  $1 \times 10^{11}$ , respectively [11,12]. This indicates a roughly linear scaling of the threshold bunch population with bunch spacing in the SPS, which is exactly opposite to the scaling expected from condition (3). We should note that the beam emittances were not the same for the three bunch spacings and that after 10 days of surface scrubbing the threshold for the 25-ns spacing further increased by a factor 2 [12]. When the Tevatron is operated with uncoalesced beam, its bunch spacing is 18.9 ns. For this beam, the threshold of multipacting was observed at  $4 \times 10^{10}$  protons per bunch [13,14], which is consistent with the SPS data for 25-ns spacing. The vacuum-chamber dimensions are similar in the two machines.

The first rough simulation of electron-cloud generation via secondary emission may have been due to S. Heifets, who studied a simplified 1-dimensional model [15]. Subsequently, a much refined simulation code, POSINST, comprising both photo-emission and secondary emission in 3 dimensions was developed by M. Furman and G. Lambertson, for the PEP-II B factory [16,17]. Furman’s and Lambertson’s work gives a succinct and comprehensive overview of the physical processes that are important for the electron cloud build up and it discusses many

of the related modeling issues. K. Ohmi upgraded his code PEI at about the same period. In February 1997, another program, E-CLOUD, was written, whose physics ingredients are similar to those in POSINST, but which differs in some technical aspects, e.g., it does not preserve the macro-particle charge. Using an early version of this code, it was predicted that an electron cloud will likely build up in the LHC [18]. The E-CLOUD simulation revealed that inside an LHC dipole field, the electrons amplify in certain preferred horizontal regions, thereby creating two vertical stripes of high electron density (similar stripes were previously found by Lambertson and Furman in PEP-II simulations [16]). At low intensity the LHC simulations show only one stripe, at the center of the LHC chamber. For a bunch population of about  $5 \times 10^{10}$  protons the stripe splits into two, whose positions move horizontally outwards as the bunch charge further increases. More recently, a third stripe was predicted to occur at higher bunch population above about  $1.1 \times 10^{11}$ , again at the center of the chamber [19]. The cascade of 1-2-3 stripes as a function of beam intensity has been confirmed by dedicated ‘strip detectors’ in the SPS [12]. The E-CLOUD code was substantially extended by O. Bruning, who studied several countermeasures such as clearing electrodes and solenoids, improved the treatment of space, and added image charges [20]. Subsequently, X.-L. Zhang, G. Rumolo, and D. Schulte made many further improvements and modifications to the code. The LHC simulations reported in [21] provide examples of several advanced capabilities. In 2001 a sophisticated 3-dimensional code, CLOUDLAND, became available, which employs finite-element methods for the field calculation and can model arbitrarily complex boundaries. The CLOUDLAND code was written by L. Wang, and it was originally developed for studies at KEKB [22]. More recently, it has been applied to the SNS accumulator ring [23].

It is a gratifying success of the early simulations that indeed electron clouds were observed at both B factories (PEP-II and KEKB) and at the LHC injectors PS and SPS when operated with LHC-type beams. In these storage rings, the electron cloud causes a tune shift along the first bunches of a train, emittance growth, both coupled and single-bunch instabilities, a reduction of specific luminosity (except for SPS and PS, where no collisions take place, but where significant beam loss can be observed at the end of a train if no countermeasures are taken), and a degradation of certain beam diagnostics signals [24,25,26]. At the SPS a whole suite of dedicated electron-diagnostics devices was installed, in preparation for the LHC commissioning. Using this suite, the electron flux, the electron energy spectrum, the spatial electron distribution, the in-situ secondary emission yield and its variation with the time of exposure (‘scrubbing’), the heat load on warm and cold surfaces for different chamber radii and beam conditions, the suppression of electron cloud build up by getter coating, and many other aspects were studied [12].

If an electron is close to the wall, in most cases it only receives a ‘kick’ (change in momentum) without noticeably changing its position during a bunch passage. By contrast, an electron near the center of the chamber oscillates in the bunch potential and its final energy depends on its initial transverse position, the bunch charge, and the bunch profile. This second regime is called the ‘autonomous’ regime by S. Berg, who derived analytical expressions and also developed numerical tools for computing the energy gain of an electron as a function of its radial distance from the beam for various beam profiles [1].

G. Stupakov was the first to develop an analytical formalism for computing the ‘effective secondary emission yield’, as a function of the horizontal electron position in a dipole field. His treatment was restricted to the interaction of electrons with a single bunch [27]. Stupakov’s work was later revisited and extended invoking several approximations, by L. Vos [28]. Taking into account the typical emission energy of secondary electrons and treating the general case of a

non-round chamber, the multipacting condition (3) can be generalized. K.Harkay and colleagues numerically identified distinct multipacting regions inside the chamber cross section, which are distinguished by different amplification factors [29].

Specific electron-accumulation patterns are also observed in simulations for magnetic fields other than dipoles, e.g., for quadrupoles, sextupoles, or z-dependent longitudinal solenoid fields. The CLOUDLAND code demonstrated, for the first time in an electron-cloud simulation, that a large fraction of electrons can remain trapped in quadrupole and sextupole fields long after the passage of a bunch train [22], which confirmed an earlier hypothesis [30].

A novel approach to the problem of electron-cloud build up is pursued by A. Novokhatski and J. Seeman [31] (if our memory is correct, this approach was first proposed by A. Krasnov, who gave it as an exercise to students in Novosibirsk). Rather than tracking macroparticles, A. Novokhatski and J. Seeman consider the electron-distribution function and solve the Vlasov equation to determine its time evolution. Some simplifications are necessary to keep the computing time in reasonable limits. From the electron distribution the electric fields are readily obtained. An important prediction of the Novokhatski/Seeman study for uniform solenoid fields is the existence of a cyclotron resonance with enhanced multipacting fields at certain values of the magnetic field. Other, higher-order cyclotron resonances were found too, at lower fields. The fundamental resonance was later confirmed in POSINST macro-particle simulations [32]. It occurs when the bunch spacing equals the time an electron needs to perform half a cyclotron oscillation, or for the following value of the solenoid field:

$$B_s^c \approx \frac{\pi m c^2}{e s_b} \quad (4)$$

The higher-order resonances correspond to situations where the travel time of an electron equals an integer multiple of the bunch spacing.

It is noteworthy, however, that for KEKB both experiments [33] and simulations with E-CLOUD [34] did not reveal any evidence of such type of resonance, but either showed a monotonic dependence on the field strength. This suggests that the existence or non-existence of the resonance depends on other model assumptions, such as the production rate of primary (photo-)electrons, the uniformity of the solenoid field, the energy and angular distribution of the emitted secondary electrons, the probability of elastic electron reflection, etc.

The effect of a clearing electrode on the electron-cloud build up is surprisingly complex. CLOUDLAND simulations reveal that the clearing field leads to one-sided multipacting (the existence this type of multipacting had also been suggested by S. Mitsunobu [35]) and to a rapid ‘polarization’ of the electron orbit. Clearing fields of intermediate magnitude, e.g., 2 kV, actually increase the multipacting [23].

#### 2.1.4 Secondary Emission Yield

We now take a closer look at the secondary emission process itself, since it is the process responsible for the multipacting. The secondary electrons consist of two or three components, the true secondaries, the elastically reflected electrons, and an intermediate state of ‘rediffused’ electrons. The true secondary yield for perpendicular incidence can be expressed by a universal function [17]

$$\delta_{true}(x) = \delta_{max}^* \frac{sx}{s-1+x^s}, \quad (5)$$

where

$$x = \frac{E}{E_{\max}^*}, \quad (6)$$

$E$  denotes the energy of the incident electron, and  $s$  is a fit parameter that is about equal to 1.35 for LHC Cu samples [36]. The two variable parameters in (5) and (6) are  $\delta_{\max}^*$ , the maximum yield for the true secondaries, which assumes values between about 1.0 and 3.0, decreasing with surface conditioning, and  $E_{\max}^*$ , the energy at which the yield assumes the maximum value, varying between 150 and 450 eV. If the impact of the ‘parent’ electron is not perpendicular to the surface, the yield is still parametrized by (5) and (6), but the values of  $\delta_{\max}^*$  and  $E_{\max}^*$  are found to be functions of the angle of incidence with respect to the surface normal,  $\theta$ , approximately described by [17,37,38]

$$\delta_{\max}^*(\theta) \approx \delta_{\max}^* \exp\left(\frac{1}{2}(1 - \cos\theta)\right) \quad \text{and} \quad E_{\max}^*(\theta) \approx E_{\max}^* \times (1 + 0.7(1 - \cos\theta)). \quad (7)$$

where the parameters  $\delta_{\max}^*$  and  $E_{\max}^*$  on the right-hand side are those for perpendicular incidence ( $\theta=0$ ).

Elastic reflection of electrons is important primarily at low energies, i.e., below about 20 eV. The measured electron reflection probability can be parametrized as

$$\delta_{el}(E) \approx \left( \frac{\sqrt{E} - \sqrt{E + E_0}}{\sqrt{E} + \sqrt{E + E_0}} \right)^2, \quad (8)$$

with only one fit parameter,  $E_0$  [39]. Since no measurements are available for the angular dependence of the elastic reflection, we at present consider the reflectivity as independent of impact angle (which might be justified by surface roughness at a microscopic level). Equation (8) implies that the reflection probability approaches 1 in the limit of vanishing electron energy, as indicated by some of the measurements [40]. Presently there is no general agreement on this point.

Ignoring ‘rediffused’ electrons, the total secondary emission yield is simply taken to be the sum of the true secondary yield and the elastic reflection yield:

$$\delta_{tot}(E, \theta) = \delta_{el}(E) + \delta_{true}(E, \theta) \quad (9)$$

The energy distribution of the emitted true secondary electrons has an influence on their survival time. The measured energy distribution is well described by a function of the form [38]

$$\frac{dN_s}{dE_s} \propto \exp\left(-\frac{1}{2}\left(\ln\left[\frac{E_s}{E_0}\right]\right)^2\right), \quad (10)$$

where  $E_s$  refers to the energy of the secondaries and  $E_0$  was fitted to values between 1.5 and 2.0 eV. The angular distribution of the true secondaries is taken to be [41]

$$\frac{dN_s}{d\Omega} \propto \cos\theta. \quad (11)$$

The key parameters determining the average electron yield and the threshold of multipacting are  $\delta_{\max}^*$  and  $E_{\max}^*$ . As indicated above, these vary greatly with material, surface treatment, history, etc. Extensive measurement campaigns have been performed for relevant technical materials in order to determine these parameters [37,40,58]. Most spectacularly, at the CERN SPS an in-situ measurement installed by N. Hilleret and his colleagues allows monitoring the time evolution of the secondary emission yield inside the beam pipe during operation [12].

### 2.1.5 Saturation

The electron-cloud build up saturates when the electron losses balance the electron generation rate. This can happen either, at low bunch charges, when the average neutralization density is reached [18] or, at high bunch currents, when the kinetic energy at emission is too low to penetrate into the space-charge field of the cloud [42]. The estimates for the equilibrium electron volume density are

$$\rho_{e,sat} \approx \frac{N_b}{\pi s_b b^2} \quad \text{for } N_b \ll N_{trans} \quad (12)$$

and

$$\rho_{e,sat} \approx \frac{E_s}{m_e c^2 b^2 r_e} \quad \text{for } N_b \gg N_{trans} \quad (13)$$

where  $b$  denotes the chamber radius (for simplicity we consider a round chamber),  $E_s$  is the average energy of the emitted secondary electrons, and  $r_e$  is the classical electron radius. The transition occurs at a bunch population of about

$$N_{trans} \approx \frac{E_s s_b}{m_e c^2 r_e}. \quad (14)$$

Therefore, if multipacting occurs, the average electron density in the steady state first increases linearly with current, until it reaches the transition intensity (14), above which the average density stays approximately constant and the density at the center of the chamber actually decreases [42], reducing the likelihood of electron-driven instabilities.

### 2.1.6 Cloud Decay and Electron Survival

The electron density decays in the gap between bunch trains. Early measurements of emittance blow up due to electron cloud at the KEKB positron ring, prior to the installation of solenoid fields, explored this decay time by injecting two short bunch trains separated by a variable distance. These studies revealed that the blow up of the first bunch in the second train disappeared for gap sizes of a few 10s of ns, while gaps of several 100 ns were required to eliminate the blow up of the second bunch [24,33]. One explanation of this phenomenon, supported by simulations [43], is that the first bunch of the second train attracts the residual electrons which have survived near the chamber wall, as a result of which the electron density at the center of the chamber strongly increases before the arrival of the second bunch of the train. The extreme length of the gap required to completely ‘reset’ the cloud that was unveiled in these experiments renders gaps a rather inefficient countermeasure.

The studies at KEKB and others at the CERN SPS determined decay times that were much longer than those naively expected from the velocity distribution of the electrons and the size of the vacuum chamber. In these studies not only the emittance growth or beam loss, but also the electron flux on the wall, as monitored by dedicated detectors, and the bunch-by-bunch coherent tune shift were used as indicators for the decay and revival of the electron cloud. The latter two signals provided information on the electron density even well below the threshold of instability. At the SPS a gap of 300 ns did not suffice to reset the cloud and there even was some circumstantial evidence that electrons might survive for as long as several seconds (namely, multipacting on the LHC cycle induced multipacting for the SPS fixed-target beam which follows almost 10 seconds later). At KEKB, with solenoids covering most of the circumference,

a gap of 1  $\mu$ s does not result in any appreciable beam-size difference between the end and start of the bunch train.

Two effects are suspected to be responsible for the long memory and lifetime of the electron cloud: First, nonuniform fields, such as quadrupoles or sextupoles, may act as magnetic bottles and trap electrons for an indefinite time period [22,30]. Second, if the probability of elastic reflection indeed approaches 1 in the limit of zero electron energy, as is suggested by measurements [39], low-energetic electrons could survive nearly forever, bouncing back and forth between the chamber walls, independently of the magnetic field. In 2004, a new electron-cloud detector will be installed inside a quadrupole magnet at the CERN SPS; this detector can observe the spatial distribution and the time evolution of the electron flux on the wall [44]. The decay in a quadrupole can then be compared with that observed by the existing detectors for bending magnets and field-free regions. The result of such a comparison may provide an indication as to whether reflection or trapping is the primary reason for the slow decay of the electron cloud.

### 2.1.7 Remedies

There are at least three possible responses to the electron cloud: (1) reducing the production rate of primary electrons or guiding their motion to a region where they do no harm, (2) suppressing the multipacting, and (3) alleviating the effect on the beam or on the diagnostics. In most cases, for example, at the LHC, the SNS, and PEP-II, a combined approach was taken.

The primary production of photoelectrons may be so high that the electron cloud could reach saturation within a few bunch passages even without any multipacting. This is the case at KEKB, the KEK Photon Factory, and even the LHC, if no countermeasures were taken. The obvious solutions are an antechamber, photon stops (as developed for the VLHC [45]), or, for dipole fields, a sawtooth pattern impressed on the chamber wall as is planned for the LHC. Weak solenoids of the order of 50 G are another possibility, which was successfully implemented at KEKB. The solenoids do not really reduce the photoemission, but they keep the photoelectrons close to the wall and, thus, mitigate the subsequent beam-electron interaction. It is difficult to imagine that the number of electrons created by gas ionization can be reduced by orders of magnitude in a similar way as for photo-electrons, since the gas ionization rate is linearly proportional to the vacuum pressure. If field ionization is important, however, a possible cure would be lengthening the bunches, though this will mainly be a concern for future projects such as linear colliders or X-ray FELs operating with positrons. Electrons generated by beam loss at a collimator can be controlled by solenoids or clearing electrodes. For example, the SNS project is installing solenoids along the collimator straights. A large number of electrons is also generated at injection stripping foils, for accelerators employing charge-exchange injection. Again at the SNS, a 10-kV clearing voltage is applied to channel the electrons liberated at the stripping foil onto a collector plate that is monitored by a TV camera.

A well established method to reduce multipacting in rf couplers is coating with TiN, a material that has a low secondary emission yield. The thickness of the coating is of the order of a micron, which should not alter the resistive impedance seen by the beam. A more favorable getter material made from TiZrV was developed at CERN [46]. This getter material is characterized by its greater structural stability than TiN and by its low activation temperature. The warm sections of the LHC, about 10% of the circumference, will be coated with this new getter. The coating was already tested at several light-source insertion devices, where

circumstantial evidence suggests an increase in the effective impedance, presumably due to a larger surface roughness. The surface roughness impedance is of no concern for the longer proton bunches in the LHC. Multipacting may also be suppressed by solenoids, though one should pay attention to the possibility of cyclotron resonances mentioned in 2.1.3. Electric clearing fields are an efficient cure in simulations. They were already used to cure electron-proton instabilities for the coasting proton beams in the CERN ISR during the early 70s. In machine experiments at BEPC, biasing the button BPMs, which are located at every arc quadrupole, with a clearing voltage of 600 V reduced the positron beam-size blow up due to the electron cloud by about 30% [47]. Also at the SNS, which will operate with long proton bunches, the capability is foreseen to bias the BPMs, with a voltage of up to 1 kV. To completely suppress the multipacting experienced by short bunches with close spacing, the clearing electrodes must be mounted all around the ring in distances of a few 10s of cm and voltages of the order 1 kV are required. The impedance introduced by many such devices could be prohibitive. However, a continuous long wire on an insulating support would not necessarily exhibit a large impedance. Other options for a practical implementation of electric clearing fields may be ‘stealth’ electrodes like those used for ion clearing in the CERN AA [48], or splitting the beam pipe into a top and bottom half, isolated from each other and held at different potential. Biasing the two jaws of a collimator against each other is a similar idea. Several authors have proposed to prevent multipacting by grooves on the chamber wall. These grooves essentially act as electron traps. Considering a wall section whose surface normal is aligned with a (dipole) magnetic field, it was calculated by S. Mitsunobu that the optimum suppression by triangular-shaped grooves is achieved, if the full angle at the bottom of the groove,  $\alpha$ , is equal to  $49.4^\circ$  [49]. A. Krasnov employed a ‘simplified 2D method of angular coefficients’ to also compute the reduction of the secondary emission yield by grooves on the surface. He found that the smaller is the angle  $\alpha$ , the larger is the reduction in secondary yield [50]. The last two results are not quite consistent, which suggests that further studies might be needed. Proper tailoring of the bunch filling patterns (bunch spacing, bunch trains and bunch charges) is yet another way of achieving an acceptable electron density. Examples here include mini-trains in PEP-II [51], the actual bunch spacings chosen for PEP-II and KEKB operation, which are twice or three times the design spacing, and satellite bunches proposed for the LHC [52]. Gaps between trains can lower the density and reset the cloud at least to some extent. Larger vacuum chambers reduce the energy gain by electrons at the chamber wall, and approximate the situation of a coasting beam, for which no multipacting occurs. An interesting prospect, first proposed by S. Heifets is that multipacting can also be controlled and electron densities be reduced by operating with close spacings and extremely high bunch charges. This currently appears the most promising approach towards higher luminosity in Super factory machines,

The electron cloud causes a large variety of undesired effects. Common stabilizing measures can be taken against the resulting coupled-bunch and single-bunch instabilities. These include transverse bunch-to-bunch feedback [25,53], increased chromaticity [25], octupoles [48], intra-bunch head-tail feedback (prototypes are under development for the PEP-II upgrade [54]), and linear coupling [55]. Degradation of diagnostics signals due to impacting electrons can be overcome with local solenoid windings, which have proven efficient at the CERN SPS [56] and PS [57].

### 2.1.8 References

1. V. Baglin, I.R. Collins, O. Gröbner, EPAC98 Stockholm, p. 2169 (1998).
2. V. V. Anashin et al., LHC Project Report 373 (1999).
3. R. Cimino et al., LHC Project Report 668 (2003).
4. K. Ohmi, PRL **75**, 1526 (1995).
5. "Tables and Graphs of electron-Interaction Cross Sections from 10 eV to 100 GeV Derived from the LLNL Evaluated Electron Data Library (EDLL), Z=1-100," UCRL-50400 Vol. 31 (1991).
6. T. Raubenheimer, P. Chen, "Ions in the Linacs of Future Linear Colliders," LINAC92, Ottawa Canada (1992).
7. S. Deng et al., "Modeling of Beam-Ionized Sources for Plasma Accelerators," PAC 2003 Portland (2003).
8. P. Thieberger et al, "Secondary-electron yields and their dependence on the angle of incidence on stainless-steel surfaces for three energetic ion beams", Physical Review A **61**, 042901 (2000).
9. P. Thieberger, private communication (2004).
10. O. Gröbner, "Bunch Induced Multipacting," 10<sup>th</sup> Int. Conference on High Energy Accelerators, Protvino, July (1977).
11. G. Arduini, presentation at E-CLOUD02, Geneva (2002).
12. M. Jiménez et al., CERN-LHC Project-Report-632 (2003).
13. B. Hanna, private communication (2002).
14. F. Zimmermann, CERN-AB-2003-004-ABP (2003).
15. S. Heifets, "Study of an Instability in the PEP-II Positron Beam: Ohmi Effect and Multipacting," CEIBA95 Tsukuba (1995).
16. M. Furman, G. Lambertson, "The Electron-Cloud Instability in PEP-II," EPAC96 Sitges (1996).
17. M. Furman, G. Lambertson, "The Electron-Cloud Instability in the Arcs of the PEP-II Positron Ring," Proc. MBI97 Tsukuba (1997).
18. F. Zimmermann, LHC Project Report 95 (1997).
19. F. Zimmermann, "Electron Cloud Simulations," Chamonix XI (2001).
20. O. Brüning, EPAC98 Stockholm (1998).
21. G. Rumolo, F. Ruggiero and F. Zimmermann, PRST-AB **4**, 012801 (2001).
22. L. Wang et al., PRST-AB **5**, 124402 (2002).
23. L. Wang et al., PRST-AB **7**, 034401 (2004)
24. H. Fukuma et al., EPAC2000 Vienna (2000).
25. G. Arduini et al., "Transverse Behavior of the LHC Proton Beam in the SPS: An Update," PAC2001 Chicago (2001).
26. K. Cornelis, "The Electron Cloud Instability in the SPS," E-CLOUD02 Geneva (2002).
27. G. Stupakov, CERN LHC Project Report 141 (1997).
28. L. Vos, CERN-AB-2003-074 (2003).
29. K. Harkay et al., PAC2003 Portland (2003).
30. P. Channell, A. Jason, "PSR Instability Induced by Electrons Trapped in Quadrupoles," LA AOT-3 TN 93-11, private communication (1994). We thank V. Danilov for drawing our attention to this reference.
31. A. Novokhatski, J. Seeman, PAC 2003 Portland (2003).
32. Y. Cai, M. Pivi and M. Furman, PRST-AB **7**, 024402 (2004).

33. H. Fukuma, ELOUD02 Geneva (2002).
34. F. Zimmermann, "New Simulations of Positron-Beam Electron Cloud Build-Up and ... for KEKB and Super-KEKB," KEK, 31. Oct. (2003).
35. S. Mitsunobu, KEKB MEMO No. 214, 29. May 2002 (2002).
36. V. Baglin, I. Collins, B. Henrist, N. Hilleret and G. Vorlaufer, LHC Project Report 472 (2002).
37. R.E. Kirby, F.K. King, NIM A**469**, 1-12 (2001).
38. B. Henrist et al., Proc. ELOUD02 Geneva (2002).
39. R. Cimino, I. R. Collins, M. A. Furman, M. Pivi, F. Ruggiero, G. Rumolo, F. Zimmermann, "Can Low-Energy Electrons Affect High-Energy Physics Accelerators?," Submitted to Phys. Rev. Let. (2004).
40. R. Cimino and I. R. Collins, LHC Project Report 669 (2003).
41. H. Seiler, J. Appl. Phys. **54** (11) (1983).
42. S. Heifets, "Electron Cloud at High Beam Currents," Proc. ELOUD02 Geneva (2002).
43. G. Rumolo, F. Zimmermann, K. Ohmi, H. Fukuma, PAC2001 Chicago (2001).
44. M. Jiménez, private communication (2004).
45. P. Bauer et al., PAC 2001 Chicago, p. 3156 (2001).
46. C. Benvenuti et al., Vacuum **60**, p. 57 (2001).
47. Z. Y. Guo, APAC 2004 Gyeongju (2004).
48. F. Caspers, presentation at ELOUD02 Geneva (2002).
49. S. Mitsunobu, KEKB MEMO No. 185, 5. April 2001 (2001).
50. A. Krasnov, Proc. EVC Berlin, and LHC Project Report 671 (2003).
51. F. Decker, presentation at ELOUD02 Geneva (2002).
52. F. Ruggiero, X. Zhang, AIP Conf. Proceedings **496**, p. 40 (1999).
53. S.S. Win et al., EPAC02 Paris (2002).
54. J. Fox, Proc. Factories03, SLAC (2003).
55. E. Métral, Proc. ELOUD02 Geneva (2002).
56. W. Höfle, Proc. Chamonix01 (2001).
57. R. Cappi et al., PRST-AB (2002).
58. N. Hilleret et al., Proc. EPAC 2000 Vienna, p. 217 (2000).
59. A. Rossi, Chamonix03 (2003).

## 2.2 Coupled-bunch instability caused by electron cloud

S. S. Win and K. Ohmi  
 mail to: [susuwin@post.kek.jp](mailto:susuwin@post.kek.jp)  
[KEK, 1-1 Oho, Tsukuba 305-0801 Japan](http://www.kek.jp/accelerator/kekb/1-1-ohmi.html)

### 2.2.1 Introduction

The coupled-bunch instability can occur due to several reasons in the accelerators. Resistive wall impedance, the higher-order modes of the rf cavities, the interaction of accelerating particles with trapped ions from residual gas, and the electrons produced as secondary charged particles from the inner wall of vacuum chamber are all capable to cause the coupled-bunch instability.

The synchrotron radiation plays major role in the electron cloud formation as the cloud electrons are originated at the chamber wall where the synchrotron radiation hits. The positrons

circulating in the ring with the relativistic energy lose their energy in every turn due to synchrotron radiation in the bending magnets. The energy loss in one turn is calculated as  $\Delta E[\text{GeV}] = C_\gamma E^4[\text{GeV}^4]/\rho[\text{m}]$  where  $C_\gamma$  is  $8.8575 \times 10^{-5} \text{ m/GeV}^3$ . Since the critical photon energy is  $\epsilon_c[\text{GeV}] = 2.218 \times 10^{-3} E^3[\text{GeV}^3]/\rho[\text{m}]$ , the quantity of emitted photons is directly proportional to their relativistic energy.

When the photons are tangentially emitted by the positron bunch and hit the wall of the vacuum chamber the electrons are produced depending on the work function of the chamber material. The accelerators are generally operated with a train of so many bunches and therefore, the electrons are continuously produced by the beam. Once a positron bunch is disturbed to oscillate by the interaction of positron bunch with the electrons being produced, the wake field left behind modifies the distribution and the density of the electron cloud which interacts with the successive positron bunch and thus affect on the subsequent bunches of the beam [1]. When bunches are in coupled motion the snap shot of the bunch oscillation are seen as if they are oscillating at some mode frequencies together. Depending on the nature of the wake, the transverse coupled bunch mode is determined either by  $f_c = (pM + \nu_\beta + \mu)f_0$  (for  $\omega - \omega_r \approx 0$ ) or by  $f_c = (-pM - \nu_\beta - \mu)f_0$  (for  $\omega + \omega_r \approx 0$ ) where  $f_c$  is the mode frequency,  $f_0$  is the revolution frequency,  $p$  is an integer,  $M$  is the number of bunches,  $\nu_\beta$  is the betatron tune and  $\mu$  is the coupled bunch mode number.

There have been experimental studies on the coupled-bunch instability caused by electron cloud in various ways in many laboratories. In 1995 Izawa et al. [2] experimentally studied the coupled-bunch instability at the photon factory (PF) at KEK by observing the coupled-bunch oscillation and a remarkable distribution of vertical betatron side-bands in positron multi-bunch beam even in a small bunch train of successive bunches followed by many vacant buckets. The vertical instability was considered to be caused by electron cloud as the instability was not affected by ion pumps and the vertical beam size reduced due to clearing electrodes. Guo et al. [3] studied the photoelectron instability in BEPC in corporation with IHEP and KEK. The coupled bunch instability was studied by observing a strong dependence of a broad distribution of betatron side bands in the mode spectrum using spectrum analyzer on the bunch spacing. The time development of the instability was studied by analyzing the oscillation in the time domain using single pass beam position monitor (SPBPM) system. Harkay and Rosenberg [4] studied the electron cloud induced beam instability at APS by the observation of a horizontal coupled bunch instability occurring at the beam-induced multipacting (BIM) resonance and also measured the electron cloud build up and the saturation over a bunch train. In the study of Holmquist and Rogers at CESR [5] the horizontal coupled-bunch instability was observed in electron and positron storage rings to grow analogously due to the photoelectrons which are trapped in the beam chamber when the distributed ion pumps (DIP) are powered.

At KEKB in the positron ring the coupled-bunch instability caused by the electron cloud is studied by measuring the coupled-bunch spectrum and growth rate with and without solenoid field [6]. The observation in the changes of the coupled-bunch mode spectrum and the growth rate when the electron cloud at the beam center is removed by the solenoid field in  $z$  direction confirms the coupled-bunch instability be caused by the electron cloud.

### 2.2.2 Characterization of Coupled-Bunch Instability from bunch oscillations

At KEKB the coupled-bunch instability is studied from the bunch oscillation data which are recorded using a high speed data recording system called bunch oscillation recorder (BOR) [7].

The BOR was developed in KEKB for the purpose of investigating the nature of multibunch instabilities. It can store the bunch oscillation data for 41 ms which is about 4000 turns.

### 2.2.2.1 Experimental procedure

The experimental parameters are listed in Table 1. In the normal operation the transverse bunch-by-bunch feedback systems are used for both horizontal and vertical planes to suppress the transverse dipole oscillation of bunches. The beam is lost as bunches oscillate if the feedback systems are switched off. In the experiments the bunch oscillation data are recorded just before the beam loss after switching off the feedback systems.

Prior to recording the data, the positron beam is accumulated in the LER up to 600 mA beam current using the feedback systems. The horizontal oscillation data were taken immediately after turning off the horizontal feedback system and the vertical data after turning off the vertical feedback system. The signals of successive bunches are recorded turn by turn at a position in the ring for 4096 turns and therefore each data set contains the position data of 1153 bunches  $\times$  4096 turns. The typical bunch oscillation recorded by the BOR is shown in Fig. 1.

**Table 1.** The machine parameters of KEKB-LER

Beam energy, $GeV$	3.5
Circumference, $m$	3016
Radius of vacuum chamber, $mm$	47
Harmonic number	5120
Number of positron train/bunches	1/1153
Bunch spacing, $ns$	8
Betatron tune $\nu_x/\nu_y$	45.52/43.57
Emittance $\varepsilon_x/\varepsilon_y$ , $nm/nm$	18/0.36
Average beta function $\beta_x/\beta_y$ , $m/m$	15/15
Bunch current, $mA$	0.52

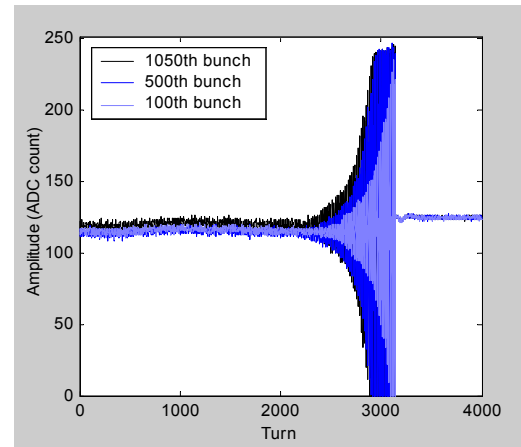


**Fig. 1.** Typical bunch oscillation

To study the characteristics of the coupled bunch instability caused by the electron cloud the bunch oscillation data are taken while solenoids are powered on and off. The typical solenoid field at the center is approximately 45 G and the chromaticity is 7.082.

### 2.2.2.2 Experimental Results

Without solenoid field, the snapshot of the positron bunches and the phase development with time along the bunch train in horizontal plane is shown in Figure 2 and 3, respectively. The coupled-bunch mode spectra from the snapshots in the horizontal and vertical plane are shown in Figure 4 and 5, respectively. As can be seen in the figures, the horizontal and the vertical mode spectrum are similar both having the peaks around the mode number 840 and 150. These mode numbers correspond to the mode frequencies of about 90 and 20 MHz (for the normal wake if  $\omega - \omega_r \approx 0$  as discussed in [8]) and 40 and 110 MHz (if  $\omega + \omega_r \approx 0$ ) depending on the wake nature. The average horizontal growth rate is 2 ms and vertical growth rate is 1.4 ms.

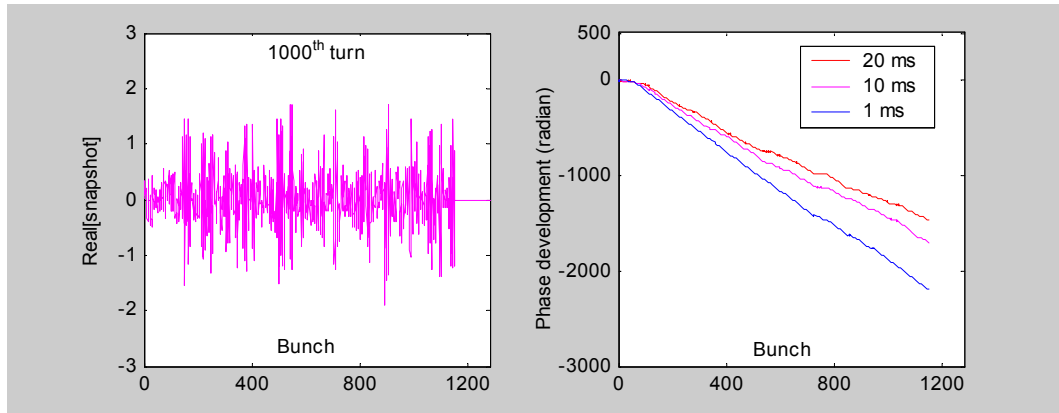


**Fig. 2.** Horizontal snapshot of the bunches at 10 ms

**Fig. 3.** Horizontal phase development along the bunch train

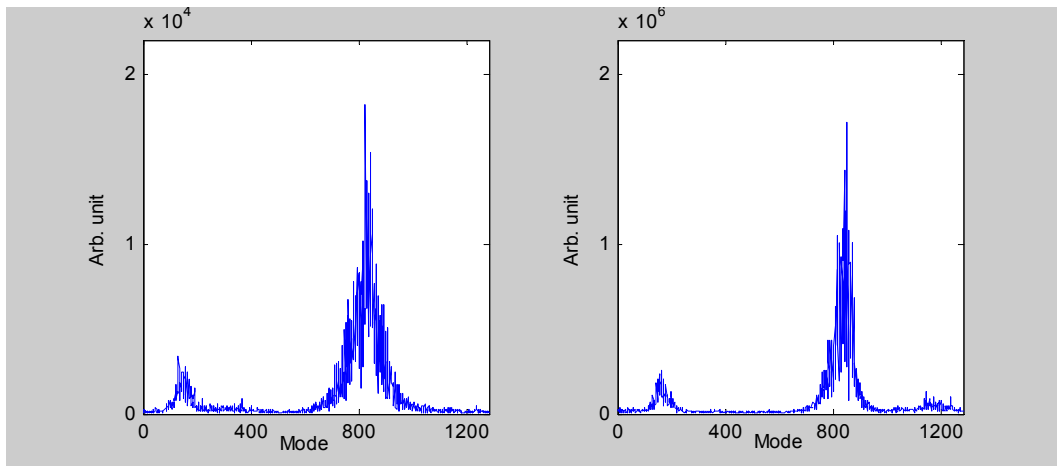


**Fig. 4.** Horizontal mode spectrum

**Fig. 5.** Vertical mode spectrum

[without solenoid field]

Fig. 6 shows the snapshots and the phase development along the bunch train with time when solenoid field is applied in the ring. Fig.6 a) and b) are due to 50% solenoid field whereas c) and d) are with 100% field strength of 45 G. The horizontal and vertical mode spectra are shown in Fig. 7 a) and b) respectively. Unlike the mode spectra observed without solenoid field, the coupled-bunch mode spectra due to the solenoid field show no peak at the mode number 840. The peak appears are at lower mode number instead. In other words, due to the solenoid field the mode frequencies are much lower than that without solenoid field. Comparing with the mode spectra due to two solenoid field strengths, it is seen that the lower mode frequency is excited as the solenoid field applied is stronger. The mode frequency is about 9 MHz for  $\omega - \omega_r \approx 0$  and 120 MHz for  $\omega + \omega_r \approx 0$  when half strength of solenoid field is applied. The mode frequency is about 1 MHz lower when solenoid field is increased to its full strength. It should be noted that the mode spectra have peaks at lower side band ( $0 \sim 640$ ) for slower resonator frequencies than  $\omega_0 \times n_{\text{bunch}}$ . Ordinary wake force with causality (or negative sign in the definition of Chao's textbook [8])

causes instability at upper side band (640~1280). This feature is the mirror of the positive phase development along the bunch train seen in Fig. 6 b) and d).

The cyclotron frequency for the solenoid field is estimated to be  $f_{\text{cyc}}=126$  MHz for 100% (45G) and 63 MHz for 50% (22.5G). Corresponding mode numbers are 1255 and 605, respectively. In the experimental data when 45 G solenoid field is applied, the mode frequency of 120 MHz (if  $\omega+\omega_r \approx 0$ ) is very close the cyclotron frequency. However, when solenoid field is reduced to its half strength, the mode frequency in the experiment is different from the cyclotron frequency. This feature is interesting and will be discussed elsewhere.

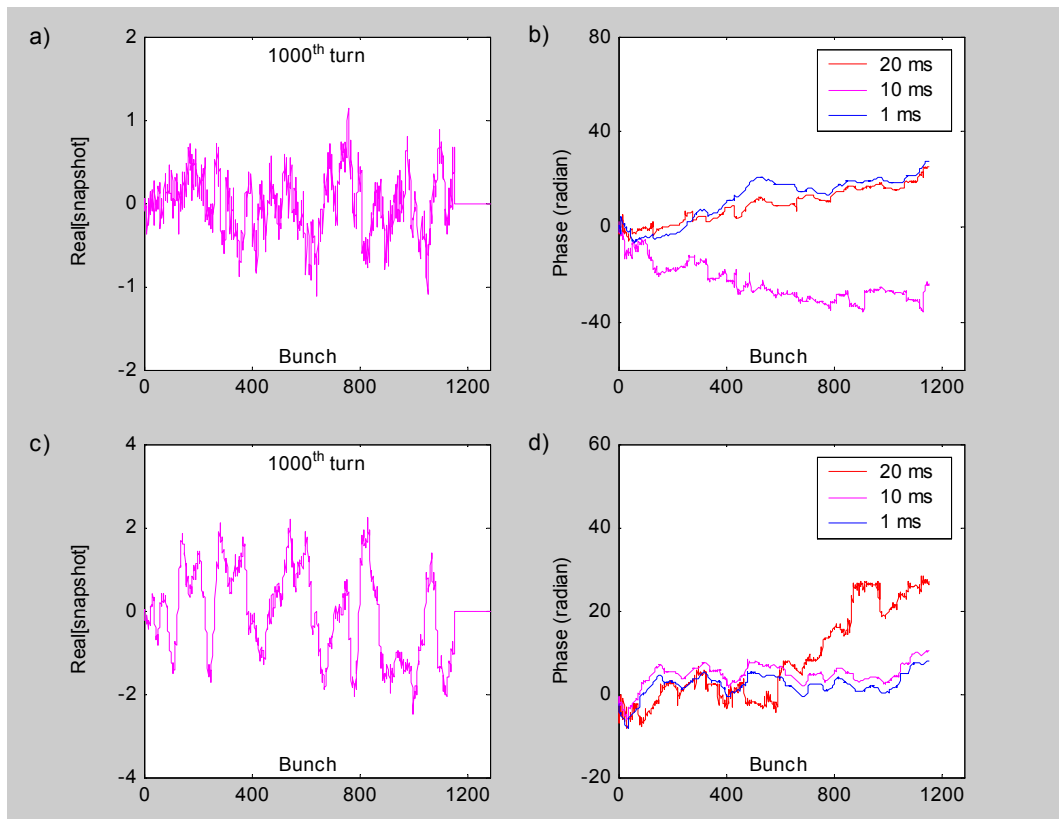


**Fig. 6.** The snapshots and the phase development with time along the bunch train in horizontal plane when solenoid field is applied a) and b) are with 50 % solenoid field strength and c) and d) with 100% solenoid field strength.

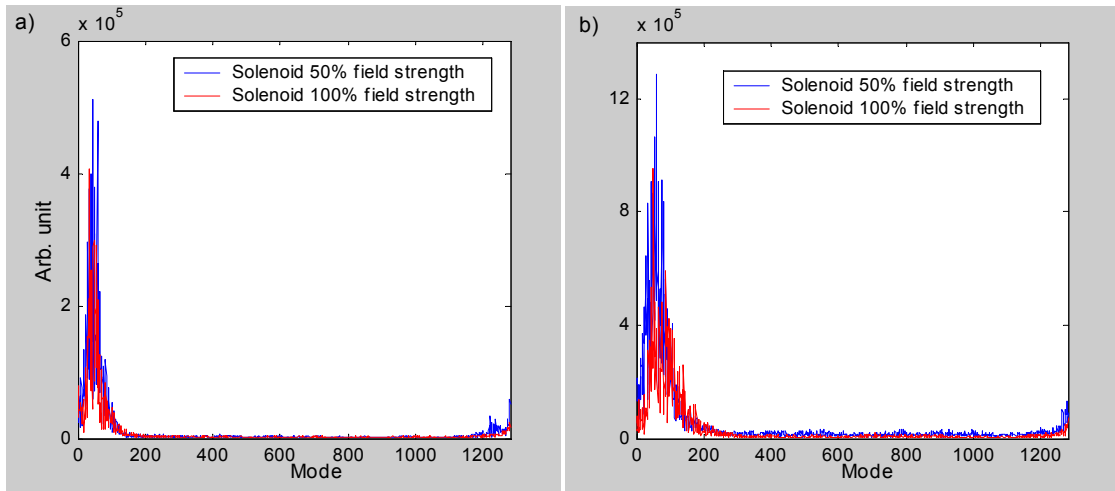


**Fig. 7.** The mode spectra in a) horizontal and b) vertical plane with different solenoid field.

Simulation studies were performed to understand the experimental results qualitatively [6]. We used a program code PEI [1,9], in which motion of electrons and positron bunches are solved self-consistently. The motion of positron bunches were analysed with the same manner as the experimental data and the experimental mode spectra with and without solenoid, which are seen in Figures 4, 5 and 7, are reproduced with consistency.

### 2.2.3 References

1. K. Ohmi, *Physical Review Letters* **75**, 1526 (1995).
2. M. Izawa et al., *Physical Review Letters* **74**, 5044 (1995).
3. Z. Guo et al., “Experiment Studies on the Photoelectron Instability in the Beijing Electron Positron Collider”, *PRST-AB* **5**, Issue 12, 124403 (2003).
4. K. Harkay et al., *PAC01 Proceedings*, Chicago, 671 (2001).
5. T. Holmquist and J.T. Rogers, *Physical Review Letters* **79**, 3186 (1997).
6. S. S. Win et al., *Proceedings of ELOUD2002*, CERN-2002-001, 199 (2002).
7. M. Tobiyama and E. Kikutani., *PRST-AB* **3**, 012801 (2000).
8. A. Chao, *Physics of Collective Beam Instabilities in High Energy Accelerators*, Wiley, New York, 1993.
9. K. Ohmi, *Physical Review E* **55**, 7550 (1997); K. Ohmi, *Proceedings of PAC97*, 1667 (1997).

## 2.3 Single bunch instabilities induced by electron cloud in short positron/proton/ion bunches

G. Rumolo

<mailto:G.Rumolo@gsi.de>

[GSI-Darmstadt](#)

Planckstrasse, 1 D-64291 Darmstadt (Germany)

E. Benedetto<sup>1,2</sup>, U. Iriso<sup>3</sup>, F. Zimmermann<sup>1</sup>

<sup>1</sup> [CERN](#), AB Department, 1211 Geneva 23, Switzerland

<sup>2</sup> INFN and Dipartimento di Energetica, [Politecnico di Torino](http://www.politecnico-torino.it), Torino, Italy

<sup>3</sup> [BNL](http://www.bnl.gov), CAD, Upton, New York, USA

### 2.3.1 Introduction

For linear accelerators, a single bunch instability of a positron bunch due to electrons created by ionization of the residual gas was discussed in Ref. [1], where a coherent oscillation of both electrons and positrons grows from any small initial perturbation of the bunch distribution, e.g. from the statistical fluctuations due to the finite number of beam particles. This instability can be considered as a two stream instability of the same type as studied in plasma physics. A similar two stream instability may occur in storage rings operating with positively charged particles, due to the interaction with electrons primarily generated via photoemission, gas ionization or particle loss and then multiplied via secondary emission [2]. Such instabilities can be very fast, since in the new generation of high intensity rings operating with many closely spaced bunches, the density of electrons can become quickly large. Even machines operating with bunches spaced by hundreds of ns can actually suffer from electron cloud because of the long survival time of low energy electrons in the beam pipe due to elastic reflection [3].

Electron clouds can also cause multi-bunch dipole mode instabilities. The multi-bunch instability is different from the instability we discuss in this article, which is a single bunch phenomenon induced by a pinched electron cloud which turn by turn carries memory of the offset bunch head to the bunch tail. Although the effect we discuss is purely single bunch, it occurs, however, only in multi-bunch operation, since the electron cloud requires several bunch passages to build up. Note also that the head tail effect we discuss here is different from the electron-proton instability observed in some machines operating with long bunches (like the Los Alamos PSR). In that case, electrons inside the beam pipe perform many oscillations during the bunch passage, and their number can be amplified if they are produced on the falling edge of the bunch and gain energy as they cross the pipe section (so called “trailing-edge multipacting” [4]). The quick multiplication of the number of electrons on the falling edge of the bunch is then responsible for the destabilization of the bunch tail. In our case, electrons can only perform about 1 oscillation while the bunch is passing by, and the bunch interacts with a pre-established cloud, which has been produced by the preceding bunches and fills almost uniformly the beam pipe prior to the bunch arrival. The number of electrons does not change appreciably during one bunch passage.

The parameter that discriminates short and long bunches in our context is thus the maximum number of oscillations performed by the electrons during one bunch passage,  $n$ . The criterion to decide whether we are dealing with a short bunch reads therefore

$$n^2 = \frac{2ZN_b\sigma_z r_e}{\pi^2\sigma_x\sigma_y} \cong 1 \quad \text{for flat beams,}$$

$$n^2 = \frac{ZN_b\sigma_z r_e}{\pi^2\sigma_x^2} \cong 1 \quad \text{for round beams,}$$

where  $Z$  is the charge state of the beam particles;  $N_b$  is the number of particles per bunch;  $\sigma_x$ ,  $\sigma_y$ ,  $\sigma_z$  the bunch rms-sizes in all three directions;  $r_e$  the electron classical radius.

However, there can exist intermediate regimes in which the electron cloud can build up as a result of a joint trailing edge and multi bunch effect, and even if the ratio  $n^2$  defined above is well above unity, a head-tail instability of the type we describe in this paper can arise (as it could be for instance expected for the GSI-SIS18 [5]). Here below we list some existing machines with their  $n^2$  parameters, their typical bunch lengths and their  $Z/(A\gamma)$  numbers.

Ring	Type of particles	Typical $\sigma_z$ (ns)	$n^2$ parameter	$Z/(A\gamma)$
DAΦNE	Positrons	$8.3 \times 10^{-2}$	0.4	1.88
SPS (LHC)	Protons	1	1.2	0.036
KEKB LER	Positrons	$1.3 \times 10^{-2}$	2	0.27
RHIC	Au <sup>79+</sup> ions	2.5	7.2	0.0037
PS (store)	Protons	2.5	7.5	0.036
SIS18	U <sup>73+</sup> ions	17	41.7	0.25
ISIS	Protons	23	177.6	0.54
PSR	Protons	54	2307	0.54

Following this table and the definition given above, only DAΦNE, KEKB LER and the SPS (with LHC-type beams) operate with rigorously short bunches. RHIC (with Au<sup>79+</sup> ions) is very close anyway, because the number of electron oscillations is very modest and gets even smaller by a factor 2 after rebucketing at top energy: in fact, the expected electron-cloud build up dynamics in RHIC resembles much more a multi-bunch accumulation than a trailing-edge phenomenon. Similar considerations apply to the CERN PS operated with 10 ns bunches stored for 10 ms (see following section). In the SIS18, in spite of the high  $n^2$  parameter, the multi-bunch multiplication effect takes over for high values of the maximum SEY, and the enhancement of electron density at the bunch tail due to the trailing edge mechanism then becomes negligible (below this threshold, the electron density in the beam chamber would not suffice to cause any instability).

The  $Z/(A\gamma)$  numbers are a measure of the sensitivity of the bunch particles to the interaction with the electron cloud. Low values indicate that the bunch particles would need to interact with very high electron cloud densities in order to feel a significant effect on their dynamics (large stiffness). High values, on the contrary, indicate that the bunch is easily destabilized even by electron clouds of moderate density.

### 2.3.2 Review of the observations and approaches to the problem

Electron-cloud induced instabilities for short bunches have been observed in form of emittance growth and beam loss at the KEKB LER, at the CERN PS and SPS, and at the PEP-II LER.

At the KEKB LER a blow up of the vertical beam size was already observed at the early commissioning time [6]. This blow up was not accompanied by any coherent beam motion, which could be easily suppressed by transverse feedback and chromaticity, and the blow up was only seen in multi-bunch operation with a narrow bunch spacing. The single bunch two-stream instability provided a plausible explanation of the observed beam blow up [7]. This explanation has since been reinforced by the simultaneous observation of a tune shift along the bunch train, which appears for the same bunches exhibiting vertical size blow up as a consequence of the

extra-focusing from the electron cloud, and by the experimental evidence that the installation of solenoids around the ring could cure the problem for currents up to 1300mA in regular operation condition for the experiments [8].

At the CERN SPS the electron cloud has appeared since the ring has been regularly operated with LHC-type bunch trains [9], and it has been held responsible for strong transverse instabilities. In the horizontal plane a low order coupled bunch instability develops within a few tens of turns after injection. In the vertical plane, a single bunch head tail instability would rise on a much shorter time. The reason of the different behavior in the two transverse planes is ascribed to the confinement of the electron cloud mostly in dipole regions, which can limit the intra-bunch electron pinching in the horizontal plane and therefore inhibit the single-bunch mechanism for instability. The horizontal instability is cured by means of a transverse feedback system. Similar to the situation at the KEKB LER, running the SPS at high positive chromaticity can cure the vertical instability here too [10].

When the nominal LHC was generated by the PS machine, it was somehow natural to investigate whether this machine was as well affected by electron cloud phenomena in LHC operation. It turned out that this was the case [11] and the standard signature, baseline drift in electrostatic devices, was observed. Interestingly enough, due to the very principle used to generate the LHC beam in the PS, the instability could not develop. Right before ejection from the PS, the proton bunches are in fact rapidly compressed from 16 to 4 ns total length within about 100 turns (about 200  $\mu$ s). This is achieved with a bunch rotation by a quarter of synchrotron period after a non-adiabatic increase of the rf voltage. The limited time for which these short bunches circulate in the ring acts as a natural protection against the electron-cloud induced instability. However, by using adiabatic rf gymnastics it was possible to reduce the total bunch length down to 10 ns and then keep the bunches circulating for about 100 ms inside the PS ring. Under these artificially created conditions, a beam instability was observed. The instability in the PS then appeared as a single bunch phenomenon in the horizontal plane, which seemed not to be affected by chromaticity changes [12]. The peculiarities of the instability observed in the PS remain somehow partly unexplained to date, because, while the presence of a horizontal instability can be justified by the structure of the PS lattice, whose magnets are combined function magnets rather than pure dipoles, it still remains unclear why its vertical counterpart gets suppressed and why chromaticity cannot cure the effect [13].

The electron cloud single bunch instability has been analyzed using a formula of the fast electron-positron bunch instability [1,2], a simplified two-particle model with finite length [7] and more sophisticated 3- and 4-particles models including space charge and beam-beam [14], tracking simulation [7,15,16,17], and the classical TMCI theory applied to the electron cloud wake field, where the latter is parametrized by a broadband resonator model [18].

In the 2-particle model, a head with finite length and a point-like tail particle are considered for an estimation of the wake force, which turns out to be proportional to the electron cloud saturated density,  $\rho_e$ . If the electrons perform more than a quarter oscillation in the beam potential, the integrated head-tail wake can be approximated as [7]

$$W_0 \approx \frac{8\pi\rho_e C}{N_b}$$

where  $C$  denotes the ring circumference and  $N_b$  the bunch population. Substituting then this expression into the BBU criterion to evaluate the threshold for instability (normally calculated in

terms of number of particle per bunch) [19], one can quickly evaluate the minimum cloud density required to excite a strong (e.g., vertical) head-tail instability on the short bunch [7]:

$$\rho_{thr} \approx \frac{2\gamma Q_s A}{\pi r_{e,p} Z C \beta_y},$$

where  $\gamma$  is the relativistic factor,  $\beta_y$  the (vertical) beta function,  $r_{p,e}$  the classical electron or proton radius, depending on whether we consider positron or proton/ion beams.

The more refined 3- and 4-particle models are used to also include the  $z$ -dependence of the electron cloud density ('pinch'), and the  $z$ -dependent space charge and beam-beam tune shifts in the analysis, showing that space charge and beam-beam can act further destabilizing and induce a head-tail motion even when electron cloud alone would only generate an incoherent emittance growth. This is a possible explanation of observations at KEKB, where the specific luminosity decreases for short bunch spacings at beam currents below the threshold of single-beam blow up [19].

The particle-tracking methods will be extensively reviewed in the next section.

The study of the electron cloud instability with the TMC theory uses a wake field approximated by a broad-band resonator whose parameters ( $Q$ ,  $R_s$  and  $\omega_r$ ) are determined either by analytical or simulation approach. The thresholds found in this case by analyzing the lowest radial mode for various values of the electron cloud density (with a finite low  $Q$  value, due to the nonlinearity of the beam force, which damps the electron oscillations in a finite time) are in good agreement with observations both for the CERN-SPS and for the KEKB-LER.

### 2.3.3 Simulation codes for single bunch instabilities and applications

A number of simulation tools have been developed in order to study the electron-cloud single bunch instability for short bunches via direct particle tracking.

The simulations of electron-cloud build up are generally treated separately, since they make use of a weak-strong approach, in which the beam is rigid and is approximated by a static transverse Gaussian distribution when computing the beam forces acting on the electrons (macroparticles) generated bunch by bunch. Build up simulations need to be run prior to the instability simulations, because they provide the necessary input on transverse distribution and saturation value of the electron cloud density. E-CLOUD, POSINST, or a variety of other simulation codes presently available can be used for this purpose (see Proceedings of *E-CLOUD'02* quoted in Ref. [4] or consult the link [21]). Fully self-consistent computations where the cloud generation over a bunch train around the ring as well as the resulting bunch instabilities are treated by a single program are an ultimate goal, but at present these would require prohibitively long computation times.

The existing simulation programs for studies of electron-cloud induced instabilities model the interaction of a single bunch with an electron cloud on successive turns. The cloud is always assumed to be generated by the preceding bunches, and is generally assumed to be initially uniform, although other initial distributions can be considered (for instance, an initial two stripe distribution, if the simulated section is a dipole region). The electrons give rise to a head-to-tail wake field, which amplifies any initial small deformation in the bunch shape, e.g., due to the finite number of macroparticles in the simulation. All simulation tools that have been developed for this study are essentially of the type strong-strong, since the purpose is to investigate how the bunch particles are affected by the electron cloud via the continuous interaction. In particular, electrons are always modelled as macroparticles with an initial transversely uniform distribution

either concentrated at one or several locations along the ring (HEADTAIL [16] and PEHTS [22] or their derivatives, the SLAC code described in Ref. [23]), or uniformly smeared along the  $z$  axis (QuickPIC [17]). The bunch consists of macroparticles [16] or of microbunches with a fixed transverse size, like in [23] or in the earlier version of PEHTS [7]. In the latest versions of PEHTS the microbunches have been changed into macroparticles, in order to also obtain information on the incoherent emittance growth [22]. The bunch is then subdivided into slices, which interact in sequence with the electrons of the cloud, creating the distortion of the initially uniform cloud distribution that can significantly affect the body and tail of the bunch. The interaction between bunch particles and cloud electrons is expressed by the following coupled equations of motion (this is the general form in the case when the kick approximation is applied and the cloud is lumped in only  $N_{int}$  locations around the ring):

$$\frac{d^2 \underline{x}_{p,i}(s)}{ds^2} + \underline{K}(s) \underline{x}_{p,i}(s) = \left( \frac{e}{\gamma m_p c^2} \right) \sum_{n=0}^{N_{int}-1} \underline{E}_e [\underline{x}_{p,i}(s); f_e(x, y, t)] \delta(s - ns_{el})$$

$$\frac{d^2 \underline{x}_{e,j}}{dt^2} = - \left( \frac{e}{m_e} \right) \left( \underline{E}_p [\underline{x}_{e,j}; f_{p,SL}(x, y)] + \frac{d \underline{x}_{e,j}}{dt} \times \underline{B}_{ext} \right)$$

The positions of electrons and bunch particles are represented by the vectors  $\underline{x}_e \equiv (x_e, y_e)$  and  $\underline{x}_p(s) \equiv (x_p, y_p, z_p)$  with  $z = s - ct$  being a co-moving longitudinal coordinate;  $\underline{K}(s)$  is the distributed 3-D focusing strength between two interaction points;  $f_e(x, y)$  and  $f_{p,SL}(x, y)$  represent the distribution functions of the electron cloud and the bunch particles within one slice, respectively;  $\underline{E}_{e,p}$  is the electric field of the electrons and of the beam, respectively, calculated by means of a Particle-In-Cell (PIC) algorithm;  $\underline{B}_{ext}$  is an external magnetic field that can significantly influence the electron dynamics in the region where the cloud is expected to be the strongest. The transformation of the relevant 6D phase-space vectors of the beam particles between two interaction points is achieved using appropriate  $6 \times 6$  matrices (HEADTAIL, PEHTS), or in QuickPIC the differential equation is simply numerically solved between two successive time steps. The summation at the RHS of the first equation of motion obviously becomes an integral over the ring circumference when the kick approximation is not used (QuickPIC). The field of the electron cloud acting on itself can optionally be included [14], though the effect during one short bunch passage is small in most cases, and hence it is normally neglected. All these simulation codes contain synchrotron motion (which is an important damping mechanism because it could introduce longitudinal mixing on a shorter time scale than the instability would take to develop) and chromaticity. HEADTAIL gives in addition the options to model the action of an independent broad-band impedance beside the electron cloud wake field, as well as space charge and detuning with amplitude.

A few example applications of these codes are shown in the following.

Fig. 1a displays the evolution of the centroid vertical position of an SPS bunch ( $N_b = 8 \cdot 10^{10}$  protons) over 500 turns. The bunch would suffer a strong dipole instability under the effect of the broad-band impedance alone, but now this effect gets damped by space charge and enhanced by the electron cloud. The instability manifests itself solely in the vertical plane. There are two good reasons to account for this behaviour: first, in the vertical plane the impedance is larger (actually due to the flat beam pipe) [24], and second, there is evidence that in the SPS the electron cloud is mostly localized in the arcs, where there is a strong vertical magnetic field, and therefore the

electrons can only be pinched vertically by the passing bunch, an effect that is taken into account in the simulation (see next section). A positive chromaticity can strongly damp the instability, as shown in Fig. 1b where the emittance growth over 5ms is plotted for three different values of chromaticity.

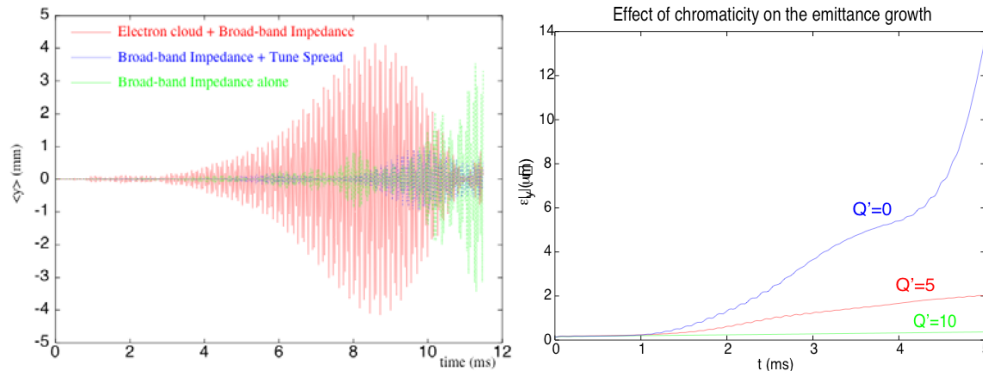


**Fig. 1.** Evolution of the centroid vertical position of an SPS bunch over 500 turns for the three labeled cases (left). Vertical emittance versus time for three different chromaticity settings (right). Broad-band impedance and space charge are included.

The stabilizing effect of chromaticity on this kind of coherent motion is found also for KEKB LER, as can be seen in Fig. 2. The simulation done with the PEHTS code by K. Ohmi clearly proves that the emittance growth can be drastically reduced by increasing the chromaticity value. Simulations with the same sets of parameters have been carried out with HEADTAIL too, confirming the very good agreement between the predictions of these two codes [16].

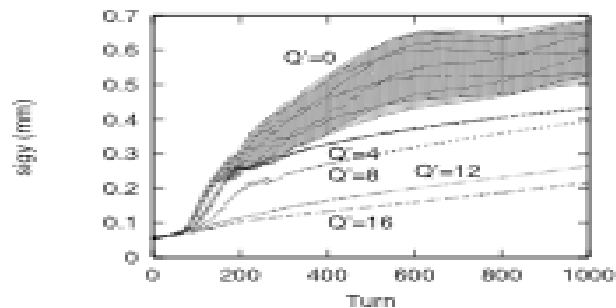


**Fig. 2.** Vertical rms-size growth of a KEK bunch for different values of the chromaticity (labelled in  $Q' = \xi_y Q_y$ )

An extensive simulation campaign is presently being carried out for LHC in order to establish which integrated value of electron cloud around the ring are tolerable in order not to render the beam unstable and not to encounter significant long-term emittance growth. LHC is a very large machine, and the one kick approximation can therefore fail, if the kick received by the bunch particles at each turn is too large. That is why, as a first example, we show in Fig. 4 the dependence of the emittance evolution in LHC on the number of interaction points along the ring (having fixed the electron cloud density  $\rho_e$  to the plausible value of  $6 \times 10^{11} \text{ m}^{-3}$ , right above the estimated threshold of the strong head-tail instability). It is clear that, while in the horizontal

plane the profiles do not significantly change with increasing number of interactions per turn, in the vertical plane they only converge for a number of interaction points larger than 5.

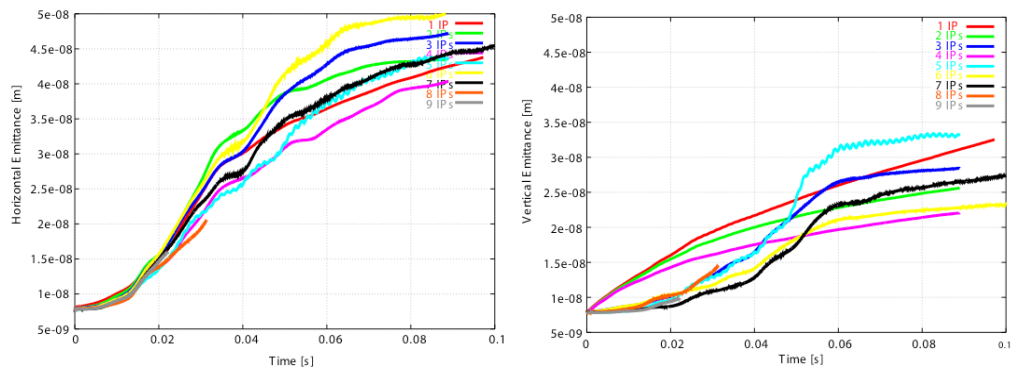


**Fig. 3.** Horizontal (left) and vertical (right) emittance growth in LHC as function of the interaction points used in the simulation.

In general, when there is coherent motion and the kick imparted on each turn by the electron cloud is not too large (by large we mean that dynamic changes in the beta function become significant; these are most likely the cause of filamentation), we expect that the 1-kick approximation is as good as modeling an electron cloud uniformly distributed around the ring (having the same integrated density). But if the kick that the beam particles receive at each turn is too large, it may happen that the coherent effect is suppressed by incoherent emittance growth, and the pattern of the emittance growth itself changes as shown in Fig. 3. The reason why this effect is only visible in the vertical plane is probably to be sought in the value of the vertical tune used in the simulation, which renders the vertical dynamics more sensitive to a large kick. Results from HEADTAIL and QuickPIC, for the purpose of comparison modified so as to model the 1-kick approximation instead of the continuous interaction, using the LHC parameters at injection is shown in Fig. 4.

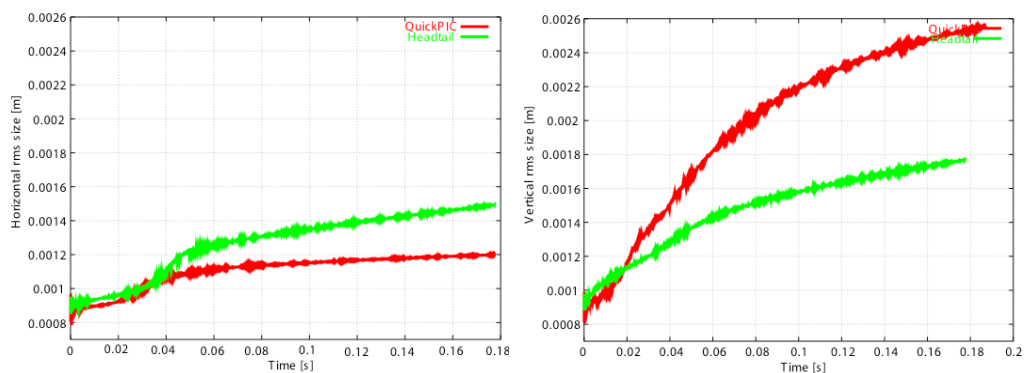


**Fig. 4.** Horizontal (left) and vertical (right) emittance growth in LHC. The green lines are simulations done with HEADTAIL, the red lines correspond to QuickPIC simulations (with the 1-kick approximation). All simulations are carried out with conducting boundary conditions on a rectangular beam pipe.

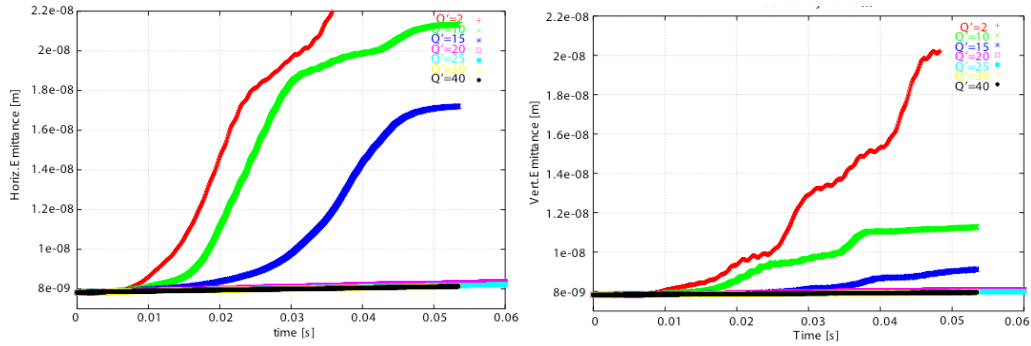


**Fig. 5.** Horizontal (left) and vertical (right) emittance growth in LHC for different chromaticity values and  $\rho_e = 6 \times 10^{11} \text{ m}^{-3}$ , simulated by HEADTAIL.

QuickPIC predicts a larger emittance growth than HEADTAIL in the vertical plane, whereas in the horizontal plane the small discrepancy might be improved by increasing the number of particles per slice when taking a larger bunch extension in HEADTAIL (the bunch extends normally from  $-2 \sigma_z$  to  $2 \sigma_z$  in HEADTAIL, and it has been extended between  $-5 \sigma_z$  to  $5 \sigma_z$  like in QuickPIC for a better comparison of the results). The other numerical parameters are exactly adjusted to the same values for both simulations. The reasons of the discrepancy in the evolution are yet to be explained, but the difference seems not to be critical.

Finally, the beneficial effect of chromaticity can be seen in LHC too, as appears from Fig. 5. Chromaticities higher than 20 (in  $Q'$  units) seem to be enough to eliminate the coherent effect of the electron cloud on a circulating bunch, if the integrated electron cloud density along the ring does not exceed  $6 \times 10^{11} \text{ m}^{-3}$ .

### 2.3.4 Peculiarities of the electron cloud wake fields

Wake fields can be evaluated using the particle tracking codes described in the previous section. In the simulation, first one bunch slice gets displaced (for instance, vertically by an amount  $\Delta y$ , given in units of  $\sigma_y$ ), and then the response of the electron cloud is evaluated in terms of electric field on axis ( $x=y=0$ ) at successive times. Normalizing this field by the amount of displacement and by the number of particles in the displaced slice yields the dipole wake function defined on axis (in  $\Omega \text{ s}^{-1} \text{ m}^{-1}$ , after multiplication by the factor  $m\gamma c^2 e^{-2}$ ). As the field on axis is not directly related to the force exerted by the cloud on the slices that follow the offset one, it can be better to evaluate an averaged dipole wake function from the net force caused by a displaced slice on later portions of the beam. In this case, instead of the field on axis, the overall force exerted by the distorted cloud on all the particles contained in a slice is calculated and then divided by the total charge in that slice in order to obtain an effective electric field. Shapes in the two cases appear to be quite different, as shown in Fig. 7.

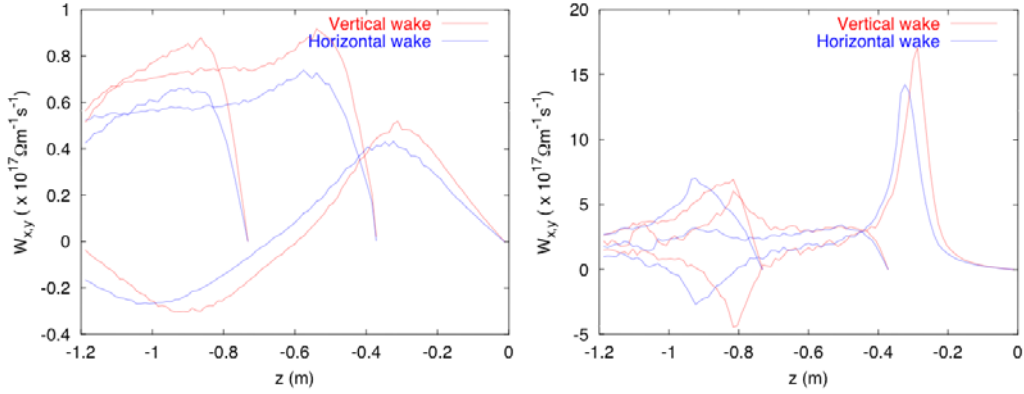


**Fig. 6.** Horizontal and vertical averaged dipole wake functions (left) or wake functions on axis (right) for an SPS bunch. They have been evaluated displacing three different bunch slices at  $t=0$ ,  $3/10 \Delta t_b$ ,  $3/5 \Delta t_b$ .

Note that the two definitions of the wake would lead to the same result for a conventional dipole wake field. Wake functions on axis reach much larger values and exhibit a spiky structure that is smoothed out to a more regular profile when the integration over the bunch slice is carried out. From the plots above we can also deduce another important feature that distinguishes electron cloud wake fields from conventional wake fields. The shape and amplitude of the wake function depend on where the displaced slice is located along the bunch that generates the wake. In particular, it is clear that if the offset slice is placed at  $3/10 \Delta t_b$  or at  $3/5 \Delta t_b$  instead of being at the very head of the bunch, the wake is about a factor two stronger and does not have any oscillatory behaviour. Besides, amplitude and frequency of the wake will also depend on the bunch charge as well as on its transverse sizes. The wake functions shown above have been calculated for an almost round beam in an SPS field-free region and for a longitudinally uniform bunch distribution. Inside a dipole region, the horizontal wake tends to disappear, whereas the vertical one remains significant. In a solenoid region, the coupling between the two planes induced by the magnetic  $z$ -field renders the pinching effect much weaker, which is very likely to cure the electron cloud instability.

The longitudinal wake field generated by an electron cloud has also been evaluated both with the 3D QuickPIC code [25] and with HEADTAIL (by assuming that electron transverse distributions at subsequent times correspond to those at subsequent longitudinal positions) [16]. The longitudinal field is found to be very small, and, therefore, it can only slightly affect the bunch shape and is not likely to be responsible for any microwave instability.

### 2.3.5 Miscellaneous

As highlighted in the Introduction, machines like RHIC and the SIS18 at GSI operate at the limit of the short bunch regime. Electrons perform more than one oscillation at each bunch passage, but the number of oscillations does not exceed 10. Beside that, the electron cloud build up (when it occurs) seems in both cases to be dominated by the multi-bunch effect rather than by the trailing edge mechanism, and the variation of the number of electrons might be negligible with respect to the accumulated density inside the beam pipe. In spite of the low  $Z/A$ , the heavy  $U^{73+}$  ions at the SIS18 can be destabilized by electron clouds of medium density (probably due to the low ion energy, see Table in the Introduction) [5]. It has been demonstrated in tracking

simulation that electron densities of  $3 \times 10^{11} \text{ m}^{-3}$  are sufficient to drive a vertical dipole mode instability, which could lead to beam loss within few tenths of ms.

In RHIC, the gold ions beams appear to be rather insensitive against single bunch instability. Figure 7 shows that the bunches before rebucketing (10 ns long) remain stable for integrated electron cloud densities up to  $10^{12} \text{ m}^{-3}$  along the ring. The incoherent emittance growth rates are in fact below the PIC noise threshold even for the higher densities, and it has been demonstrated that this modest linear increase completely disappears by simply distributing the electron cloud kick over more interaction points along the ring (see discussion below on the monopole instability).

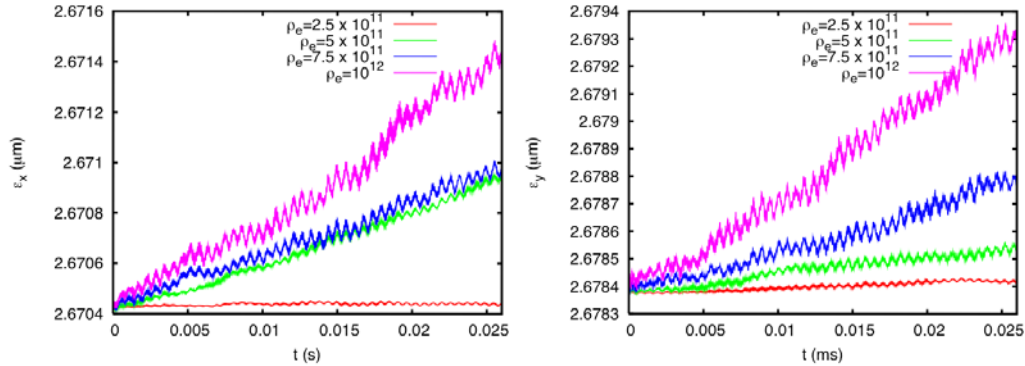


**Fig. 7.** Horizontal (left) and vertical (right) emittance growth for a long  $\text{Au}^{79+}$  bunch in RHIC and different integrated electron cloud densities.

It is interesting to observe that compressed bunches in RHIC (5 ns long) also have a very high threshold for the instability. This is probably because the bunch length gets halved and the synchrotron tune becomes much higher (the synchrotron period,  $n_s = I/Q_s$ , decreases by one order of magnitude with rebucketing), even if the RHIC bunches after rebucketing completely fill their holding buckets, which causes the head and tail particles of the bunch to have an extremely slow synchrotron motion and thus could give rise to a BBU type instability. We have estimated the threshold for instability of short bunches to be above a few  $10^{12} \text{ m}^{-3}$ .

The table below shows five sets of some selected RHIC and LHC parameters, which can be used to estimate the sensitivity of these rings in different operations to electron-cloud induced single bunch instability (at injection and at top energy). The number in the last row,  $L_b/\sigma_z$ , represents the filling factor of the bucket (from 1 to  $\sim 10$ , it means that the bunch tails significantly fill also the nonlinear region of the bucket; above 10, the full bunch essentially occupies only the linear region of the bucket)

**Table.** Selected RHIC and LHC parameters

	RHIC (inj)	RHIC (top) before rebuck.	RHIC (top) after rebuck.	LHC (inj)	LHC (top)
$C$ (m)	3833			26659	
$n^2$	4	7.2	3.6	5.8	54
$Z/(A\gamma)$	0.038	0.0037		0.0021	0.00013
$n_s=1/Q_s$	724	2790	290	167	472
$\sigma_z$ (ns)	5	2	1	0.434	0.257
$\delta p/p_0$ ( $10^{-4}$ )	4.7	1.8	8.9	4.7	1.1
$L_b/\sigma_z$	7.1	17.7	5.0	5.7	9.7

There is no significant difference between LHC at injection and RHIC at top energy after rebucketing. But being the ring circumference by one order of magnitude larger in the LHC, it is reasonable to expect that the threshold for instability in RHIC (in terms of average electron cloud density around the ring) will be about 10 times higher than in LHC at injection. LHC at top energy operates at the limit of the short bunch regime, but we know that the electron cloud build up is in this case essentially a multi-bunch process. The numbers given in the table above seem to suggest that LHC at top energy should be somewhat less stable than RHIC at top energy after rebucketing, because while the larger stiffness is balanced by the larger ring extension, synchrotron tune and momentum spread are both smaller. RHIC at injection energy is expected to be the least stable because of the high  $Z/(A\gamma)$ , of the relatively small synchrotron tune and small filling number. A comparison of (normalized) emittance growth for a cloud density of  $10^{12} \text{ m}^{-3}$  in RHIC at injection, top energy before rebucketing and top energy after rebucketing is shown in Fig. 8.

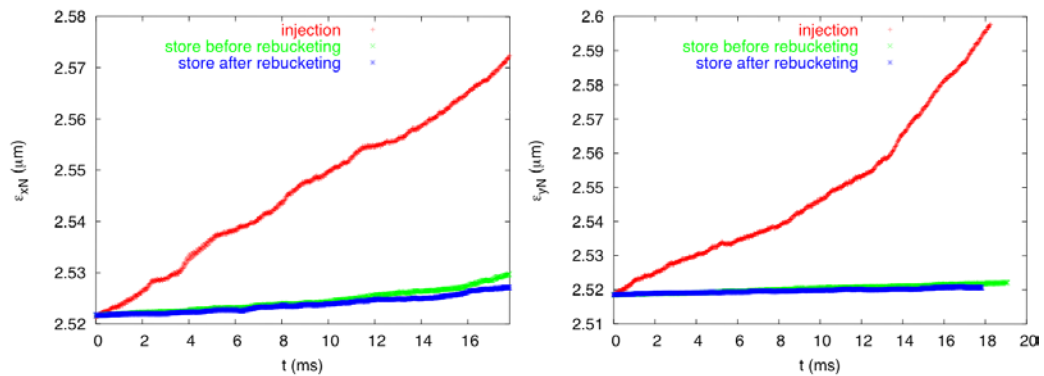


**Fig. 8.** Horizontal (left) and vertical (right) normalized emittance growth for a  $\text{Au}^{79+}$  bunch in RHIC at injection (red), at top energy before rebucketing (green) and at top energy after rebucketing (blue). The electron cloud density is  $10^{12} \text{ m}^{-3}$

Actually the assumption that we can neglect the variation of the electron-cloud density for the quasi-short bunches in the SIS18 or in RHIC probably needs closer attention and further study to be either completely validated or replaced by a more refined model. If we take a look at Fig. 9a (left), showing the electron cloud build up in a RHIC Interaction Region (IR) for instance, it is clear that the electron cloud at saturation still oscillates between bunches by 42% of its

average saturated value. How much of the steep density increase occurs while the bunch is still going by, can be seen in Fig. 9b (right).

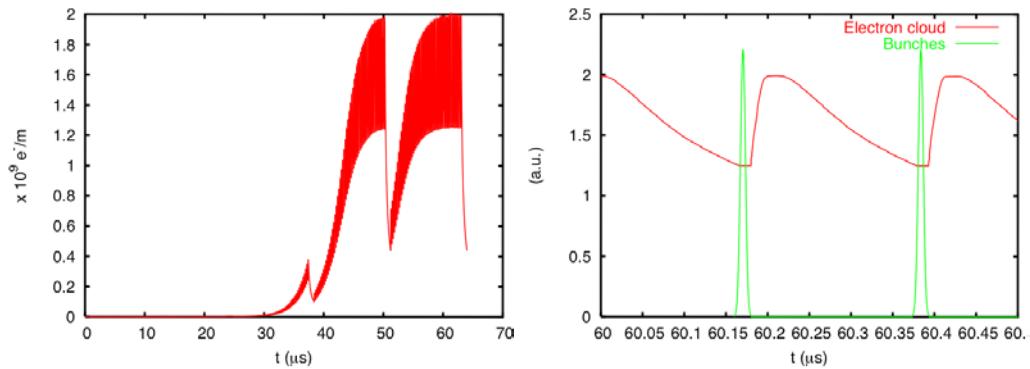


**Fig. 9.** Electron cloud build up in an IR in RHIC (left) and with bunch structure in the saturation regime (right)

Even if it does not seem to be a dominant effect, the small variation along the bunch, as well as the detailed position and momentum distribution of the electrons prior to a bunch arrival, could probably be considered and included in the study of the single bunch instability. With this complication the wake field approach becomes even more difficult to handle and apply, because any contributing trailing edge multiplication introduces a strong dependence of the electron-cloud wake field on the bunch shape. This is a very important point to be taken into account because, while for quasi-short bunches particle tracking is still viable both for electrons and bunch particles (a bunch slicing by about 200 is still acceptable without exceeding the memory requirements of the code), for longer bunches (like in ISIS or PSR) a wake field approach would be preferable, in which the dipole wake field is calculated once at the beginning of the simulation and then stored in a matrix and used turn by turn to calculate the bunch evolution. The 3D QuickPIC, which runs on parallel processors and can track huge numbers of bunch particles, unfortunately does not (yet) contain the possibility of electrons hitting the walls and generating secondaries, which makes its present version unsuitable for the kind of applications that we are discussing in this section.

The last item that we would like to address in this paper is the transverse ‘monopole’ instability driven by the electron cloud [26]. A small long-term emittance growth like that observed in RHIC simulations for long bunches and cloud density above  $2.5 \times 10^{11} \text{ m}^{-3}$  or in some LHC simulations [26], could be important for rings where the storage time of the beam amounts to several hours. It is therefore essential to distinguish whether this growth is purely numerical and introduced by the algorithm noise or it has a physical meaning. Earlier simulations seem to have ruled out the possibility of a slowly developing pure monopole instability, because the simulated emittance growth disappears, if either the beam and electron distributions are fully symmetrized or if any incurring dipole moment is suppressed slice by slice at each interaction point. The incoherent growth often observed in simulations with nonzero dipole motion strongly depends on the number of interaction points and on the inter-IP phase advances. It is presently not clear whether the growth converges to zero or against a finite nonzero value as the number of IP’s increases. In the limiting case of a bunch continuously interacting with an electron cloud (QuickPIC), the beam size blow up for SPS reduces to a value compatible with zero for a cloud density of  $10^{12} \text{ m}^{-3}$ , whereas the 1-kick codes had foreseen a linear blow up for the same density.

Alternatively, in other cases the incoherent emittance growth is replaced by a coherent growth distributed along the bunch for an increasing number of IP's. In these cases, we believe that the coherent effect had probably been overcome by the quick emittance blow up due to the strong electron cloud kick for low number of IP's (see LHC in the section above, or Ohmi's notes published in [21]) and shows up again when the artificial incoherent mechanism is cured by an appropriately high number of IP's.

In reality the existence of a long-term emittance growth or monopole instability of the space charge type cannot be completely excluded on the basis of the previous considerations. All simulation codes used for the electron cloud instability do not account in fact for the bunch envelope modulation along the ring due to the lattice beta functions. Similarly to what happens because of space charge in very intense and low energy beams, this modulation can be responsible for a long-term incoherent emittance growth [27]. To quantify this phenomenon is presently one of the main challenges in the progress of the electron-cloud instability studies.

### 2.3.6 Acknowledgements

The authors would like to thank F. Ruggiero, K. Ohmi, W. Fischer, M. Blaskiewicz, A. Ghalam, T. Katsouleas, D. Schulte, S.Y. Zhang, R. Tomàs, R. Calaga, O. Boine-Frankenheim, I. Hofmann, G. Bellodi for helpful comments and discussion.

### 2.3.7 References

1. T. Raubenheimer and F. Zimmermann, *Phys. Rev. E* **52**, 5487 (1995)
2. F. Zimmermann, Report No. CERN-SL-Note-2000-004 AP, 2000.
3. R. Cimino, I. Collins, M. Furman, M. Pivi, F. Ruggiero, G. Rumolo, and F. Zimmermann, "Can low energy electrons affect high energy physics accelerators ?", submitted to *Phys. Rev. Letters*.
4. J. Wei and R. Macek, in *Proceedings of E-CLOUD'02, CERN, Geneva, 2002*, edited by G. Rumolo and F. Zimmermann (CERN Yellow Report No. CERN-2002-001, 2002), p. 29.
5. G. Rumolo and O. Boine-Frankenheim, GSI-Acc-Note-2003-10-001 (October 2003).
6. K. Oide et al., in *Proceedings of International Workshop on Performance Improvement of Electron-Positron Collider Particle Factories (KEKB Report No. 99-24, 2000)*.
7. K. Ohmi and F. Zimmermann, *Phys. Rev. Letters* **85**, 3821 (2000).
8. H. Fukuma, in *Proceedings of E-CLOUD'02, CERN, Geneva, 2002* p. 1
9. G. Arduini et al., in *Proceedings of the Workshop LEP-SPS Performance Chamonix X (2000)* pp. 119-122
10. G. Arduini, K. Cornelis, W. Höfle, G. Rumolo and F. Zimmermann, in *Proceedings of PAC 2003, 12-16 May, Portland, USA (2003)*.
11. R. Cappi, M. Giovannozzi, E. Métral, G. Métral, and F. Zimmermann, in *Proceedings of PAC 2001, Chicago, USA*, edited by P. Lucas and S. Webber (2001) p. 685
12. R. Cappi, M. Giovannozzi, E. Métral, G. Métral, G. Rumolo and F. Zimmermann, *PRST-AB* **5**, 094401 (2002).
13. M. Giovannozzi, E. Métral, G. Métral, G. Rumolo and F. Zimmermann, *PRST-AB* **6**, 010101 (2003)
14. G. Rumolo and F. Zimmermann, CERN-SL-2001-0067-AP (2001).
15. G. Rumolo, F. Ruggiero, and F. Zimmermann, *PRST-AB* **4**, 012801 (2001).

16. G. Rumolo and F. Zimmermann, PRST-AB **5**, 121002 (2002)
17. G. Rumolo, A. Ghalam, T. Katsouleas, C.K. Huang, V.K. Decyk, C. Ren, W.B. Mori, F. Zimmermann, and F. Ruggiero, PRST-AB **6**, 081002 (2003)
18. K. Ohmi, E. Perevedentsev, and F. Zimmermann, Phys. Rev. E **65**, 016502 (2001)
19. Y. Funakoshi, Proc. Factories 2001 (2001)
20. A. W. Chao, "Physics of collective beam instabilities in high energy accelerators", John Wiley & Sons (1993)
21. Code comparison page: <http://wwwslap.cern.ch/collective/ecloud02/ecsims/index.html>
22. K. Ohmi, T. Toyama, and C. Ohmori, in Proceedings of E-CLOUD'02, CERN, Geneva, 2002 p. 163
23. Y. Cai, in Proceedings of E-CLOUD'02, CERN, Geneva, 2002 p. 141
24. H. Burkhardt, G. Rumolo, and F. Zimmermann, CERN-SL-Note-2001-043-MD (2001)
25. T. Katsouleas et al., in Proceedings of E-CLOUD'02, CERN, Geneva, 2002 p. 239
26. E. Benedetto et al., in Proceedings of PAC 2003, 12-16 May, Portland, USA (2003)
27. K. Ohmi, private communication.

## 2.4 Measuring the Properties of the Electron Cloud at the Advanced Photon Source

Katherine C. Harkay<sup>‡</sup> and Richard A. Rosenberg  
[Advanced Photon Source](#), Argonne National Laboratory, Argonne, IL 60439, USA

Laura J. Loiacono  
 Loyola University, Chicago, IL 60626, USA  
<sup>‡</sup>Corresponding author; mail to: [harkay@aps.anl.gov](mailto:harkay@aps.anl.gov)

### Abstract

Dedicated electron cloud diagnostics developed at the Advanced Photon Source (APS) enabled for the first time detailed characterization of the electron cloud (EC) properties in a high-intensity positron and electron storage ring. From *in situ* measurements of the electron flux and energy distribution at the vacuum chamber wall, electron cloud production mechanisms and details of the beam-cloud interaction could be inferred. Strong amplification of the cloud was observed under certain machine conditions, sometimes referred to as beam-induced multipacting (BIM). Significant longitudinal variation of the cloud was also observed, due primarily to geometrical details of the vacuum chamber. These experimental data have contributed to a better understanding of the physics of the EC and its interaction with the beam, in particular, details of EC amplification and the sensitivity of key parameters relating to EC generation. The former (amplification) involves modeling studies of the beam-cloud dynamics. The latter (parameter sensitivity) involves benchmarks of the simulation code POSINST using APS data. More recently, there are plans to install a superconducting undulator (SCU) in the APS storage ring. Preliminary calculations show that EC-induced heating under specific machine conditions may impact the SCU design. Highlights of experimental data for both positron and electron beams are given, as well as modeling results.

### 2.4.1 Experimental results

The study of electron clouds in high intensity storage rings remains an important area of R&D 30 years after the first observations were made. The list of EC-induced effects grows as new observations are reported. Data from dedicated electron cloud diagnostics, used at the APS and elsewhere in combination with standard beam diagnostics, have contributed to a better understanding of the physics of the electron cloud and its interaction with the beam. This paper highlights what we have learned from experiments carried out at the APS with both positron and electron beams, and what needs to be better understood.

In order to directly measure the properties of the electron cloud, a special vacuum chamber was installed in 1997 in a field-free region of the APS storage ring. The chamber was equipped with several compact, planar electron energy retarding field analyzers (RFAs) (Figs. 1a, 1b). The APS was operated from 1996-98 with positron beam, after which it was converted to electron beam operation; this allowed EC study with both beams. The chamber over most of the ring is made of Al, which has a relatively high secondary electron yield coefficient  $\delta$  [1] due to oxidation of the surface. Details of the RFA are described elsewhere [2,3,4], and dedicated electron detectors based on the APS RFA are now widely implemented (e.g., [5,6,7]). Briefly, the RFA is an integrating device that collects electrons colliding with the chamber walls with energies greater than an applied retarding field. The differentiated collector current gives the electron energy spectrum convolved with the detector response. In addition to measuring the distribution of electrons, the RFA signal can be directly correlated with standard diagnostics that indicate any anomalous vacuum pressure rise, collective beam instability, or beam lifetime changes – all of which have been observed at the APS for positron beams and/or electron beams. An important benefit of the RFA is that it is nonperturbative and gives a quantitative measure of the wall flux and spectrum, unlike a biased electrode or BPM. Secondary emission from biased electrodes is a clear disadvantage in using these devices to characterize the EC [4]. However, the RFA has some limits in energy resolution and collector efficiency, and small signal errors due to SEs produced in the device are possible. A device that in principle improves on some of these limits, the Bessel Box Analyzer, was also developed and studied at the APS [3], but will not be discussed here.

The experimental studies at the APS were designed to address two issues: to characterize the EC distribution and to allow better prediction of cloud-induced effects by providing realistic limits on key ingredients in computer models of EC production. Key factors contributing to the EC include chamber-surface characteristics such as roughness, photoelectron and secondary electron yield coefficients, and secondary electron (SE) distribution; machine parameters such as bunch current and spacing, and the presence of an external electric or magnetic field; and vacuum chamber geometry such as cross-sectional dimensions and the presence of an antechamber or synchrotron radiation absorbers. The APS experimental data were compared with calculations from the code `POSINST` [8] to model the EC generation. The version (8) of `POSINST` we used models all the properties listed above, with the exception of surface roughness and the absorber.

The major results of the APS studies [4,9] can be summarized as follows. The electron cloud was very sensitive to the bunch intensity and spacing. A dramatic amplification was observed for positron beams with a 20-ns bunch spacing (7 rf wavelengths,  $\lambda$ ), and for bunch currents above 1.5 mA (5.5 nC) (Fig. 2a). This gain was attributed to beam-induced multipacting (BIM) and was accompanied by an anomalous vacuum pressure rise, measured also in the special chamber. At

the BIM condition for long bunch trains, the EC grows exponentially until a saturation limit, beyond which the EC grows linearly (Fig. 2b). The saturation level and time at which the limit is reached (i.e., position along the train) were observed to depend nonlinearly on the bunch current. In addition, what appears to be a cloud-induced horizontal coupled-bunch instability (CBI) was observed for positrons with about 2 mA (7 nC) per bunch [4]. This instability was observed for conditions in which the EC was in saturation and has not been observed for electron beams at identical operating conditions. Finally, the measured electron cloud signals decrease over time as the chamber surfaces are irradiated, giving evidence of a beam-induced conditioning effect (inset, Fig. 2a). This decrease is consistent with measurements showing the reduction of  $\delta$  under electron or photon bombardment [1,10,11]. The data in the main plot in Fig. 2a were acquired shortly after the new chamber was installed (<1 Amp-hours (Ah) of operation). The inset shows the normalized signal after >60 Ah. The accumulated electron dose ( $2 \times 10^{-4}$  C/mm<sup>2</sup>) was calculated using the measured wall current for the standard machine configuration, which is used the majority of the time. It is interesting to note that EC amplification was never observed until the dedicated EC study: standard user operation with positron beams typically used  $1-\lambda$  or  $54-\lambda$  bunch spacing, well outside the position of the resonant peak. For electron beams, EC amplification was also observed, but centered instead around a 30-ns ( $11-\lambda$ ) bunch spacing (Fig. 3a). The measured amplification of the cloud, however, is more modest with an electron beam (Fig. 3b).

Electron cloud effects do not presently limit the performance of the APS storage ring, now operating with electron beams. To date, the only indication of cloud-induced effects in electron beams was a significant beam lifetime change that occurred with certain bunch patterns. We filled 85 mA in nine bunch trains of four bunches each; the beam lifetime was half as long and the vacuum pressure was a factor of two higher with a  $2-\lambda$  gap between bunch trains, compared to a gap of  $12 \lambda$ . The RFA signals were a factor of three to five higher with the smaller gap. These observations are consistent with electron-stimulated gas desorption. When these bunch patterns were repeated after additional surface conditioning, the vacuum pressure rise and lifetime reduction were negligible. It should be noted that EC effects can in principle be important for both positively and negatively charged beams, occurring albeit at a higher threshold for electron beams. Preliminary calculations, discussed later, indicate that EC-induced heating may be an important factor in the design of a superconducting undulator (SCU) planned for future installation in the APS.

#### 2.4.2 Beam-cloud interaction and EC amplification

For a fixed beam energy, the average total number of primary electrons is expected to be linear with beam current and independent of the temporal distribution of the beam. In the APS, this contribution consists of photoelectrons and SEs produced in the collision of synchrotron radiation photons with the walls [12] (ionization electrons are not considered important). In the absence of multipacting (described below) and in a storage ring like the APS (with antechambers), the local electron density will depend primarily on the distance from the main electron source (end absorber, EA; see Fig. 1a), and in a minor way on electrons produced by the bending magnet radiation and by fluorescence x-rays emitted from EA (in the upstream direction to the beam). The influence of EA on the azimuthal variation in the EC distribution can be seen in Fig. 2b: with one bunch (no multipacting) the RFA signal near EA is an order of magnitude greater than about one meter upstream. In storage rings without antechambers, primary

photoelectrons can dominate the cloud (e.g., KEK Photon Factory, Japan [13] and Beijing Electron Positron Collider (BEPC) (Institute of High Energy Physics (IHEP), P.R. China) [5,14]).

In contrast, the total number and energy distribution of SEs, produced in collisions with the walls by electrons accelerated by the beam will be highly dependent on the bunch charge and spacing. SEs emitted from the chamber surface have an intrinsic energy distribution (mean energy of a few eV); this governs the electron dynamics between bunch passages. Acceleration by the beam can increase the average collision energy of the electrons during bunch passages. Because  $\delta$  is energy-dependent, the beam-cloud interaction can strongly influence the electron cloud gain. Amplification can be significant if the collision energies are such that  $\delta > 1$ . The azimuthal variation in the EC distribution, this time for multiple bunches spaced at  $7\lambda$ , can be seen in Fig. 2b: for RFAs 65 cm apart, the gain in the cloud buildup differs by almost two orders of magnitude, and the wall flux at saturation differs by a factor of three.

If secondary electron emission processes dominate, the electron cloud can build up significantly if a BIM resonance condition is satisfied. In its classical form [15], cold electrons at the wall are accelerated by the beam and traverse the chamber in precisely the time between bunch passages. It was noted by M. Furman [16] that the range of bunch spacings over which amplification was observed for APS positrons ( $4\lambda$  to  $16\lambda$ ) is consistent with the classical BIM condition for trajectories ranging between the minor and major chamber axes. However, the cold electron assumption is clearly incomplete, since the sharp peak at  $7\lambda$ , seen in Fig. 2a, cannot be readily explained.

M. Furman and S. Heifets proposed a general BIM resonance that includes the intrinsic SE energy [17]. SEs created between bunch passages drift near the chamber center and receive a large energy gain during the bunch passage. At resonance, the sum of the two drift times, before and after the bunch passage, equals the bunch spacing [4]. J. Galayda made a similar proposal: for a given bunch spacing, the multipacting resonance “selects” electrons at a certain radius. If  $\delta > 1$  for this resonant energy, amplification is observed [18]. At APS the energy gain for electrons at the wall is typically a few tens of eV, whereas electrons that drift to within about 1 cm of the beam gain a few hundred eV. The peak  $\delta$  ( $\delta_{\max}=2.8$ ) was measured to occur at 330 eV ( $E_{\max}$ ) (Fig. 4) [1], so general BIM could yield higher amplification than the classical case. Interestingly, there is some indication of a range of “resonant energies” in the differentiated RFA data for  $2\lambda$  ( $> 110$  eV) and  $4\lambda$  (40-100 eV), but not for  $7\lambda$  (Fig. 5).

To test the general BIM theory, a simple computer model was developed to study the dependence of multipacting resonances on the emitted SE energy [19]. The interaction between a single electron and a train of beam bunches was modeled as a series of drifts and instantaneous kicks. Several simplifying assumptions were made. Space charge is not applicable for bunch trains of less than 20 bunches (verified in simulation, Sect. 2.4.3). The electron is constrained to move on a 1D trajectory that passes through the center of the bunch in a plane perpendicular to the beam’s path. For electrons that do not drift too close to the beam (initially assumed true and sufficient to model the dynamics), the “impulse kick” approximation is valid; i.e., the distance traveled by the electron is short compared to the bunch length. With each collision with the wall, SEs are assumed to be produced with a constant energy, chosen by the user, and with gain  $\delta$  from Fig. 4. For improved accuracy, the chamber shape was modeled according to design drawings. The beam has a bi-Gaussian transverse distribution.

Indeed, a rich set of general resonance conditions were found for SE energies ranging from approximately 1.2 to 3.8 eV (50% of the measured distribution) and for bunch spacings ranging from  $4\lambda$  to  $9\lambda$  (the bunch current was fixed at 2 mA) [19]. Typically, the resonances were

established before 20 bunches (within the validity of no space charge, see Sect. 2.4.3). Notably,  $7\lambda$  has the largest number of resonances corresponding to  $\delta \geq 2$ , followed by  $6\lambda$ . This is qualitatively consistent with the experimental data. However, the results do not seem to agree quantitatively with the degree of amplification in the sharp peak at  $7\lambda$ .

Two further refinements were made in the model: on each collision, the SE energy was randomly generated using the measured SE distribution, rather than assigning all SEs a fixed energy, and the beam-cloud interaction was integrated over a finite bunch length (typically  $\sim 12$  mm rms in APS). If one tracks the path of an electron whose starting position is within  $10\times$  the beam size (vertically), it oscillates in the beam potential. Figure 6 shows comparisons of an electron-positron beam interaction for 2-mA and 10-mA bunches. Preliminary calculations were performed for the  $7\lambda$  bunch spacing. Interestingly, there is no longer any sign of a true resonance. Instead, the dynamics appear to be a random process, yet a preliminary investigation shows that significant amplification is still possible [20]. Quite independently, L. Wang (BNL) and his colleagues have come to the same conclusion (although amplification was not discussed) and have suggested a term “random multipacting” [21]. We prefer to call this process “beam-induced amplification.”

### 2.4.3 Simulations

The experimental results were compared with the code `POSINST` developed by M. Furman and M. Pivi at LBNL [8]. `POSINST` calculations at the center of a long field-free section were compared to RFA 6. The code output was scaled by 0.5 to account for the transmission attenuation in the experiment (Fig. 1b), and  $\delta_{\max}=3.1$  was assumed for an unconditioned Al surface. Figure 2a shows the comparison between the modeled and measured electron wall current for ten positron bunches as a function of bunch spacing. The model reproduced the broad peak centered at a  $7\lambda$  bunch spacing; however, the sharp, resonant peak at  $7\lambda$  is not reproduced. The position of the peak in the modeled result was very sensitive to the secondary-electron energy spectrum, the mean energy in particular [16,22]. In the code, the distribution assumes the form  $E \exp(-E/E_s)$ , where  $E_s = 1$  eV gave good agreement. The width of the broad peak was quite sensitive to assumptions about the rediffused electron component (inelastic scattering);  $E_r = 35$  eV gave the best fit, consistent with stainless steel [8]. Notably, the average wall-collision energy was also reproduced: 111 eV calculated in `POSINST` averaged over the chamber surface vs. 88 eV measured at the RFA location.

The measured electron cloud buildup over a bunch train was reproduced reasonably well by `POSINST` when space charge was included (Fig. 2b). It should be noted that space charge was found not important for bunch trains less than about 20 bunches in length [22]. Curiously, while the buildup rate was sensitive to  $\delta_{\max}$ , the saturation level seemed relatively insensitive, differing by only a factor of two for  $\delta_{\max}$  ranging from 2.2 to 3.1. Recall that the variation from one RFA location to another was greater, about a factor of three.

Using the same input parameters, the modeling was repeated for electron beams. To account for the additional surface conditioning,  $\delta_{\max}=2.2$  was used (EC scales by about a factor of two compared to  $\delta_{\max}=3.1$  [22]). The broad measured peak at  $11\lambda$  was nearly reproduced (`POSINST` peak is  $9\text{--}10\lambda$ ), but the overall width does not agree nearly as well for the electron beam case (Fig. 3a). Two RFA locations are shown. In addition, the average collision energy is overestimated by about an order of magnitude. This was a bit surprising, given the good

agreement with the positron data. We can speculate on the possible reasons for the disagreement: a careful review of all parameters, including photon reflectivity,  $\delta(0)$ , and  $E_r$  might be undertaken, as well as a parameter sensitivity analysis for the electron beam case. Perhaps  $E_r$  changes with surface conditioning.

#### 2.4.4 Superconducting undulator (SCU)

The design of the cryogenic systems for superconducting magnets requires reliable estimates of all sources of heating. The electron cloud can contribute to this heating through bombardment of the chamber surfaces, a widely-studied issue for the Large Hadron Collider (LHC) project. At the APS, there is interest in installing a superconducting undulator [23]. Simulations were undertaken with `POSINST` to calculate the cloud-induced heat load. In the smaller-aperture undulator vacuum chambers, the synchrotron radiation fan can intercept the upper and lower chamber surfaces (full height 5-8 mm), so the photoelectron contribution is more significant (note the antechamber channel height is 10 mm (Fig. 1b)). For an 8-mm undulator chamber, calculations for 1- $\lambda$  bunch spacing give the highest wall current, and 5 mA/bunch gives a power deposition on the walls of 1 W/m. However, this may be overestimated, given the discrepancies in the average collision energies for electron beams. Firm conclusions are not yet possible, but the results have encouraged us to plan installation of RFAs on a small-aperture chamber in the ring to measure the EC-driven wall current and, possibly, the heat load. Also, U. Iriso's work [24] on EC maps developed at RHIC may help explain the strong beam lifetime dependence on electron bunch train spacing at APS.

#### 2.4.5 Summary

Special, dedicated electron diagnostics known as RFAs installed in the APS storage ring have enabled detailed characterization of the electron cloud under various machine and surface conditions. Dramatic amplification of the cloud was observed for certain temporal bunch distributions, especially for positron beams. The beam-cloud interaction giving rise to amplification appears to be more complex than the simple resonant process given by the classical beam-induced multipacting (BIM) formula. A simple model shows that a seemingly random interaction can lead to "beam-induced amplification," a modification of BIM. The secondary electron (SE) energy spectrum plays a critical role in the amplification process. Benchmarks using the code `POSINST` show good agreement with the positron data if  $\delta$ , the SE energy spectrum, and the rediffused electron component are taken into account. Discrepancies with electron beam data, perhaps due to subtle surface conditioning effects, need to be better understood. The EC-driven heat load on a SCU at APS is under investigation.

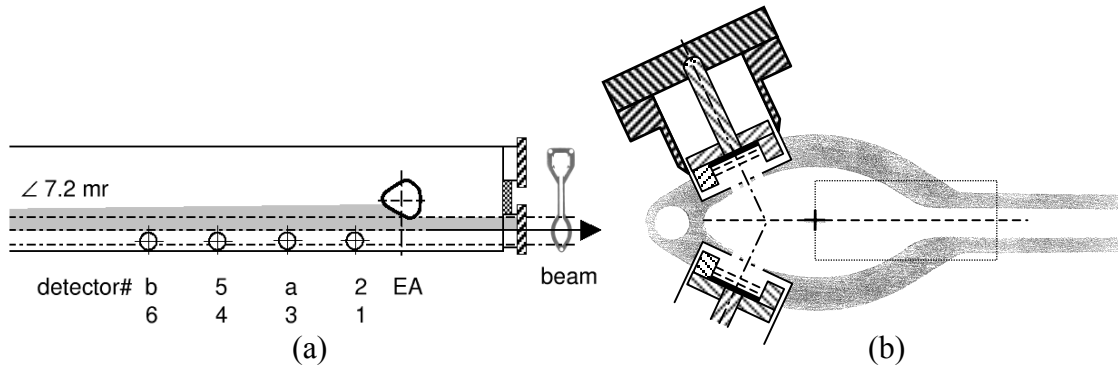


**Fig 1.** (a) RFA detectors (1-6) and BPMs (a,b) mounted on an APS chamber, top view, also showing the bending magnet synchrotron radiation fan and the absorber EA that intercepts high-energy photons. RFA 6 is 80 cm upstream of EA. (b) Standard vacuum chamber cross-section showing mounted RFA detectors. The RFA grid transmission is 0.8, while the transmission through the vacuum penetration is 0.6, giving a total of 0.5. The rectangle represents the limits of the radiation fan at RFA 6 for photon energies above the photoelectron work function.

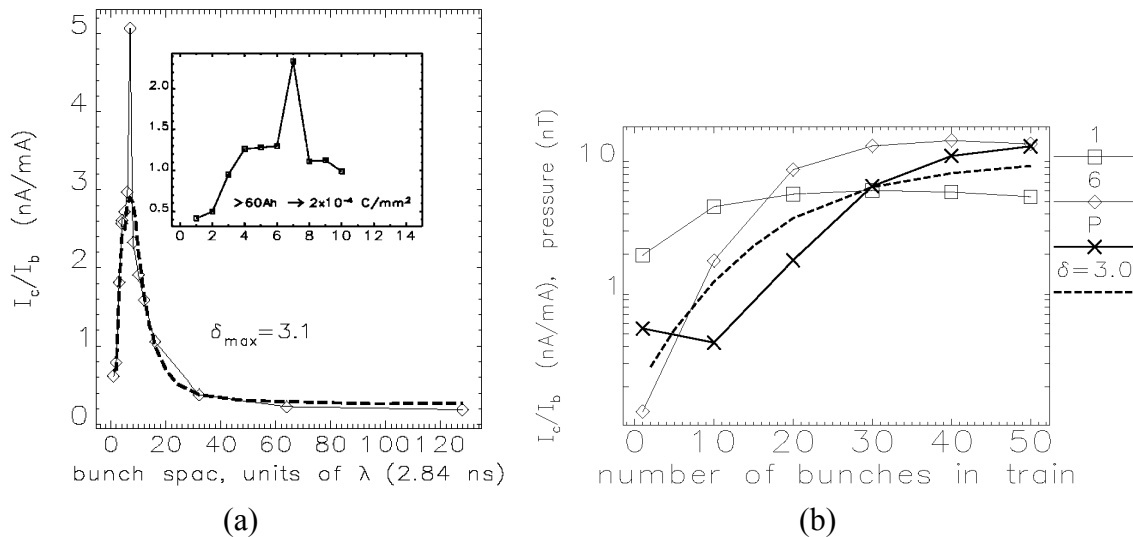


**Fig 2.** Positron beam: (a) Measured (RFA 6, diamonds) and simulated (dashed line,  $\delta_{\max}=3.1$ ) electron wall current ( $I_c$ ) as a function of bunch spacing, normalized to the total beam current ( $I_b$ ) (ten bunches; 2 mA/bunch). The inset shows a conditioning effect of more than a factor of two reduction after 60 Ah of beam operation. (b) Measured (RFA 1,6) and simulated (dashed line,  $\delta_{\max}=3.0$ ) electron wall current as a function of bunch train length, comparing RFAs 65 cm apart. Anomalous pressure rise P is also shown.

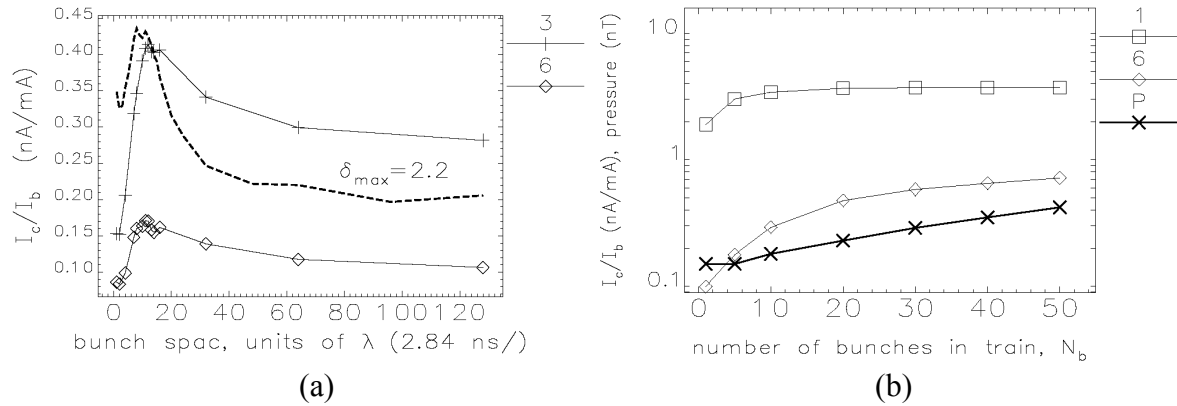


**Fig 3.** Electron beam: (a) Measured (RFA 3,6) and simulated (dashed line) wall current vs. bunch spacing. There is additional conditioning of 100 Ah for these data compared to Fig. 2a, main plot. (b) Measured wall current as a function of bunch train length. The signal near EA (RFA 1) is always higher than RFA 6. No anomalous pressure rise is observed.

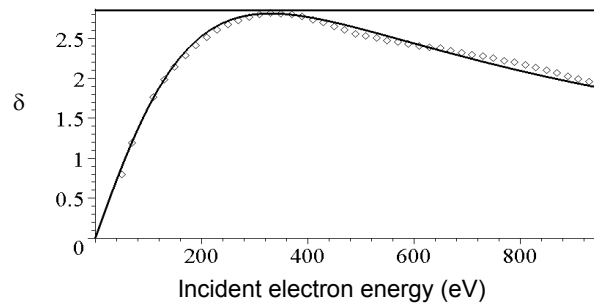


**Fig 4.** Measured  $\delta$  for Al APS chambers, fitted to empirical formula in Ref. [8].

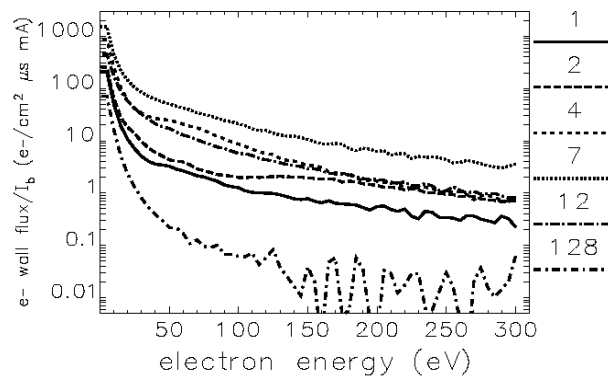


**Fig 5.** Energy distributions from differentiated RFA signals as a function of bunch spacing (units of  $\lambda$ ) (10 bunches, 2 mA/bunch). Low-energy part is well fit by a Lorentzian with  $\langle E \rangle$  2.5 eV and width 4 eV. There is a long exponential tail on all but 128  $\lambda$ . Energy bumps are observed for 2  $\lambda$  and 4  $\lambda$ , but not on longest tail for 7  $\lambda$ .

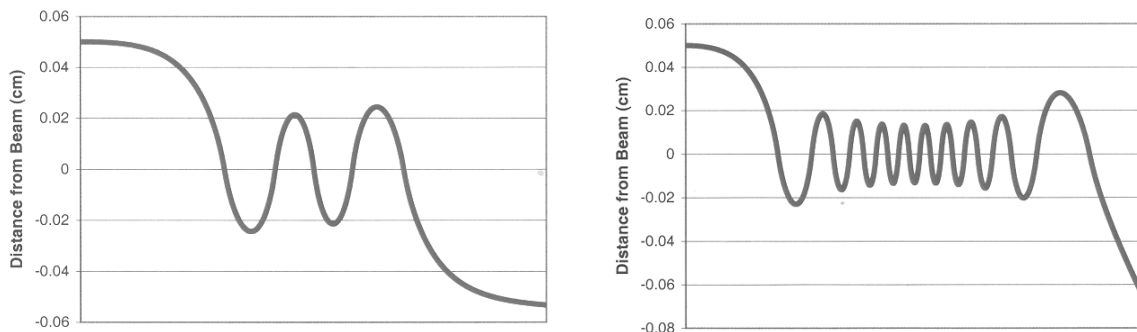


**Fig 6.** For 40-ps-long (12-mm) positron APS bunches, electrons that are within about 500  $\mu\text{m}$  of the beam center oscillate several times in the bunch potential (calculations are for vertical plane). The bunch current is 2 mA on the left, 10 mA on the right. The transverse rms beam size is 350  $\mu\text{m}$  (horizontal) and 50  $\mu\text{m}$  (vertical).

#### 2.4.6 Acknowledgement

The authors thank J. Galayda for initially suggesting and encouraging this study; G. Goepfner, J. Gagliano, J. Warren, and M. McDowell for engineering and technical assistance; and M. Furman, M. Pivi, R. Macek, R. Kustom, and S. Heifets for stimulating discussions. This work was supported by the U.S. Department of Energy, Office of Basic Energy Sciences under Contract No. W-31-109-ENG-38.

#### 2.4.7 References

1. R. A. Rosenberg, M. W. McDowell, Q. Ma, and K. C. Harkay, *J. Vac. Sci. Technol. A* **21**(5), 1625 (Sep/Oct 2003).
2. R. A. Rosenberg and K. C. Harkay, *Nucl. Instrum. Methods Phys. Res., Sec. A* **453**, 507 (2000).
3. R.A. Rosenberg and K.C. Harkay, in *Proc. of 2001 Particle Accelerator Conf.*, Chicago, 2069 (IEEE, Piscataway, NJ, 2001).
4. K. C. Harkay and R. A. Rosenberg, PRST-AB 034402 (2003).
5. K. Harkay, R. Rosenberg, Z.Y. Guo, and Q. Qin, in *Proc. of 2001 Particle Accelerator Conf.*, Chicago, 671 (IEEE, Piscataway, NJ, 2001).
6. R. J. Macek, A. Browman, D. Fitzgerald, R. C. McCrady, F. E. Merrill, M. A. Plum, T. Spickermann, T.-S. Wang, K. C. Harkay, R. Kustom, R. A. Rosenberg, J. E. Griffin, K. Y. Ng, and D. Wildman, in *Proc. of 2001 Particle Accelerator Conf.*, Chicago, 688 (IEEE, Piscataway, NJ, 2001).
7. H. Fukuma, in *Proc. of Mini-Workshop on Electron-Cloud Simulations for Positron and Proton Beams*, CERN Yellow Report No. CERN-2002-001, 1 ( <http://slap.cern.ch/collective/ecloud02/> ) (2002).
8. M. A. Furman and M. T. F. Pivi, PRST-AB **5**, 124404 (2002).
9. K. C. Harkay and R. A. Rosenberg, in *Proc. of 1999 IEEE Particle Accelerator Conf.*, New York, 1641 (IEEE, Piscataway, NJ, 1999).
10. R. Kirby and F. King, *Nucl. Instrum. Methods A* **469** (1), 1 (2001); also SLAC Report No. SLAC-PUB-8212 (Oct. 2000).

11. V. Baglin, I. Collins, B. Henrist, N. Hilleret, and G. Vorlaufer, CERN Report No. CERN-LHC-Project-Report-472 (Aug. 2001).
12. R. Cimino, I. R. Collins, and V. Baglin, PRST-AB **2**, 063201 (1999).
13. M. Izawa, Y. Sato, and T. Toyomasu, Phys. Rev. Lett. **74**, 5044 (1995).
14. Z. Y. Guo, K. Ohmi and H. Fukuma, in *Proc. of 1998 European Particle Accelerator Conf.*, 957 (Institute of Physics, Bristol, UK, 1998); and Z.Y. Guo et al., in *Proc. of 1997 Particle Accelerator Conf.*, Vancouver, 1566 (IEEE, Piscataway, USA, 1998).
15. O. Gröbner, in Proc. 10<sup>th</sup> Int'l. Conf. on High-Energy Accel., Protvino, 277 (1977); also in Proc. of 1997 Particle Accelerator Conf., Vancouver, 3589 (1997).
16. M. A. Furman, M. Pivi, K. C. Harkay, and R. A. Rosenberg, in *Proc. of 2001 Particle Accelerator Conf.*, Chicago, 679 (IEEE, Piscataway, NJ, 2001).
17. M.A. Furman and S. Heifets (private communication, 2000).
18. J. Galayda (private communication, 1998).
19. K. C. Harkay, L. Loiacono, R. A. Rosenberg, in *Proc. of 2003 Particle Accelerator Conf.*, Portland, 3183 (2003).
20. K. C. Harkay and L. J. Loiacono (to be published).
21. L. Wang et al., in *Proc. of ELOUD04*, Napa, CA, (2004) (<http://icfa-ecloud04.web.cern.ch/icfa-ecloud04/>).
22. K.C. Harkay, R.A. Rosenberg, M.A. Furman, M. Pivi, in *Proc. of Mini-Workshop on Electron-Cloud Simulations for Positron and Proton Beams*, CERN Yellow Report No. CERN-2002-001, 69 (2002).
23. R.L. Kustom, in *Proc. of Workshop on Superconducting Undulators and Wigglers*, Grenoble, France (2003) ([http://www.esrf.fr/Accelerators/Conferences/ID\\_Workshop/](http://www.esrf.fr/Accelerators/Conferences/ID_Workshop/)).
24. U. Irizo, in *Proc. of ELOUD04*, Napa, CA (2004) ( <http://icfa-ecloud04.web.cern.ch/icfa-ecloud04/> ).

## 2.5 Measurement of electron cloud effects in KEKB

H. Fukuma

mail to: [hitoshi.fukuma@kek.jp](mailto:hitoshi.fukuma@kek.jp)

[High Energy Accelerator Research Organization \(KEK\)](http://www.kek.jp/)

Tsukuba, Ibaraki 305-0801, Japan

### 2.5.1 Introduction

A large number of electrons called "an electron cloud" can be generated in positively charged beam. Main sources of the electrons in positron storage rings are photoelectrons generated by the synchrotron radiation and secondary electrons. The electrons are attracted by positive charge of the beam and form the electron cloud around the beam. Amplification of the electrons can be occurred by the beam-induced multipacting. The electron cloud causes various effects on the beam. In the KEKB low energy positron ring (LER) the electron cloud effects are observed as a vertical beam blow-up, a tune shift along a bunch train and a coupled bunch instability. Among them most serious has been the vertical beam blow-up which severely limited the luminosity. The beam size as a function of the beam current started to increase at a threshold beam current

and was almost doubled at 300 mA in an early operation period. According to the model by K. Ohmi and F. Zimmermann [1] the blow-up is explained as the head-tail instability of a positron bunch due to the electron cloud. The instability will occur only in multi-bunch operation since the electron cloud is built up by the successive passage of the bunches.

A measure taken to mitigate the electron cloud effects has been the installation of solenoid magnets to sweep out the electrons [2]. The solenoid magnets were installed first in September 2000. The effect of the solenoids on the blow-up was confirmed by the measurements of the vertical beam size and the luminosity [3]. Now about 10000 solenoids cover 78% of the circumference of the ring. As the result a measurement in February 2002 showed no blow-up up to 1600 mA in regular operation condition. Nevertheless the blow-up is an issue of the luminosity upgrade because it is still observed at large average bunch current.

This article describes a measurement of the electron cloud effects at the KEKB LER.

### 2.5.2 Measurement of electron cloud

An electron yield was measured by retarded field analysers (RFA's) [4] which were located at 1.2 m and 8.0 m downstream from a bend. The measurement at the beam current of 500 mA and with the bunch spacing of 8 ns showed the electron current of 7.5  $\mu\text{A}$  and 1.5  $\mu\text{A}$  at the upstream- and downstream-RFA respectively. A simulation gives an electron current of 10  $\mu\text{A}$  and 1  $\mu\text{A}$  at the corresponding RFA's [5]. The measurement is roughly consistent with the simulation. Energy distribution of the electrons was also measured by the RFA [6]. Measured energy distribution is reproduced by a simulation [7]. Two dips in the energy distribution might be explained by a recent simulation work [8].

Gradient of the electric field generated by the electron cloud causes a tune shift along the bunch train. The tune shift can be a good measure of the electron density according to a model [9]. In the KEKB the tune of each bunch is measured by a gated tune meter [10]. The tune of the bunches increased along the train then saturates [11]. The saturated tune shift in vertical plane was consistent with the result of a simulation [12]. Build-up time of the tune shift along the train was about 20 bunches which was also consistent with the build-up time of the electron cloud density calculated by the simulation. Measured vertical tune shift was about 80% larger than horizontal one [13]. The difference cannot be explained by that of horizontal and vertical beta function on which the tune shift depends linearly [14].

The measurement of the decay time gives information of the electron cloud such as quantity of the low energy electrons and a trapping of the electrons inside magnets. A test bunch was injected at the end of a train with variable distance between the last bunch of the train and the test bunch, then the tune shift and the vertical beam size were measured. The decay time was 28 ns from the data of the tune shift [15] and 24 ns from the data of the blow-up [6]. Two measurements are roughly consistent with each other. Another experiment also indicated the decay time of the electron cloud [11]. Two trains which were separated by 64 ns were injected in the ring, then the vertical beam size of each bunch was measured by a gated camera. While the blow-up started at about 7th bunch in the first train, second bunch already blew-up in the second train. The result is supported by a simulation [7]. The former measurement suggests the decay time of about 30 ns. The latter suggests the decay time longer than 64 ns. There may be two components which govern the decay time.

### 2.5.3 Beam size blow-up

If the blow-up is caused by the head-tail instability it should be a single bunch effect and be sensitive to the chromaticity. A test bunch was injected immediately behind a train to prove the single bunch nature of the blow-up [11]. The beam size of the test bunch was measured at several bunch currents of the test bunch. The beam size of the test bunch increased when its bunch current increased, which demonstrates that the blow-up is a single bunch effect. The effect of the vertical chromaticity on the blow-up was measured by the gated camera [11,16]. The measurement showed that the blow-up along the train became weaker when the chromaticity was increased.

The average beam size at various bunch spacing was measured by an interferometer as a function of the beam current [11]. The threshold intensity  $I_{b,th}$  was proportional to the bunch spacing  $s_b$ . After many small permanent magnets called C-Yokes were attached on the chamber wall  $I_{b,th}$  was proportional to square root of  $s_b$ . According to a model of the single bunch instability caused by the electron cloud  $I_{b,th}$  is proportional to  $s_b$  for the regular or strong head-tail instability and is proportional to the square root of  $s_b$  for the beam break-up instability [17]. The reason why the scaling changed after the installation of C-Yokes is not understood yet.

Two-dimensional longitudinal and vertical distribution of the bunches was measured by a streak camera in order to detect the head-tail motion of the bunches [18]. The result showed that the vertical beam size started to increase at the third or fourth bunch when the solenoids were powered off, while such increase was not seen when the solenoids were powered on. A vertical tilt within a bunch was not clearly observed even in the tail part of the train where a large cloud density is expected. Increase of the light intensity may be necessary in order to get a clearer result.

A bunch by bunch luminosity was measured by the "zero-degree luminosity monitor [19]". A droop of the luminosity along the train was not clearly observed. It may be difficult to separate the single beam blow-up from the beam-beam blow-up because the beam size is intentionally optimized by automatic programs and/or operators to obtain the high luminosity.

### 2.5.4 Transverse coupled bunch instability

The coupled bunch instability was studied in the LER. Mode spectra of the instability were totally different with and without solenoid field, which strongly suggests that the instability is caused by the electron cloud because usual wake fields are not affected by the weak DC solenoid field [20]. Peaks of the mode spectra in horizontal and vertical planes appeared at almost same position when the solenoids were turned off. A simulation showed that the observed mode spectra, especially position of the peaks, were well reproduced if the electrons are produced uniformly on the chamber wall. Growth rates of the instability were roughly consistent with the simulation.

### 2.5.5 Effect of solenoid

The solenoids were installed several times in the LER to sweep out the electrons since September 2000. The maximum longitudinal magnetic field at the centre of a solenoid is about 45 Gauss [2].

The effect of the solenoids on the beam blow-up was confirmed by the measurement of the vertical beam size with the interferometer after first installation of the solenoids where about 800

m was covered by the solenoids [3]. The threshold current of the blow-up increased by 80% after turning on the solenoids. The beam size of each bunch along the train was measured by the gated camera [3]. The blow-up started at 7th bunch with solenoids-off while it started at 30th bunch with solenoids-on. The effect of the solenoids was also confirmed by the luminosity measurement [3]. The specific luminosity decreased when all solenoids were turned off.

The mode spectrum of the coupled bunch instability was changed with and without solenoid field. The effect of the solenoids on the growth rate of the instability was also observed. The mode spectrum can be explained by a simulation assuming the effective solenoid field of 5 to 20 Gauss [20].

After about 95% of the drift space was covered by the solenoids several measurements were performed in order to obtain information to mitigate the electron cloud effects further. The results are summarized as follows [13,14,18].

- 1) When the solenoids were turned on the horizontal tune shift almost disappeared. The vertical tune shift decreased, but still remained.
- 2) The threshold current was measured as a function of the field strength of the solenoids. In the case of 3 and 4 rf bucket spacing the threshold current was not saturated even at the maximum solenoid field. In case of 2 rf bucket spacing the threshold current saturated at 20G and was not improved by the stronger solenoid field.
- 3) The contribution of the solenoids in various places on the electron cloud was studied by turning off the solenoids locally. The result showed that the solenoids in Fuji and Tsukuba straight sections where photoelectrons produced by the synchrotron radiation are not expected large are effective as well as in the arc sections in suppressing the blow-up.
- 4) The solenoids were initially arranged such that the integrated longitudinal field vanishes between adjacent quadrupole magnets in order to suppress the x-y coupling due to the solenoids. This arrangement brings regions where the polarity of the solenoid field changes. To see the effect of these regions on the blow-up and the tune shift, the polarity of the solenoids in three arcs among four was changed such that the polarity-changing-regions were removed. The result showed that the blow-up and the tune shift did not change.

### **2.5.6 Effect of wiggler magnets**

KEKB has two long straight sections occupied by wiggler magnets of 0.75 T. Total length of the wiggler sections are about 100 m. The blow-up of the beam size and the tune shift were measured with and without wiggler field to see the effect of the bending field on the electron cloud effects [14]. The result showed that 1) the horizontal and vertical tune shift did not change and 2) the beam size changed largely after powering on the wigglers. The result is not understood yet. More study is necessary.

### **2.5.7 Summary**

Cloud build-up studied by the measurements of the electron yield, the energy distribution, the tune shift along the train, the build-up time of the tune shift and the beam blow-up along the train

is explained by the simulations. Observations of the blow-up such as single bunch characteristics and the scaling of the threshold beam current on the bunch spacing seem consistent with the single bunch head-tail instability model. It is unclear whether the chromaticity dependence of the beam blow-up is well explained by the theory of the transverse mode coupling instability (TMCI) or not [21]. Mode spectrum of the coupled bunch instability can be explained by the simulation assuming a uniform production of the electrons on the chamber wall. Growth rate of the coupled bunch instability is roughly consistent with the simulation. Effect of the weak solenoid field on the electron cloud was confirmed by the measurements of the beam size, the luminosity, the tune shift and the coupled bunch instability.

Several open questions remain in the electron cloud effects at KEKB:

- 1) Beam blow-up has been observed in the vertical plane and not observed in the horizontal plane. A calculation based on the TMCI theory gives almost same horizontal and vertical threshold cloud density of the instability [21].
- 2) The decay time of the cloud density is a puzzle. A measurement showed a short decay time while another measurement did a long decay time.
- 3) Very slow blow-up along the train was observed. This slow blow-up is not explained by simulations yet.
- 4) The vertical beam size increases gradually as a function of the beam current even below a threshold of the blow-up.
- 5) Mode spectrum of the coupled bunch instability suggests the round distribution of the electron cloud though a large number of the electrons are produced at an illumination point of the synchrotron radiation.
- 6) The observed vertical tune shift is larger than the horizontal tune shift. The vertical tune shift does not disappear even after 95% of the drift space was covered by the solenoids.
- 7) The specific luminosity with 3 rf bucket spacing is lower than that with 4 rf bucket spacing even below a threshold beam current of the blow-up [23]. A combined phenomenon of the electron cloud and the beam-beam effect might be applicable to explain the observation [23].
- 8) The blow-up is still observed after a large number of the solenoids were installed. Questions are where the electrons are and how can they be removed. Trapped electrons inside the magnets might be a source of the electrons [24].

### 2.5.8 References

1. K. Ohmi and F. Zimmermann, "Head-Tail Instability Caused by Electron Clouds in Positron Storage Rings", *Phys. Rev. Lett.* **85**, 3821- 3824 (2000).
2. H. Fukuma et al., "Status of Solenoid System to Suppress the Electron Cloud Effects at the KEKB", *Proceedings of the 20th ICFA Advanced Beam Dynamics Workshop on High*

- Intensity and High Brightness Hadron Beams", 2002, FNAL, Batavia, Illinois, 2002 (AIP Conference Proceedings 642), p. 357.
3. H. Fukuma et al., "Study of Vertical Beam Blowup in KEKB Low Energy Ring", Proceedings of HEAC2001, Tsukuba, 2001.
  4. Y. Ohnishi et al., "Detection of Photoelectron Cloud in Positron Ring at KEKB", Proceedings of HEAC2001, 2001, Tsukuba.
  5. K. Ohmi, private communication.
  6. H. Fukuma, "Electron Cloud Effects at KEKB", Proceedings of ELOUD'02, CERN, Geneva, 2002 (CERN-2002-001), p. 1.
  7. F. Zimmermann, "Electron Cloud at the KEKB Low Energy Ring: Simulations of Central Cloud Density, Bunch Filling Patterns, Magnetic Fields, and Lost Electrons", CERN-SL-2000-017 (AP) (May, 2000).
  8. L. Wang et al., "Energy Spectrum of Electron Cloud with Short Bunch", to be appeared in Proceedings of 31st Advanced ICFA Beam Dynamics Workshop on Electron-Cloud Effects, 2004, Napa, California.
  9. K. Ohmi, S. Heifets and F. Zimmermann, "Study of Coherent Tune Shift Caused by Electron Cloud in Positron Storage Rings", Proceedings of Second Asian Particle Accelerator Conference (APAC'01), 2001, Beijing, p.445.
  10. T. Ieiri et al., "Bunch-by-bunch measurements of the betatron tune and the synchronous phase and their applications to beam dynamics at KEKB", PRST-AB **5**, 094402 (2002).
  11. H. Fukuma et al., "Observation of Vertical Beam Blow-Up in KEKB Low Energy Ring", Proceedings of EPAC2000, Vienna, June 2000.
  12. F. Zimmermann, "Electron-Cloud Studies for the Low Energy Ring of KEKB", CERN SL-Note-2000-004 AP (2000).
  13. T. Ieiri et al., "Estimation of Electron-Cloud Density by Means of Measuring Betatron Tune at KEKB Low Energy Ring", Proceedings of the 14th Symposium on Accelerator Science and Technology, 2003, Tsukuba.
  14. H. Fukuma, "Electron cloud effects in the KEKB", to be appeared in Proceedings of 31st Advanced ICFA Beam Dynamics Workshop on Electron-Cloud Effects, 2004, Napa, California.
  15. T. Ieiri et al., "Measurement of Betatron Tune Along Bunch Train in The KEKB Low Energy Ring", Proceedings of HEAC2001, 2001, Tsukuba.
  16. J. Flanagan et al., "High-Speed Gated Camera Observations of Transverse Beam Size Along Bunch Train at the KEKB LER", Proceedings of EPAC2000, 2000, Vienna, p. 1119.
  17. F. Zimmermann, "The Electron Cloud Instability: Summary of Measurements and Understanding", Proceedings of PAC2001, 2001, Chicago, p. 666.
  18. H. Fukuma et al., "Recent Observations of Collective Effects at KEKB", to be appeared in Proceedings of 30th Advanced ICFA Beam Dynamics Workshop on High Luminosity  $e^+e^-$  Collisions, 2003, Stanford, California.
  19. T. Uehara, private communications.
  20. S. S. Win et al., "Effect of Electron Cloud on the Bunch Oscillations in KEKB LER", Proceedings of ELOUD'02, CERN, Geneva, 2002 (CERN-2002-001), p.199.
  21. K. Ohmi et al., "Wake-field and fast head-tail instability caused by an electron cloud", Phys. Rev. E **65**, 016502 (2002).

22. Y. Funakoshi, "KEKB Accelerator Physics Report", in Proceedings of 23rd ICFA Advanced Beam Dynamics Workshop on High Luminosity  $e^+e^-$  Colliders, 2001, Cornell University, Ithaca.
23. K. Ohmi and A. W. Chao, " Combined phenomena of beam-beam and beam-electron cloud interactions in circular  $e^+e^-$  colliders ", PRST-AB **5**, 101001 (2002).
24. L. F. Wang et al., " Photoelectron trapping in quadrupole and sextupole magnetic fields", Phys. Rev. E **66**, 036502 (2002).

## 2.6 Measurement of ion effects in KEKB

H. Fukuma

mail to: [hitoshi.fukuma@kek.jp](mailto:hitoshi.fukuma@kek.jp)

[High Energy Accelerator Research Organization \(KEK\)](http://www.kek.jp)

Tsukuba, Ibaraki 305-0801, Japan

### 2.6.1 Introduction

So far ion effects are not serious problems in the KEKB electron ring (HER) except for the operation after a recovery from vacuum troubles, where a strong transverse coupled bunch oscillation which is suspected to be an ion induced instability is observed.

Several experiments about the ion instability were performed in the HER. One is the experiment for the fast ion instability which was done in 2000. Another experiment is the measurement of the coupled bunch oscillation which was done to identify the source of the transverse coupled bunch instability observed in the HER.

### 2.6.2 Experiment of the fast ion instability [1]

In high intensity and low emittance electron rings ions can make the beam unstable even when they are not trapped for a long time. The instability is called the fast ion instability (FII) [2]. Since the growth time of the bunch oscillation in the FII increases along a bunch train, the oscillation amplitude of the bunches also tends to increase from a head to a tail of the train. The growth time of the FII depends on the transverse beam size as a characteristic of ion instabilities.

The vertical coupled bunch oscillation in the HER was measured and analyzed to study the FII. In usual operation the coupled bunch oscillation is suppressed by a bunch by bunch feedback system. In the experiment the oscillation was measured by a bunch oscillation recorder (BOR) [3] after turning off the feedback system. The turn by turn positions of all bunches passing through a beam position monitor were stored in a memory up to 4096 turns. Eight bunch trains were stored in the ring. A train contained 120 bunches. The bunches in the trains were equally spaced at an interval of 8 ns, i.e. 4 rf buckets. The gaps between neighboring bunch trains were 160 ns. A gap of 1 ms was put between the last and the first train. The beam current was 240 mA and the average pressure was  $1.4 \times 10^7$  Pa in presence of the beam.

Singular Value Decomposition (SVD) was applied to analyze the coupled bunch oscillation. The data from the BOR was stored in a matrix  $Y$  which was composed of  $K$  rows and  $M$  columns, where  $K$  is the total number of turns and  $M$  the total number of bunches. The matrix  $Y$  was decomposed by SVD as  $Y = U^T W V$ , where  $U$  and  $V$  are orthogonal matrices. The

eigenvectors which are row vectors of  $U$  represent time patterns and those of  $V$  represent spatial patterns. The singular values corresponding to the eigenvectors appear in the diagonal matrix  $W$ .

The spatial pattern which corresponds to the largest singular value showed a snake-like shape where the oscillation amplitude grew from the head to the tail. The vertical oscillation was measured for several vertical beam sizes which were controlled by the vertical dispersion at sextupoles. The wavelength of the oscillation was obtained from the spatial pattern as a function of the vertical beam size and compared with a calculation using an analytic formula based on the FII theory. In the calculation the ion of carbon monoxide ( $\text{CO}^+$ ) was assumed and the beam size measured by an interferometer [4] was used. The measured wavelength agreed with the calculation if the vertical emittance was smaller than 2 nm. At the vertical emittance of 3.5 nm it was 1.5 times larger than the calculated wavelength.

The growth time of the coupled bunch oscillations was obtained from the time evolution of the oscillation. The head-tail damping rate, which was estimated to be  $6.4 \text{ msec}^{-1}$  from the dependence of a tune shift on the beam current, was subtracted from the observed growth rate. In the case of the vertical emittance of 0.98 nm, the growth time was 0.15 msec at the bunch number 100 in the first train. Using the number of the ions estimated from the relative pressure of the  $\text{CO}^+$  measured by a residual gas analyzer, the growth time was calculated from the FII theory as 0.48 ms which was not far from the measurement.

The above results show that the observed coupled bunch instability is likely the FII.

### 2.6.3 Measurement of transverse coupled bunch instability [5]

The transverse coupled bunch oscillation in the HER was studied to investigate sources of beam aborts accompanied by the horizontal oscillation. A bunch train of 1152 bunches was injected in the HER. The bunch spacing was 8 ns and the beam current was 600 mA. The bunch positions were measured using the BOR after switching off the bunch by bunch feedback system. The results are summarized as follows:

- 1) While the horizontal oscillation amplitude showed a tendency to increase along the train, the amplitude of the vertical oscillation was almost uniform among the bunches.
- 2) A saturation of the amplitude was observed in the horizontal oscillation.
- 3) The horizontal average growth rate of the instability was  $6 \times 10^{-4} \text{ turn}^{-1}$  and 5 times smaller than that of the vertical average growth rate.
- 4) The mode distribution of the coupled bunch instability obtained by Fourier transform of the bunch oscillation had a peak at a mode number about 10 in the horizontal plane and at the mode number 0 in the vertical plane.

The measurements showed the different characteristics of the horizontal and vertical oscillation.

A simulation of the horizontal instability in the HER was done by F. Zimmermann [6]. The simulation assumed four sources of the instability; 1)  $\text{CO}^+$  ions, 2) hydrogen ions ( $\text{H}^+$ ) in a dipole field, 3) a resistive wall wake and 4) the electron cloud. The results of the simulation are summarized as follows:

- 1) The oscillation amplitude grows along the bunch train in the cases of the ions.
- 2) While the oscillation increases exponentially in the resistive wall wake and the electron cloud case, it shows complicated structure such as the saturation of the amplitude in the cases of the ions.
- 3) The mode spectrum has a peak at the mode number 10, 300, 0 and 0 in the case of the  $\text{CO}^+$  ions, the electron cloud, the  $\text{H}^+$  ions and the resistive wall wake, respectively.
- 4) The growth time of the oscillation is 1, 2, 4000 and 5 ms in the case of the  $\text{CO}^+$  ions, the electron cloud, the  $\text{H}^+$  ions and the resistive wall wake, respectively.

The simulation assuming the  $\text{CO}^+$  ions as a source of the instability is consistent with the observations of the horizontal instability because 1) the peak of the mode spectrum appears at about 10, 2) the saturation of oscillation amplitude is seen, 3) the amplitude grows along the train and 4) the growth time is order of 1 ms. The reason why the vertical instability did not show the characteristics of the ion instability is an open question.

The observed average horizontal growth rate at 600 mA is 20 times smaller than the damping rate of the bunch by bunch feedback system. The measured growth rate does not explain why the beam abort was not cured by the bunch by bunch feedback system.

#### 2.6.4 References

1. Y. Ohnishi et al., "Study of Fast Ion Instability at KEKB Electron Ring", Proceedings of the 7th European Particle Accelerator Conference, 2000, Vienna.
2. T. O. Roubenheimer and F. Zimmermann, "Fast beam-ion instability. I. Linear theory and simulations", Phys. Rev. E **52** 5487 (1995).
3. M. Tobiyama and E. Kikutani, "Development of a high-speed digital signal process system for bunch-by-bunch feedback systems", PRST-AB **3**, 012801 (2000).
4. T. Mitsuhashi et al., "Optical Diagnostic System for the KEKB B-Factory", Proceedings of the 7th European Particle Accelerator Conference, 2000, Vienna.
5. H. Fukuma et al., "Recent Observations of Collective Effects at KEKB", to appear, Proceedings of 30th Advanced ICFA Beam Dynamics Workshop on High Luminosity  $e^+e^-$  Collisions, 2003, Stanford, California.
6. F. Zimmermann et al., "Simulation Study Of Coupled-Bunch Instabilities Due To Resistive Wall, Ions, or Electron Cloud", Proceedings of the 2003 Particle Accelerator Conference, 2003, Portland.

## 2.7 Studies on Electron Cloud Instability in the BEPC

Z.Y. Guo, Y.D. Liu, Q. Qin, J.Q. Wang, J. Xing  
 Mail to: [guozy@mail.ihep.ac.cn](mailto:guozy@mail.ihep.ac.cn)  
 Institute for High Energy Physics  
 P.O. Box 918, Beijing 100039, China

### 2.7.1 Introduction

The luminosity of a collider may be degraded due to the Electron Cloud Instability (ECI). A series of studies on the ECI has been processing since 1996 [1] in Beijing Electron Positron Collider (BEPC). Many of these studies are under the cooperation between IHEP and KEK. It was called photoelectron instability (PEI) during the first stage studies because we did not find the secondary electron effect at that time. The progress of the ECI studies is reviewed in this report first, we then focus to introduce the recent study results in detail. The BEPC is an electron positron storage ring as a collider, and it also can be operated as a synchrotron light source with single electron beam. It can be injected with positron beam bunch by bunch, so the ECI can be studied experimentally in BEPC. Now, a plan to upgrade the machine to be a double-ring collider, BEPCII [2], is being progressed to enhance the luminosity as two orders higher than the BEPC. The ECI could be a limitation to the performance of BEPCII.

The parameter dependence on the ECI has been investigated in experiments in BEPC such as the chromaticity effect, the solenoid effect, the octupole effect, and the clearing electrode effect using beam position monitor (BPM), etc. The electron cloud (EC) has been measured by a few detectors, which are mounted on the vacuum chamber specially. The different codes have been developed, including the EC build-up process in the antechamber structure. The beam instability behaviours for multi- and single bunch cases are simulated in detail. The potential methods to cure the ECI in a positron storage ring are issued from the experimental and simulation studies, and the meaningful study results are discussed in this report.

### 2.7.2 Experimental studies

#### *2.7.2.1 ECI parameter dependence*

The first experiment on the ECI was performed in 1996 [1]. The typical vertical betatron sidebands were observed on the spectrum analyzer when the positron beam was injected with uniformly distributed bunches. The vertical coupled bunch oscillation was also detected on the synchrotron light monitor. Any other betatron sidebands caused by HOMs at the corresponding frequency in the RF cavities were not found. The similar phenomena were not found with the electron beam under the same conditions.

We then started the experiments on the parameter dependence. The machine chromaticity effect, the bunch spacing effect, the beam energy effect, the beam emittance effect and the closed orbit effect, etc., were studied. The observed results showed that the bunch spacing effect is very sensitive to the ECI. The threshold of ECI decreased markedly when the bunch spacing increased. The chromaticity can control the ECI near the threshold current, suppressing the ECI when the chromaticity increased. The ECI is not influenced so strongly at the different beam energy as the beam instabilities caused by the impedance. Other beam parameters are not very important on the ECI.

A fast beam position monitor system which is borrowed from KEK, has been once used to observe the bunch oscillation process in the experiment in 1998. The damping time and the oscillation modes issued by fitting and doing FFT to the data. The mode analyses can more clearly show that it was definitely different between positron and electron beams under the same conditions [3].

### 2.7.2.2 *Electron cloud measurement*

Electron cloud (EC) detectors were installed in the BEPC since 1999 [4]. The typical structure of the detector is similar with that used in APS [5]. The detector current  $I_c$  varied linearly with the total beam current  $I_b$ , and it did not saturate as the  $I_b$  was not yet strong enough in the experiment. The EC energy distribution was resulted from the bias voltage scan. The longer distance from bending magnet, the better result. The multi-pacting effect has been investigated under the different bunch spacing, but no clear events to show that the electron motion was resonated by the bunch train passing as we used a detector near by the magnet.

### 2.7.2.3 *Solenoid effect on ECI*

It was verified in KEKB [6] and PEP-II that the solenoid field could wave the electron cloud partially to weaken the instability. We wound solenoid around a detector, from which the measured  $I_c$  was different when solenoid was off and on. This encourages us to wind solenoid on as more straight sections as we can in BEPC [7]. The total length of the solenoid wound on the vacuum chamber of the straight sections is 42 meters, covering about 18% of the ring circumference. A current up to 35A in the coils can be offered by a DC power supply, which corresponds to about 30 Gauss magnetic field longitudinally. When the current was applied on all of the solenoids, the betatron sidebands disappeared and the vertical bunch size reduced by about 20% clearly. The solenoid is more effective in the arc section nearby the magnet than it locates in the long straight section far away from magnet. The polarity of the solenoid is not important.

### 2.7.2.4 *Octupole effect on ECI*

The suppressive effect on ECI has been observed using an existing octupole in the ring. It can be clear to find that the vertical sidebands of the coupled bunch instability and the vertical bunch size were decreased when the octupole was excited as the positron beam was higher than the ECI threshold [7].

### 2.7.2.5 *Clearing electrode to decrease electron cloud*

A special detector as a model electrode was used to test to clean the electron cloud first. We do find it is effective [4]. This result encourages us to do more experiments using the buttons of BPMs as electrodes. There are 32 BPMs in BEPC ring, with 4 buttons in each BPM. A DC voltage from -600V to +600V can be applied to all of the buttons under the different patterns to be connected. The amplitudes of sidebands and the vertical bunch sizes along the bunch train were measured vs. the voltages applied on the BPM buttons. The results showed that the betatron sidebands and the beam size were decreased, and the effect may saturate at the applied voltage of 600V [8].

## 2.7.3 **Simulation studies**

### 2.7.3.1 *Code development*

Many simulation codes have been developed to study the ECI in the different laboratories, such as KEK [9] and IHEP. In the early simulation studies [10], the electron cloud distribution has been modelled in the vacuum chamber with a round shape transverse cross section, and photoelectrons are involved only. Later on, a code involving secondary electron emission was

developed [11] to simulate the EC distribution and the coupled bunch oscillation. A new computer code was developed in recent years to simulate the EC distribution in the antechamber, which will be used in BEPCII, to simulate the coupled bunch oscillation and the single bunch effect under the different conditions [12].

### 2.7.3.2 *Electron cloud build-up process*

We simulate the EC distribution and its build-up process along the bunch train in the different shape of the beam tube under the different yield  $Y$ , the different reflectivity  $R$ , and the different secondary electron yield (SEY). The results are used to simulate the behaviour of ECI. From the simulation we understand that the characteristics of the wake field by the EC are: short-ranged propagating along the bunch train longitudinally, varying along transverse direction of the beam tube linearity in the central part of the chamber, following the beam, and treating the wake field in a macro-particle way. The results of the simulation show that the electron density in the central region of the vacuum chamber can be reduced by about 5 times as the antechamber is adopted, by about 6 times if the TiN is coated inside the chamber, by about 3 times if the photon absorber is made in the wall of the chamber, by about 5 times if the electrode is installed in the chamber [13]. In the recent BEPCII design, the antechamber, the absorber, and the TiN coating have been decided to use. The electron density will then be decreased about 90 times from  $1.1 \times 10^{13} \text{ m}^{-3}$  to  $1.3 \times 10^{11} \text{ m}^{-3}$ , which is much lower than the case without any special measures used in the chamber.

### 2.7.3.3 *Single bunch effect*

For the single bunch effect, the EC is described as macro-particles in transverse direction of the chamber, and the bunch is described as macro-particles in the different slices from head to tail of the bunch. The macro-particles move in a 3-dimensional space affected by the EC, including the movement in the different slices as the particle synchrotron oscillation. The clear pictures of blown-up process can be printed from the simulation results [12]. The chromaticity effect is also involved in the simulation, in which the result can be compared with the experiment observation and with the conventional theory of the head tail instability. The threshold of the blown-up occurs at the central EC density is about  $9.2 \times 10^{11} \text{ m}^{-3}$ , which corresponds to a wake of  $1.47 \times 10^6 \text{ m}^{-2}$ .

### 2.7.3.4 *Coupled bunch oscillation*

For the simulation of the coupled bunch oscillation, the EC simulated along the build up process in a bunch train is described as macro-particles in transverse direction of the chamber, and each bunch is as one macro-particle to interact with the electron cloud. The vertical coupled bunch oscillation progresses in BEPCII conditions and its mode analyses are resulted [12]. The growth time fitted from the progress is about 0.08 ms as the central EC density is taken  $1.0 \times 10^{13} \text{ m}^{-3}$ , it will be about 6 ms if the central EC density is  $1.3 \times 10^{11} \text{ m}^{-3}$ . The simulated mode spectrum distribution is comparable with the observation in the experiment qualitatively.

## 2.7.4 **The potential methods to cure ECI issued from studies**

The suggested methods to reduce the EC density and ECI from simulation studies as: using antechamber, coating TiN on the inner surface of the beam tube, which lowers the secondary

electron yield, making the structure on the vacuum chamber inside as a saw-tooth shape, using photon absorber at the end of each section antechamber, designing lattice with a larger chromaticity by the limit of the dynamic aperture, etc.

The suggested methods to reduce the ECI from experiment studies as: winding solenoids outside of the vacuum chamber on the possible straight sections, especially nearby the magnet, designing lattice with a larger chromaticity by the limit of the dynamic aperture, installing an octupole in the ring at the position with large betatron function, using clearing electrodes in the vacuum chamber such as BPM buttons or other components, using a bunch to bunch feedback system to cure the possible coupled bunch oscillations, etc.

The ECI studies in BEPC have got quite rich meaningful results in the experiment and in the simulation. The study will continue before the machine shutdown for its upgrading. The recent experiment results need to be further confirmed with higher quality data when there is much machine time. Some more factors will be involved in the simulation code, such as the octupole effect, 3-D electromagnetic field caused by BPM buttons, etc.

### 2.7.5 References

1. Z. Y. Guo et al, "The Experiment Study on Beam-Photoelectron Instability in BEPC", PAC'97 Proceedings, Vancouver, 1566, 1997.
2. BEPCII Group, "BEPCII Design Report", IHEP-Proceedings, Aug. 2001.
3. Z. Y. Guo et al, "Experiment Studies on the Photoelectron Instability in the Beijing Electron Positron Collider", PRST-AB, Vol. 5, Issue 12, 124403, 2003.
4. J. Xing et al, "Simulation Study on ECI for BEPC and its Upgrade Plan BEPCII", ECLOD'02 Workshop, CERN, 2002.
5. Harkay, et al, PAC01 Proceedings, Chicago, 671, 2001.
6. H. Fukuma et al., Proceedings EPAC2000, Vienna, 2000.
7. Q. Qin et al, "Recent Experiment Study on ECI at the BEPC", APAC2004 Proceedings, Gyeongju, Korea, 2004.
8. Z. Y. Guo et al, "The Studies of Electron Cloud Instability", APAC2004 Proceedings, Gyeongju, Korea, 2004.
9. K. Ohmi, Phys. Rev. Lett. **75**, 1526, 1995.
10. Z. Y. Guo et al, "Simulation Study of the Beam-Photoelectron Instability in BEPC", EPAC98 Proceedings, Stockholm, 957 (1998).
11. Y. Luo, Doctoral thesis, 2001.
12. Y. D. Liu et al, "Simulation of the Electron Cloud Instability for BEPCII", APAC2004 Proceedings, Gyeongju, Korea, 2004.
13. Y. D. Liu et al, "Simulation of the Electron Cloud Density in BEPCII", HEP & NP **28**(3) (2004) p. 222.

## 2.8 Electron Cloud effect in the Linear Colliders

M. Pivi                    [mpivi@slac.stanford.edu](mailto:mpivi@slac.stanford.edu) SLAC, Menlo Park, California 94025, US  
 T. Raubenheimer       [tor@slac.stanford.edu](mailto:tor@slac.stanford.edu)    SLAC, Menlo Park, California 94025, US

### 2.8.1 Introduction

Beam induced multipacting, driven by the electric field of successive positively charged bunches, may arise from a resonant motion of electrons, generated by secondary emission, bouncing back and forth between opposite walls of the vacuum chamber. The electron-cloud effect (ECE) has been observed or is expected at many storage rings [1].

In the beam pipe of the Damping Ring (DR) of a linear collider, an electron cloud is produced initially by ionization of the residual gas and photoelectrons from the synchrotron radiation. The cloud is then sustained by secondary electron emission. This electron cloud can reach equilibrium after the passage of only a few bunches. The electron-cloud effect may be responsible for collective effects as fast coupled-bunch and single-bunch instability, emittance blow-up or incoherent tune shift when the bunch current exceeds a certain threshold, accompanied by a large number of electrons in the vacuum chamber.

The ECE was identified as one of the most important R&D topics in the International Linear Collider Report [2]. Systematic studies on the possible electron-cloud effect have been initiated at SLAC for the GLC/NLC and TESLA linear colliders, with particular attention to the effect in the positron main damping ring (MDR) and the positron Low Emittance Transport which includes the bunch compressor system (BCS), the main linac, and the beam delivery system (BDS). We present recent computer simulation results for the main features of the electron cloud generation in both machine designs. Thus, single and coupled-bunch instability thresholds are estimated for the GLC/NLC design.

The results are obtained by the computer simulation codes POSINST vers. 12, HEAD-TAIL vers. 02/04 and CLOUD\_MAD vers. 2.3, which were developed at LBNL, CERN and SLAC [3,4,5] respectively, to study the electron-cloud effect in particle accelerators. The former code is used to simulate the electron cloud generation, to estimate the equilibrium electron-cloud density and to estimate the coupled bunch instability, while the latter two codes are used to estimate the single-bunch head-tail instability and the emittance growth. Electron-cloud studies for CLIC are discussed in [6].

The GLC/NLC MDR stores 3 trains, separated by 65 nsec with each train consisting of 192 bunches having 1.4 nsec bunch spacing. The aluminum vacuum chamber is specified to be a cylindrical perfectly-conducting round pipe with a 20 mm radius and includes an antechamber to remove most of the synchrotron radiation. The TESLA main damping ring stores 2820 bunches with a 20 nsec bunch spacing. The vacuum chamber in the long straight sections is a round aluminum pipe with a 50 mm radius without an antechamber. The arc vacuum chambers are assumed to be round chambers without an ante-chamber and with 22 mm radius. The TESLA bunch spacing in the linac increases to 337 nsec from the 20 nsec in the damping ring. A complete set of parameters assumed for the simulations can be found in [2,7,8].

In the following, the present status of the studies on the electron cloud generation and effects in the linear colliders will be described. In general, the electron cloud effects are so severe that the generation of a cloud in a significant fraction of the rings or beam lines will have deleterious effects. Finally, possible remedies to mitigate the effect are presented.

### 2.8.2 Generation of the cloud

The simulation code POSINST for the generation of the electron cloud and the detail model of the secondary electron yield (SEY or  $\delta$ ) are described in [9,10]. The code offers the possibility

of simulating multiple field configurations including solenoid, arc dipole, quadrupole, sextupole and wigglers sections and includes a model for the fringe fields ends.

The secondary electron yield, number of secondary electrons generated, is a function of the primary incident electron energy and angle and, together with the secondary electron energy, is the key parameter for the electron-cloud effect. The main SEY parameters are the peak SEY value  $\delta_{\max}$  and secondary emitted-electron energy spectrum  $d\delta/dE$ .

Typically the electron-cloud develops under the conditions where the average SEY of the electrons hitting the wall is larger than one. The cloud develops until an equilibrium electron density level is reached which arises due to a balance between the space charge forces, the beam potential well, and the rate of electron generation. The equilibrium density level is typically close to the neutralization level which is defined as the point where the average number of electrons equals the average number of positively charged particles. In the damping rings, the neutralization level is typically between  $4.0E+11$  and  $1.0E+13$   $e/m^3$  depending on the beam intensity and vacuum chamber sizes. In these studies, we are mainly interested in the estimate of the equilibrium electron density as a function of the peak value of the SEY.

### 2.8.3 Thresholds for the development of the cloud: SEY Thresholds

The typical peak SEY for *as received* aluminum 6063 technical vacuum chamber material is  $\sim 2.7$ . Simulation results for the GLC/NLC main damping rings [10] indicate that the secondary electron yield threshold for the development of the electron-cloud is  $\delta_{\max} = 1.6$  in field free regions, and 1.4, 1.3, and 1.25, respectively in the arc dipole, wiggler and arc quadrupole sections of the GLC/NLC main damping ring. See table I.

Simulations for the TESLA positron damping ring suggest that the electron cloud develops in the long straight sections when  $\delta_{\max} > 2.1$ . This threshold appears to be safe, however, a serious issue is the multipacting in the  $\sim 400$  m long damping wigglers. In the wiggler sections the vacuum chamber size are smaller and as a consequence the multipacting conditions are enhanced, resulting in an electron-cloud threshold given by  $\delta_{\max} = 1.3$ , see Fig 1.

Furthermore, the TESLA damping ring arcs vacuum chamber design actually does not include an antechamber. Without an antechamber, the synchrotron radiation generates a large amount of photoelectrons at the wall and the electron-cloud is present independently of the SEY. In our simulations, we have also considered the possibility to include an antechamber design and switched off the synchrotron radiation. In this case, in the arc quadrupoles and dipoles the thresholds are given by  $\delta_{\max} = 1.6, 1.5$ , respectively.

Therefore to avoid the detrimental effect given by the electron-cloud in the damping rings, a SEY as low as 1.2 needs to be achieved in at least the damping wiggler sections of either ring design machines. The aim is to reduce the SEY of the vacuum chamber material below the specified thresholds.

Studies have also been made of the electron cloud generation in the positron transport lines. This is only expected to be an issue in the normal conducting colliders where the bunches are closely spaced while, in the TESLA design, the bunch spacing is 337 ns after extraction from the damping ring. In the GLC/NLC transport lines, the peak electron cloud density is a strong function of the vacuum chamber radius as well as the SEY. Assuming the worst case of a 1 cm chamber radius and an SEY = 2, the cloud density grew to the neutralization level of  $6E+13$   $e/m^3$ . However, decreasing the SEY to 1.5 or increasing the vacuum chamber radius to 2 cm decreased the peak cloud density to  $2E+11$   $e/m^3$ . Further decreases were seen with addition reduction of

the SEY or increase of the chamber aperture however the electron cloud due to the photoelectrons must still be estimated. An antechamber in the bunch compressor arcs and the BDS arcs may be required to keep the photo-electrons at a sufficiently low level.

**Table 1.** Secondary electron yield thresholds for the development of the electron-cloud in the GLC/NLC and TESLA DRs. The TESLA damping ring arcs vacuum chamber design does not include an antechamber. Without an antechamber and assuming a photoelectron yield of 10%, the photoelectrons dominate and an electron-cloud is present independent of the SEY.

Damping Ring location	Parameters	$\delta_{\max}$ threshold	neutralization Cloud density
<b>GLC/NLC</b> field free region		1.5÷1.6	2E13 m <sup>-3</sup>
“ arc dipole	$B_y=0.675$ T	1.3÷1.4	2E13 m <sup>-3</sup>
“ arc quadrupole	$G=30$ T/m	1.2÷1.25	2E13 m <sup>-3</sup>
“ damping wiggler	$B_y=2.1$ T, $\lambda_w=0.27$ m	1.2÷1.3	6E13 m <sup>-3</sup>
<b>TESLA</b> long straight sections		2.0÷2.1	4E11 m <sup>-3</sup>
“ arc dipole without antechamber	$B_y=0.194$ T	Photo e <sup>-</sup>	2E12 m <sup>-3</sup>
“ arc dipole with antech.	$B_y=0.194$ T	1.4÷1.5	2E12 m <sup>-3</sup>
“ arc quadrupole without antechamber	$G=21.7$ T/m	Photo e <sup>-</sup>	2E12 m <sup>-3</sup>
“ arc quadrupole with antechamber	$G=21.7$ T/m	1.5÷1.6	2E12 m <sup>-3</sup>
“ damping wiggler	$B_y=1.6$ T, $\lambda_w=0.4$ m	1.2÷1.3	5E12 m <sup>-3</sup>

#### 2.8.4 Head-Tail single-bunch and coupled bunch instabilities

We have estimated the electron cloud density threshold for the head-tail instability in the GLC/NLC MDR with the simulation code HEAD-TAIL. In the field free regions of the MDR, a head-tail instability is observed to occur for an average electron-cloud density close to 2.0E+12 e/m<sup>3</sup>, see Fig. 2, leading to a strong vertical emittance blow-up and particle loss. The growth time of the instability is in the order of 100  $\mu$ sec. In particular, this electron-cloud density threshold occurs when the secondary electron yield at the wall exceeds  $\delta_{\max} \sim 1.5$  in the field-free regions. Study of the head-tail instability in the arc dipole and damping wiggler sections of both GLC/NLC and TESLA DR are underway. Simulations confirm that a slightly positive chromaticity or a larger synchrotron tune increase the threshold for the instability as expected but this is unlikely to provide the margin of safety that is desired.

Similarly, the code CLOUD\_MAD has been used to estimate the single bunch thresholds in the positron transport lines of the BCS, the main linac, and the BDS. The electron cloud effects manifest in different ways in each of these different regions. For example, the thresholds for single-bunch emittance increase and beam size blow up in the BDS is  $\sim 1.0\text{E}+11$  e/m<sup>3</sup> [11] where the effect mainly arises from the mismatch of the optical functions due to the focusing from the electron cloud. Unfortunately, it is not possible to simply retune the BDS optics because the electron cloud density, and thus the focusing mismatch, changes along the bunch length. The thresholds in the main linac and the BCS are  $\sim 5.0\text{E}+13$  e/m<sup>3</sup> [12]. In the main linac and the

bunch compressor pre-linac, the instability manifests itself by modulating the position within a single bunch while in the arcs of the bunch compressor the instability arises from a mismatch of the optical functions much like that in the BDS.

Finally, the threshold for a coupled bunch instability in the GLC/NLC main damping ring is estimated for a cloud density  $> 1.0E+13$  e/m<sup>3</sup>. Feedback may correct the coupled bunch instability at a growth time of 100  $\mu$ s estimated for this density level. Coupled bunch instabilities have not been estimated for the transport lines but are not expected to be a limitation.

### 2.8.5 Remedies for the electron-cloud build-up

The SEY for *as received* aluminum vacuum chamber material is unacceptably high for both machines damping ring designs. Thus, we are planning to coat the aluminum vacuum chamber. An experimental program is well developed at SLAC, to measure the secondary yield of TiN and TiZrV thin film coating materials and the reduction of the SEY due to electron bombardment or ion sputtering. The non-evaporable TiZrV getter material provides pumping after its activation; activation is obtained by means of heating which reduces also the SEY.

The electron bombardment, so called conditioning or scrubbing effect, is effective in reducing the SEY of technical vacuum chamber materials. The peak SEY of TiN is reduced below 1.2 by applying an electron dose of  $\sim 0.5$  mC/mm<sup>2</sup>. In the case of TiZrV material, an order of magnitude larger electron dose is needed to reduce the secondary yield to the same value. Recontamination of the material under vacuum results in an increase of the SEY; this effect is still under study.

The electron wall current of the cloud itself will provide the necessary conditioning. Assuming nominal GLC/NLC MDR beam parameters, the estimated average electron-cloud current hitting the surface of the vacuum chamber is  $0.5\mu$ A/mm<sup>2</sup>. At the initial stage of machine operations it will be necessary to run with lower beam intensity. When operating the MDR with a beam current just above the threshold to develop electron-cloud for conditioning purpose, but below the threshold for head-tail, simulations estimate an electron wall current of  $2.5$  nA/mm<sup>2</sup>. Thus, ramping the beam current up, the required electron conditioning dose may be achieved in  $\sim 2.0E+05$  sec or during few tenth hours of beam operation in the commissioning period.

Concern has been expressed [13] about the possibility that TiN coating materials may evaporate in time under continuous machine operations, i.e. photons, ions and electrons hitting and degrading the surface coatings. The issue needs to be addressed.

A promising remedy is given by fabricating the vacuum chamber surface with a particular design profile. We have studied the secondary electron emission from a metal surface with a grooved triangular and rectangular design profile [14,15]. Secondary electrons emitted from the grooved surface are likely to hit other wall of the groove causing a partial trapping of electrons which results in a suppression of the effective secondary emission yield (SEY). Thus, the special groove design is expected to reduce the escape probability of electrons in the proximity of the surface, reducing considerably the effective SEY at the surface. Analytic estimates [15] show that a SEY reduction by a factor  $\sim 2$  is achieved with a groove angle design of  $40^\circ$ . The proposed mechanism of SEY reduction might be important for suppression of the electron-cloud effect in particle accelerators. Aluminum and copper samples with the special groove surface profile are being produced and measurements of the SEY are underway.

Among possible remedies we consider also solenoid windings. A longitudinal solenoid field of 10-20 Gauss has been extremely effective in reducing the electron cloud effect in the PEP-II

and KEKB, with considerable enhancement of luminosity performance. Solenoid field is effective in field free regions. It may be applied in the BDS regions and a small fraction 15% of the GLC/NLC main damping ring. *In situ* ion sputtering is also under study.

As mentioned in section 2.8.3, simulations show that reduction of the SEY or increase of the chamber aperture in the BDS region, decrease the peak cloud density during a single bunch train pass. The 8 msec bunch spacing between trains should be sufficient for the electron-cloud to dissipate.

### 2.8.6 Miscellaneous discussions

We have estimated the equilibrium density level in both linear collider damping rings and the thresholds for the single- and coupled-bunch instability in the GLC/NLC main damping ring. Simulations indicate that a reduction of the secondary electron yield below a peak value of  $\sim 1.2$  is required to avoid the electron-cloud effect in the damping wiggler sections of both damping rings. The electron-cloud effect is an issue in the arc sections of both DRs.

To reduce the electron-cloud effect in the GLC/NLC, various possible remedies are meant to decrease the SEY to a value  $\sim 1.1$ - $1.2$  in a stable way.

Due to the estimated high electron wall current at the GLC/NLC main damping ring vacuum chamber, the required electron conditioning dose may be achieved in few hours of beam operations during the commissioning period.

To apply extra measure of security, we are developing a metal surface with a special groove profile design, which is estimated to reduce the secondary yield by a factor 2 from an initial value 2.0 to  $\sim 1.1$ . The groove profile design under study is expected to be effective mainly in field free regions.

Solenoid windings are effective in reducing the effect in the GLC/NLC beam delivery system and bunch compressor system and in a fraction of the main damping ring. Increasing the chamber aperture is beneficial in reducing the cloud density in the beam delivery system.

### 2.8.7 Acknowledgments

We are particularly grateful to our colleagues for many stimulating discussions, especially to R. Kirby, F. Le Pimpec, A. Wolski, K. Kennedy and G. Stupakov. We are grateful to NERSC for supercomputer support.

### 2.8.8 References

1. For an updated summary and links on electron cloud studies, see E-CLOUD02: <http://slap.cern.ch/collective/ecloud02/>. See also the proceedings of the E-CLOUD04 workshop, April 2004, <http://icfa-ecloud04.web.cern.ch/icfa-ecloud04/>.
2. ILC-TRC Report 2003, <http://www.slac.stanford.edu/xorg/ilc-trc/2002/2002/report/03rep.htm>
3. M. A. Furman and G. R. Lambertson, "The Electron-Cloud Instability in the Arcs of the PEP-II Positron Ring," LBNL-41123/CBP Note-246, PEP-II AP Note AP 97.27, 1997.
4. F. Zimmermann and G. Rumolo, "Electron Cloud Simulation: Build Up and Related Effects," in *Proceedings of the Mini-Workshop on Electron-Cloud Simulations for Proton and Positron Beams, CERN Geneva, 2002* [Yellow Report No. CERN-2002-001 (unpublished)], p. 97.

5. CLOUD\_MAD, T. Raubenheimer reference page:  
[http://www-project.slac.stanford.edu/lc/local/AccelPhysics/Codes/Ion\\_MAD-Cloud\\_Mad/dbates/nlc\\_cloudmadtools\\_doc/cloud\\_mad/index.html](http://www-project.slac.stanford.edu/lc/local/AccelPhysics/Codes/Ion_MAD-Cloud_Mad/dbates/nlc_cloudmadtools_doc/cloud_mad/index.html)
6. F. Zimmermann, "CLIC Damping Ring," LC02 Workshop at SLAC, Menlo Park, CA, US, February 4-8, 2002. <http://www-conf.slac.stanford.edu/lc02/wg1/schedule.html>.
7. A. Woslki and M. Woodley, "The NLC Main Damping Ring Lattice" NLC LCC-0113, LBNL CBP Tech Note-276, February 2003.
8. R. Brinkmann, K. Flöttmann, J. Roßbach, P. Schmüser, N. Walker, H. Weise "TESLA Technical design Report," March 2001.
9. M. A. Furman and M. T. F. Pivi "Probabilistic model for the simulation of secondary electron emission" PRST-AB **5**, 124404 (2002).
10. M. Pivi, T. O. Raubenheimer and M. A. Furman "Recent Electron Cloud Simulation Results for the NLC and for the TESLA Linear Colliders" in the Proc. PAC 2003, Portland, Oregon, US, May 12-16, 2003.
11. D. Chen, et al, "Single Bunch Electron Cloud Effects in the NLC Beam Delivery System," NLC LCC-0126, September 2003.
12. D. Chen, et al, "Single Bunch Electron Cloud Effects in the NLC Bunch Compressor System," NLC LCC-0131, October 2003.
13. R. Kirby and A. Kulikov, SLAC, private communication, 2004.
14. A. Krasnov "Molecular pumping properties of the LHC arc beam pipe and effective secondary electron emission from Cu surface with artificial roughness", CERN LHC Project Report 671.
15. G. Stupakov and M. Pivi "Suppression of the effective SEY for a grooved metal surface" in preparation for the upcoming E-CLOUD04 workshop [1], and to be published as to be LCC Note [http://www-project.slac.stanford.edu/lc/ilc/TechNotes/LCCNotes/lcc\\_notes\\_index.htm](http://www-project.slac.stanford.edu/lc/ilc/TechNotes/LCCNotes/lcc_notes_index.htm)

## 2.9 Electron-cloud build-up in hadron machines

M. A. Furman<sup>(\*)</sup>

mail to: [mafurman@lbl.gov](mailto:mafurman@lbl.gov)

[Lawrence Berkeley National Laboratory](#)

Bldg. 71R0259, 1 Cyclotron Rd., Berkeley, CA 94720-8211, USA

(\*)Work supported by the U.S. DOE under Contract DE-AC03-76SF00098.

### 2.9.1 Introduction

The first observations of electron-proton coupling effect for coasting beams and for long-bunch beams were made at the earliest proton storage rings at the Budker Institute of Nuclear Physics (BINP) in the mid-60's [1]. The effect was mainly a form of the two-stream instability. This phenomenon reappeared at the CERN ISR in the early 70's, where it was accompanied by an intense vacuum pressure rise. When the ISR was operated in bunched-beam mode while testing aluminum vacuum chambers, a resonant effect was observed in which the electron traversal time across the chamber was comparable to the bunch spacing [2]. This effect ("beam-induced multipacting"), being resonant in nature, is a dramatic manifestation of an electron cloud

sharing the vacuum chamber with a positively-charged beam. An electron-cloud-induced instability has been observed since the mid-80's at the PSR (LANL) [3]; in this case, there is a strong transverse instability accompanied by fast beam losses when the beam current exceeds a certain threshold. The effect was observed for the first time for a positron beam in the early 90's at the Photon Factory (PF) at KEK, where the most prominent manifestation was a coupled-bunch instability that was absent when the machine was operated with an electron beam under otherwise identical conditions [4]. Since then, with the advent of ever more intense positron and hadron beams, and the development and deployment of specialized electron detectors [5-9], the effect has been observed directly or indirectly, and sometimes studied systematically, at most lepton and hadron machines when operated with sufficiently intense beams. The effect is expected in various forms and to various degrees in accelerators under design or construction.

The electron-cloud effect (ECE) has been the subject of various meetings [10-15]. Two excellent reviews, covering the phenomenology, measurements, simulations and historical development, have been recently given by Frank Zimmermann [16,17]. In this article we focus on the mechanisms of electron-cloud buildup and dissipation for hadronic beams, particularly those with very long, intense, bunches.

## 2.9.2 Primary sources of electrons and secondary electron emission

Depending upon the type of machine, the EC is seeded by primary electrons from three main sources: photoelectrons, ionization of residual gas, and electrons generated when stray beam particles hit the chamber walls. In addition, for HIF drivers, an important expected source of electrons is a combination of two of the above, namely: gas will be desorbed by stray ions striking the chamber walls which will subsequently be ionized by the beam. These electrons get kicked by successive bunches mostly in the direction perpendicular to the beam; as they strike the walls of the chamber, they generate secondary electrons which add to the existing electron population.

Of all hadron machines presently existing or under construction, only the LHC will be affected by the photoelectric effect. Indeed, this source is expected to be the dominant source of seed electrons at top beam energy, with an effective photoelectric yield of  $\sim 10^{-3}$  photoelectrons per proton per meter in the arcs [18]. For all other hadron machines, the dominant source of electrons is ionization of residual gas and/or electron production off the walls from stray beam particles. For the PSR, for example, it is estimated that the proton loss rate is  $\sim 4 \times 10^{-6}$  per stored proton per turn, and that the electron yield per proton striking the wall is  $\sim 100-200$  [19]. For heavy ions striking a chamber wall, such as  $\text{Au}^{79+}$  used at RHIC, the electron yield is significantly higher than for protons [20]. For  $\text{K}^+$  ions used in present HIF test drivers, the yield appears to be comparable to that for protons at the PSR, at least a low ion energies [21]. In order to minimize activation, designs of newer spallation neutron sources place a premium on minimizing particle losses [22]. In this case, the dominant source of electrons may be ionization of residual gas.

In many (perhaps most) cases of practical interest, the secondary electron emission process has a more significant effect on the overall electron density than the primary source mechanism. The primary relevant quantity is the secondary emission yield (SEY)  $\delta$  for the vacuum chamber surface material, which is defined to be the average number of electrons emitted per incident electron. The SEY is a function of the incident electron energy and angle,  $E_0$  and  $\theta_0$  respectively, as well as the type of material and its state of conditioning. Also important in some cases is the

secondary electron emission spectrum. For a given incident-electron energy  $E_0$ , the emitted electrons range in energy from 0 to  $E_0$ . If  $E_0$  is larger than  $\sim 50$  eV, the emitted spectrum exhibits three fairly well-defined regions: true secondaries (emitted with energies in the range 0–50 eV), rediffused (emitted with energies in the range  $\sim 50$  eV up to  $E_0$ ), and reflected electrons (emitted within a sharp peak,  $\sim \pm 2$  eV, about  $E_0$ ). Depending on the bunch spacing of the beam and the state of conditioning of the chamber, these three components can contribute significantly different amounts to the growth of the electron-cloud density, and to its dissipation rate [23].

In practice, it is the *effective value* of the SEY that determines the rate of growth or dissipation of the electron cloud density. This quantity,  $\delta_{\text{eff}}$ , is the convolution of  $\delta(E_0, \theta_0)$  with the energy-angle distribution of the electrons striking the chamber wall. If  $\delta_{\text{eff}} > 1$ , the electron density grows exponentially until the space-charge forces become strong enough to effectively suppress further electron emission. Simulations show that, in practice, this saturation is reached when the electron density roughly equals the beam neutralization level. If  $\delta_{\text{eff}} < 1$ , the vacuum chamber wall acts as an effective electron absorber, and an equilibrium is reached when the primary electron production rate equals the net absorption rate. A quantity that is commonly used to gauge  $\delta_{\text{eff}}$  is the peak value of the SEY,  $\delta_{\text{max}}$ , since, in general,  $\delta_{\text{eff}}$  is a monotonically increasing function of  $\delta_{\text{max}}$ . Nevertheless, it should be kept in mind that details of the energy-angle distribution of the electron flux at the wall may be important. For this reason, the value of  $E_0$  at which the normal-incidence SEY peaks,  $E_{\text{max}}$ , is quite relevant. In most positron and hadron machines presently operating or planned, the energy spectrum of the electrons striking the chamber walls is concentrated below  $\sim 100$  eV, while  $E_{\text{max}}$  is typically in the range 250–350 eV.

### 2.9.3 Electron-cloud formation and dissipation

For the purposes of addressing electron-cloud effects, particularly the build-up and dissipation, hadron accelerators or storage rings can be roughly separated into two classes: (a) those for which few of the electrons in the vacuum chamber are trapped within the bunch when it traverses a given sector of the machine, and (b) those in which most of the electrons are trapped within a bunch. Although the basic physical mechanisms are common to all machines that exhibit ECEs, this effective criterion is convenient in classifying the dominant electron-cloud manifestations and appropriate detection techniques. This criterion combines several parameters of the beam and vacuum chamber, namely bunch intensity, bunch length, transverse bunch size, vacuum chamber geometry and size, etc. There is, apparently, no single (and simple) combination of the above-mentioned parameters that describes the classification in all cases. Nevertheless, in practice, when the machines operate at their nominal specification, the bunch length appears to be a single convenient parameter to separate the two classes. Among those accelerators in class (a) are the LHC, SPS, RHIC, TEVATRON and possibly others, for which the bunch length is roughly in the range  $\sim 10$ –100 cm. Among those in class (b) are spallation neutron sources such as the PSR, ISIS, SNS and ESS, for which the bunch length is in the range  $\sim 10$ –100 m. Although heavy-ion fusion (HIF) drivers are not circular accelerators, they represent, from the electron cloud perspective, a rather extreme case of this second class of machines.

#### 2.9.3.1 Short-bunch case

For hadron machines in the first class, the ECEs are similar to those in positron rings such as those used in light sources or B factories. In particular, the dimensionless parameter

$$G = \frac{ZNr_e s_b}{b^2} \quad (1)$$

plays a special role [2]. Here  $Z$  is the beam-particle charge (e.g.,  $Z = 1$  for proton beams,  $Z = 79$  for fully stripped gold ions, etc.),  $N$  is the number of particles per bunch,  $r_e = 2.82 \times 10^{-16}$  m is the classical electron radius,  $s_b$  is the bunch spacing, and  $b$  is the half-height of the vacuum chamber (or radius, if round). The value  $G = 1$  defines the beam-induced multipacting resonance condition, in which an electron “born” at the chamber wall crosses the chamber along a diameter by the action of a single bunch passage in a time equal to the bunch spacing,  $s_b/c$ . This condition is valid in the impulse approximation, neglects space-charge and image forces, and assumes that the electron is born at rest. This parameter roughly defines two regimes, separated by the value  $G = 1$ : the long-bunch-spacing regime, corresponding to  $G > 1$ , and the short-bunch-spacing regime, for which  $G < 1$ . The condition  $G = 1$  is necessary but not sufficient to lead to beam-induced multipacting: in addition to  $G = 1$ ,  $\delta_{\text{eff}}$  must be  $> 1$  for multipacting to take place [23]. For the LHC, for example,  $G \approx 7$  for electrons crossing the chamber vertically, while for the SPS,  $G \approx 3$ . For positron beams in B factories,  $G$  is closer to 1, and may be quite different whether it is computed along the vertical or horizontal direction.

Regardless of the value of  $G$ , the build-up of the electron cloud typically proceeds in similar fashion following injection of a beam into an empty chamber: primary electrons are generated by one or more of the mechanisms described above, the bunches kick the electrons primarily in the direction perpendicular to the beam, the electrons strike the chamber wall leading to more electrons, and the process repeats with the passage of successive bunches. In most practical cases, the secondary emission is of key importance owing to its compounding effect on the electron-cloud density. If  $\delta_{\text{eff}} > 1$ , and if the bunch train is sufficiently long, the electron-cloud density increases in time until a saturation level is achieved, as described above.

### 2.9.3.2 Long-bunch case

In the case of long bunch machines, the primary mechanisms for the build-up of the electron cloud is typically “trailing-edge multipacting” [24-26]. In these machines the longitudinal bunch profile is typically roughly parabolic or triangular. As the bunch traverses any given section of the ring, the beam potential from the leading edge of the bunch rises in time to a peak value of ~many kV, and traps electrons quite efficiently. Once the peak of the potential passes, the trapped electrons are released during the passage of the trailing edge and strike the wall, leading to secondary emission. The trailing-edge multipacting mechanism is quite sensitive to the longitudinal bunch profile. The electron cloud saturates typically within a few bunch passages. During the gap between bunches, electrons dissipate and the remaining slow electrons that remain in the chamber are trapped by the head of the next bunch [27-29]. Fig. 1 shows a sample measurement at the PSR. Comparative simulated studies have been carried out for several spallation neutron sources [30-33].

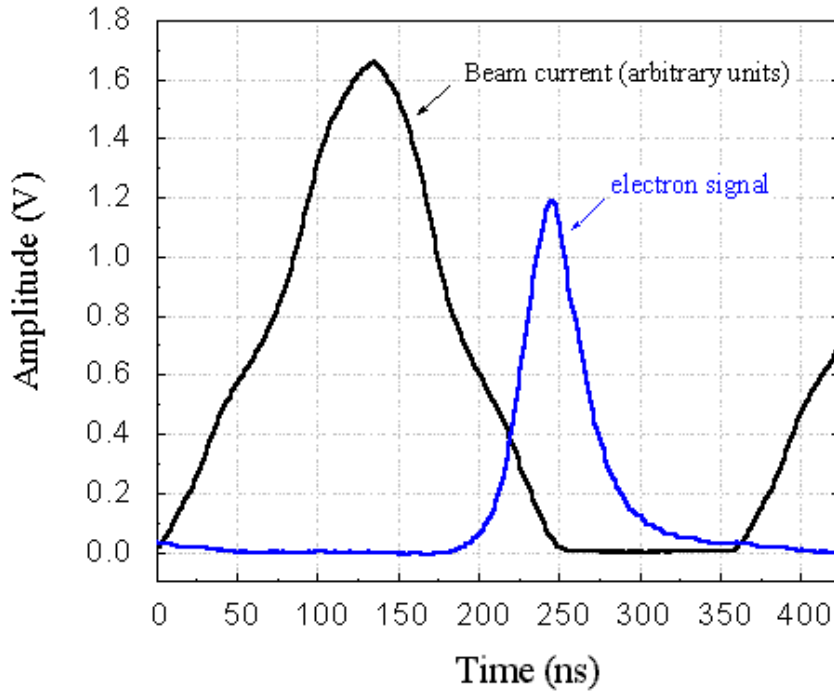


**Fig. 1.** Beam current signal and electron flux at the chamber wall at one specific field-free region of the PSR. The ring contains only one bunch with a revolution period of 357 ns. The peak electron detector signal of 1.2 V corresponds to a flux of  $435 \mu\text{A}/\text{cm}^2$ . In this case, the bunch charge was  $8 \mu\text{C}$ . Courtesy R. Macek.

### 2.9.3.3 *ElectronDissipation.*

When the beam is extracted from the machine, or during a sufficiently long beam gap, the surviving electrons are gradually absorbed by the chamber walls. Once the space-charge forces within the electron cloud become negligible, the electron density decays exponentially in time with a time constant  $\tau$ , which is closely related to the electron kinetic energy  $E$ , the chamber half-height  $b$ , and  $\delta_{\text{eff}}$ . In the simplest approximation, these quantities are related by [23,33]

$$\delta_{\text{eff}} = \exp\left\{-\frac{b}{c\tau}\sqrt{\frac{2mc^2}{E}}\right\} \quad (2)$$

Measurements [19] and simulations [33] show that an exponential decay is indeed observed at the PSR following beam extraction. By measuring  $\tau$ , and assuming a typical energy  $E \sim 3\text{-}5 \text{ eV}$  (which is suggested by basic electron emission spectrum data), Eq. (2) yields a value for  $\delta_{\text{eff}}$  which, in this particular case (stainless steel chamber), is in the range 0.4-0.6. This value is consistent with independent lab measurements of  $\delta(0)$ , as it should be expected. Recent measurements for copper surfaces, however, show that the SEY has a non-monotonic dependence on  $E_0$  below  $\sim 10\text{-}15 \text{ eV}$  [34]. In such a case, the approximation  $\delta_{\text{eff}} \approx \delta(0)$  has to be modified to take into account the low-energy details of the SEY.

## 2.9.4 Acknowledgments

I am grateful for many discussions over time with A. Adelman, G. Arduini, V. Baglin, M. Blaskiewicz, O. Brüning, Y. H. Cai, R. Cimino, R. Cohen, I. Collins, F. J. Decker, A. Friedman, O. Gröbner, K. Harkay, S. Heifets, N. Hilleret, J. M. Jiménez, R. Kirby, G. Lambertson, R. Macek, A. Molvik, K. Ohmi, M. Pivi, C. Prior, A. Rossi, G. Rumolo, D. Schulte, J.-L. Vay, A. Wolski, A. Zholents and F. Zimmermann.

## 2.9.5 References

1. A review of the early work, with numerous references, has been recently given by V. Dudnikov, "Diagnostics for e-p Instability Observation," Ref. 14 (below).
2. O. Gröbner, "Bunch-Induced Multipactoring," Proc. 10th Intl. Accel. Conf., Serpukhov, 1977, pp. 277-282.
3. R. Macek, "Measurements of Electron Cloud Effects at PSR" and references therein, this Newsletter.
4. M. Izawa, Y. Sato and T. Toyomasu, "The Vertical Instability in a Positron Bunched Beam," Phys. Rev. Lett. **74** (1995), pp. 5044-5047.
5. R. A. Rosenberg, K. C. Harkay, "A rudimentary electron energy analyzer for accelerator diagnostics," NIMPR A **453** (2000), pp. 507-513.
6. R. Macek, M. Borden, A. Browman, D. Fitzgerald, T.-S. Wang, T. Zaugg, K. Harkay, R. Rosenberg, "Electron Cloud Diagnostics in Use at the Los Alamos PSR," Proc. PAC03, Portland, OR, May 12-16, 2003, paper ROAB003.
7. V. Baglin and B. Jenninger, "Experimental Results of a LHC Type Cryogenic Vacuum System Subjected to an Electron Cloud," Proc. ELOUD04 (Ref. 15 below).
8. J. M. Jiménez, "Electron Clouds And Vacuum Effects in the SPS - Experimental Program for 2004," Proc. ELOUD04 (Ref. 15 below).
9. A. Rossi, "SEY and Electron Cloud Build-Up with NEG Materials," Proc. ELOUD04 (Ref. 15 below).
10. Workshop on Multibunch Instabilities MBI97, KEK, Tsukuba, Japan, July 15-18, 1997, KEK Proc. 97-17 (1997). Proceedings: <http://www-acc.kek.jp/www-acc-exp/Conferences/MBI97-N/MBI97.html>
11. ICFA Workshop on Two-Stream Instabilities in Particle Accelerators and Storage Rings, Santa Fe, NM, Feb 16-18, 2000, <http://www.aps.anl.gov/conferences/icfa/two-stream.html>
12. Int'l Workshop on Two-Stream Instabilities in Particle Accelerators and Storage Rings, KEK, Tsukuba, Japan, Sept 11-14, 2001, <http://conference.kek.jp/two-stream/>
13. Mini-Workshop on Electron-Cloud Simulations for Proton and Positron Beams "ELOUD02," CERN, April 15-18, 2002, <http://slap.cern.ch/collective/ecloud02/>
14. 13th ICFA Beam Dynamics Mini-Workshop on Beam-Induced Pressure Rise in Rings, BNL, Dec. 9-12, 2003, <http://www.c-ad.bnl.gov/icfa/>
15. 31st ICFA Advanced Beam Dynamics Workshop on Electron-Cloud Effects "ELOUD04," Napa, California, April 19-23, 2004, <http://icfa-ecloud04.web.cern.ch/icfa-ecloud04/>
16. F. Zimmermann, "Review of Theoretical Investigations on Electron Cloud," ICFA Beam Dynamics Newsletter No. 31.

17. F. Zimmermann, "Review of Single Bunch Instabilities Driven by an Electron Cloud," Proc. E-CLOUD04 (Ref. 15 above).
18. G. Rumolo, F. Ruggiero, and F. Zimmermann, "Simulation of the Electron-Cloud Build Up and its Consequences on Heat Load, Beam Stability, and Diagnostics," PRST-AB **4**, 012801 (2001).
19. R. Macek and the PSR Development Team, "Measurements of Electron Cloud Effects at PSR" and references therein, this Newsletter.
20. P. Thieberger, A. L. Hanson, D. B. Steski, V. Zajic, S. Y. Zhang, and H. Ludewig, "Secondary-Electron Yields and their Dependence on the Angle of Incidence on Stainless-Steel Surfaces for Three Energetic Ion Beams," Phys. Rev. A **61**, 042901.
21. A. W. Molvik, M. Kireef-Covo, LLNL; F. M. Bieniosek, L. Prost, P. A. Seidl, D. Baca, and A. Coorey, LBNL; A. Sakumi, CERN, "Gas Desorption and Electron Emission From 1 MeV Potassium Ion Bombardment of Stainless Steel," LBNL-55045, Mar. 16, 2004, submitted to PRST-AB.
22. L. Wang and J. Wei, "Electron Cloud in the SNS Accumulator Ring" and references therein, this Newsletter.
23. M. A. Furman, "Formation and Dissipation of the Electron Cloud," Proc. PAC03, Portland, OR, May 12-16, 2003, paper TOPC001.
24. V. Danilov, J. Galambos, D. Jeon, J. Holmes, D. Olsen, ORNL-SNS; D. Fitzgerald, R. Macek, M. Plum, LANL LANSCE; J. Griffin, A. Burov, FNAL, "A Study on the Possibility to Increase the PSR e-p Instability Threshold," Proc. PAC99, New York City, March 29th-April 2nd, 1999, paper TUA52.
25. V. Danilov, A. Aleksandrov, J. Galambos, D. Jeon, J. Holmes, D. Olsen, "Multipacting on the Trailing Edge of Proton Beam Bunches in PSR and SNS", Workshop on Instabilities of High Intensity Hadron Beams in Rings, BNL, June 28-July 1, 1999, <http://www.agsrhichome.bnl.gov/AGS/Workshop99/>. T. Roser and S.Y. Zhang, editors, AIP Conf. Proc. No. 496 (AIP, New York, 1999), p. 315.
26. R. Macek, "Sources of Electrons for Stable Beams in PSR", PSR Tech-Note PSR-00-10.
27. M. Pivi and M. A. Furman, "Mitigation of the Electron-Cloud Effect in the PSR and SNS Proton Storage Rings by Tailoring the Bunch Profile," Proc. PAC03, Portland, OR, May 12-16, 2003, paper RPPG024.
28. L. Wang, "Mechanism of Electron Multipacting with Long Bunched Proton Beams: Theory and Simulation," Ref. 14 (above).
29. L. Wang, M. Blaskiewicz, H. Hseuh, P. He, Y.Y. Lee, D. Raparia, J. Wei, S.Y. Zhang, BNL; R. Macek, LANL; "Multipacting and Remedies of Electron Cloud in Long Bunch Proton Machines," Proc. E-CLOUD04 (Ref. 15 above).
30. K. Ohmi, T. Toyama and C. Ohmori, "Electron Cloud Instability in High Intensity Proton Rings," PRST-AB **6**, 114402 (2002); erratum: **6**, 029901 (2003).
31. M. A. Furman and M. T. F. Pivi, "A Preliminary Comparative Study of the Electron-Cloud Effect for the PSR, ISIS and the ESS," LBNL-52872/CBP Note 516, June 23, 2003, <http://mafurman.lbl.gov/LBNL-52872.pdf>
32. G. Bellodi, "Electron Cloud Buildup in the ISIS Proton Synchrotron and Related Machines," Proc. E-CLOUD04 (Ref. 15 above).
33. R. Macek, A. Browman, M. A. Furman and M. Pivi, "Extraction of the Low-Energy Secondary Emission Yield from Electron-Cloud Measurements at the PSR," to be published.

34. R. Cimino, LNF-INFN and CERN; I. R. Collins, CERN; M. A. Furman, LBNL; M. Pivi, SLAC; F. Ruggiero, CERN; G. Rumolo, GSI; F. Zimmermann, CERN, “Can Low Energy Electrons Affect High Energy Physics Accelerators?,” CERN-AB-2004-012 (ABP), LBNL-54594, SLAC-PUB-10350, Feb. 9, 2004 (to be published in Phys. Rev. Lett. vol. **93**).

## 2.10 Theory of Electron Cloud Instability in High Intensity Proton Machines

Mike Blaskiewicz  
mail to: [mmb@bnl.gov](mailto:mmb@bnl.gov)

[Collider-Accelerator Department, BNL](#)  
BNL 911B Upton NY 11973-5000

### 2.10.1 Introduction

The electron cloud instability was first discovered at BINP [1-3] when attempting to overcome the space charge limit by neutralizing the beam. Then, it manifested in the ISR [4,5] and later showed up in the LANL PSR [6-8]. Since that time it has appeared in many positron storage rings as well as in the SPS when working with beams for LHC. Of these, the PSR is most similar to the ORNL SNS and other proposed high intensity proton machines so we begin with a review of the electron cloud instability in the PSR.

### 2.10.2 Review of Data from the PSR [6-9]

Figure 1 shows the time evolution of the instability. The set of traces on the bottom of the figure show the situation at the onset of the instability. The difference signal from the vertical BPM (blue) is small, but clearly present. The signal from the electron detector is also small at 120  $\mu$ s. As the instability progresses the electron detector signal grows. Other electron detectors

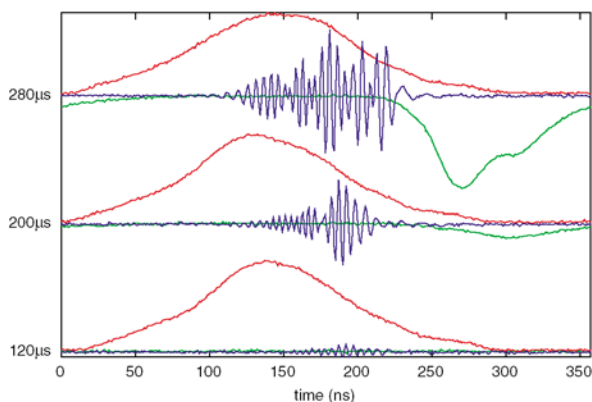


**Fig 1.** Courtesy R.J. Macek. Evolution of the ep instability for a 4.4  $\mu$ C beam. The red trace is the wall current monitor, the blue trace is a vertical beam position monitor difference signal, and the green trace is the electron detector current.

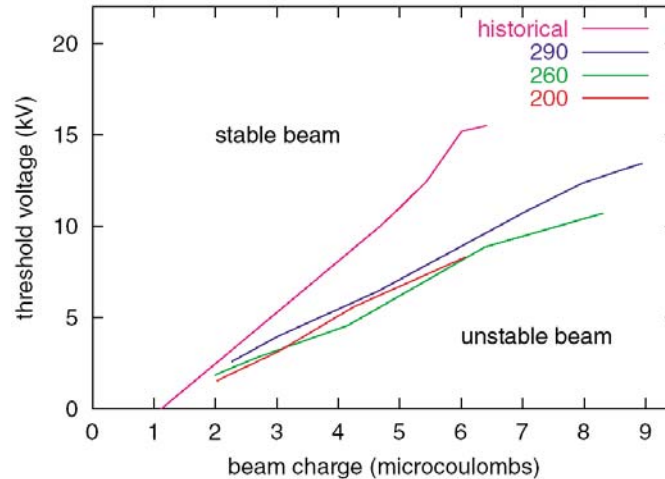


**Fig 2.** Courtesy R.J. Macek. Threshold RF voltage versus beam charge. The historical curve represents the situation before the direct H- injection upgrade. Threshold curves near the end of the extended 2001 run for injected bunch lengths of 200, 260, and 290 ns. are shown for comparison.

showed strong signals at 120  $\mu$ s, but it is clear that the electron cloud does not always fill the entire ring at the onset of the instability. The central set of traces in Figure 1 show the situation at 200  $\mu$ s after injection. Assuming exponential growth, the e-folding time of the instability is about 40  $\mu$ s. Using the cold, coasting beam, transverse instability formula implies a transverse resistance of 100 k $\Omega$ /m. Other data have given twice this value. Also, the carrier frequency of the instability scales as the square root of the beam intensity.

Figure 2 shows the minimum required voltage (threshold voltage) for stable beams as a function of the beam charge, for different epochs and bunch lengths. The historical curve (pink) shows the situation before extended running. Historically, typical bunch lengths were 250 ns. The blue, green and red curves show the situation after extended running for injected bunch lengths of 290, 260, and 200 ns, respectively. There are two striking features. Extended running reduced the threshold voltage, for a given bunch charge, by as much as a factor of two and, the threshold voltage depends on the total charge per bunch but only weakly on the bunch length. In earlier work the threshold voltage even decreased as the bunch length was shortened.

### 2.10.3 Coasting Beam Theory

The carrier frequency of the instability in Figure 1 is of order 200 MHz, while the equivalent bunch length is about 150 ns. With so many oscillations within the bunch it is natural to suppose that the instability can be understood in terms of a coasting beam theory [4-18]. Assume the instability is in the vertical direction ( $y$ ) and, for the purpose of estimating thresholds, that the force due to the electron cloud can be linearized in  $y$ . For no frequency spread in the proton beam the fastest growing transverse mode has a tune shift given by

$$\Delta Q_0 = \Delta Q_{sc} + i \frac{Q_p^2 Q_r}{2Q_y},$$

where  $\Delta Q_{sc}$  is the space charge tune shift,  $Q_y$  is the vertical betatron tune,  $Q_r$  is the quality factor of the oscillating electrons and,

$$Q_p^2 = \frac{e\lambda_e}{2\pi\epsilon_0(\omega_0 a/c)^2 E_T}$$

where  $\lambda_e$  is the magnitude of the line charge density of the electrons,  $\omega_0$  is the angular revolution frequency,  $a$  is the beam radius, and  $E_T$  is the total energy per proton. The electron cloud and beam radii are assumed to be the same. Note that  $Q_p$  is the betatron tune calculated assuming all transverse focusing is due to the electron cloud. The carrier frequency of the instability is the same as the oscillation frequency of the electrons,

$$\omega_e = \omega_0 Q_e = \left(\frac{c}{a}\right) \sqrt{\frac{e\lambda_p}{2\pi\epsilon_0 E_e}},$$

where  $\lambda_p$  is the line charge density of the protons and  $E_e = 511keV$  is the electron rest mass energy. Of course, real beams have some frequency spread and this frequency spread can damp the instability. For carrier frequencies appropriate to the PSR and SNS, the betatron frequency spread is nearly equal to the frequency spread of the nearest revolution line,  $\delta\omega = \omega_0 \delta Q = \omega_e |\eta| \delta p/p$ , where  $\eta$  is the frequency slip factor and  $\delta p/p$  is the fractional momentum spread of the beam. Whether a beam is stable or not depends on the complex number  $\Delta Q_0/\delta Q$  with the threshold corresponding to a magnitude of order one. For PSR and SNS parameters, the magnitude of  $\Delta Q_0$  is dominated by the space charge tune shift. For a given bunch charge and RF voltage, a short bunch has a higher peak current and a lower momentum spread than a long bunch. If one assumes that the instability threshold is dominated by the space charge contribution it is easy to show that RF voltage  $V_{rf}$ , bunch length  $\tau_b$ , and number of protons per bunch  $N_p$ , satisfy  $N_p \propto V_{rf} \tau_b^3$  at the instability threshold [9]. Looking back at Figure 2 an immediate problem arises. While the linear scaling with RF voltage is reproduced, the simple model predicts a strong dependence on bunch length. The data show little, if any, dependence on bunch length, so this coasting beam theory is missing a fundamental ingredient. One obvious point is that the PSR beam is bunched longitudinally. Another, more subtle, difference between this coasting beam theory and the actual PSR is that the transverse distribution of the PSR beam is roughly Gaussian. For a Gaussian distribution, the space charge tune shift depends on betatron amplitude and the spread in space charge tune shift with betatron amplitude is comparable to the average value of the space charge tune shift. The following two sections address these points.

#### 2.10.4 Bunched Beam Theory

For long bunched beams, the linearized theory of the electron cloud instability is theoretically similar to the theory of impedance driven transverse instabilities [9-14].

There are two main differences. The electron oscillation frequency depends on the longitudinal position within the bunch, varying as  $\omega_e \propto \sqrt{I_p(t)}$ , where the instantaneous proton beam current varies in time as it passes through the, nearly stationary, electron cloud. Also, the electron line density can undergo a sharp increase near the trailing edge of the proton bunch (see

the top trace in Fig 1). The first of these effects has been considered via tracking [9,11] and analytically within the context of a centroid or beam breakup model [14]. The instability threshold for the simulations has been compared with the predictions of the coasting beam theory [9]. It was found that the coasting beam theory using values near the center of the beam gave similar thresholds. Similar agreement was found for a semi-analytic method based on rectangular bunches [9]. The effect of varying electron line density was also considered in the beam breakup formalism [14], but threshold estimates are difficult. In any case, it seems unlikely that increasing the electron density near the tail of the proton bunch leads to stabilization. Adding the complication of bunched beams did not reproduce the insensitivity to bunch length shown in Figure 2.

### 2.10.5 Nonlinear Space Charge

For beams with a roughly Gaussian cross section, the space charge tune shift varies strongly with betatron amplitude. There has been much discussion on this effect, and varied opinions exist.

Consider a coasting beam with transverse coordinates  $x$  and  $y$  in the smooth focusing approximation. We assume that the effect of the electrons can be modeled via a linear impulse response function so their effect is formally equivalent to a transverse impedance. We will consider the Vlasov equation to first order in perturbation theory. Assume that the instability is vertical and consider a single, unstable betatron sideband. The coherent force is generated by a phase space density given by

$$f_0(J_x, J_y) \rho(\delta) + f_1(J_x, J_y, \delta, t) \exp(in[\theta - i\omega_0 t] + iQ_y \omega_0 t - i\psi_y)$$

where  $\theta$  denotes ring azimuth,  $n$  is the longitudinal harmonic number of the perturbation,  $\delta = \omega - \omega_0$  is the main source of Landau damping,  $\rho(\delta)$  is the longitudinal frequency distribution in the unperturbed beam,  $J_y$  is the vertical action,  $\psi_y$  is the vertical angle, and  $f_1$  varies slowly in  $t$ .

Approximate the vertical position by  $y = \sqrt{2J_y/Q_y} \sin \psi_y$  and similarly for  $x$ . The relation is approximate since the nonlinear space charge forces might (and probably do) yield a non-integrable system even for the unperturbed distribution. There are two terms to the coherent force. The electrons (and space charge images) can be handled by an effective impedance. The other part of the coherent force is due to direct space charge. The potential for this force is generated by a translationally invariant Green function  $G(x, y)$  and is given by

$$U_{sc}(x, y, t) = \iint dx_1 dy_1 G(x - x_1, y - y_1) \rho(x_1, y_1, \theta, t),$$

where  $\rho(x, y, \theta, t)$  is the charge density in regular (3 dimensional) space. Next, one needs to insert the assumed form for the distribution and phase average to obtain the potential due to all the coherent forces

$$U_c = U_0(J_x, J_y) + U_1(J_x, J_y, t) \exp(in[\theta - i\omega_0 t] + iQ_y \omega_0 t - i\psi_y)$$

The linearized Vlasov equation reads

$$\frac{\partial f_1}{\partial t} - iU_1 \frac{\partial f_0}{\partial J_y} + i \frac{\partial U_0}{\partial J_y} f_1 + i\delta(n - Q_y + \xi_y / \eta) f_1 = 0,$$

where  $\xi_y$  is the vertical chromaticity and  $\eta$  is the frequency slip factor. Notice that the form of this equation is not changed when we set  $n = 0$ . This means that we are free to choose an equivalent 2 dimensional problem, with no  $\theta$  dependence.

A simple physical model is to consider a set of “particles” which are parallel, charged rods. The x component of the direct space charge force between two particles is

$$F_{sc,x} = C_{sc} (x_1 - x_2) / [(x_1 - x_2)^2 + (y_1 - y_2)^2 + \varepsilon^2],$$

where  $\varepsilon$  is a smoothing length,  $C_{sc}$  quantifies the strength of the space charge force, and a similar expression holds for y. The x component of the coherent force is proportional to the centroid position and velocity and is given by  $F_c = W\bar{x} + \alpha\bar{v}_x$ , and similarly for y. If all the particles have the same horizontal and vertical bare tunes it is straightforward to show that the equations of motion for the centroid do not depend on  $C_{sc}$ . Direct space charge has no effect on the coherent tunes. When there is a distribution of bare tunes things get more difficult. This problem was considered analytically, for a single transverse dimension in [14] and nonlinear space charge was found to have a modest effect for smooth momentum distributions. With very large space charge nonlinearity and a parabolic momentum distribution, a sizeable effect was predicted [9]. More realistic parameters showed a 30% effect [10]. On the other hand, analytical and numerical work by the Princeton group [17] suggest a significantly stronger effect. An additional point is that if nonlinear space charge is important for the electron cloud problem it should also have some impact on impedance driven transverse instabilities.

### 2.10.6 Other effects

For most electron cloud studies the transverse fields due to the beam and the cloud have been calculated in the pancake approximation. In this approximation the beam is sliced longitudinally and for each slice the scalar potential  $\Phi$ , is calculated using a 2-dimensional Poisson equation. The vector potential for the beam is related to the scalar potential via  $A = \hat{z}\nu\Phi$  where  $\nu$  is the average beam velocity. The vector potential for the electrons is usually neglected. Recently, the effect of the actual time dependence has been included in a coasting beam model with one transverse dimension [18]. When the electron oscillation wavelength is large compared to the beam radius the effect is fairly small. However, for some electron cloud simulations the longitudinal bin size is comparable to the beam radius and the Lorentz factor is not too large. For these kinds of simulations it may be necessary to consider the actual space-time dependence of the fields. A finite difference time domain approach is probably overkill. However, optimizing smoothing lengths based on physical considerations seems easy enough.

### 2.10.7 Conclusions

It is difficult to say that we have a good theory of the electron cloud instability in high intensity proton machines. The data shown in Figure 2 are well documented and any good theory should accurately reproduce the scaling laws. Reasonable, quantitative agreement is needed too. To the author's knowledge, only [8] presents a derivation which reproduces the observed scaling. However, the space charge force is neglected in that derivation and one needs a first principles justification for neglecting the largest term in the coherent force. When linear space charge is included, the theory is pessimistic with regard to accelerator performance. Since the theory is pessimistic, a machine designed to be stable using the theory has a good chance of avoiding the instability in practice. This was the philosophy used when designing the SNS.

It is difficult to say what the best approach to solving this problem is. With the lack of bunch length dependence in Fig. 2 it seems unlikely that a coasting beam theory will suffice. The bunched beam models with linearized space charge have not worked either so the next natural step is to include nonlinear space charge in bunched beams. One way is to try a fully 3 dimensional simulation for the bunch and take an impulse response model for the electron cloud. This seems tractable in principle but significant work will be needed to push things far enough to get general results. Adding realistic electrons, even in the pancake approximation, makes things much harder. An alternate approach is to use a "stripped down" version of the direct space charge Green function and approximate it with something like  $G(x, y) \approx A \cos(kx) \cos(ky)$ . The point here is that the sum rule for cosines can be used to create a fast algorithm. Another approach is to consider the bunched beam stability problem with nonlinear space charge in a semi-analytic way. One might try the techniques used in Y. H. Chin's MOSES and other bunched beam eigenvalue codes. The difficulty here is that the coherent tune will be "buried" inside dispersion integrals associated with the nonlinear space charge and octupole forces. The author is looking into a model, based on the theory of beam transfer functions, that might alleviate this difficulty, but no solid results have been obtained.

### 2.10.8 References

1. G. I. Budker, G. I. Dimov, V. G. Dudnikov, "Proceedings of the International Symposium on Electron and Positron Storage Rings", VIII-6-1, Saclay 1966.
2. G. I. Budker, G. I. Dimov, V. G. Dudnikov, A. A. Sokolov, V. G. Shamovsky, "Sixth International Conference on High Energy Accelerators", A-103, Cambridge Massachusetts, 1967.
3. V. Dudnikov, 8th ICFA Beam Dynamics Mini-workshop, Santa Fe, (2000), available online at <http://www.aps.anl.gov/conferences/icfa/two-stream.html>
4. H. G. Hereward, CERN 71-15 (1971).
5. E. Keil, B. Zotter, CERN/ISR-TH/71-58, (1971).
6. D. Neuffer, E. Colton, D. Fitzgerald, T. Hardek, R. Hutson, R. Macek, M. Plum, H. Thiessen, T.S. Wang NIM A **321**, p. 1 (1992).
7. M. A. Plum, D. H. Fitzgerald, D. Johnson, J. Langenbrunner, R. J. Macek, F. Merrill, P. Morton, B. Prichard, O. Sander, M. Shulze, H. A. Thiessen, T. S. Wang, C. A. Wilkinson, PAC97 p 1611.
8. R. Macek, AIP Conf. **448**, p. 116, (1998).
9. M. Blaskiewicz, M. A. Furman, M. Pivi, R. J. Macek, PRST-AB **6**, 104203 (2003).

10. M. Blaskiewicz, PAC03, p. 302.
11. K. Ohmi, T. Toyama, C. Ohmori, PRST-AB **5**, 114402 (2002).
12. E. Perevedentsev, CERN-2002-001, p. 171 (2002).
13. K. Ohmi, F. Zimmermann, E. Perevedentsev, Phys Rev E **65**, 016502 (2001).
14. T. S. Wang, P. J. Channell, R. J. Macek, R. Davidson, PRST-AB **6**, 014204 (2003).
15. M. Blaskiewicz, PRST-AB **4**, 044202 (2001).
16. R. C. Davidson, H. Qin, P. H. Stoltz, T. S. Wang, PRST-AB 054401, 1999.
17. H. Qin, E. Startsev, R. C. Davidson, PRST-AB **6**, 014401 (2003).
18. R. A. Bosch, PRST-AB **6**, 074201 (2003).

## 2.11 Measurements of Electron Cloud Effects at PSR\*

Robert Macek and the PSR development team\*\*

mail to: [macek@lanl.gov](mailto:macek@lanl.gov)

[Los Alamos National Laboratory](#)

P.O Box 1663 Los Alamos, NM 87544, USA

\*Work conducted at the Los Alamos National Laboratory, operated by the University of California for the U.S. Department of Energy under Contract No. W-7405-ENG-36

\*\* A. A. Browman, M. J. Borden, D. H. Fitzgerald, R. C. McCrady, T. Spickermann and T. J. Zaugg, LANSCE Division, Los Alamos National Laboratory.

### 2.11.1 Abstract

Various electron cloud effects (ECE) including the two-stream (e-p) instability at the Los Alamos Proton Storage Ring (PSR) have been studied extensively for the past five years with the goal of understanding the phenomena, mitigating the instability and ultimately increasing beam intensity. The specialized diagnostics used in the studies are two types of electron detectors, the retarding field analyzer and the electron sweeping detector - which have been employed to measure characteristics of the electron cloud as functions of time, location in the ring and various influential beam parameters - plus a short stripline beam position monitor used to measure high frequency motion of the beam centroid. Highlights of this research program are summarized along with more detail on recent results obtained since the ECLOUD'02 workshop. Recent work includes a number of parametric studies of the various factors that affect the electron cloud signals, studies of the sources of initial or "seed" electrons, additional observations of electron cloud dissipation after the beam pulse is extracted, studies of the "first pulse instability" issue, more data on electron suppression as a cure for the instability, and observations of the effect of a one-turn weak kick on intense beams in the presence of a significant electron cloud.

### 2.11.2 Introduction

Well-established electron cloud effects (ECE) at the Los Alamos Proton Storage Ring (PSR) include the two-stream e-p instability and electron-cloud generation by trailing-edge multipactor [1-6]. After a brief review of these, the main focus of this paper will be on the results of more

recent work on issues regarding e-cloud buildup, some unresolved issues still under study and first results on the beam response to a weak kick.

### 2.11.2.1 Two-stream e-p instability at PSR

The fast transverse instability observed since the commissioning of PSR has long been characterized [1] as a two-stream instability arising from the coupled motion of the proton beam and a low energy electron cloud. Some of the most convincing evidence for this conclusion is the observed frequency spectra (modes) for the unstable beam motion near threshold examples of which are shown in Figure 1 for two different beam intensities. The central frequencies for each band occur at the calculated “bounce” frequency for electrons in the space charge potential of the proton beam and vary as the square root of beam intensity as expected from the coasting beam formula below for the electron bounce frequency,  $f$ .  $N$  is the number of protons in the ring,  $a$  and  $b$  the horizontal and vertical half sizes of the beam cross-section,  $R$  the mean radius of the ring and  $f_e$  (the fractional neutralization) is the ratio of the electron density to the beam density.

$$\omega_e = Q_e \Omega_0 = 2\pi f = \sqrt{\frac{2Nr_e c^2 (1 - f_e)}{\pi b(a + b)R}}, \quad f \approx 230 \text{ MHz (6.1 } \mu\text{C)}$$

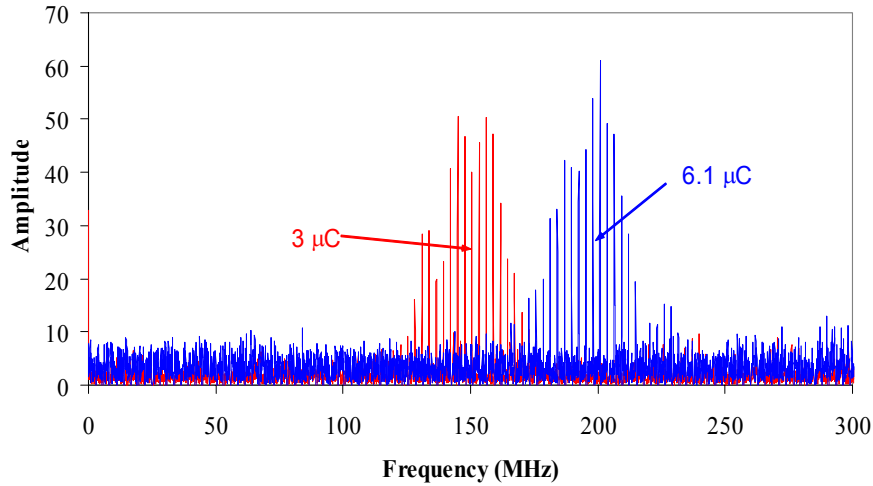


**Fig. 1.** Plot showing the spectra of betatron sidebands from a stripline BPM (vertical difference signal) taken during unstable motion near threshold for two different intensities (6.1 and 3  $\mu\text{C}$ /pulse respectively).

Another important feature of the instability is the threshold behaviour plotted in Figure 2. The definition of threshold (for bunched beams with the rf on) used at PSR is based on an experimental procedure that yields reproducible results at the 3-5% level (on buncher voltage). A fixed amount of charge is accumulated and stably stored for  $\sim 500 \mu\text{s}$  before extraction. The buncher voltage is slowly lowered until the instability appears near the end of the store as evidenced by the appearance of significant high frequency beam centroid motion on a stripline BPM, accompanied by significant beam loss ( $\sim 5\%$ ) for  $\sim 50\%$  of the macropulses.

The linear behaviour in Figure 2 is a feature that has been reproduced many times since 1998. It is predicted in coasting beam centroid models if the fractional neutralization is constant

over the entire range of intensity variation. Since the evidence shown later does not support a constant fractional neutralization, explanation of this behaviour is still an open issue.

Control of the instability at PSR has been achieved by various measures which increase Landau damping including higher buncher voltage (more momentum spread), inductive inserts (equivalent to more rf voltage), multipole fields (magnetic sextupoles and octupoles), and coupled Landau damping using a skew quad [2,3]. There is some evidence that the transverse coupling introduced by vertical closed orbit offsets in sextupoles is responsible for much of the improvement using sextupoles. Mitigation by measures to suppress the electron cloud is more ambiguous and is discussed later in this paper.

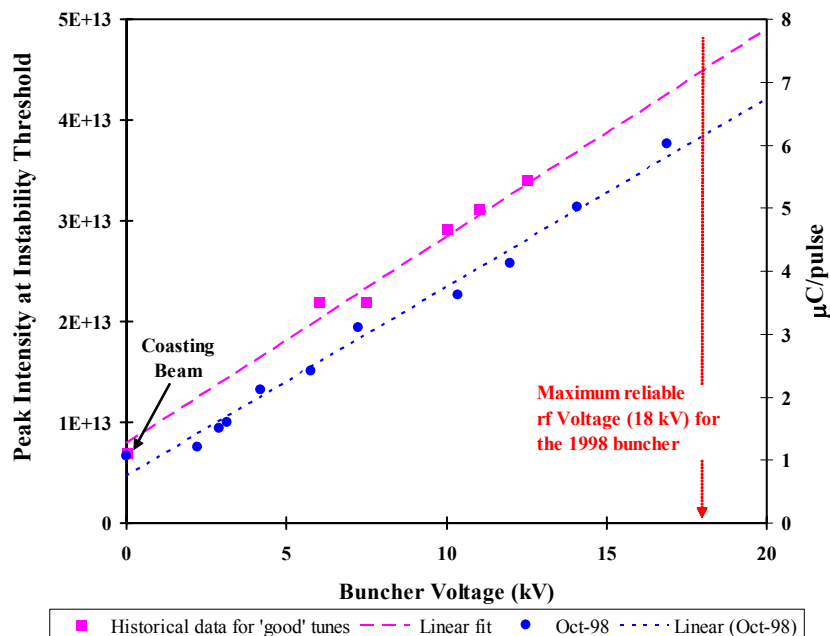


**Fig. 2.** Plot of threshold intensity as a function of rf Buncher Voltage. The square points are historical data for operational beams prior to the direct H<sup>-</sup> injection upgrade in 1998 and the blue circles in Oct 1998 after the upgrade.

### 2.11.2.2 Trailing edge multipactor

The origin and characteristics of the electron cloud driving the instability have been key issues in the search for greater understanding of the e-p instability at PSR. Biased collection electrodes were the first diagnostics used to detect electrons in PSR. They provided indications of significant numbers of electrons being generated in some type of avalanche process [7] for beams close to instability threshold but the signals were not easily interpreted. Since then, two types of more suitable detectors have been used successfully to better characterize the electron cloud at PSR. The first is the Harkay-Rosenberg retarding field analyzer (RFA) [8] to which were added fast electronics in order to observe the time structure of the electrons striking the wall [9]. The time information was important for identifying trailing edge multipactor.

Representative samples of the signals from such a detector located in a relatively low-loss straight section and for stable beams are shown in the plot of Figure 3. Signals for several values of the repeller voltage are shown in proper time relationship to the beam current signal. The

detectors collect electrons striking the wall with energies higher than the value set by the negative repeller voltage, thus providing data on the cumulative energy spectrum, an example of which is plotted in Figure 4.

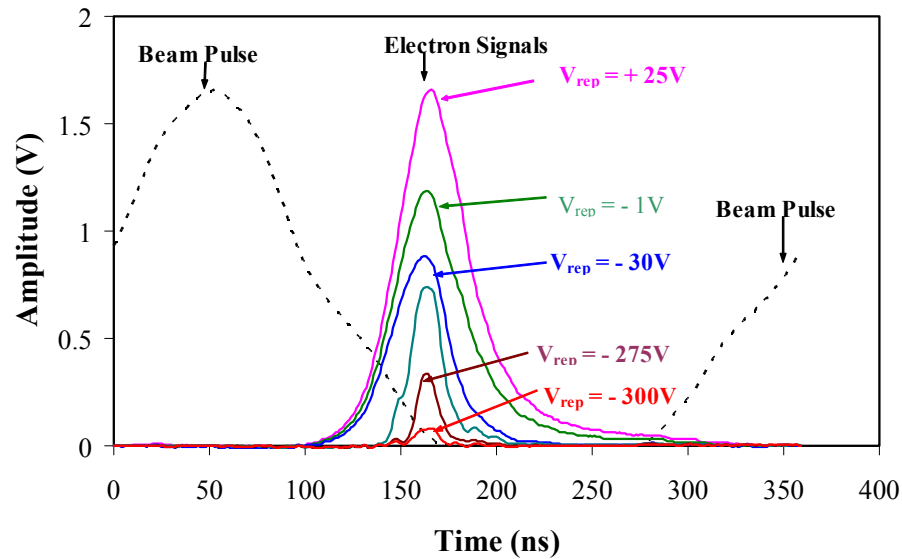


**Fig. 3.** Examples of electrons signals observed with an RFA shown in time relation to the beam.

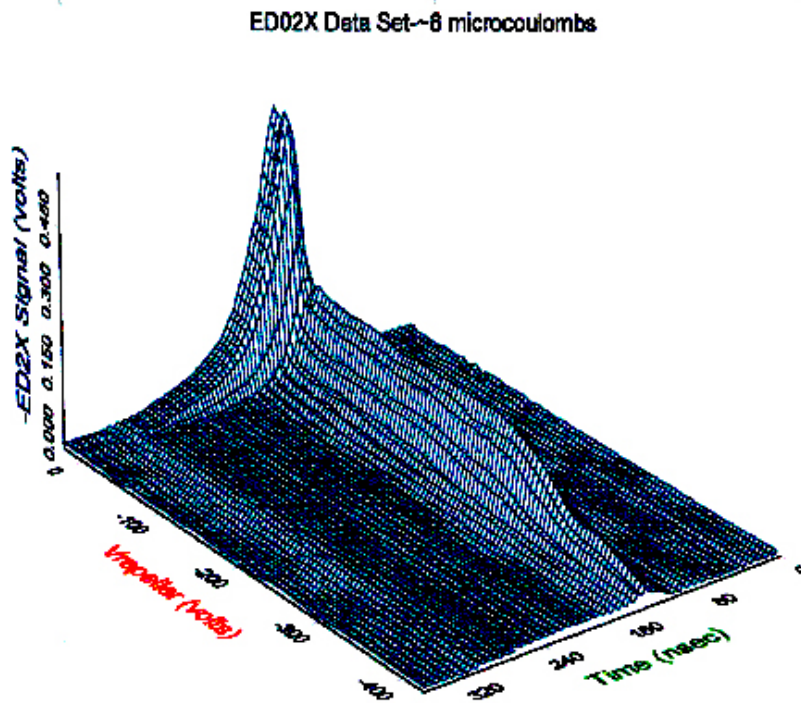


**Fig. 4.** The three-dimensional plot of RFA signals as a function of time and repeller voltage shown here provides a cumulative energy distribution of electrons striking the wall.

Relatively “cold” electrons born at the wall (say from beam losses) after the peak of the beam will be accelerated and then decelerated by the beam space charge fields and will strike the

wall with some additional energy beyond their initial value. These “multipacting” electrons build up exponentially on the trailing edge of the beam pulse and peak at the end of the beam pulse. In addition to multipactor electrons, electrons captured from the gap at the beginning of the pulse will also be ejected at the end of the bunch. In general, the higher energy electrons appear in a shorter pulse. The signal level at the peak implies  $\sim 400\text{-}500 \mu\text{A}/\text{cm}^2$ . This is a large flux of electrons, in fact it is 5 orders of magnitude higher than the  $\sim 2\text{nA}/\text{cm}^2$  expected from residual gas ionization, assuming that the electrons generated in one passage of the beam pulse emerge in an approximately 40 ns pulse at the end of each beam pulse.

The electrons signals from the RFA which peak at the end of the bunch are referred to as “prompt” electron signals in contrast to electrons surviving the “gap” between successive passages of the beam bunch.

Simulations of electron cloud build-up for the long-bunch proton beams of PSR [5,10] are in good agreement with the shape, timing and energy spectra of prompt (multipactor) signals measured in drift spaces. The amplitude is also in reasonable agreement, given the large uncertainties on the number of seed electrons and the SEY of PSR chambers.

### 2.11.2.3 Observation of electrons surviving the gap between bunch passages

A key issue for understanding the instability is the number of electrons surviving passage of the gap to be captured by the next beam pulse, oscillate against the protons throughout the pulse and therefore drive the two-stream instability. These are not determined by the flux striking the wall at the end of the gap. To resolve this issue the electron sweeping diagnostic was developed which could measure the number surviving the gap.

The electron sweeper [9] is basically an RFA with an electrode opposite the RFA opening which can be pulsed to sweep electrons from the pipe into the RFA. Figure 5 shows signals from the electron sweeper in a drift space of section 4. The blue curve is the beam pulse. The green is the signal from the collector of the electron sweeper and the red is the high voltage pulse applied to the sweeper. These are shown in proper time relation with the beam pulse. Prompt electrons are observed at the end of the beam pulse since the detector functions as a large area RFA until the HV pulse arrives. The “swept” electron signal at the end of the gap is narrow, as expected, and its integral provides a lower limit of  $\sim 1\%$  on the average beam neutralization by the electrons that survive the gap. This is in the range needed to explain the instability threshold in a simple centroid model [1,3].

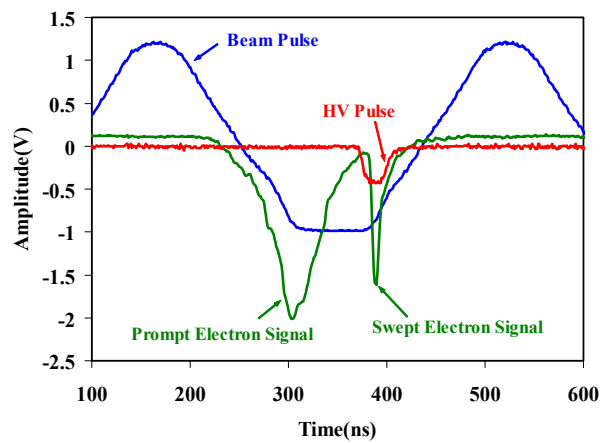


**Fig. 5.** Signal from the electron sweeping diagnostic.

The electron sweeping diagnostic has been used to measure the electrons in the pipe as a function of time after the passage beam pulse. By sweeping electrons after passage of the last pulse in the ring (just before extraction) one measure electrons surviving well beyond the usual 100 ns gap. As can be seen in Figure 6, where both the peak and the integral of the swept electron peak are plotted, either of these signals has a long, approximately exponential tail which is still observable after 1 microsecond.

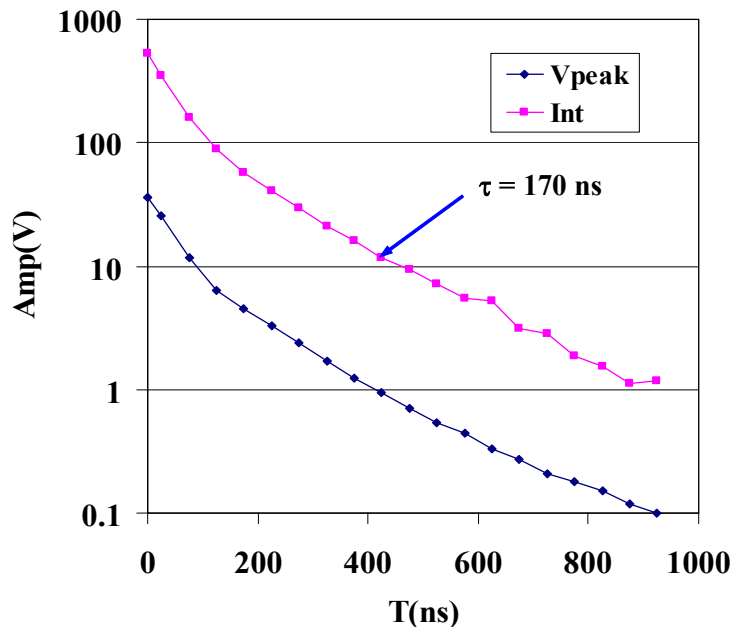


**Fig. 6.** Electron dissipation as measured with the electron sweeping diagnostic.

The decay time constant for the exponential tail is  $\sim 170$  ns and implies a high reflectivity for the low energy electrons left in the pipe. A simple calculation yields a secondary emission yield (SEY or  $\delta$ ) of  $\sim 0.5$  for electrons with energies of 2-5 eV (the peak energy of true secondary electrons). Simulations of electron dissipation by Furman and Pivi [10] agree in detail with this data for a value of  $\delta(0)$  of  $\sim 0.5$ . This somewhat surprising result is consistent with more recent measurements of SEY down to very low energy incident electrons.

Parametric studies of electron dissipation decay time (in the region of the approximately exponential tail beyond 200-300 ns) over the past 3 years show that it is insensitive to beam intensity, TiN coating, beam scrubbing and location in the ring or the extraction line. This suggests that the SEY for very low energy electrons (2-5 eV) is insensitive to the same variables.

The electron sweeper was also used to simultaneously measure the prompt and swept electrons as a function of intensity as shown in Figure 7. In this experiment all control variables were held constant - buncher voltage, accumulation time etc - except the intensity which in this example was varied by moving the stripper foil to control the amount of beam injected.

These plots show that the prompt electron signal varied strongly with intensity, in fact, as the 10th power over the entire range. The swept electrons measured at the end of the gap varied somewhat more slowly as the 7th power but saturated above 5-6  $\mu\text{C}/\text{pulse}$ . This high intensity region is the region of greatest interest for the PSR improvement program and could explain why

the threshold intensity doesn't hit a brick wall in this region since the fractional beam neutralization from the electrons surviving the gap is roughly constant in the saturation region.

Saturation of the electrons surviving the gap is presumably due to the space charge forces in the electron cloud in the beam free region. These forces will tend to cause more rapid expansion of the cloud which counters the rapid build-up of electrons fed into the gap by the prompt electrons striking the wall at the end of the bunch.

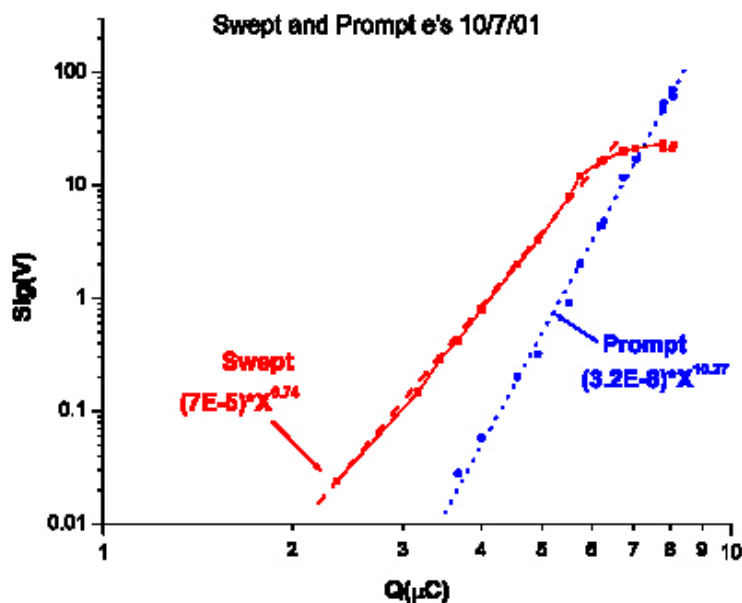


Fig. 7. Prompt and swept electrons signal amplitudes plotted as functions of beam intensity ( $Q$ ).

### 2.11.3 Recent studies on electron-cloud buildup

#### 2.11.3.1 Parametric Studies

In the past 2-3 years numerous parametric studies of e-cloud signals have been made to determine the parameters that have the most influence on e-cloud characteristics. Table 1 summarizes the results of the many parameter variations and their effect on the prompt or multipacting electron signal. As shown earlier (e.g. Figure 7), beam intensity has a strong effect on the multipacting signal. A power law fits the data reasonably well with an exponent that varies from 2-10 depending on location and amount of beam scrubbing. The effect of several variables will be discussed in later sections. The effect of added beam in the gap was observed to increase both the prompt electron signal and the electrons surviving the gap. The increase in the latter is consistent with enough additional electrons to neutralize the added beam in the gap.

**Table 1.** Summary of Parametric Studies

Variable	Effect on the prompt electron signal
Beam intensity	Strong effect $\sim I^n$ , $n=2-10$
Longitudinal bunch profile	Significant effect
Transverse profile	Strong effect, more electrons in direction of major axis
Beam scrubbing	Factor of $\sim 5$ reduction over several months
Beam losses	Linear in local losses
Ring vacuum	Linear in local pressure
Location in ring	Significant effect related to other variables at that location
TiN coatings	Mixed results
Weak solenoid field	Factor of $\sim 50$ reduction at 20 G
Added beam in gap	Increase in signal and in electrons surviving the gap

Parametric studies of the cumulative energy spectra as functions of intensity, location in the ring, beam scrubbing and TiN have been made but are still being analyzed. In addition, observations have been made of electron signals in the presence of sub-threshold coherent motion and some for unstable beam.

### 2.11.3.2 Source strengths of primary electrons

The primary initial or seed electrons are a crucial input to the simulations. Most simulations have assumed that the dominant source is electrons born at the wall from grazing angle proton beam losses taken as uniform around the ring with 100 electrons per lost proton. The measured beam losses at PSR for  $\sim 8 \mu\text{C}/\text{pulse}$  beams imply an average loss rate of  $4 \times 10^{-6}$ /proton/turn if taken as uniform around the ring. These parameters are a useful starting point in the absence of better information and yields simulation results in rough agreement with measurements for the drift space of section 4 in PSR. The agreement is fortuitous since the beam losses in PSR are far from uniform around the ring and the angular distribution of beam particles striking the wall near the electron detectors is not measured or simulated.

The 100 e/proton has been justified using the model by Sternglass [11,12] which is supported by the measurements of Thieberger et al at BNL [13]. In this model, depicted in Figure 8, electrons liberated by energy loss (dE/dx) processes can emerge from the surface if they are produced in the thin,  $\sim 1\text{nm}$ , escape zone. This leads to  $1/\cos(\theta)$  dependence, which implies that the number of electrons is a very strong function of the grazing angle of incidence.

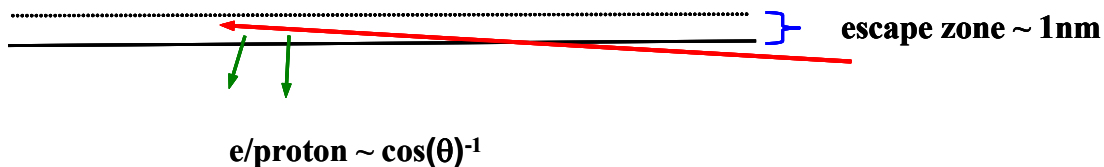


**Fig. 8.** A schematic is shown which illustrates the Sternglass model for electron production from grazing angle interactions of a beam halo particle (red line) with the wall.

Detailed information on the angular distribution for the lost protons incident on the chamber walls near the electron detectors is not available and therefore the 100e/lost proton number is probably best treated as an upper limit. Furthermore, the loss rates are far from uniform around ring and vary by as much as a factor of 1000. Grazing angle losses from foil scattering occur mainly in the quads and it would be largely secondary particles scattered from the primary loss points that would reach the regions where the various electron detectors are located.

When the information from the local loss monitors is considered the resulting picture still remains puzzling. A stronger prompt signal is consistently observed in section 4 than in sections 2 and 9 where the losses, as measured by local loss monitors or local activation, are an order of magnitude higher. See the Appendix and Figure 24 for a layout of the PSR including the various electron detectors. The ratios of electrons ( $R_e$ ), local beam losses ( $R_L$ ) and activation ( $R_A$ ) with respect to those in section 4 are listed in Table 2. Even in section 1, where the losses are a factor of 50 higher, the electron signal is only a factor of 6 higher after accounting for the smaller solid angle.

There are a number of possible explanations for the higher relative signals in section 4 of the ring. The local loss monitor or activation data does not provide suitable information on the angular distribution of the radiation striking the walls which could be different in the various sections of the ring. More precise information on the distributions of radiation striking the walls in the vicinity of the various electron detectors is needed before one can know if there is a true discrepancy. Better information on the distributions may be possible from detailed simulation and tracking of lost protons and their secondary products but would require a significant effort to carry out.

**Table 2.** Ratios of electrons ( $R_e$ ), local beam losses ( $R_L$ ) and activation ( $R_A$ ) with respect to section 4 of the ring

Section	$R_e$	$R_L$	$R_A$
9	$\sim 1/3$	$\sim 17$	7-35
2	$\sim 1/2.5$	$\sim 7$	$\sim 2$
1	$\sim 6$	$\sim 55$	$\sim 50$

The SEY could be different at the locations of the various detectors. Perhaps the higher loss regions were scrubbed at a higher rate. In addition, the vacuum pressure in section 4 was consistently higher than in sections 2 and 9 by a factor of 5-10 and might be responsible for the higher electron signals in that region.

With these issues in mind, a number of experiments were performed where the beam losses and vacuum pressure were systematically varied. Results are presented and discussed in the next two sub-sections.

### 2.11.3.3 Primary Electrons from Beam Losses

Beam losses were varied by either moving the stripper foil at injection or by local closed orbit bumps. Moving the stripper into the beam systematically increased the losses from foil scattering but changed no other beam parameter. Relative changes in the losses were monitored by measuring the foil current which is a measure of foil hit by the stored beam. In the other method, local closed orbit bumps were introduced and relative losses measured with a local loss

monitor. In both cases it was found that the electron signals showed considerable linear variation with the beam losses as shown in Figures 9 and 10 below.

The equations shown on the graphs of Figures 9-11 are linear fits to the data and  $R^2$  is the “coefficient of determination” for the fit. In Figure 9 the prompt electron signal is plotted as function of changes in beam losses from foil scattering as monitored by the foil current. It shows that the electron signal is linear in the change in losses. The intercept at zero foil current is the contribution from the other loss components (primarily excited states of  $H^0$ ) plus any contribution from the vacuum. The excited states do not change with foil position so do not contribute to the slope of the curve.

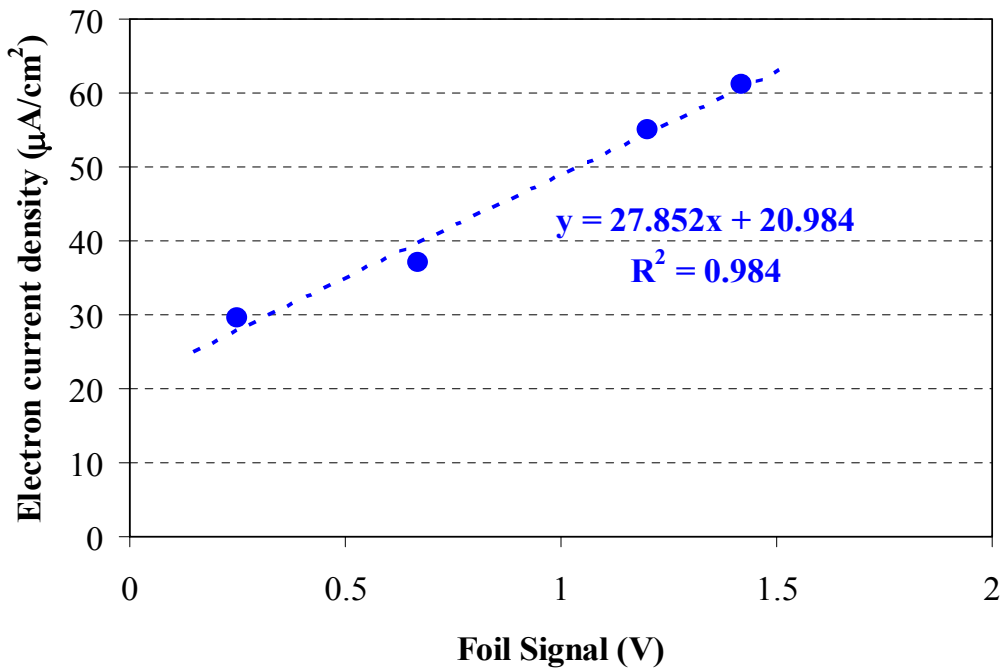


**Fig. 9. Effect** of varying losses (from foil scattering) on the prompt electron signal in drift section 4 for a beam intensity of  $5.8 \mu\text{C}/\text{pulse}$ .

Local losses were changed by local horizontal closed orbit bumps (-6 to +8 mm) for the curves plotted in Figure 10. Two identical RFAs were installed at this location, one in the horizontal and the other in the vertical. Local losses were monitored by a nearby loss monitor, designated as LM59. Here, as in Figure 9, the prompt electrons signals are linear in the losses over the range loss variation. It should be noted that the vertical signal is an order of magnitude larger, presumably due to the larger beam size in the vertical. It is also worth noting that two parameters are changed simultaneously - the losses and the horizontal beam center. The latter could influence the space charge fields and therefore the multipactor “gain”.

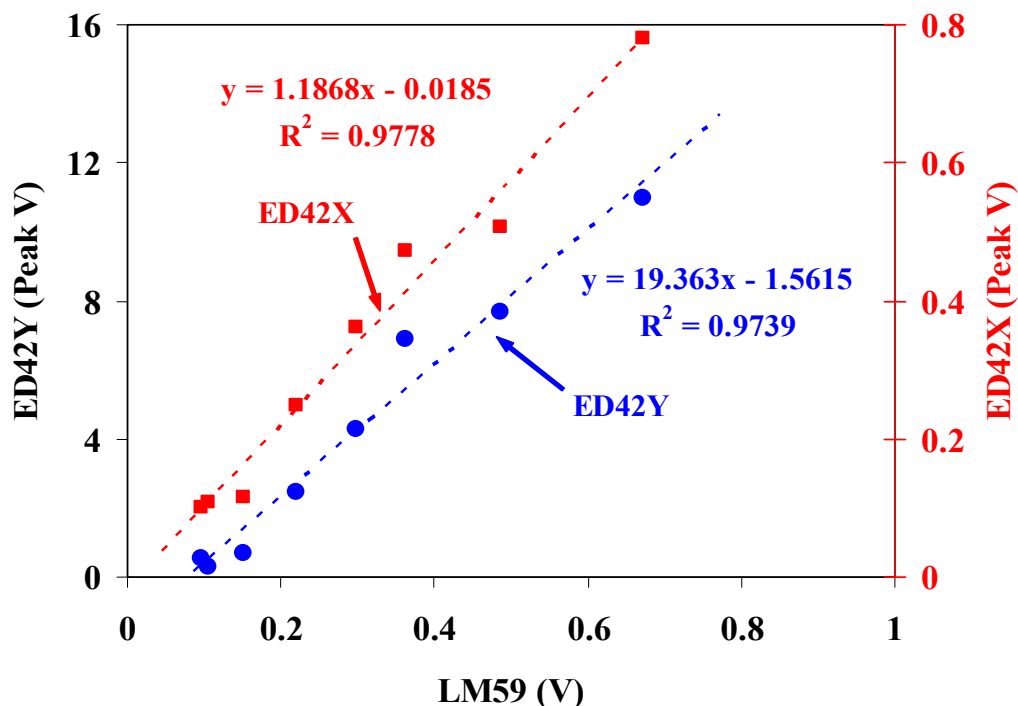


**Fig. 10.** Prompt electron signals from ED42X (detector in the horizontal plane) and ED42Y (detector in the vertical plane) plotted against the variation of local losses produced by horizontal closed orbit bumps in section 4 of PSR. The beam intensity was  $8.1 \mu\text{C}/\text{pulse}$  ( $5 \times 10^{13}$  protons per pulse).

The sizeable change in electron signals with losses indicates that losses make a significant, possibly dominant, contribution to the primary or seed electron strength. The linear response with losses indicates that the multipactor amplification process has not yet saturated for these conditions. If the multipactor gain could be estimated, say from simulations, then it would be possible to estimate the number of seed electrons from the electron signals. In addition, if the flux of lost particles striking the wall in the vicinity of the electron detectors were known, then it would be possible to estimate the number of seed electrons per lost particle. There is some expectation that the particle tracking code ORBIT [14], under development at ORNL, could be used to simulate both the beam losses and the multipactor signal. Another code such as LAHET or MCNPX would be needed to simulate the production of secondary products at the proton loss points.

#### 2.11.3.4 Primary Electrons from Residual Gas Ionization

In the experiment discussed in this section, the vacuum pressure was varied in a number of sections of the ring by turning off ion pumps and monitoring both the pressure and electron signals while the pressure gradually rose. Ion gauges in the drift spaces near the electron detectors monitored the vacuum pressure.

The graph of Figure 11 is one example that illustrates the effect of vacuum pressure on both the prompt and swept electron signals. The vacuum pressure measured by an ion gauge, IG41, in section 4 varied from  $\sim 100$  nTorr to 2000 nTorr and the prompt signals in these two detectors (ES41Y and ED42Y) increased linearly by approximately a factor of 6 over this range. However, the electrons surviving the gap (swept electrons labeled as ES41Y swept) were unchanged. Other detectors in sections 2 and 5 (ED22Y and ED51Y) gave similar results. Beam intensity was  $8.2 \mu\text{C}/\text{pulse}$  ( $5 \times 10^{13}$  protons per pulse) during the data collection.

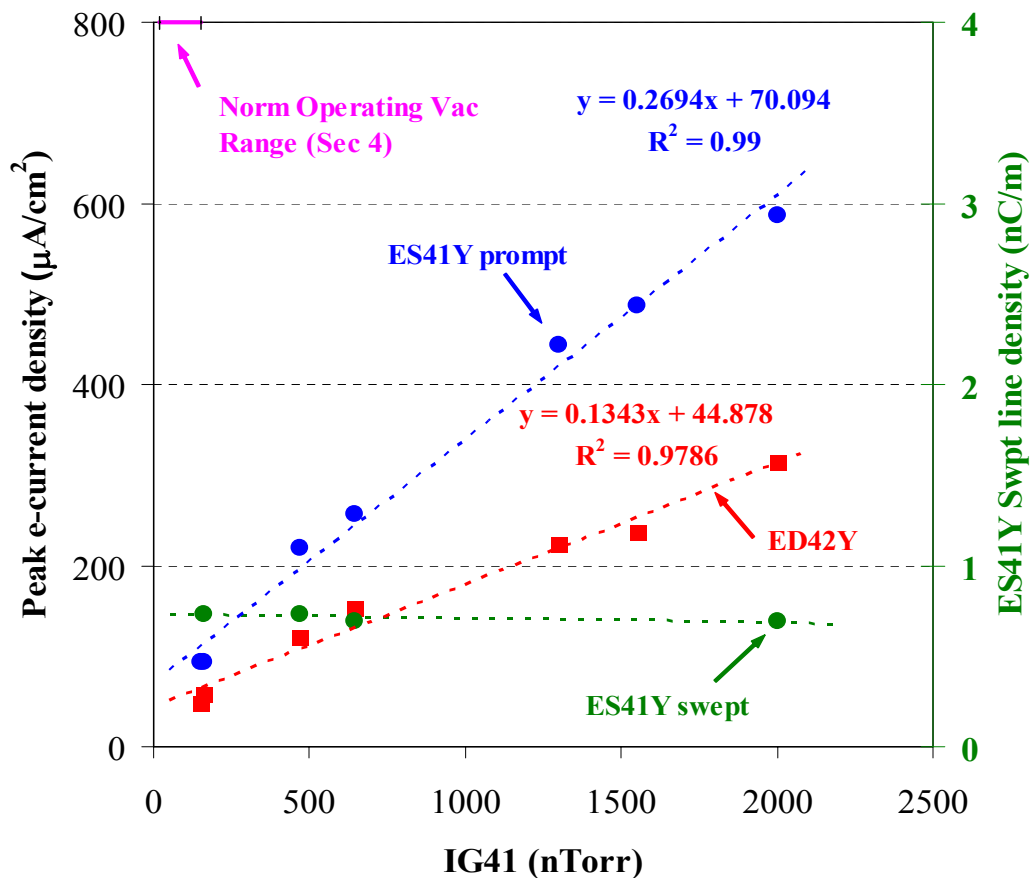


**Fig. 11.** Prompt electron signals (ES41Y and ED42Y) plus the swept electron signal at the end of the gap (ES41Y swept) are plotted as a function of the vacuum pressure in section 4. Beam intensity was  $8.2 \mu\text{C}/\text{pulse}$  ( $5 \times 10^{13}$  protons per pulse).

From the fits to these curves we can infer that the vacuum pressure contributes 25-30% of the signal at  $10^{-7}$  Torr where section 4 was operating at the time of these measurements. This section has typically run with somewhat higher pressures than most but not all of the other sections of the ring. The slope of the ES41Y fit is approximately twice that of the ED42Y fit which could be due to a difference in the multipactor gain at these locations. The two detectors are  $\sim 1$  m apart and the beta functions will be somewhat different at these two locations hence slightly different beam sizes.

This experiment suggests that residual gas can make a non-negligible contribution to the seed electrons (depending on the actual vacuum pressure). The assumption in most simulations to date has been that residual gas ionization can be neglected because it is small and the electrons are created near the beam not the wall. However, the vacuum effect might be from the ions that are driven to the wall by the beam potential. These hit with as much as 2-3 keV and can release secondary electrons at the wall ( $\sim 0.3$  for 2 keV ions) [14]. To our knowledge, this effect has not yet been included in the published results from simulations.

#### 2.11.3.5 *Suppression of the electron cloud formation*

Suppression of the electron cloud build up is widely expected to provide a cure for electron cloud instabilities. Over the years various measures to suppress electrons have been tried at PSR with rather limited results. Initially, various clearing fields over as much as 15% of the ring circumference were tried [3, 16]. However, it can be argued that these measures were not implemented everywhere in the ring and therefore may have had only a very limited effect on the average electron cloud density.

In recent years TiN coatings and solenoid windings were tested. Beam scrubbing as a result of ongoing beam operations over time has been effective in reducing the electron cloud and improving the instability thresholds.

Tests of TiN coatings gave mixed results which are tabulated in Table 3 below.

**Table 3.** Tests of TiN coatings.

<b>Test</b>	<b>Date</b>	<b>Beam Intensity</b>	<b>Prompt electron reduction factor</b>
Section 5	1999	8.5 $\mu\text{C}/\text{pulse}$	>100
Section 9	2002	8 $\mu\text{C}/\text{pulse}$	$\sim 40$
Section 4	2002	7 $\mu\text{C}/\text{pulse}$	None initially
Section 4 after beam scrubbing*	2002	8 $\mu\text{C}/\text{pulse}$	$\sim 5$

\*After 2 months of operations at 100  $\mu\text{A}$  @ 20 Hz.

TiN coatings suppressed the prompt signal by a factor of 100 or more for the same beam intensity in our first test in section 5 in 1999 but provided no improvement in more recent tests in section 4 while TiN gave a factor of 40 reduction of the prompt signal in section 9. The TiN coated section 4 has improved with beam scrubbing but at the same rate as other sections in the ring. The section 4 results are a puzzle since the components were coated at SLAC at the same time as those for section 9. While the section 4 results are disappointing and not understood, one can not rule out some contamination or compromise of the coated surfaces without destructive testing.

Weak solenoidal magnetic fields suppressed prompt electron signals by a factor  $\sim 50$  at 20 G [3] in a short section of PSR but when solenoid windings were installed over about 10% of the ring they had no effect on the instability threshold. This suggests that the drift spaces with windings may not be a significant source of electrons that drive the instability.

We have found that beam conditioning (scrubbing) over time reduced the prompt electron signal and improved the instability threshold curves. The first evidence at PSR for the beneficial effects of beam scrubbing on the e-p instability was the repeated observation starting in 1997 that

the e-p instability had a lower threshold ( $\sim 20\text{-}30\%$ ) during start-up after a 4-6 month down period for annual maintenance activities and improved a few weeks later. It was studied more systematically in 2000 as shown in Figure 12 where the threshold intensity is plotted as a function of rf buncher voltage while holding other beam parameters such as accumulation time, bunch length, injection offset fixed. The improvement is rapid at first and slows down after a few days of operation but was still improving after a few weeks of operation at  $\sim 100\ \mu\text{A}$  (at 20 Hz). The threshold intensity curves continued to improve into 2001 and 2002 and appear to have stopped improving by late summer of 2002.

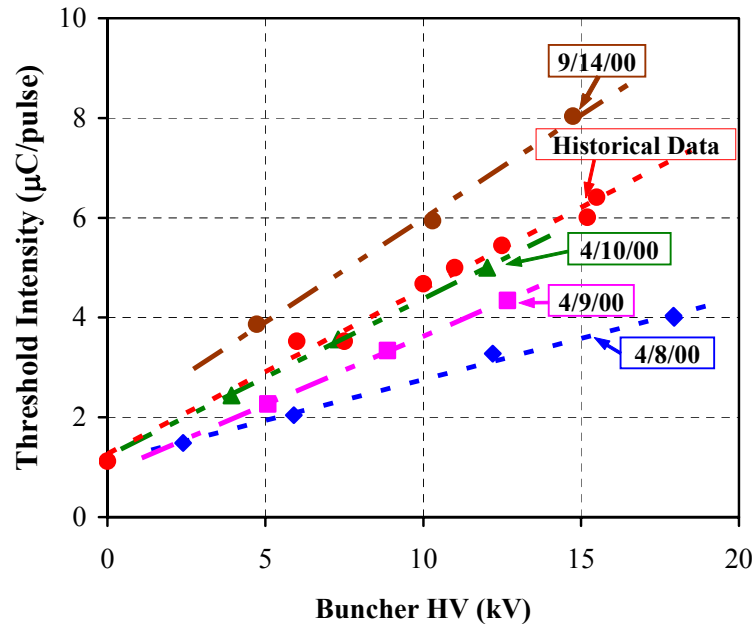


**Fig. 12.** Threshold intensity curves showing the benefit of beam conditioning (scrubbing) during 2000 when there were no inductive inserts in PSR.

In the 2002 run cycle we embarked on a systematic effort to correlate the improvement in instability threshold curves with changes in the electron signals. The two plots in Figures 13 and 14 show the prompt electron signals as functions of time over a several month period in 2002 for an  $8\ \mu\text{C/pulse}$  beam.

The four electron detectors plotted in Figures 13 and 14 are located in three different sections of the ring. ED02X (in horizontal plane) is located 0.6 m downstream of the injection stripper foil and ED22Y (in vertical plane) is in the centre of the drift space of section 2. ED42Y and ES41Y (both in vertical plane) are both located in the drift space of section 4 and are about 1 m apart.

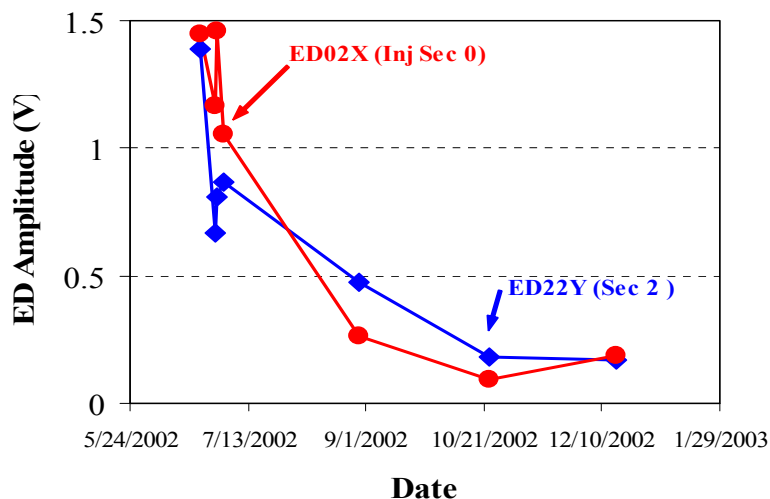


**Fig. 13.** Plot showing the reduction of the prompt electron signal amplitudes for two RFAs (ED02X and ED22Y) during 2002 operations.

Signals from these 4 detectors show a similar factor of 5-10 reduction in signal over this period of time during which PSR operated rather continuously at  $100\text{-}120\ \mu\text{A}$  @ 20 Hz. It should also be mentioned that the swept electron signal (in the drift space of section 4) at the end of the gap showed only a factor of two reduction during this period.

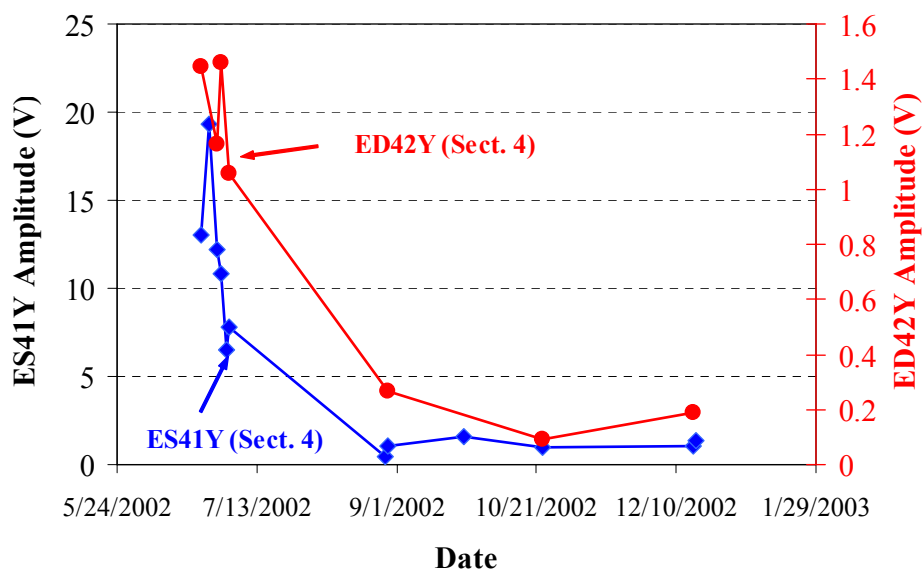


**Fig. 14.** Plot showing the reduction of the prompt electron signal amplitudes for two RFAs (ED42Y and ES41Y in section 4 of the ring) during 2002 operations.

#### 2.11.4 Some unresolved issues

Several rather puzzling phenomena which appear to be unique to PSR will be discussed in this section.

### 2.11.4.1 Recovery after sweeping the gap

An interesting and not understood effect of sweeping electrons from the gap is shown in Figure 15. The next prompt signal after sweeping the gap is reduced substantially and takes several turns to recover. Such behaviour does not appear to this extent in most simulations for PSR.

Electrons surviving the gap are captured by the next passage of the beam pulse and will be ejected at the end of the beam pulse and thereby make a contribution to the prompt signal. Sweeping the electrons from the gap means they will be removed from the next prompt signal. It is surprising if they account for 75% of the prompt signal and take several turns to build up as the data in Figure 15 suggests. We have taken data [17] with the sweeper pulsed every turn for 10 turns with the result that the swept signal has the same amplitude for each of the successive turns. This means the electrons surviving the gap and captured by the beam pulse are not changing after sweeping the gap. Some other mechanism is needed to explain the recovery of the prompt signal.

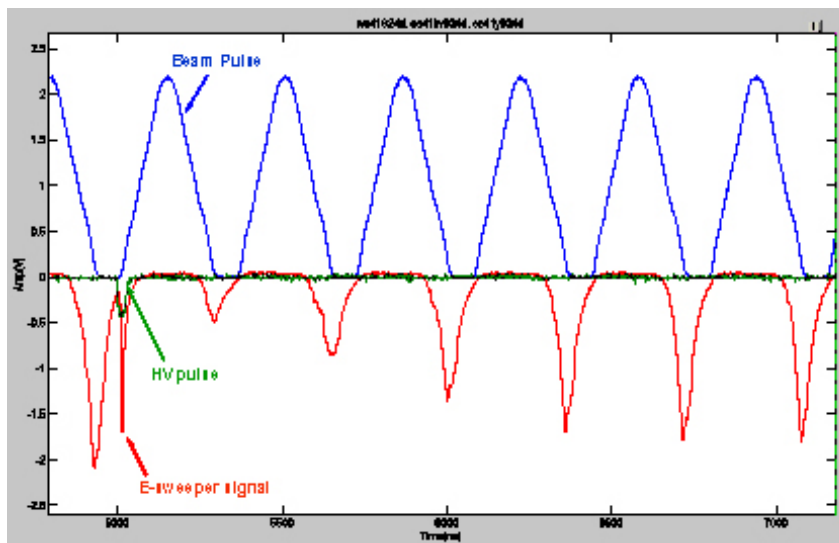


**Fig. 15.** Recovery after sweeping the gap. The red signal is from the electron sweeping diagnostic, the green is the high voltage pulse (500 V) applied to the sweeping electrode and the blue signal is the beam current signal from a wall current monitor (WC41) in the ring.

### 2.11.5 Electron bursts

Many of the traces shown earlier have been averages over a number (typically 32) of macropulses and don't reveal the turn-to-turn fluctuations. A rather puzzling phenomenon that is not yet understood is the burst character of prompt electron signals shown in Figure 16 for detectors in section 4 of the ring.

The simultaneous traces in Figure 16 cover 110 turns near the end of accumulation. The prompt electron signals vary greatly from turn to turn with some coherence over several turns. The phenomenon varies from day to day and is much more pronounced now than 3 years ago and maybe connected to the gradual decline in strength of the electron signals due to scrubbing of the surface. The electron detector signals in Figure 16 show more fluctuations than are typical

in order to illustrate the range of the fluctuations. Another set of traces shown in Figure 17 are more typical of the bursts observed during the past 2-3 years.

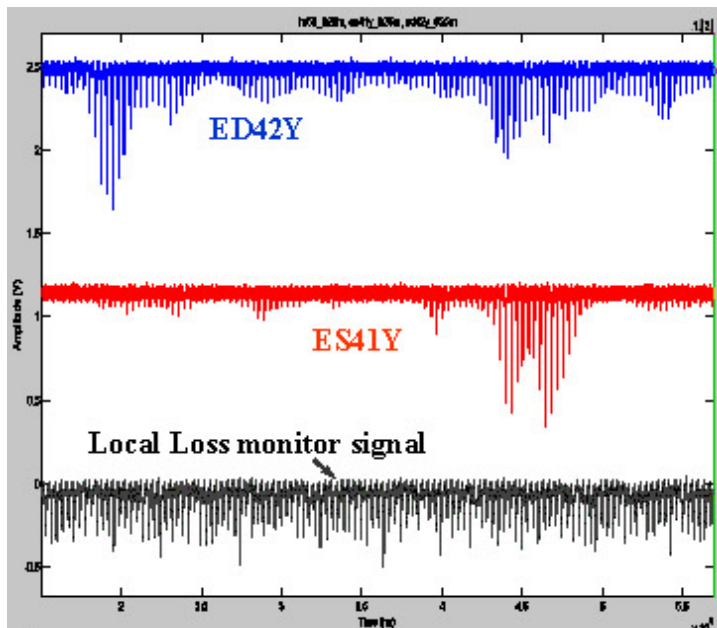


**Fig. 16.** Multi-turn (110) sequence of signals from two electron detectors (ES41Y and ED42Y) and a local loss monitor in section 4 of the ring.

The bursts show no correlation with fluctuations in the local losses but do show some correlation with detectors in other locations around the ring as shown in Figure 17, which suggests that the beam structure somehow causes the bursts. In fact, large increases in the prompt signals and the bursts have been observed when the ring was operated under conditions of low buncher voltage where a microwave-like longitudinal instability introduces  $\sim 60$  MHz modulation on the beam pulse. The coherence of the bursts over several turns suggests that the betatron oscillations of the beam centroid might be involved. However, no clear correlation with BPM signals has been found. Not all locations show the same levels of fluctuations e.g., the fluctuations near the stripper foil are much lower than those in section 4. Basically the bursts are an unresolved issue. It is hard to claim understanding of the electron cloud buildup without some reasonable understanding of the cause of the fluctuations.

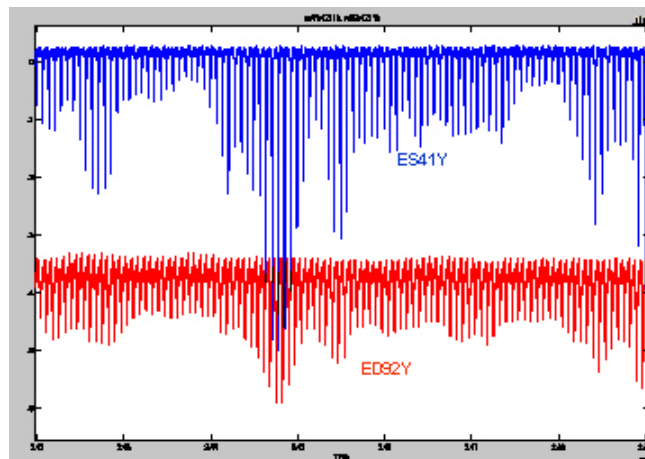


**Fig. 17.** Multi-turn ( $\sim 100$ ) sequence of signals from two electron detectors (ES41Y and ED92Y) located in section 4 and section 9 respectively.

#### 2.11.5.1 1<sup>st</sup> pulse instability

Another curious phenomenon and one that has an adverse impact on single pulse operation of PSR is the so-called 1st pulse instability. It shows up on the 1st pulse in the ring after the beam has been off the several minutes. We see that the 1st pulse is unstable but subsequent pulses are stable. There is a significant difference in the instability threshold curves for the 1st pulse compared with those for subsequent pulses as shown in Figure 18.

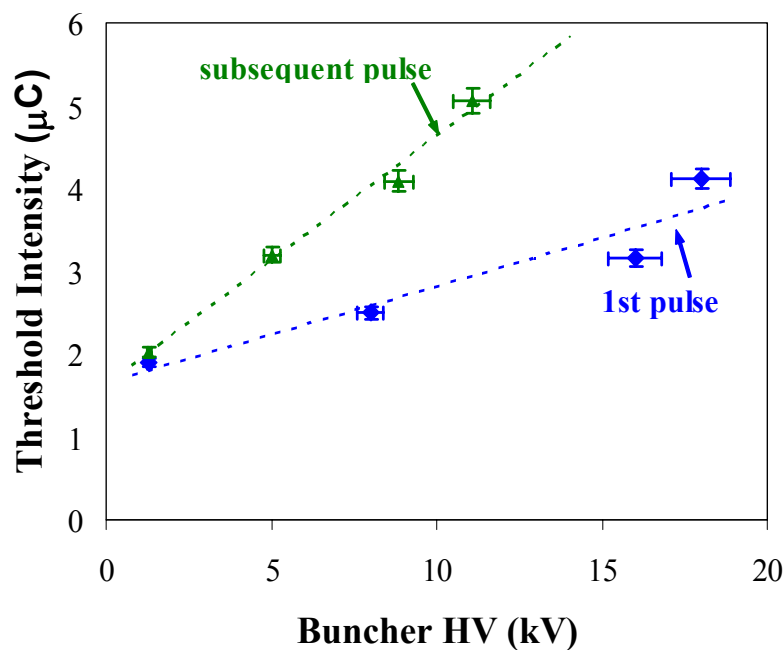


**Fig. 18.** Instability threshold curves for the 1<sup>st</sup> unstable pulse (blue) and subsequent pulses (green).

The transverse emittance for the beam used for the typical single pulse operation of PSR is perhaps a factor of two smaller than used for the spallation neutron program at the Lujan center. Such a beam was used during the measurements for Figure 18 but is not required for the 1st pulse instability which is also observed for larger emittance beams.

The 1<sup>st</sup> pulse instability phenomenon has been observed for several years especially when resuming operations after the annual shutdown for maintenance when the ring has been up to air. The instability disappears after a few weeks of beam operations, presumably due to some sort of beam conditioning. It is interesting that the minimum wait time increases gradually with continual beam operations. Another curious observation is the increased foil current for the 1st pulse compared with others even for a stable first pulse as shown in Figure 19. Yet another interesting observation was made by the operators who found that a low intensity precursor (down a factor of 50) generally prevents the 1st pulse instability.

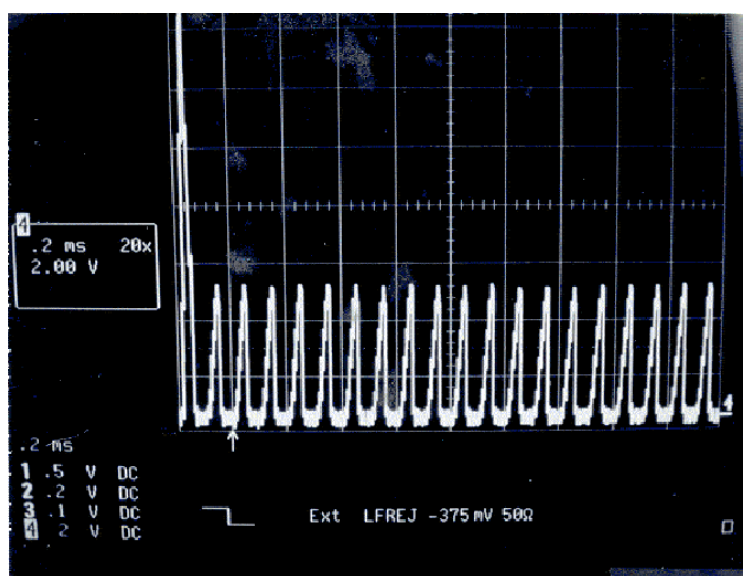


**Fig. 19.** Sequential capture of the foil current signal for 20 consecutive macro pulses after a several minute beam off time.

A satisfactory explanation for the 1<sup>st</sup> pulse instability phenomenon has not yet been developed although there are several ideas (speculations) being offered. The wait time is comparable to the monolayer formation time for the vacuum pressures in the ring, which suggests that adsorption and desorption of gases on vacuum surfaces may be involved.

One hypothesis assumes that certain gases (water?) that increase the secondary emission yield and are slow to pump down are slowly adsorbed on the vacuum chamber walls during the wait time. The strong electron cloud from beam induced multipacting on the first pulse creates an unstable pulse which further increases the electron bombardment. Gases under electron bombardment are desorbed quickly (a strong pressure pulse is observed on a fast ion pump monitor) and the secondary emission yield is reduced for subsequent pulses. It is difficult to understand how the low intensity precursor pulse would create an electron cloud intense enough to desorb the gas and reduce the SEY sufficient to avoid the instability. The foil current data of Figure 19 and the precursor result suggest that it may be related to gas re-adsorption on the stripper foil. At this time we do not have a plausible model that explains all of the observations.

### 2.11.6 Beam response to weak kick

Another interesting set of observations is the beam response to a weak kick. For these experiments we were motivated by the possibility of obtaining information on wake functions/impedance in the presence of an electron cloud from the time-domain analog of beam transfer function measurements. The conditions for the plot shown Figure 20 are: a beam intensity of  $5 \mu\text{C}/\text{pulse}$  and a buncher voltage of 11 kV which is twice as much as at the instability threshold for this intensity.

It took a surprisingly weak, single-turn kick (1kV) at the end of injection to elicit a strong beam response at  $5 \mu\text{C}/\text{pulse}$ . At lower intensities, 4 times this kick was needed to measure betatron tunes. For the experiment shown in Figure 20, the beam centroid motion grew to a large enough amplitude to cause significant beam losses 300-400  $\mu\text{s}$  after the kick. In many ways the response is similar to what is seen in the e-p instability.

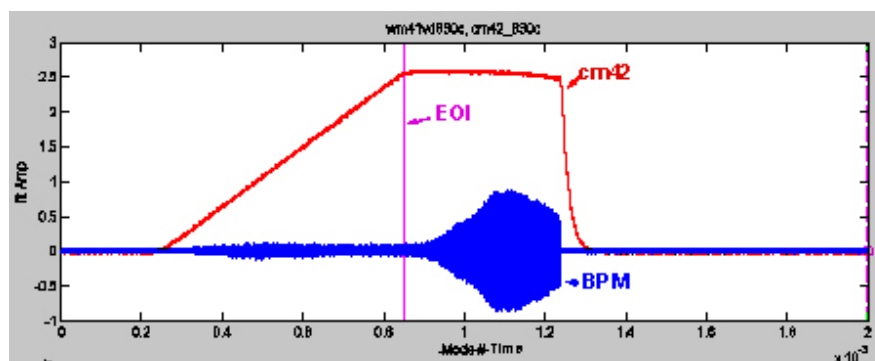


**Fig. 20.** Beam response to a weak one-turn vertical kick applied at the end of injection (EOI). The blue trace is the vertical difference signal from a stripline BPM and the red trace is current monitor (CM42) showing the stored current in the ring during accumulation and a 500  $\mu\text{s}$  store.

A spectrogram of the stripline BPM signal after the kick is shown in Figure 21. The initial response to the kick is a low level betatron oscillation that is barely visible. After  $\sim 100 \mu\text{s}$  or so higher frequency betatron sidebands emerge. They quickly broaden to encompass modes up to  $\sim 55$ , which is somewhat lower than you would get for the standard e-p instability at this intensity. For comparison, see Figure 22 which shows the spectrogram of the BPM signal for a  $5 \mu\text{C}/\text{pulse}$  beam that was unstable (buncher 6.81 kV).

Additional data was collected over a grid of intensity, kick strength and “distance” to the instability threshold in the buncher voltage space. In general, the response is stronger both at higher intensity and closer to the standard e-p threshold. This is as far as we have gone in analyzing the data. In time we will try to extract wake functions from the data provide the concept proves applicable to the electron cloud. There are also a few details that need to be worked out such as converting the BPM stripline signal to a position signal.

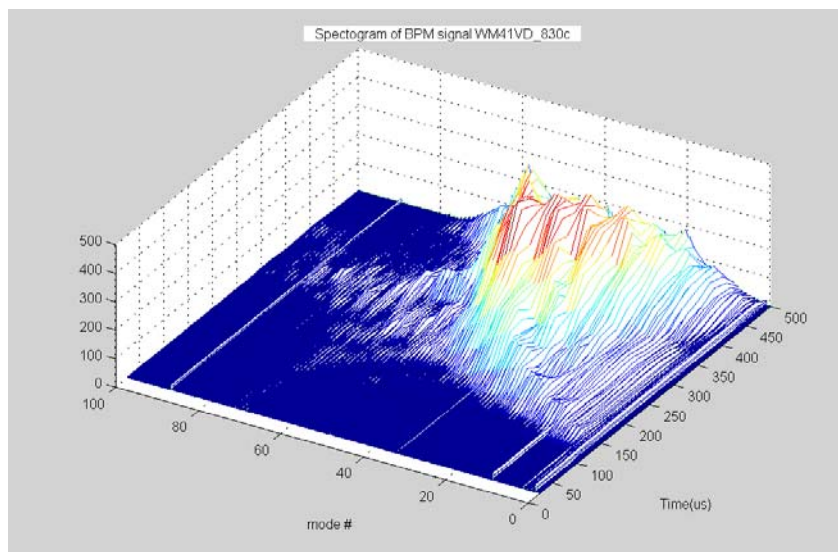


**Fig. 21.** Spectrogram of the BPM signal from the beam response to a weak kick. The origin of the time axis is the time of application of the one-turn kick. The vertical axis is the fft amplitude of the BPM signal.

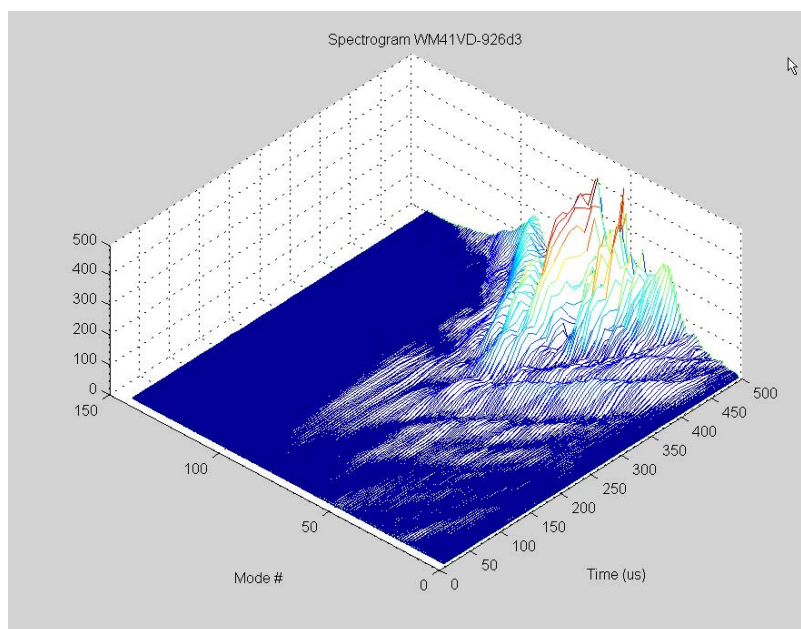


**Fig. 22.** Spectrogram of the BPM signal collected for a  $5 \mu\text{C}/\text{pulse}$  unstable beam. The time origin is the end of injection. The vertical axis is the fft amplitude of the BPM signal.

### 2.11.7 Summary and Conclusions

The long-observed two-stream e-p instability is the most serious ECE at PSR and much work has been done to understand its various aspects. The source and characteristics of the electron cloud driving the instability have been long-standing issues and the subject of much beam physics research at PSR in the past several years. Trailing edge multipactor has been shown in experiments and simulations to generate many electrons in the drift spaces by amplification of primary electrons born near the vacuum chamber walls. The electrons left after the beam pulse passes dissipate more slowly than initially expected with the consequence that a significant number survive the  $\sim 100$ ns gap between successive passages of the beam bunch. The line density of those surviving the gap (in drift spaces) is about 1% of the average proton beam line density (at  $\sim 5$   $\mu\text{C}/\text{pulse}$  beam intensity). An average line density neutralization of 1% is in the range needed to explain the appearance of the e-p instability in centroid models.

This paper has provided a sampling of results from numerous parametric studies made to identify the control variables having a significant effect on e-cloud signals. Beam intensity was found to have the strongest effect on the prompt (multipacting) electron signals. Beam profile shape both longitudinal and transverse also had a strong effect. The prompt electron signals were found to be linear in beam losses and vacuum pressure up to the highest intensity studied (8  $\mu\text{C}/\text{pulse}$ ) indicating that the multipactor amplification process has not saturated at PSR.

The experiments and parameter variations that have been simulated show reasonable agreement between simulations and experiments. More data is available for comparisons but require additional simulations.

The source terms for seed electrons from losses have large uncertainties which could be improved with appropriate beam loss and beam scattering simulations. Primary electrons associated with the residual gas make a non-negligible contribution in some sections of PSR. These may be due to electrons born at the wall from ions driven to the wall by the beam potential.

We have obtained mixed results on methods for suppressing trailing-edge multipactor as a cure for e-p. One of three tests of TiN coatings showed no suppression of the electron cloud while the other two tests showed very encouraging suppression of the multipactor electrons. A test of weak solenoids showed a good suppression (factor of  $\sim 50$ ) of the prompt electron signal but solenoid windings in drift spaces over  $\sim 10\%$  of the ring circumference showed absolutely no effect on the instability threshold. On the other hand, beam scrubbing over time has had a noticeable effect on both the strength of the electron cloud in drift spaces and on the instability threshold. These results might be explained if drift spaces are not the dominant source of electrons driving the instability.

We do not yet have reliable electron cloud diagnostics installed in PSR dipoles or quadrupoles and therefore can not rule out these regions as the dominant source(s) of electron clouds that drive the instability. Quadrupoles could be the dominant source for two reasons: grazing angle beam losses are expected to be largest in quadrupoles where the beta functions are largest and electrons can be trapped in the quadrupole fields after the beam passes. Various simulations are not yet in agreement on the importance of multipacting in quadrupoles at PSR.

The beam response to a weak kick is interesting but awaits further analysis. The 1st pulse instability is an unexplained puzzle as are the electrons bursts and the recovery following a sweeper pulse. Other open issues include the electron clouds in dipoles and quadrupoles and the effectiveness of active damping for e-p instability.

### 2.11.8 Proposals for future work

There is no shortage of issues regarding ECE at PSR that would benefit from additional work in theory, simulations and experiments. In addition to continuing to analyze data already collected and continuing to exploit electron cloud diagnostics presently installed, we can identify crucial issues whose resolution would likely have a major impact on our understanding and control of ECE for long bunch proton machines. These would include understanding the cause(s) of the electron bursts, measuring the electron cloud in magnets especially quadrupoles and testing the feasibility of active damping of the e-p instability at PSR.

#### 2.11.8.1 Electrons in quadrupoles

Electrons in quadrupoles are an unresolved issue for PSR. Simulations by Pivi [18] indicate significant multipacting plus trapping in the quadrupole field after the beam pulse passes. For the same number of seed electrons, he found a prompt signal that is a factor of 5 less than in a drift space. However, the source terms for the seed electrons from grazing angle losses should be considerably larger in the quads. If these are correct then quads might be the location of the strongest electron cloud density.

Not all simulations indicate strong multipacting in quads. Thus, for many reasons it seems crucial to measure the electron cloud in a PSR quad, especially those that are trapped between bunch passages. A concept for doing this sketched below. Fortunately we have extra aperture in the PSR quads where a 17 cm diameter aperture is available but only 10 cm is used for the beam chamber. Thus we can envisage installing an RFA assembly and a sweeper plate and use the assembly much like the sweeping diagnostic installed in drift spaces.

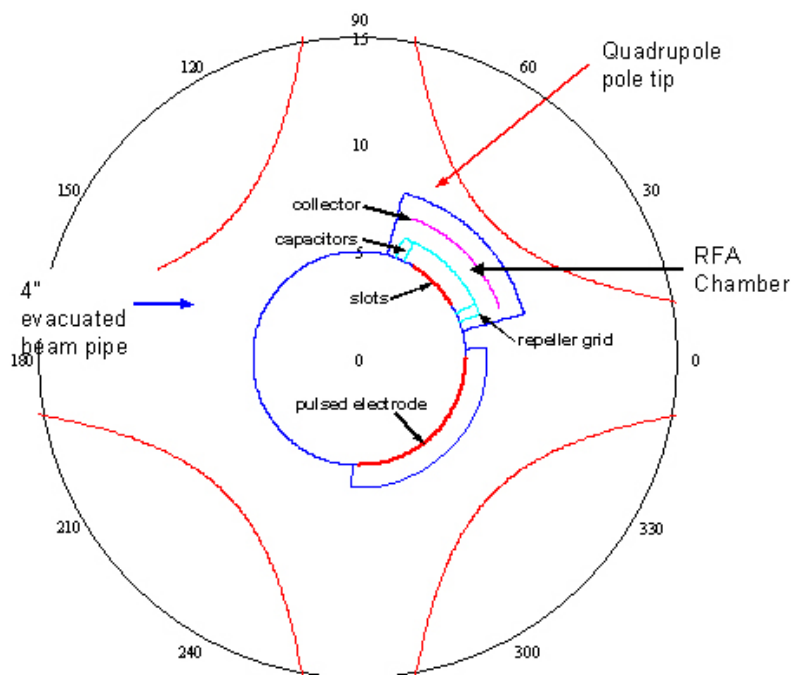


**Fig. 23.** Schematic layout of a proposed electron sweeping diagnostic in a PSR quadrupole.

### 2.11.8.2 Active damping of the e-p instability

Active damping is a possible means for controlling the transverse two-stream e-p instability. The fast growth time and broad frequency content present significant challenges. We are looking at this possibility in collaboration with Prof. S.Y. Lee and students at Indiana University and the accelerator physics group (lead by Stuart Henderson) with Spallation Neutron Source (SNS) project at Oak Ridge National Laboratory. The feasibility of a test of the method at PSR is being discussed.

### 2.11.9 Acknowledgements

Robert Macek would like to acknowledge many useful discussions and other collaborative efforts on ECE in the past few years with Miguel Furman, Mauro Pivi, Katharine Harkay, Richard Rosenberg, Robert Kustom, Mike Blaskiewicz, Ron Davidson, Hong Qin, Slava Danilov, Sasha Alexandrov, Jie Wei, Lanfa Wang, Mike Plum, Tai Sen Wang, Paul Channel, S. Y. Lee and Stuart Henderson. All of the authors wish to acknowledge the technical support from the LANSCE-2 and LANSCE-6 groups who maintain, develop and operate the LANSCE accelerator facilities and who made many valuable contributions to the PSR studies reported here.

### 2.11.10 Appendix: PSR Layout

The present layout of the PSR including the various electron cloud and e-p diagnostics referred to in this paper is shown in Figure 24.

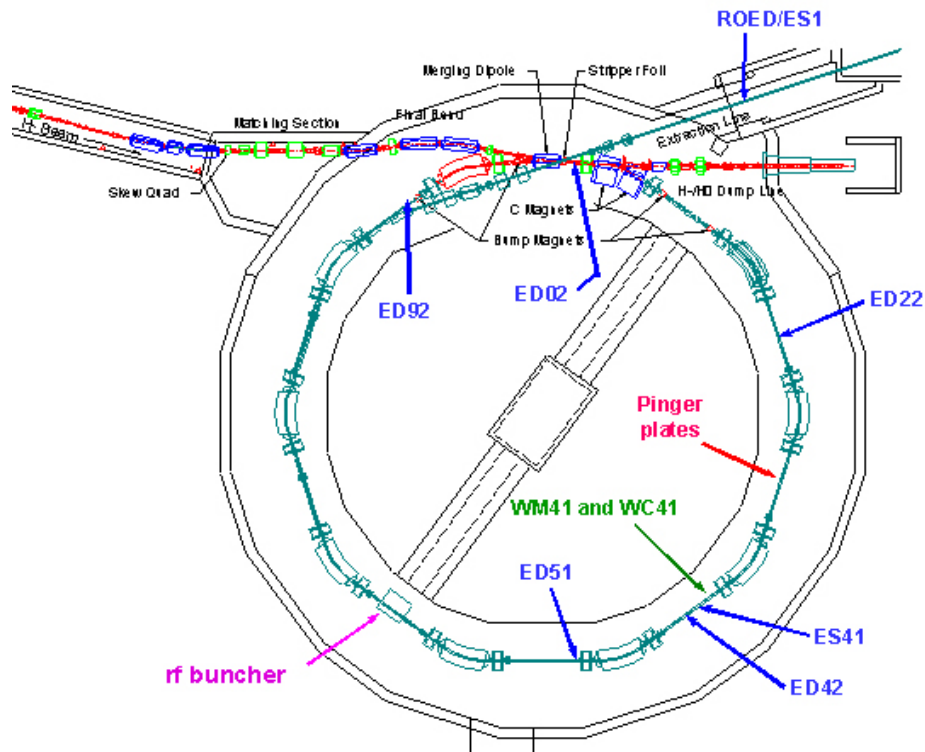


**Fig. 24.** PSR layout including electron detectors and e-p diagnostics.

### 2.11.11 References

1. D. Neuffer et al, NIM **A321**, p.1-12(1992).
2. R. Macek et al, FOAB007, PAC'01, 688(2001).
3. R. Macek, E-CLOUD'02 Proceedings, CERN-2002-001, 259(2002).
4. See contributions to the PRST-AB special collection on Electron Cloud and Two-Stream Interactions in Long-Bunch Proton Beams, at the website: <http://prst-ab.aps.org/speced/TwoStreamSC/>.
5. A comprehensive collection of recent presentations on ECE at PSR can be found at the Midwest Accelerator Physics collaboration website (3/15-18, e-p feedback collaboration meeting), <http://physics.indiana.edu/~shylee/ap/mwawpc/>
6. M. Blaskiewicz et al, PRST-AB **6** 014203 (2003).
7. M. Plum et al, RAR23, PAC'95, 3406 (1995)
8. R. Rosenberg and K. Harkay, NIM A **453** p. 507 (2000)
9. R. J. Macek et al, ROAB03, PAC2003, p. 508 (2003)
10. M. T. F. Pivi and M. A. Furman, PRSTAB **6**, 034201 (2003).
11. E. J. Sternglass, Phys Rev **108**, 1 (1957).
12. M. Plum, PSR TechNote PSR-95-001(1995).
13. P. Thieberger et al, Phys Rev A **61**, 042901 (2000).
14. J. D. Galambos et al, ORBIT Users Manual, SNS/PRNL/AP Technical Note Number 011, Rev.1.
15. E. W. Thomas ed., Atomic Data for Fusion, Vol 3: Particle Interactions with Surface, ORNL-6088 (ORNL-6086 V3) (1985), see p. C-4, C-8, and C-12, <http://www-fadc.phy.ornl.gov/redbooks/three/c/c/c.html>
16. M. Plum et al, PAC'97, p. 1611 (1997).
17. R. J. Macek, PSR Dev Log Book 98, p 60 and 63, (9/17/2001).
18. M. Pivi, private communication to R. Macek, Oct 2003.

## 2.12 Electron Cloud in the SNS Accumulator Ring

L. Wang<sup>\*</sup>, J. Wei<sup>†</sup>, BNL, Upton, NY, USA

Mail to : [\\*WANGL@BNL.GOV](mailto:*WANGL@BNL.GOV)  
[†WEI@BNL.GOV](mailto:†WEI@BNL.GOV)

### 2.12.1 Introduction

Most operators of high-beam intensity machines have encountered electron cloud instability since it was first reported at INP PSR in 1965 [1-12]. For a coasting beam, electrons accumulate at the chamber center due to trapping by the beam potential rather than the beam inducing multipacting. Multipacting, induced by bunched beams apparently causes electrons to accumulate inside the vacuum chamber [13,14] and then interact with the proton- or positron-beam, causing its instability. Experimental observations of electron-cloud instabilities are distinctively different for “short bunches”, where multi-bunch multipacting is expected to be important (PS, SPS, and B factories) and for “long bunches”, where it is dominated by single-bunch, trailing-edge multipacting [15]. The mechanism of beam-induced multipacting is quite

different for the two. The SNS beam is a bunched beam wherein the electron cloud is mainly produced by multipacting. Many studies of electron-cloud buildup in long-bunch proton machines have been done based on numerical methods [16–21]. This report briefly recalls the results of some of our main researches on electron-cloud multipacting in the SNS ring and possible remedies to suppress it. Interested readers are encouraged to consult the formal publications given in the references.

### 2.12.2 Multipacting mechanism

The so-called “trailing edge multipactor” was used to qualitatively explain the mechanism of electron multipacting with a bunched long proton beam [4,15]. Analysis shows that electrons generated before the center of the bunch can be trapped by the beam potential. The oscillation amplitude of trapped electrons can be described by the adiabatic invariant [20].

The many surviving electrons from the last bunch gap modulate the beam dynamics; they may destabilize the beam because they can be deeply trapped inside it. They have weak effect on multipacting due to their long-term trapping and low energy at the chamber surface. On the other hand, electrons born at the wall after the peak of the pulse passes will be accelerated towards the beam center and decelerated after passing through it. They will drift straight to the opposite wall of the chamber, gaining certain energy as they reach it. If the gain is high enough, then the secondary emission yield (SEY) can exceed unity, and be further amplified on each successive traversal of the beam pipe. Electrons born at the wall between the bunches center and tail are the only source of multipacting due to their having a short transit time and sufficient energy when they hit the chamber surface.

A more detailed analysis shows that the electron energy at the wall surface is proportional to the derivative of the beam-line density and inversely proportional to its square root [20]. Therefore, the electrons’ energy at the wall is usually bigger around the bunch tail due to the small beam-line density there, and hence, multipacting is stronger. That can explain why cutting the bunch tail can effectively reduce multipacting [17]. An experiment carried out at the LANL PSR shows that variation of the RF buncher phase can change the beam longitudinal profile and electron signal [22]. Thus, we can optimize the design of a real machine to lower the electrons energy gain. The energy spreader and corrector in the SNS ring can significantly suppress the beam tail [23] and hence, reduce multipacting. Simulation also verified the effect of the beam longitudinal profile on multipacting [20]. The longitudinal profile factor can be used to explain the mechanism involved. Simulation demonstrated that a beam with a Gaussian profile exhibits stronger multipacting than do beams with sinusoidal and elliptical ones. The electron density in SNS ring is close to that with the sinusoidal profile. For the SNS beam, the electron peak energy at the wall is about 300 eV and multipacting starts at 500 ns with 700 ns bunch length. Therefore, multipacting time is about 200 ns. Electrons can cross the chamber more 15 times on average during this period. Assuming the same secondary-emission parameters and electron yield per turn for the SNS and PSR, the simulated electron density is close for these two rings.

### 2.12.3 Important parameters related to multipacting

For a beam with a fixed longitudinal profile shape, both the energy gain and multipacting frequency are proportional to the square root of the beam intensity. Accordingly, the electron cloud is very sensitive to the beam intensity. For example, the electron density inside vacuum

chamber can increase with a factor of 20 if increase the beam intensity from 32  $\mu\text{C}$  to 64  $\mu\text{C}$ . Simulation shows that the signal for electron multipacting does not saturate at high intensity although the density of electrons trapped inside the beam does due to the stronger space-charge effect at the bunch gap since multipacting is stronger for high-intensity beams. This finding agrees with observations from the LANL PSR experiment.

The azimuthal distribution of the electron cloud is related to the shape of the beam transverse profile: there is more of the electron cloud in the orientation of the beam larger dimension. The space-charge force in the direction of the larger direction is stronger and it confines electrons moving along it; then, stronger multipacting occurs there. Browman observed a similar phenomenon in the LANL PSR [24]. There is stronger electron signal in the direction of the larger betatron function. Consequently, the electron cloud may differ in horizontal and vertical directions.

A smaller beam size contributes to a stronger space-charge field and therefore, a larger electron-energy gain and stronger multipacting. The simulated electron density inside the chamber is roughly inversely proportional to the beam transverse size. However, the electron-volume density inside the beam exponentially decreases with its transverse size. Therefore, a big beam is very helpful in reducing instabilities caused by the electron cloud. This is consistent with the PSR experimental study [25] wherein the instability threshold rose by a factor of two when the beam size was increased from 15 mm to 34 mm.

Both analysis and simulation show that electrons surviving from the last bunch gap can be soundly trapped inside the beam until the end of the passage of the next bunch; these electrons are the main source of electron-proton instabilities [26]; those electrons outside the beam have little effect upon its dynamics. Although strong multipacting occurs at the bunch tail, most electrons remain outside the beam. The electron density inside the beam at the tail is the same as at other times. Therefore, the surviving electrons from the last bunch gap cause instabilities. We note that the bunch gap has a very weak effect on the peak electron-line density inside the chamber due to the mechanism of single-bunch multipacting. Therefore, the peak electron-line density inside the vacuum chamber is almost the same during the passage of the first turn and of the following turns. However, the bunch gap contributes to decreasing electron density inside the beam. If the gap is long compared with the decay time of the electron cloud during the bunch gap, the electron density inside the beam will be lowered significantly, and hence the beam instabilities also. When the bunch gap is short, such that the electron cloud cannot decay to zero by the end of the gap, a clearing electrode can be applied to remove the electron cloud at the bunch gap. A weak clearing field is very helpful in reducing the number of electrons inside the beam during the bunch passage.

The protons that remain at the bunch gap because of their wider momentum spread and large pulse width can slow down electron loss at the gap because of the space-charge effect. The percentage of protons at the gap is less than  $1 \times 10^{-4}$  for the SNS design beam. The simulated electron-line density inside the chamber increases 18% and 33%, respectively, for  $1 \times 10^{-4}$  and  $1 \times 10^{-2}$  protons at the gap. However, the electron density inside the beam increases 30% and 300%, respectively, due to their slow decay during the passage of the gap. Because the growth rate of the beam instability is proportional to the electron density inside it, instability may be highly sensitive to the beam at the gap, even though that parameter itself has a weak effect on the average electron density inside the chamber.

The simulated electron density inside the chamber roughly increases linearly with peak SEY, at a rate slower than exponential growth due to the space-charge effect. In contrast, the average

volume electron-density inside the beam approaches saturation for a big peak SEY due to the strong space-charge effect. Because the beam instability is governed primarily by electron volume density inside beam, we conclude that instabilities will saturate at certain peak SEY. However, the heat load generated when the electron cloud hits the chamber surface does not saturate until the peak SEY reaches 2.5.

The gain in electron energy with a long beam, which usually is less than the energy at peak SEY, is much smaller than that with short bunch, such as in B-Factories. Accordingly, a long beam is more sensitive to the energy at peak SEY. Both the electron-line density inside the chamber and the electron-volume density inside the beam increase linearly with the decrement of energy at peak SEY. The latter does not reach saturation because the electron-line density inside the chamber is insufficient. If the energy at peak SEY in the SNS beam falls from 330 eV to 246 eV, the electron density inside the chamber will rise from 12 nC/m to 67 nC/m; the effect is the same as increasing the SEY from 1.74 to 2.07. However, the effect on electron density inside the beam is stronger than increasing the SEY from 1.74 to 2.5. Therefore, a bigger energy at peak SEY can significantly reduce the beam instability.

The number of electrons generated by the residual gas depends on its pressure and temperature. When the vacuum is good, the yield usually is more than one order-of-magnitude less than the yield of electrons by proton loss. These electrons have low initial energy [27] and cannot efficiently obtain energy from the beam when they are released at the bunch tail according to the adiabatic invariant. Because of the absence of multipacting, the electron-cloud density caused by ionization electron is negligible compared with that due to the electrons generated by proton loss, provided vacuum pressure is satisfactory. When the vacuum is poor, notable numbers of electrons will be generated by ionization and all of them can be trapped inside the beam and destabilize it without strong multipacting. However, when ions liberated by beam ionization hit the wall with sufficient energy, they may create a significant number of electrons born at the wall and then these electrons can excite multipacting with the same mechanism as the electrons by beam loss. The estimation of multipacting by these electrons is under way.

#### **2.12.4 Multipacting inside dipole and quadrupole magnetic fields**

Analysis shows that the electron energy gain at the chamber wall surface in a strong dipole magnet has a peak value at the chamber horizontal center that is equal to the energy gain in the drift region, and decreases at both sides [20]. Consequently, multipacting in a dipole magnet depends on the horizontal coordinate. It is the strongest at the chamber center and becomes weak with the increment of the horizontal coordinate. Thus, in dipole magnets, only electrons moving near the center of the horizontal chamber have enough energy at the wall surface so that a multipacting cloud forms there at bunch tail. In today's proton machine, multipacting only can happen at the chamber horizontal center because electron energy peaks there below a few hundreds eV. It is less than 300 eV in the SNS dipole magnet. However, in short-bunch machines, for example, the SPS and B-factories, the energy of an electron hitting the wall surface at the center of the horizontal chamber could be more than thousands of eVs under normal operation. This causes multipacting at two strips near the chamber center [11, 28]. The electron-cloud density inside dipole magnet is about two times less than that in drift region because the area for multipacting is limited in the dipole magnet. The electron cloud is trapped vertically at the chamber center by the beam space-charge force during its passage.

In quadrupole and sextupole magnets, very weak multipacting occurs around the middle of each magnetic pole because only those electrons moving along these field lines might receive enough energy through a mechanism similar to that inside a dipole magnet. The simulated electron-cloud is more than two orders-of-magnitude smaller than in the drift region due to the electrons low energy at the wall surface. Quadrupole and sextupole magnetic fields are mirror fields that may trap electrons via the mirror-field trap mechanism. However, trapping requires that the bunch length is shorter than the period of gyration [29]. Therefore, electrons emitted from the chamber surface cannot be trapped in these magnets due to the long bunch length. The simulated distribution of the electron cloud implies that there is no mirror-field trap. Compared with the drifting region, the decay time of the electron cloud at the bunch gap in quadrupole and sextupole magnets is much longer due to the weak effect of the space-charge and the confinement of the electron orbit by the magnetic fields. In contrast with long bunch case, electron cloud can be deeply trapped inside quadrupole and sextupole magnet in short bunch case, such as in B-factories [29].

### 2.12.5 Electron cloud clearing with solenoids and electrodes

A 30-Gauss weak solenoid can be invaluable in confining the electron cloud to the region near the wall and limiting the energy of electrons hitting the wall surface to below the multipacting level. It can reduce the electron density inside the chamber by a factor of a thousand. There is a non-electron circle at the chamber center with a radius more than the beam transverse size. Macek's PSR experiment demonstrated that a 20-Gauss solenoid field reduces the electron signal by a factor of 50 [22]. When the periodic solenoids are arranged in the coil with their currents in the same direction, this geometry is called equal polarity configuration. When the solenoids currents take alternative directions, it is termed an opposite polarity configuration. The electron density in the latter case is six times larger than that in the former. Importantly, most electrons stay around the chamber center under opposite polarity; there are no electrons near the chamber center with an equal polarity configuration. Therefore, the solenoids should be arranged in the latter configuration in operating the real machine. The same conclusion holds for B-factories [30,31]. Simulation shows that the electron cloud in an opposite configuration is trapped inside the solenoids, rather than in the gap between them. The distribution of electrons reflects the combined effect of the space-charge force and the solenoid fields.

With short bunches, such as B-factories, resonance occurs when the time for an electron to emerge from the wall and be bent back by the magnetic field coincides with the interval between two consecutive bunches [32,33]. Both the bunch length and the gap between subsequent bunches in the SNS ring, which are 700ns and 300ns, respectively, are much longer than the electron gyration period in the clearing solenoid fields. Therefore, the SNS exhibits no such kind of resonance phenomenon, which agrees with our simulation.

The effect of a clearing electrode is more complicated because it disturbs the electron orbit. A weak voltage round 200 V can effectively suppress multipacting. On the other hand, a median clearing voltage, which is 2000 V in the SNS, can excite stronger multipacting than can any clearing fields. We suggested how electron motion under a clearing field could explain the mechanism of action of the clearing field [21]. At the SNS accumulator ring, the Beam Position Monitors (BPMs) around the ring were designed as clearing electrodes to apply a voltage of up to 1000 V; this is not enough to completely suppress the electron cloud. However, our study

shows that such a voltage is effective with the “half multipacting frequency” mechanism. With a clearing field around 300 V, an electron bounces only from one side of the chamber surface, the frequency at which it hits the wall surface will be reduced by about half, and hence, the density of the electron cloud could be less than when there is no clearing field. A main source of electrons is at the stripping foil in the injection region of SNS ring. Multiturn charge-exchange injection often is preferred for high-intensity rings to enhance the phase-space density of the accumulated beam. Near the injection stripping-foil, we expect a high concentration of electrons with a broad energy-spectrum. With an H- beam, the stripped electrons carry twice the current of the injecting H- beam with a kinetic energy of  $mc^2(\gamma-1)$ , where  $\gamma$  is the beam relativistic factor. The injecting- and circulating-beams impacting on the foil produce a secondary emission of low-energy electrons (tens of eV). Both beams also generate knock-on electrons at high energy (up to several MeV). The electrons are guided by a magnetic field and collected by a water-cooled device of heat-resistant material. The electron collector consists of carbon material attached to a water-cooled copper plate. Its inner surfaces are coated with 100 nm thick TiN. An installed clearing electrode can apply 10,000 V. The clearing efficiency for electrons with energy up to several MeV still is unknown, and a study is underway. Also, the combined effect of the guiding magnetic field and clearing field needs to be considered.

### 2.12.6 References

1. G. I. Budker, G. I. Dimov, V. G. Dudnikov, Proceedings of the International Symposium on Electron and Positron Storage Rings, Saclay, 1966 (Orsay, Universitaires De France, 1966), page VIII-6-1.
2. H. G. Hereward, CERN Report No. 71-15, 1971
3. E. Keil and B. Zotter, CERN Report No. CERN-ISR-TH/71-58, 1971
4. R. J. Macek, et. al., Proceedings of the Particle Accelerator Conference, Chicago, 2001 (IEEE, Piscataway, NJ, 2001), p. 688.
5. M. Blaskiewicz, Workshop on Instabilities of High Intensity Hadron Beams in Rings, edited by T. Roser and S.Y. Zhang, AIP Conf. Proc. No. 496 (AIP, New York, 1999), p. 321.
6. M. Izawa, Y. Sato, and T. Toyamasu, Phys. Rev. Lett. **74**, 5044-5047 (1995).
7. K. Ohmi, Phys. Rev. Lett. **75**, 1526-1529 (1995).
8. H. Fukuma, Mini-Workshop on Electron Cloud Simulation for Proton and Positron Beams, Proceedings E-CLOUD'02, CERN-2002-001, Edited by G. Rumolo and F. Zimmerman, 2002, pp.1-10.
9. S. Heifets, Proceedings of 8th Advanced Beam Dynamics Mini-workshop on Two-stream Instabilities in Particle Accelerators and Storage Rings, Santa Fe, New Mexico, USA, 2000. URL: <http://www.aps.anl.gov/conferences/icfa/two-stream.html>
10. Z. Y. Guo, et. al., 1998, Proceedings of 1st Asian Particle Accelerator Conference. Tsukuba, Japan, 1998 (KEK, Tsukuba, Japan), pp. 432-434
11. J. M. Jiménez, G. Arduini, P. Collier, G. Ferioli, B. Henrist, N. Hilleret, L. Jensen, K. Weiss, F. Zimmermann, “Electron Cloud with LHC-type beams in the SPS : a review of three years of measurements”, LHC-Project-Report-632 (2003).
12. K. Cornelis, Mini-Workshop on Electron Cloud Simulation for Proton and Positron Beams, Proceedings E-CLOUD'02, CERN-2002-001, Edited by G. Rumolo and F. Zimmerman, 2002, pp.11-16.

13. O. Gröbner, Proceedings of the 10th International Accelerator Conference, Protvino, Russia, 1977 (Institute of High Energy Physics, Protvino, 1977), p. 277.
14. O. Gröbner, Proceedings of the 17th IEEE Particle Accelerator Conference (PAC 97), Vancouver, Canada (IEEE, Piscataway, NJ, 1998), p. 3589.
15. R. Macek, "Sources of electrons for stable beams in PSR", PSR Technical Note, PSR-00-10; also V. Danilov, A. Aleksandrov, J. Galambos, D. Jeon, J. Holmes, D. Olsen, "Multipacting on the Trailing Edge of Proton Beam Bunches in PSR and SNS", Workshop on Instabilities of High Intensity Hadron Beams in Rings, edited by T. Roser and S.Y. Zhang, AIP Conf. Proc. No. 496 (AIP, New York, 1999), p. 315.
16. M. Blaskiewicz, M. A. Furman and M. Pivi, PRST-AB **6**, 014203 (2003).
17. M.T.F. Pivi and M.A. Furman, PRST-AB **6**, 034201 (2003).
18. K. Ohmi, T. Toyama and C. Ohmori, PRST-AB **5**, 114402 (2002).
19. J. Wei and R. J. Macek, Mini-Workshop on Electron Cloud Simulation for Proton and Positron Beams, Proceedings E-CLOUD'02, CERN-2002-001, Edited by G. Rumolo and F. Zimmerman, 2002, pp. 29-40.
20. L. Wang, et.al., BNL/SNS TECHNICAL Note 132, Brookhaven National Lab, 2003. Presented at the 13th ICFA Beam Dynamics Mini-Workshop Beam Induced Pressure Rise in Rings, BNL, Upton, NY, December 9 - 12, 2003, <http://www.c-ad.bnl.gov/icfa/>
21. L. F. Wang, D. Raparia, J. Wei, and S.Y. Zhang, PRST-AB **7**, 34401; BNL/SNS Technical Note 128, Brookhaven National Lab, 2003.
22. R. J. Macek, Mini-Workshop on Electron Cloud Simulation for Proton and Positron Beams, Proceedings E-CLOUD'02, CERN-2002-001, Edited by G. Rumolo and F. Zimmerman, 2002, pp. 259-268
23. Jie Wei, Reviews of Modern Physics **75** (2003), pp.1383-1432.
24. A. Browman, Proceedings of 8th advanced beam dynamics mini-workshop on two-stream instabilities in particle accelerators and storage rings, Santa Fe, New Mexico, USA, 2000, <http://www.aps.anl.gov/conferences/icfa/two-stream.html>.
25. M. Plum, D. Johnson, R. Macek, F. Merrill, B. Prichard, PSR TECH NOTE PSR-97-19 (1997)
26. K. Ohmi and F. Zimmermann, Phys. Rev. Lett. **85**, p.3821-3823 (2000).
27. Lapique F. and Piuz F., Nucl. Instrum. Methods Phys. Res. **175** (1980), pp. 297-318.
28. L. F. Wang, H. Fukuma, K. Ohmi, S. Kurokawa and K. Oide, F. Zimmermann, PRST-AB **5**, 124402 (2002)
29. L. F. Wang, H. Fukuma, S. Kurokawa, K. Oide, Phys. Rev. E **66**, 036502 (2002).
30. L. Wang, H. Fukuma and K. Ohmi, KEK Report 2001-3, 2001.
31. Y. Suetsugu, Y. Tanimoto, Y. Hori, M. Kobayashi and K. Kanazawa, Proceedings of the International Workshop on Two-Stream Instabilities in Particle Accelerators and Storage Rings, 2001, KEK, Tsukuba, Japan, <http://conference.kek.jp/two-stream/> .
32. Y. Cai, M. Pivi, M. Furman, PRST-AB **7**, 024402 (2004); SLAC-PUB-1-164, 2003
33. A. Novokhatski, J. Seeman, "Simulation Study of Electron Cloud Multipacting in Straight Sections of PEP-II," SLAC-PUB-9950, Jun 2003. Contributed to Particle Accelerator Conference (PAC 03), Portland, Oregon, 12-16 May 2003.

## 2.13 Electron Cloud studies in J-PARC and KEK-PS

T. Toyama and K. Ohmi  
mail to: [takeshi.toyama@kek.jp](mailto:takeshi.toyama@kek.jp)

KEK, 1-1 Oho, Tsukuba 305-0801 Japan

### 2.13.1 Introduction

J-PARC [1] is a Japan Proton Accelerator Research Center as a joint project of KEK and JAERI. Construction of J-PARC is in progress and commissioning is scheduled to start from 2007. J-PARC equips two circular proton accelerators: one is a 3 GeV rapid cycling synchrotron (RCS) and the other is a 50 GeV proton synchrotron (MR). RCS is used as a source of neutrons and mesons, and as an injector to MR. It accelerates proton beams from 400 MeV (180 MeV in phase I) to 3 GeV at the repetition rate of 25 Hz. MR is used for experiments of nuclear physics and neutrino physics. It accelerates the beam up to 50 GeV and supply with fast and slow extraction. In the slow extraction, coasting beam operation is adopted. The parameters of the two rings are summarized in Table 1.

**Table 1.** Parameters of J-PARC proton synchrotrons

		RCS		MR	
		injection	extraction	injection	extraction
Circumference	(m)	348.3	348.3	1567.5	1567.5
gamma		1.43	4.20	4.20	54.29
bunch population		4.15E+13	4.15E+13	4.15E+13	4.15E+13
Number of bunches		2	2	8	8
harmonic number		2	2	9	9
beam size	(m)	0.019	0.012	0.011	0.0035
bunch length	(m)	110	82	82	16
momentum spread	(%)	0.6	0.7	0.7	0.25
slippage factor		-0.48	-0.047	-0.058	-0.0013
synchrotron tune		0.00580	0.00050	0.00260	0.00010
beam pipe radius	(cm)	12.5	12.5	6.5	6.5

The bunch structure, the population of  $4 \times 10^{13}$  and the length of 16-110 m, is comparable with PSR. Therefore electron cloud effect may affect the accelerator performance. The electron cloud effect has been studied by computer simulations and investigated by experiments at the KEK 12 GeV PS.

### 2.13.2 Simulation studies

#### 2.13.2.1 Instability for bunched beam in the RCS and MR

Electron cloud build-up is estimated by analyzing motion of electrons produced at the chamber wall due to primary and secondary productions [2]. We assume that primary electrons are produced at the chamber wall with an yield per traveling of 1m of a proton,  $Y_1 = 4 \times 10^{-6} / (\text{m.p})$ .

The secondary emission yield  $\delta_2(E)$ , which is the number of electrons created by an electron incidence with energy (E), is approximated by the formula

$$\delta_2(E) = \delta_{2,\max} \times \frac{E}{E_{\max}} \frac{1.44}{0.44 + (E/E_{\max})^{1.44}}$$

where  $E_{\max}=200\text{eV}$ ,  $\delta_2(0)=0.5$  and  $\delta_{2,\max}=2.1$  are assumed. The simulation was improved including electron elastic reflection and space charge force between electrons [3].

Electron density at build up is obtained by tracking the electrons with the primary yield and by estimating the amplification due to secondary emission. The neutralization factor, defined by electron line density divided by bunch average line density, is shown in Table 2. In the table, the neutralization factors at peak and bottom densities due to bunch induced multipacting are written.

Instability threshold is estimated by coasting beam approximation. The approximation is reliable, because of  $\omega_e \sigma_z / c \sim 100 \gg 1$ . The threshold of the neutralization factor is seen in Table 2.

The neutralization factor is close to the threshold in every case at the peak density except for injection of RCS. The electron cloud gets to the peak density at the tail of bunch. MR is more serious than RCS, because of the low slippage factor. The primary yield,  $Y_1=4 \times 10^{-6} /(\text{m.p})$ , is used in all cases. The yield has been estimated in detail according to the cases. The neutralization factor strongly depends on the secondary yield,  $\delta_{2,\max}$ . The value 2.1 is given for stainless steel with a conditioning, but it may be more 2.5~3 at the early stage of commissioning. In this case the neutralization factor exceeds the threshold value. To make easy the commissioning program, cures for example, TiN coating, is indispensable.

**Table 2.** Amplification factor of electron cloud and notarization factor

	RCS inj.	RCS ext.	MR inj	MR ext.
Ae(bottom)	17	18	5.1	1.7
Ae(peak)	50	68	115	9.5
Neutralization factor (bottom)	0.01	0.0067	0.0019	0.0001
Neutralization factor (peak)	0.024	0.025	0.042	0.0007
Neutralization factor (threshold)	0.28	0.03	0.03	0.00043

### 2.13.2.2 Instability for coasting beam at the MR

A coasting beam operation is planned for slow extraction in the 50 GeV main ring. The neutralization factor of the threshold is extremely low for the top energy of the MR as is shown in Table 2, because of the low slippage factor. If electrons created by ionization were just trapped, their density would reach the threshold value with a short time, 0.2 ms for a vacuum pressure of  $2 \times 10^{-7}$  Pa ( $Y_1=8 \times 10^{-9} /(\text{m.p})$ ). Considering the transverse momentum conservation, electrons whose density is 0.4% of proton beam are strongly swung by small perturbation of the proton beam. How the instability is observed actually depends on production rate of the electrons, namely the beam flicks the electrons immediately if they are accumulated up to the threshold value. The simulation of motion of the proton beam and electrons was performed [4], and showed that the beam amplitude does not grow to visible level for such low production rate of electrons  $Y_1=8 \times 10^{-9} /(\text{m.p})$ .

On the other hand, electrons created at the chamber wall are produced by higher rate, typically  $Y_1=4 \times 10^{-6}/(\text{m.p})$  as is discussed for bunched beam. A simulation was carried out for interaction between a coasting beam and electrons produced at the chamber, and shows that the beam amplitude grew to visible value for such high production rate. The results mean that electrons produced at the chamber wall with high rate were essential even for the instability of coasting beam.

### 2.13.3 Experiments at the KEK 12 GeV Proton Synchrotron (KEK-PS)

The observation of electron clouds at the Main Ring (MR) of the KEK-PS is going on to benchmark the computer simulation and to test materials such as TiN coating on stainless steel and alumina ceramic pipes. The scaled version of electron sweeping detector developed by the LANL team [5] was recently installed in the ring. The KEK-PS MR accelerates nine proton bunches from 500 MeV to 12 GeV. The parameters of the ring are summarized in Table 3.

**Table 3.** Parameters of KEK 12 GeV PS MR

		MR	
		injection	extraction
Circumference	(m)	339.3	339.3
gamma		1.53	13.8
bunch population		$\leq 9 \text{ E}+11$	$\leq 9 \text{ E}+11$
Number of bunch		$\leq 9$	$\leq 9$
harmonic number		9	9
beam size (rms)*	(m)	$\sim 0.005 / \sim 0.007$	$\sim 0.002 / \sim 0.003$
bunch length	(m)	$\sim 20$	$\sim 18$
momentum spread	(%)	0.4	0.4
slippage factor		-0.40	0.017
synchrotron tune		$\sim 0.008$	0.0004
beam pipe radius*	(cm)	$\sim 6$	$\sim 6$

\*) Value estimated at the position of the electron sweeping detector.

#### 2.13.3.1 Observation of bunched beams

Previous observation indicated the existence of electron clouds for bunched beams at the phase transition ( $\sim 5.3$  GeV) and the flat top energy (12 GeV) [6]. Recent observation shows concrete evidence of the electron clouds. Collective beam instabilities are not observed due to electron clouds so far.

The electron sweeping detector comprises slits, a grid, a collector and a HV plate as shown in Fig. 1.

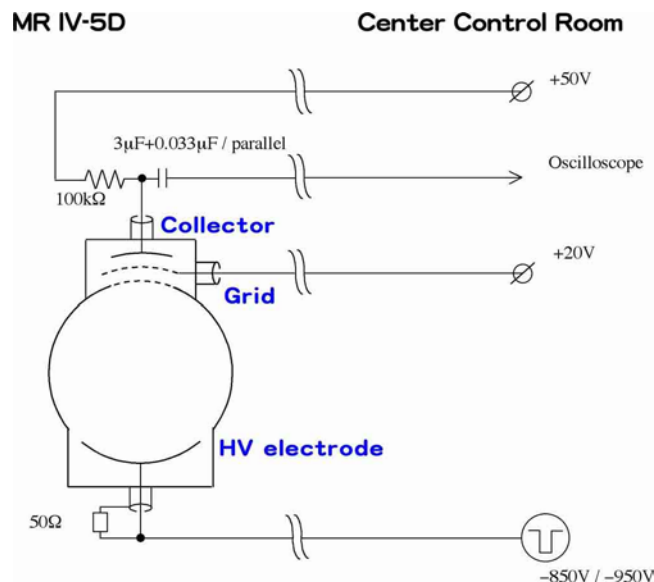


**Fig. 1.** Electron sweeping detector at the KEK-PS Main Ring.

The typical signals from the collector without sweeping voltage are shown in Figs. 2 and 3. Upper plots are the signals from the collector. Lower plots are the signals from a wall current monitor just downstream of the e-sweeping detector. The accumulation of electrons is clearly seen, comparing the collector signals of two different number of bunches, nine and six. There are no collector signals less than or equal to 5 bunches.

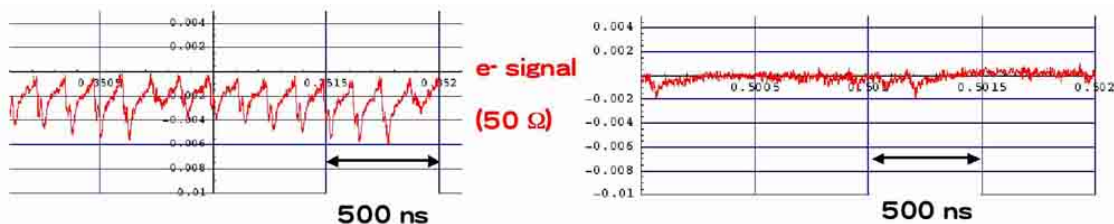


**Fig. 2.** Signals from the collector and wall current monitor for nine bunches.

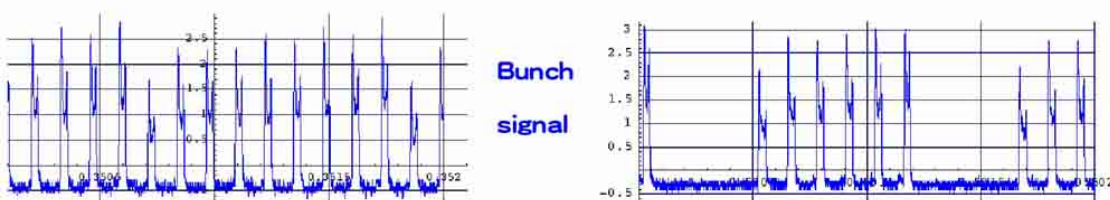


**Fig. 3.** Signals from the collector and wall current monitor for six bunches.

With a HV pulse of 50 ns,  $-850$  V (at the output of the pulser), a large signal was detected as Fig. 5. Just after sweeping the electrons, the electron signal is reduced and gradually increasing within a few bunch passages, which is similar to that observed at LANL [5].

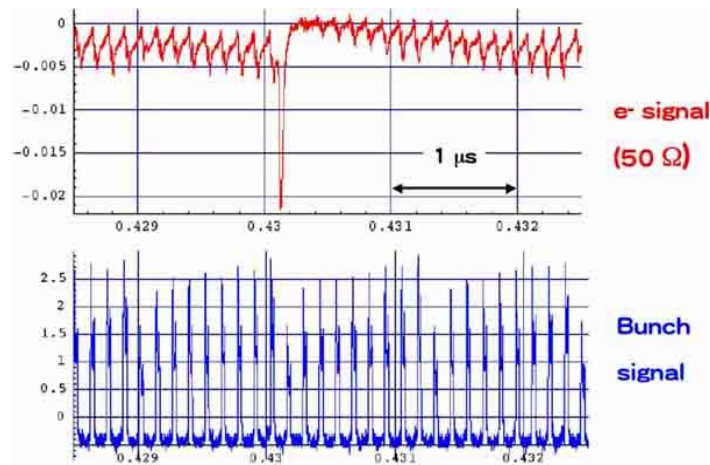


**Fig. 4.** Signals from the collector and wall current monitor for nine bunches. A large electron signal around the middle of the trace corresponds to the HV sweeping pulse.

### 2.13.3.2 Observation of coasting beams

A model that assumes continuous ionization of a residual gas by the proton beam, diffusion of electrons and multipacting due to beam oscillation is described in 1.1.2. It predicts saturation of electron cloud density. The goal of the experiments is to confirm the above picture. The result of an experiment with the e-sweeping detector is shown in Fig. 5: electron cloud build-up for several coasting beam intensities and with artificial beam loss.

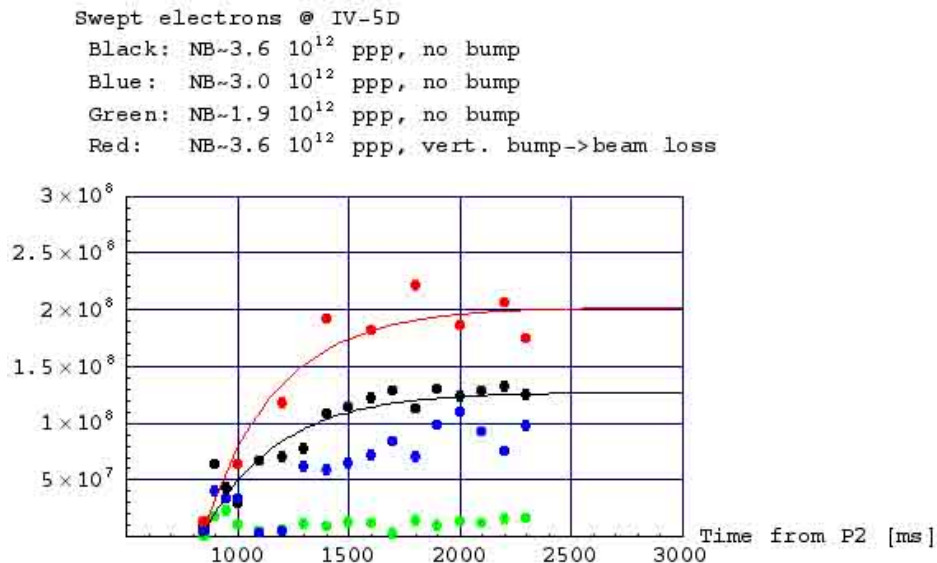


**Fig. 5.** Number of electrons swept out with HV ( $\sim -850$  V, 100 ns) after a time from the acceleration starting trigger. RF is turned off at  $\sim 850$  ms.

Using the following expression for electron cloud build-up:

$$\mu\tau(1 - e^{-t/\tau}) \quad \tau : \text{decay constant [s] ,}$$

$$\mu : \text{production rate [e}^-/\text{m} \cdot \text{s] ,}$$

we obtain the production rate of  $1 \times 10^{10}$  e<sup>-</sup>/m·s and decay constant of 0.3 s for the beam intensity of  $3.6 \times 10^{12}$  ppp. Saturated electron density is  $3 \times 10^9$  e<sup>-</sup>/m, assuming detector efficiency of 0.04, which is the ratio of the number of ejected electrons from the beam pipe to the detector, and the number of electrons in the pipe volume of one meter in the beam direction. The local neutralization factor is about 30 %.

With the artificial beam loss, the production rate increased by 60 % comparing to the above case. The loss amount was so small that an air-filled loss monitor could not detect it and only a scintillation counter did detect.

Reducing the beam intensity caused rapid decrease of the electron cloud density.

#### 2.13.4 Conclusion

Using the J-PARC beam parameters, electron cloud build-up and collective beam instabilities are simulated for bunched and coasting beams. The bunched beams at the extraction of the 3 GeV RCS and at the injection and extraction of the 50 GeV MR are close to the instability threshold, assuming  $\delta_{2,\text{max}}$  is 2.1. The inner surface of the ceramic pipe of the 3 GeV RCS will be coated by TiN, which will drastically suppress the electron cloud build-up due to smaller secondary electron yield [2]. The SEY suppression depends on the coating process [7]. We plan to make TiN coating samples with the same process for mass production, install it in the electron-sweeping detector and check the electron yield.

Another important issue is to examine the beam loss at each stage of acceleration. The above calculation relies on the beam loss rate of  $Y_1 = 4 \times 10^{-6}$  /(m.p) and primary electron production rate of  $\sim 100$  e<sup>-</sup>/p. Less amount of beam losses causes smaller electron density and more amount of beam losses more electron density [3], which means that the electron density is not saturated in J-PARC. Reducing an amount of losses is important. Preliminary estimate at each acceleration stages shows smaller losses than the one above mentioned [8]. We will pursue better accuracy of prediction, follow up an improving design of collimators and try to keep the beam loss small.

The measurements using the electron sweeping detector at the KEK-PS shows the existence of the electron cloud both in the bunched and coasting beams. Comparing the results to the simulation is foreseen.

#### 2.13.5 References

1. "Accelerator Technical Design Report for J-Parc" edited by Y. Yamazaki, KEK-report 2002-13.
2. K. Ohmi, T. Toyama, C. Ohmori, PRST-AB **5**, 114402 (2002).
3. [http://www-accps.kek.jp/J-PARC/beam\\_instability/epi\\_ohmi\\_2002Jun12.pdf](http://www-accps.kek.jp/J-PARC/beam_instability/epi_ohmi_2002Jun12.pdf) .
4. K. Ohmi, T. Toyama and M. Tomizawa, Proceedings of PAC03 (2003).
5. R. J. Macek, Proc. of E-CLOUD'02 workshop, CERN Yellow Report, CERN-2002-001, p. 259 and references therein. The radial dimension was scaled up as an inner radius from 5 cm to 8 cm.
6. T. Toyama *et al.*, Proc. of E-CLOUD'02 workshop, CERN Yellow Report, CERN-2002-001, p.155.

7. Y. Saito, Private communication.
8. T. Toyama *et al.*, Proc. of E-CLOUD'04 workshop, in preparation.

## 2.14 RHIC Two Stream Effects

S.Y. Zhang  
 mail to: [syzhang@bnl.gov](mailto:syzhang@bnl.gov)

Brookhaven National Laboratory  
 911B, Upton, New York, USA

### 2.14.1 Introduction

**RHIC luminosity has been limited by beam induced pressure rise, which is mainly due to the two stream effect. In this article, the pressure rises observed at the RHIC will be discussed. Also, the scenario of the electron-ion collider at the RHIC, i.e. eRHIC, will be described.**

### 2.14.2 Injection pressure rise

Pressure rise at the beam injection has been observed for gold, deuteron, and proton operations in the RHIC. This pressure rise limits operation of 112 bunches with bunch intensity of  $10^9$  gold ions, and  $10^{11}$  for protons [1].

It has been diagnosed that the injection pressure rise is due to the electron cloud. The evidence include:

1. Electron detector signals are very closely related to the pressure rise, at onset, saturation, and drooping.
2. Pressure rise and electron signal are very sensitive to the bunch spacing, 112 bunch mode is much worse than 56 bunch mode.
3. Bunch gap helps.
4. Solenoid field of 2 to 50 Gauss can suppress both pressure rise and electron signal, but not completely.
5. Beam scrubbing has been demonstrated helpful in reducing pressure rise.

It is noticed that the electron cloud observed at the RHIC is different from other machines. For example, the RHIC electron cloud takes place at the bunch spacing of 108 ns or even 216 ns. All other machines have much smaller bunch spacing:

1. The B factories, KEKB and PEP-II, have bunch spacing of 4 ns to 8 ns [2,3].
2. Electron activity was peaked at 20 ns of bunch spacing at the APS of Argonne [4].
3. SPS observed electron cloud at 25 ns bunch spacing with the threshold of  $(3-4) \times 10^{10}$  protons per bunch. At the bunch spacing 130 ns, no electron cloud was observed at the bunch intensity of  $2.5 \times 10^{11}$  protons [5].

4. Tevatron observed electron cloud at 18.9 ns bunch spacing with bunch intensity of  $4 \times 10^{10}$  protons [6]. The situation is very similar to SPS. The Tevatron Run II plan calls for 132 ns bunch spacing with bunch intensity of  $2.7 \times 10^{11}$  protons [7].

The RHIC pressure rise and electron cloud also have several distinguished characteristics from other machines:

1. It only occurs in warm sections, and the pressure rise distribution is very un-uniform in the ring. When pressure rise at certain location(s) is high enough to close the vacuum valve, some locations have none. The worst locations also change time by time.
2. The beam intensity threshold at the Q3 to Q4 straight section, 34 meters long, is only 60% of that at the interaction straight section, which is 17 meters long. Other conditions of the chamber are the same.
3. No noticeable cryogenic heat load has been observed. Together with the absence of electron cloud induced beam instability and emittance growth, it is believed there is no electron multipacting at the RHIC cold region.
4. RHIC pressure rise decreases at the ramp, and it is non-existent at the store. In SPS, the electron activity was stronger at the store than at the injection [8].

It is suspected that the beam halo scraping at the wall, which generates mostly positive ions, may have helped the secondary electron to survive long bunch gap, and makes electron multipacting possible.

During the 2003 polarized proton run, a beam scrubbing was tested. Total high intensity beam scrubbing time was less than 1 hour. However, the scrubbing effect was observed not only in the locations with highest pressure rise, but also in others with non-trivial pressure rise [9].

For RHIC operation, the complete elimination of the injection pressure rise is not necessary. Therefore, a limited time of high intensity beam run might be sufficient to allow higher beam intensity operation.

### 2.14.3 Transition pressure rise

The beam transition pressure rise for heavy ion operations is another intensity limit for RHIC [1]. The characteristics of this pressure rise are as follows:

1. The pressure rise is quasi-exponentially proportional to the total beam (charge) intensity.
2. No difference between 56 bunch and 112 bunch modes can be identified. The absence of bunch spacing effect indicates that the transition pressure rise is not dominated by the electron cloud.
3. The beam loss is not a dominant factor in the transition pressure rise.
4. The pressure rise is not related to the ion species. Since the gold ion gas desorption cross section is about 79 times larger than the deuteron, this indicates that the gas desorption is not a dominant factor in the transition pressure rise.

It is found that the transition pressure rise is, on the other hand, related to the beam momentum spread:

1. The beam momentum spread is 0.17% at the injection, it is peaked at 0.3% at the transition, and decreases afterwards. The pressure rise follows this pattern. In proton run, the beam momentum spread decreases in the acceleration, and the pressure rise decreases as well.
2. The bunch length seems not a dominant factor in the transition pressure rise. At the bunch rebucketing, where the beam was captured in 200 MHz storage cavity, the bunch length reduces to 5 ns, the same as that at the transition (the beam potential at the rebucketing is actually 37% higher than that at the transition due to the smaller transverse size), yet the rebucketing pressure rise was not a problem in the d-Au run.
3. The total storage cavity voltage was 2.5 MV in d-Au run. At the rebucketing, the beam momentum spread was a little larger than that at the injection, and much lower than 0.3% at the transition.

In Run 4, two more common cavities have been commissioned to increase the total rebucketing voltage to  $> 4$  MV. The rebucketing pressure rise was observed at several interaction regions. Much higher storage voltage and the better rebucketing imply also higher beam peak current and beam potential. Accordingly, some electron multipacting may have been observed at the rebucketing.

The transition pressure rise had caused serious experiment background problem in d-Au run. For same luminosity, 56 bunch mode requires 30% less total intensity than the 112 bunch mode. Switching from 112 bunch mode to 56 bunch, the experiment background was significantly improved.

Eleven NEG (non-evaporable-getter) pipes have been installed in the RHIC rings for test [10,11]. To alleviate the transition pressure rise, ion desorption reduction might be important. The data on this aspect is, however, less than sufficient [12]. The NEG pipes in RHIC have made possible for the evaluation of ion desorption, and other relevant issues such as the activation condition, saturation effect, aging, venting effect, possible dust, and impedance problem, etc.

For same purpose, a test stand has been built at the BNL Tandem Van de Graaff. Different activations will be tested, and also the ion desorption on the shallow angle ion beam scraping on stainless steel and NEG surface will be compared.

#### **2.14.4 Scenario of 360 bunches in eRHIC**

The electron-ion collider at the RHIC, i.e. eRHIC, calls for 360 bunches in the ring. It is expected that not only the injection and transition pressure rises, but also a usual electron cloud may occur for both proton and heavy ion operations. With the bunch spacing of 35 ns, eRHIC is very similar to SPS and LHC in terms of electron multipacting [13].

For normal electron cloud, eRHIC have several new issues to deal with:

1. Electron multipacting in cold region. The chamber radius at the cold region is 3.5 cm, compared with 6.1 cm at warm sections. The multipacting threshold at the cold region is, therefore, lower, and the cryogenic heat load might be of concern. Experimental data at the SPS shows that the heat load is larger than 1.2 W/m under electron multipacting [13], which is not acceptable at the RHIC.

2. Since the cold region consists 3/4 of the RHIC ring, the electron cloud induced beam instability and beam emittance will be of concern.
3. Electron cloud will present not only at the injection, but also at the ramp and storage.
4. Electron activity in dipole and quadrupole becomes relevant [14]. The multipacting threshold at the dipole is lower than that at the straight section. Moreover, since the electron dose stripes in dipoles vary according to the bending field and beam intensity [8], the scrubbing is more difficult. As for quadrupole field, it is suspected the electrons are trapped there and stay for a long time.

Given luminosity unchanged, it is of interest to study the benefit of using larger bunch spacing and higher bunch intensity.

Issues related to the 180 bunch mode, with the 70 ns bunch spacing and 40% increase in bunch intensity, include:

1. Electron activity will be reduced compared with the 360 bunch mode. The decrease of the electron activity is more than linearly proportional to the inverse of bunch spacing [15].
2. In 180 bunch scenario, the total beam intensity is reduced. This will benefit at least the pressure rise in warm sections, perhaps more.

#### 2.14.5 References

1. S.Y. Zhang et al, PAC03, Portland, Oregon, 2003.
2. Y. Suetsugu, Workshop of Beam Induced Pressure Rise in Rings, BNL, Dec. 2003.
3. U. Wienands, Workshop of Beam Induced Pressure Rise in Rings, BNL, Dec. 2003.
4. K. Harkay, Workshop of Two Stream Instabilities, Santa Fe, Feb. 2000.
5. W. Höfle, Chamonix X, CERN, 2000.
6. F. Zimmermann, CERN-AB-2003-004, Jan. 2003.
7. RunII Handbook, Fermilab, 2000.
8. J. M. Jiménez, Workshop of Beam Induced Pressure Rise in Rings, BNL, Dec. 2003.
9. S.Y. Zhang, W. Fischer, H. Huang, and T. Roser, C-A/AP Tech Note, 123, Nov. 2003.
10. S.Y. Zhang, H.C. Hseuh, and T. Roser, C-A/AP Tech Note, 99, June, 2003.
11. P. Chiggiato, LHC-VAC/ChR/mpt, CERN, 2001.
12. E. Mahner, Working group report, Workshop of Beam Induced Pressure Rise in Rings, BNL, Dec. 2003.
13. F. Ruggiero, Workshop of Beam Induced Pressure Rise in Rings, BNL, Dec. 2003.
14. R. Macek, Working group report, Workshop of Beam Induced Pressure Rise in Rings, BNL, Dec. 2003.
15. G. Arduini, Chamonix XIII, 2004.

## 2.15 Vacuum limitations due to electron clouds during the Relativistic Heavy Ion Collider Run-4

Wolfram Fischer

Mail to: [Wolfram.Fischer@bnl.gov](mailto:Wolfram.Fischer@bnl.gov)

Brookhaven National Laboratory  
Upton, New York, USA

### 2.15.1 Introduction

The Relativistic Heavy Ion Collider (RHIC) at Brookhaven National Laboratory consists of two superconducting rings, denoted Blue and Yellow. The machine can accelerate and store particles from protons to fully stripped gold ions [1]. The current operating period (Run-4) began in November 2003, and will last until May 2004. In Run-4 gold ions were accelerated to and stored at 100 GeV/u and 31.2 GeV/u. Later in the run the machine will also be operated with polarized protons.

The two most severe luminosity limitations in heavy ion operation are intrabeam scattering, and vacuum pressure rises with intense beams. Intrabeam scattering leads to luminosity lifetimes of about 2.5 hours, and fast refills are needed to achieve a high average luminosity. Ultimately beam cooling at full energy is required to overcome intrabeam scattering. Pressure increases with intense beams limit the luminosity in two ways. First, they limit the beam intensity that can be accelerated and stored. Second, they create backgrounds that are not acceptable to the experiments. Experimental observations indicate that the pressure increases are predominately caused by electron clouds.

### 2.15.2 Beam current limitations

Pressure increases with intense ion beams can be observed in various warm locations in the two RHIC rings. The pressure increases are especially pronounced at transition, and after rebucketing (see Fig. 1). One location in each ring limits the intensity that can be accelerated and stored.

When the beams cross the transition energy, the bunch length is reduced to 4ns, from 18ns at injection, while the peak current and the momentum spread are increased. At rebucketing the bunches are transferred from the accelerating rf system, with 36ns bucket length, into the storage rf system, with 5ns bucket length. The shorter bunches have again a higher peak current and a larger momentum spread. Simulations show that shorter bunches with the same intensity are more likely to trigger an electron cloud formation [2,6].

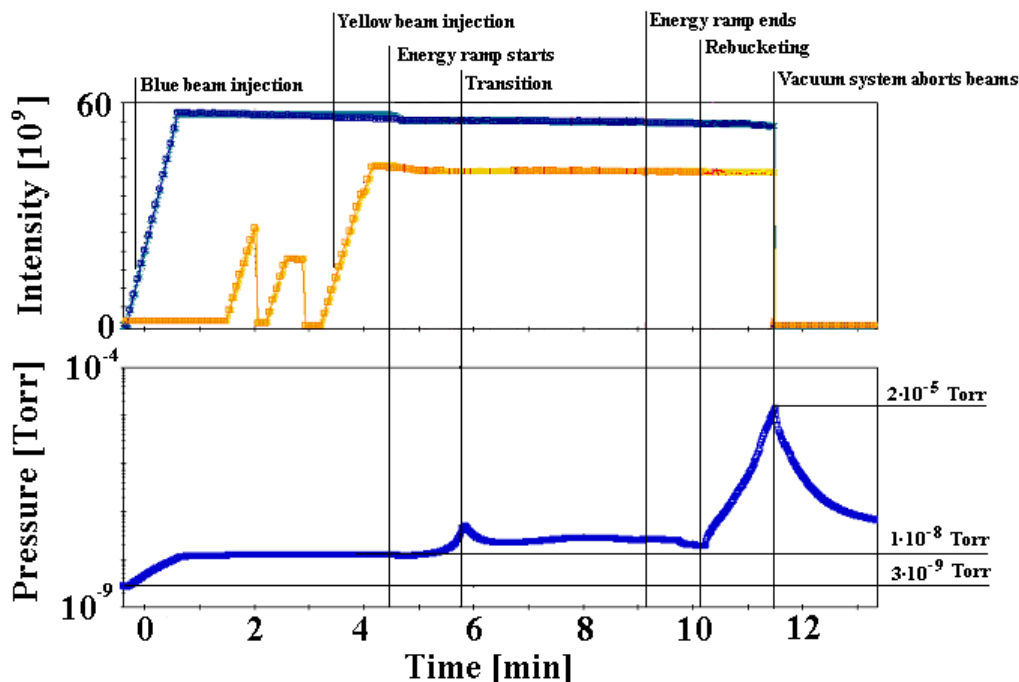


**Fig. 1.** Vacuum instability in Blue sector 8 (unbaked collimators), with 56 bunches per ring. The upper part shows the beam intensities during injection, acceleration and rebucketing. The lower part shows the pressure changes during injection, transition crossing and after rebucketing.

In Run-4 the Blue beam intensity was limited by the vacuum in sector 8, at the location of a newly installed unbaked collimator. In the Yellow ring the intensity was limited by the vacuum in sector 4, at the location of a stochastic cooling kicker, also unbaked initially. Both devices had not been baked, since they were installed late during the last shutdown, and not enough time was available for a bake-out before operation began. The Yellow stochastic cooling kicker was baked later during the run, raising the intensity threshold by some 10%.

Fig. 1 show a vacuum instability in Blue sector 8. The static pressure before the beam is filled is  $3 \times 10^{-9}$  Torr. The pressure rises to  $1 \times 10^{-8}$  Torr after 56 bunches are injected. At transition the pressure rises to  $5 \times 10^{-8}$  Torr and drops back as the acceleration continues. After rebucketing the pressure increases exponentially over 1.5 minutes until  $2 \times 10^{-5}$  Torr are reached. The vacuum system then aborts the beam.

With 61 bunches in both rings,  $0.95 \times 10^9$   $\text{Au}^{97+}$  ions per bunch can be accelerated and stored in the Blue ring, and  $0.80 \times 10^9$   $\text{Au}^{97+}$  ions per bunch in the Yellow ring. With 56 bunches in both rings,  $1.00 \times 10^9$   $\text{Au}^{97+}$  ions per bunch can be accelerated and stored in the Blue ring, and  $0.90 \times 10^9$   $\text{Au}^{97+}$  ions per bunch in the Yellow ring. With 45 bunches, the available bunch intensity is not sufficient to exceed the vacuum limit in either ring.  $1.15 \times 10^9$   $\text{Au}^{97+}$  ions per bunch can be accelerated and stored in both rings.

The fact that shorter bunches raise the pressure, and longer bunch spacings can suppress the pressure rise, point to electron clouds as a driving mechanism for the pressure rise. Furthermore, in proton-proton operation during the RHIC Run-3, an electron cloud signal was observed directly in conjunction with a pressure rise, although at a different location [3,4].

There are two observations that are not fully understood. First, if the pressure increases were only the result of electrons bombarding the wall, one would expect a pressure increase linear in time, not exponential. Furthermore, in deuteron-gold operation during Run-3, the transition pressure rise appeared to be mainly dependent on the total intensity, not the bunch spacing [5].

### 2.15.3 Experimental background limitations

One of the four RHIC experiments, PHOBOS, has experienced high backgrounds from increased pressure in the experimental area. In some of the stores, the pressure rises after rebucketing by about an order of magnitude, and drops back after some time, typically an hour. During the time of increased pressure, experimental backgrounds are too high to allow for data taking.

In Fig. 2 the history of the pressure rise problem in PHOBOS is shown. The machine was initially run with 56 bunches per ring, which was then increased to 61 bunches. At the same time the bunch intensity was continuously increased. After some time with 61 bunches, the pressure rise problem became visible for the first time. A reduction in the bunch number to 56 eliminated the problem, even with further increases in the bunch intensity. With 56 bunches, all bunches are spaced by 6 buckets, while with 61 bunches, some bunches are spaced by only 3 buckets. The short bunch spacing was found to trigger electron cloud formation much earlier in simulations [6].

After some running time with 56 bunches, the problem resurfaced, although the bunch intensity had not been increased. At the same time the static pressure had slightly increased from 20 pTorr to 40 pTorr. The bunch number was again reduced, to 45, accompanied by an increase in the bunch intensity to maintain the luminosity. In this configuration the bunch intensity available from the injectors became the luminosity limit. The bunch number was adjusted when not enough bunch intensity was available.

With 45 bunches the pressure rise problem was suppressed for a number of stores, but gradually the number of stores that exhibited a pressure rise problem increased, until almost all stores had high pressures during the early part of the store. The pressure rise problem was observed with beams of 100 GeV/u and 31.2 GeV/u.

The fact that the pressure rise is triggered after a bunch shortening, that an increase in the bunch spacing helps suppressing it, and that it is independent of the beam energy points again to electron clouds as the driving mechanism [7]. The PHOBOS experimental beam pipe is a 12 m section of beryllium that has a high secondary emission yield. Detailed simulations indicate that the electron clouds are concentrated near the ends of the beryllium pipe [7].

Not all stores show a pressure rise problem. This suggests that a threshold in some parameter set must be crossed to trigger the pressure increase; a threshold is also crossed when the pressure drops back sharply after about an hour. From the data displayed in Fig. 2 one cannot find, however, a narrow range in either the bunch intensity or initial pressure that would lead to a pressure rise upon rebucketing. Neither can one find a narrow range in either the bunch intensity or the pressure that are sufficiently low to switch off the effect after some time.

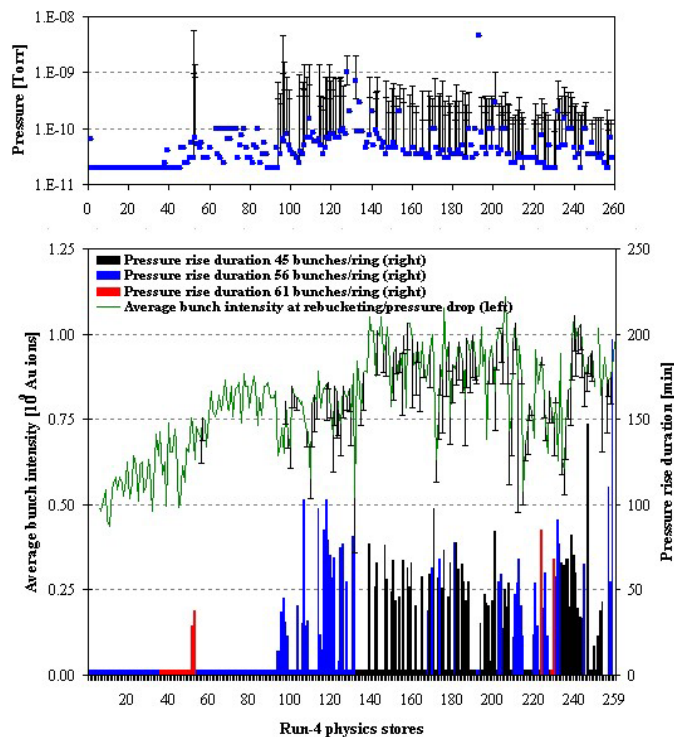


**Fig. 2.** History of the PHOBOS pressure rise problem during the RHIC Run-4. In the upper part, the pressure at PHOBOS is shown at rebucketing for the physics stores of Run-4. For stores with a pressure rise after rebucketing, also shown are the maximum pressure and the pressure when it begins to drop sharply. In the lower part on the left hand scale the bunch intensity, averaged over all bunches in the Blue and Yellow rings, is depicted. Stores with a PHOBOS vacuum problem also show the average bunch intensity at the time when the pressure begins to drop sharply. In the lower part on the right hand scale, the duration of the pressure problem is shown, ordered into stores with 45, 56, and 61 bunches per ring. Note that the last 14 stores are with Au<sup>79+</sup> beams at 31.2 GeV/u, all other stores are with Au<sup>79+</sup> beams of 100.0 GeV/u.

A second experiment, STAR, has also seen, at times, higher backgrounds from pressure increases in the experimental area [8]. This pressure rise, however, is not likely to be caused by electron clouds. The STAR magnet provides a solenoidal field of 0.5 T in the central part, and fringe fields of more than 5 mT in all of the experimental area. The magnetic field should suppress electron clouds. The central part of the experimental beam pipes in STAR cannot be baked at temperatures above 100°C, and the pressure increase may be caused by a different effect.

#### 2.15.4 Summary

The RHIC luminosity is limited by pressure increases with intense ion beams. Observations point to electron clouds as the dominant source for most of the pressure increases. The increased pressure limits the intensity that can be injected, accelerated, and stored. Even lower intensity limits are set by the background requirements of some of the experiments. While electron clouds are the most likely source of the increased pressure, the mechanism leading to an exponential pressure increase is not understood.

To increase the intensity thresholds that trigger vacuum problems, the replacement of warm beam pipes with NEG coated ones, especially in the experimental regions, is under consideration.

### 2.15.5 Acknowledgements

The author would like to thank for information and discussions: M. Blaskiewicz, A. Drees, H.C. Hseuh, U. Iriso, G. Rumolo, T. Roser, L. Smart, P. Thieberger, D. Trbojevic, D. Weiss, and S.Y. Zhang.

### 2.15.6 References

1. H. Hahn (editor), “RHIC design manual”, revision of October 2000, [http://www.rhichome.bnl.gov/NT-share/rhicdm/00\\_tocli.htm](http://www.rhichome.bnl.gov/NT-share/rhicdm/00_tocli.htm) (2000).
2. W. Fischer, J.M. Brennan, M. Blaskiewicz, and T. Satogata, “Electron Cloud Measurements and Simulations for the Brookhaven Relativistic Heavy Ion Collider”, *Phys. Rev. ST Accel. Beams* 5, 12440 (2002).
3. U. Iriso, A.K. Drees, W. Fischer, D. Gassner, O. Gould, J. Gullotta, P. He, H.C. Hseuh, R. Lee, V. Ponnaiyan, L. Smart, D. Trbojevic, and S.Y. Zhang, “Electron cloud observation at RHIC in Run-3 (2002/03)”, BNL C-A/AP/129 (2003).
4. U. Iriso, this Newsletter.
5. S.Y. Zhang, “Experiment Background in RHIC Deuteron-Gold Run”, BNL C-A/AP/107 (2003).
6. W. Fischer and U. Iriso-Ariz, “Bunch patterns and pressure rise in RHIC”, BNL C-A/AP/118 (2003).
7. G. Rumolo and W. Fischer, “Observations on background in PHOBOS and related electron cloud simulations”, BNL C-A/AP/146 (2004).
8. A. Drees and W. Christie, private communication (2004).

## 2.16 Electron Cloud observations at RHIC

U. Iriso

<mailto:ubaldo@bnl.gov>

[C-AD Department](#)

Brookhaven National Laboratory, Upton, NY – 11973, USA

### 2.16.1 Introduction

Since the second running period (Run-2) of the Relativistic Heavy Ion Collider (RHIC) occurred in 2001, pressure rises in its warm vacuum sections have been observed during operations with high intensity beams [1-3]. This pressure rise was suspected to be due to electron stimulated desorption (ESD) produced by electron cloud (EC) effects, ion desorption, or even beam halo scraping [1]. The analysis of the measured coherent tune shift along the bunch train showed to be consistent with the tune shift due to an electron cloud (EC) density, calculated using computer simulations codes in Ref. [4]. In order to obtain a careful diagnostic, and

properly study the phenomenon during Run-3 (December 2002 until May 2003), devoted instrumentation was installed during the 2002 shutdown. Presently, this instrumentation (updated at [5]) is listed as follows:

- 16 electron detectors (ED) installed in the RHIC ring. These detectors also allow ion collection by switching its bias voltage. Detailed information about these ED can be found in Refs. [6-8].
- Pin Diodes to evaluate the beam halo scraping.
- Several vacuum gauges, including Residual Gas Analyzer (RGA) allow pressure rise analysis.

The use of solenoids and NEG (Non Evaporable Getter) coated beam pipes have been explored as possible cures to the electron cloud problem. Solenoids were wrapped along 64 m of the warm beam pipes during 2002 shutdown. The maximum attained magnetic field with the solenoids is 68 Gauss. During the 2003 summer shutdown, 60 m of beam pipe in the warm vacuum sections were coated with NEG. Also, in order to minimize the detrimental effects of the EC (and thereby optimize machine luminosity) the effect of bunch gaps along the bunch train were studied [9,10].

Two main types of pressure rises have been observed during Run-3: At injection, EC effects have been proved to be responsible for the pressure rises [7,9,10]; And at transition, beam loss seems to have a large influence in the pressure rise [11]. The presence of EC in this process has not been fully understood yet, and it is currently under study [12]. As a consequence of the pressure rise, intolerable experimental backgrounds in the Interaction Regions arise and limit machine operation [11-13].

Table 1 summarizes the pressure rises, beam characteristics and beam pipe surfaces for the reported fills. In the following, Section 2.16.2 will focus on the experimental electron multipacting evidences, while Section 2.16.3 deals the case of EC in the Interaction Regions. Section 2.16.4 will discuss the results of the possible cures attempted during Run-3. Finally, Section 2.16.5 summarizes the whole set of observations shown in this paper.

**Table 1.** Main beam characteristics for the fills reported in this paper. In each fill, the pressure values refer to the gauge in which the maximum pressure reading was logged. The two later cases refer to the Interaction Region 12, with two beams circulating in the same beam pipe. The values listed for these two cases always refer to the average numbers for each beam.

Fill #	Average Bunch Intensity – N	Bunch Spacing	# Bunches Injected	Initial Pressure	Maximum Pressure	Surface material
3460	$0.95 \cdot 10^{11}$ p	108 ns	110	$3 \cdot 10^{-10}$ torr	$4 \cdot 10^{-6}$ torr	Unbaked steel
3530	$1.1 \cdot 10^{11}$ p	108 ns	41	$3 \cdot 10^{-10}$ torr	$2 \cdot 10^{-6}$ torr	Unbaked steel
3812	$1.7 \cdot 10^{11}$ p	108 ns	39	$3 \cdot 10^{-10}$ torr	$6 \cdot 10^{-6}$ torr	Unbaked steel
4791	$1.1 \cdot 10^9$ Au <sup>79+</sup>	216 ns	56	$3 \cdot 10^{-11}$ torr	$2 \cdot 10^{-9}$ torr	Baked steel
4794	$0.95 \cdot 10^9$ Au <sup>79+</sup>	108 ns	110	$5 \cdot 10^{-11}$ torr	$7 \cdot 10^{-8}$ torr	Baked steel

## 2.16.2 Experimental results

### 2.16.2.1 EC influence on the pressure rise

During Run-3, gold ions ( $\text{Au}^{79+}$ ) were accelerated in the counterclockwise ring (yellow ring), and deuteron (d) were accelerated in the clockwise ring (blue ring). In April 2003, the Collider had 5 weeks of polarized proton-proton operation. EC effects have been held to be responsible for the pressure rises at injection with all the species ( $\text{Au}^{79+}$ , d, and p) [6,7,9,11]. Figure 1 shows a significant case (fill 3460) in which the correlation of electron flux into the wall is shown as a primary source of pressure rise: after filling the blue ring with 45 bunches (out of 110), bunch intensity of  $0.95 \cdot 10^{11}$  p, and bunch spacing of 108 ns. The fill is interrupted due to the strong pressure rise. The injection is resumed after some minutes. Correlation between the time evolution of pressure and electron signal readings in the same region is visible, thereby showing EC as a primary trigger for the pressure rise. Note that the pressure is plotted in logarithmic scale, while the voltage in the ED is shown in a linear scale.

A priori, one would expect a linear dependence between the electron flux into the wall and the pressure depending on the ESD coefficient ( $\eta$ ) of the beam pipe surface. However, this dependence breaks up overall the injection process (see Fig. 1). However, linear dependence (if any) can only be assumed in absence of other desorption processes, which is unlikely to happen once vacuum breakdown occurs. Previous calibration of the ED [8, 9], the flux into the wall ranges from about  $0.5$  to  $2 \mu\text{A}/\text{cm}^2$ .

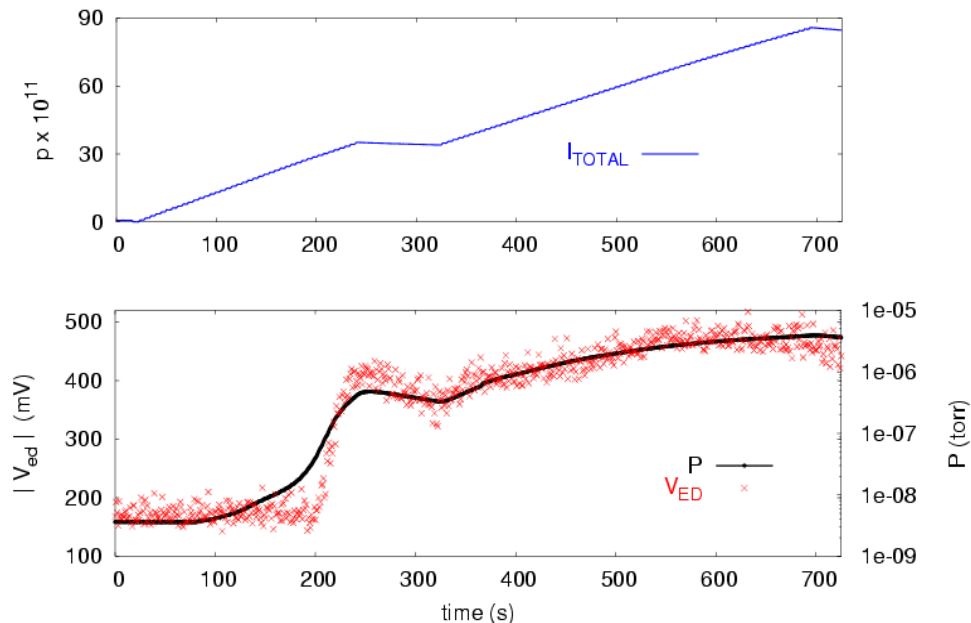


**Fig. 1.** The top figure shows the total beam current injected in RHIC. Note that injection was temporally interrupted after injection of 45 bunches ( $t=250$  s), and resumed at  $t=320$  s. The bottom picture shows the pressure evolution (black line) and the voltage (absolute value) in the ED (red crosses) while this injection takes place. The noise in the ED is about 150 mV.

### 2.16.2.2 Electron energy spectrum

The build up of the EC, as well as the corresponding pressure rise, has a strong dependence on the wall surface parameters. The Secondary Emission Yield (SEY) is the main responsible for the EC build up, whereas the above-mentioned ESD coefficient ( $\eta$ ) is the main responsible for the pressure rise. These parameters are a function of the electron energy of the impinging electrons. Therefore, the electron energy spectrum is a significant piece of information for the EC understanding.

Using the Retarding-Field Analyzer electron detector, several energy sweeps were carried out during fill 3812, whose characteristics can be seen in Table 1. Figure 2 shows the absolute value of the voltage collected in the ED for two different energy sweeps (red and blue curves), and the electron energy distribution (black line), given by the numerical derivative of both curves. Note that the oscillations in the sweeps produce as well oscillation in the spectrum. The two main aspects to stress is first the large peak of low energy electrons (15 eV), and second how the spectrum extends to about 350 eV. Unfortunately, as mentioned earlier the noise in the ED is around 0.15 V, so we cannot definitely conclude the upper energy limit for the energy spectrum.

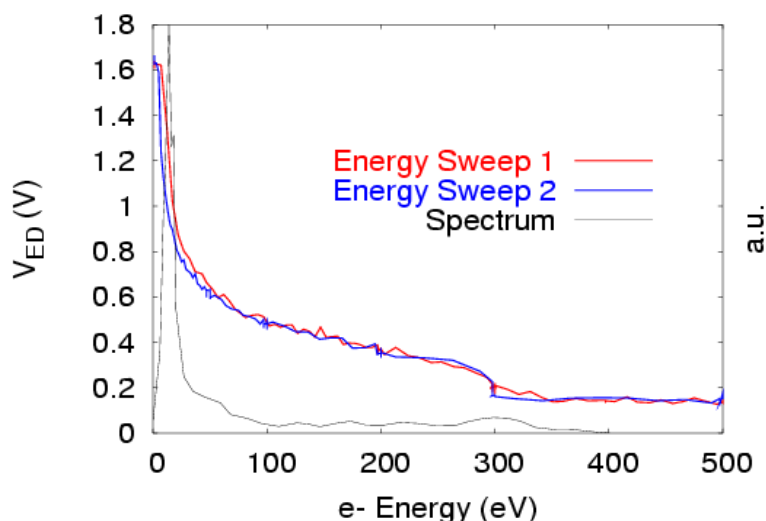


**Fig. 2.** The red and blue traces show the electron signal in the ED when filtering the electron energy from 0 to 500 eV. The corresponding differentiated spectrum is shown by the black trace. Note that the noise in the ED is about 0.15 V.

### 2.16.3 Electron Cloud in the Interaction Regions

Sudden pressure rises in the Interaction Regions (IR) provoke high experimental backgrounds through beam-gas scattering, becoming a machine limitation at RHIC (yet the pressure rise itself does not produce any machine damaging). During both Run-3 and Run-4 (2003/2004), the interaction regions have been main bottle necks in machine operation due to high experimental backgrounds [13].

However, the EC analysis in the IRs raises some extra difficulties compared to the straight sections. The two beams circulating in opposite senses produce an uneven bunch spacing that

changes along the beam pipe locations. Eventually, when the two beams collide in the Interaction Point (IP), the bunch charge at IP is double than for a single beam. This case was studied for LHC in [14], and more recently at RHIC [12].

An experimental analysis of the EC in the IRs was carried out during Run-4 ( $\text{Au}^{79+}$  -  $\text{Au}^{79+}$  operation). The analysis was focused on IR12, where special EC instrumentation is placed. Figure 3.a and 3.b (fills 4791 and 4794, respectively) summarize this study. Firstly, we inject 56 bunches ( $N=1.1 \cdot 10^9 \text{ Au}^{79+}$ , 216ns bunch spacing) in each ring (Fig. 3.a), named blue (circulating clockwise) and yellow (counterclockwise). The pressure rise up to  $2 \cdot 10^{-9}$  torr in the gauges 1m away from the IP, but it did not rise in the gauges placed at each extreme of the IP. The EC signal, if any, did not overcome the noise in the ED. Nonetheless, one can see a solenoid field of  $\sim 5$  Gauss decreased the pressure by a factor of 10. When the beams were shifted with respect to each other they were lost, and the experiment ended.

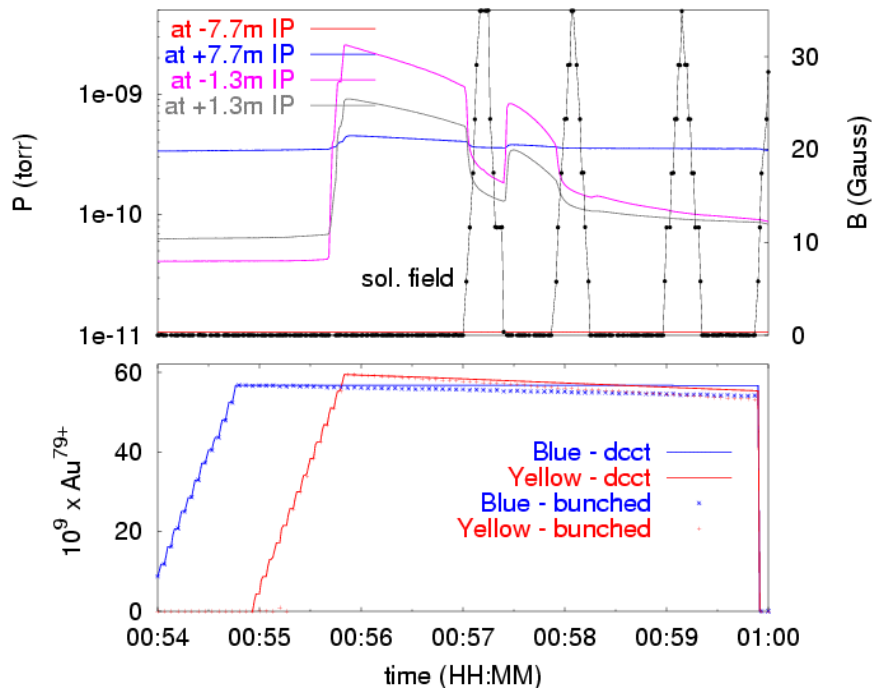


**Fig. 3a.** Pressure rise (top plot) while injecting 56 bunches in each ring, spaced by 216 ns (bottom plot) in fill 4791. Note that weak solenoid fields (around 10 Gauss) decrease the pressure value by a factor of 10.

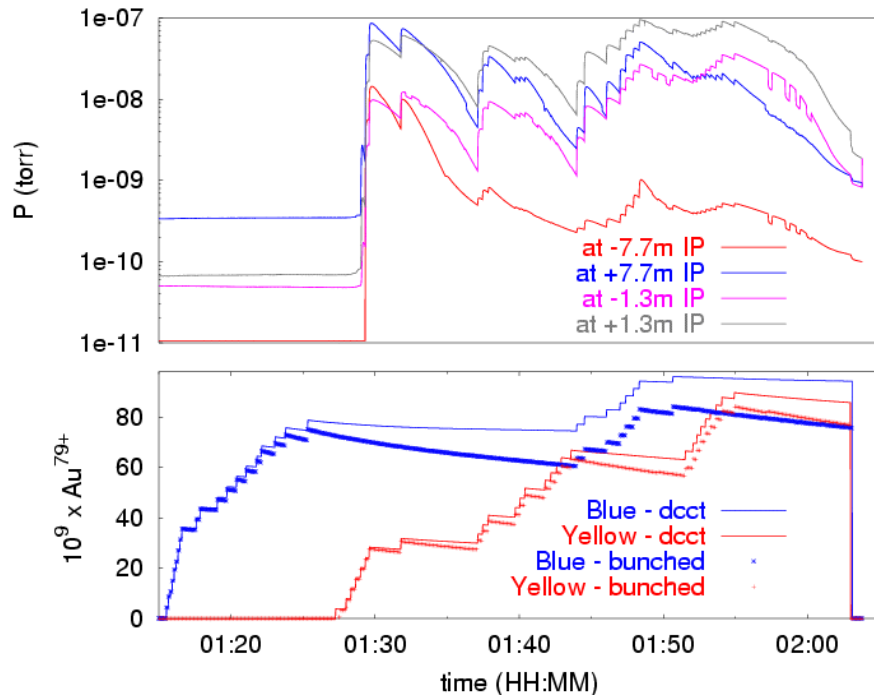


**Fig. 3b.** Pressure rise in the different gauges of IR12 while injecting 110 bunches in each ring, spaced by 108 ns (fill 4794). In this case, the pressure only decayed by a factor of 2 when applying solenoid fields.

The next injection into RHIC (Fig. 3.b corresponding to fill 4794) was carried out using 110 bunches ( $N=0.95 \cdot 10^9 \text{ Au}^{79+}$ ) with 108 ns bunch spacing in RHIC. Note that injecting 80 blue bunches does not produce any pressure rise. However, after injecting only 28 yellow bunches, the EC threshold is reached and the pressure rise to  $7 \cdot 10^{-8}$  Torr. After some time, the large amount of debunched beam causes the pressure to decay and more bunches could be injected. By repeating this process over 40 minutes, we managed to inject up to 110 bunches in either ring. In this case, the solenoid field only decreased the pressure by a factor of 2. Compared to results in Fig. 3.a, the less efficient solenoid field in this case can be due to extended EC along the whole beam pipe, therefore, reducing EC only in the location of the solenoid field does not produce the same effect. Note that gauges at 7.7 m from IP did not see any pressure increase in the first case (Fig. 3.a), unlike the case in Fig. 3.b.

Figure 4 shows a snapshot of  $12.8 \mu\text{s}$  (a RHIC revolution) taken by an ED placed one meter away from the IP, and the bunch intensity logged by the Wall-Current Monitor for each beam. One can see that EC only appears during the time intervals that the beams are overlapping: the top plot shows a snapshot of the electron signal collected by the ED, whereas the bottom plot shows the position of yellow bunches relative to the blue ones when the injection is finished (110 bunches in each ring).

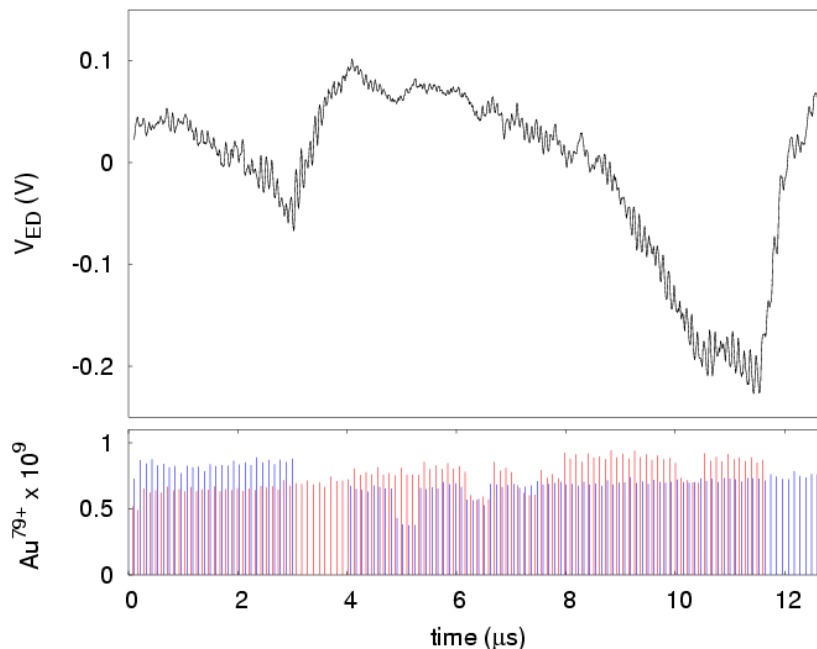


**Fig. 4.** The top plot shows the EC build-up in IR12 during a RHIC revolution (12.8  $\mu\text{s}$ ). The bottom plot shows the bunch intensity of both blue (blue lines) and yellow (red lines) beams and the relative time position between them. Note a single beam produces a decay in the electron signal (between 2.8 and 4  $\mu\text{s}$  – blue abort gap, and 11.6 and 12.8  $\mu\text{s}$  – yellow abort gap).

#### 2.16.4 Possible cures

One of the tested solutions to suppress the EC in RHIC is the use of solenoid fields [15, 18], which bend the trajectory of an electron before it gains enough energy from the bunch to produce secondary electrons when hitting the wall. The second tested method against the build up of the EC is the use of gaps in the bunch train. Since the growth (or build up) time is longer than the decay time, the goal is to look for a bunch pattern, which does not trigger the EC, or that the pressure rises due to EC can be handled by the vacuum system. Therefore, we intentionally did not fill certain buckets in such a way that the EC does not have enough time to build up.

In fill 3530 (see Table 1), we attempt to fill RHIC with 84 bunches with the usual 108 ns bunch spacing and a bunch charge of  $1.1 \cdot 10^{11}$  p. However, every 16 consecutive bunches, we leave a gap corresponding to 4 “ghost” bunches (not filled buckets). As we can see in Fig. 5 and due to the so-called “memory” effect producing long lived electrons [16], after 41 bunches the EC is clearly triggered and the injection had to be stopped due to pressure rise. The bottom plot in Fig. 5 shows the filling pattern for this particular fill. The effect of the different bunch patterns in the pressure rise has been evaluated in [10], which finally led to develop a software to unevenly fill the buckets in RHIC (thus, create a given bunch pattern with different bunch spacing). Bunch spacing of 3, 6, 9, ... buckets (corresponding to 108, 216, 324, ... ns) allow to fill the RHIC circumference with 45, 56, 68, ... bunches, depending on the available bunch intensity, and thus allowing the optimization of luminosity at each fill.

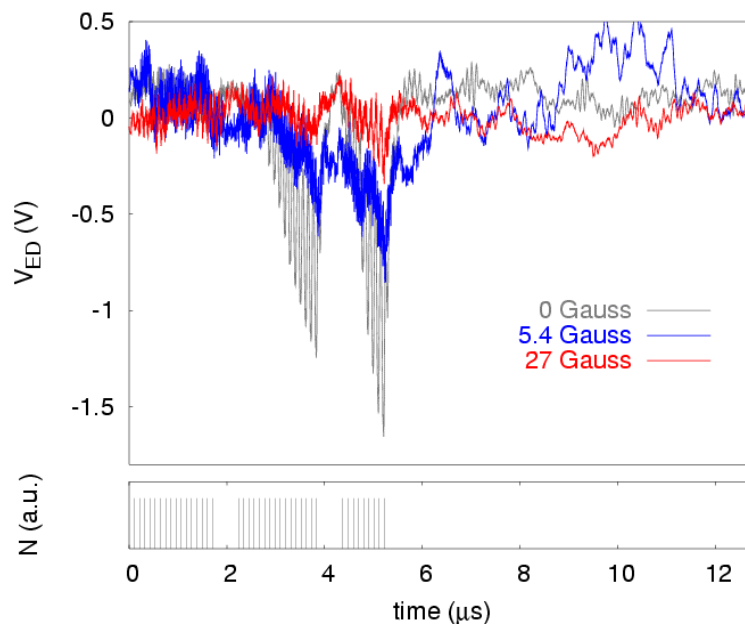


**Fig. 5.** The bottom plot shows a bunch pattern tested to suppress the EC: 16 successive bunches are followed by 4 “ghost” bunches with a bunch spacing of 108 ns. However, as can be seen in the top plot (grey trace), EC signal already appears when 41 bunches were injected in RHIC. The top plot also shows the effect of applying different solenoids fields: at 5.4 Gauss the electron signal has already decreased by a factor  $\sim 2$ , and at 27 Gauss (red trace), the EC signal is already within the noise level of the ED.

Figure 5 also shows the effect of applying different solenoid fields. The effect of a solenoid field of 5.4 Gauss already decreases the flux into the wall by a factor of 2 (blue trace). For a solenoid field of 27 Gauss, the signal is already at the noise level of the ED, and not additional benefit could be concluded by applying more than 27 Gauss (red trace). The final effectiveness of the solenoid fields for RHIC is being evaluated with computer code simulations [17]. As seen in [18], two solenoid fields must be arranged with equal polarity configuration to optimize the benefit from a solenoid field.

### 2.16.5 Conclusion

Experimental results indicate EC effects as responsible for the pressure rise at injection. Observations show a pronounced low energy peak (15 eV) in the energy distribution of the electrons, and the tail extends up to  $\sim 350$  eV, although this upper bound cannot be precisely determined. Solenoid fields decrease the multipacting effect, and detailed studies to evaluate its effectiveness are currently being carried out. In order to maximize RHIC luminosity by minimizing the detrimental effects of the EC, bunch spacing of 3, 6, 9, ... buckets allow filling RHIC with 45, 56, 68, ... bunches, depending on the available bunch intensity, and thus optimizing luminosity at each fill.

For a given surface, observations show that IR regions are more EC prone, as a result of the two beams coming from opposite directions, which produce shorter bunch spacing. Although

solenoid fields can significantly reduce the EC, practical difficulties arise from wrapping solenoids in the experimental locations, and therefore surface coatings (NEG) facilities are currently being developed at BNL [19].

### 2.16.6 Acknowledgements

The author is indebted for helpful discussions to M. Blaskiewicz, A. K. Drees, W. Fischer, D. Gassner, J. Gullotta, P. He, H. Hseuh, H. Huang, J-M. Laurent, R.C. Lee, S. Peggs, G. Rumolo, L. Smart, P. Thieberger, D. Trbojevic, K. Zeno, and S.Y. Zhang.

### 2.16.7 References

1. W. Fischer et al., "Vacuum pressure rise with intense ion beams in RHIC". Proceedings of EPAC'02, Paris, France, 2002.
2. H. Hseuh, L. Smart, et al. "Analysis of beam induced pressure increases in RHIC warm vacuum sections". Proceedings of EPAC'02, Paris, France, 2002. EPAC02.
3. S.Y. Zhang. "RHIC vacuum pressure bump". BNL C-A/AP/67 (2001).
4. W. Fischer, M. Blaskiewicz, M. Brennan, T. Satogata. "Electron cloud measurements and simulations for the Brookhaven Relativistic Heavy Ion Collider". PRST-AB **5**, 124401 (2002).
5. <http://www.rhichome.bnl.gov/AGS/Accel/Vacuum/RHICindex.html>
6. J. Gullotta, D. Gassner, et al. "RHIC electron detector signal processing design". Proceedings of PAC03, Portland, USA, 2003.
7. U. Iriso et al. "Electron detectors for vacuum pressure rise diagnostics at RHIC". Proceedings of PAC03, Portland, USA, 2003
8. P. He et al. "Calibration of RHIC electron detectors". Proceedings of PAC03, Portland, USA, 2003.
9. U. Iriso et al. "Electron Cloud Observations at RHIC in Run-3 (2002/03)." BNL C-A/AP/129.
10. W. Fischer and U. Iriso. "Bunch patterns and pressure rise in RHIC". BNL C-A/AP/118.
11. S.Y. Zhang, et al. "RHIC pressure rise and electron cloud". Proceedings of PAC03, Portland, USA, 2003.
12. G. Rumolo and W. Fischer. "Analysis of PHOBOS experimental background". BNL C-A/AP/146.
13. S. Y. Zhang. "Experimental background in RHIC deuteron-gold run". BNL C-A/AP/107.
14. A. Rossi, G. Rumolo, and F. Zimmerman. "A simulation study of the electron cloud in the experimental regions of the LHC". LHC-PROJECT-REPORT-581. Jul 2002 .
15. R. Macek et al. "Recent experimental studies studies of the electron cloud at the Los Alamos PSR". KEK Workshop, Sept. 2001.
16. R. Cimino, I. Collins, et al. "Can low energy electrons affect high energy physics accelerators?". CERN-AB-2004-012-ABP.
17. L. Wang, private communications.
18. L. Wang, H. Fukuma, K. Ohmi. "Numerical study of photoelectron cloud in KEK LER". Proceedings of APAC'01. Beijing, China, 2001.
19. H. Hseuh, private communications.

## 2.17 Measurement of Electron Cloud Effects in SPS

J. M. Jiménez

Mail to [jose.miguel.jimenez@cern.ch](mailto:jose.miguel.jimenez@cern.ch)

European Organization for Nuclear Research – CERN  
CH-1211 Geneva 23 - Switzerland

### 2.17.1 Introduction – SPS and LHC Issues

The electron cloud is not a new phenomenon, indeed, it was observed already in other machines like the proton storage rings in BINP Novosibirsk [1,2] or in the CERN ISR (Intersecting Storage Ring) [3-5]. Inside an accelerator beam pipe, the electrons can collectively and coherently interact with the beam potential and degrade the performance of the accelerators operating with intense positively charged bunched beams. Most of the positive beam rings are suffering from the electron cloud which induces e-p instabilities, emittance growth or pressure rises. This is the case of the two B factories at SLAC [6] and KEK [7], the Relativistic Heavy Ion Collider at BNL [8], the Los Alamos Proton Storage Ring [9,10] and the Super Proton Synchrotron (SPS) at CERN [11-13].

In the SPS and with LHC-type\* beams, the electrons created at the vacuum chamber wall will be accelerated by the proton bunches and will cross the vacuum chamber in less than 5 ns. A significant fraction of the electrons will be lost with the nominal bunch spacing of 25 ns, except the low energy electrons will have a significant chance to survive the gap potential [14-16] between bunches and be kicked up to several keV by the following bunches. This non resonant single pass mechanism may lead to an electron cloud build up if the maximum secondary electron yield (SEY)  $\delta_{\max}$  of the chamber wall is larger than a critical value, typically around 1.3 [17,18]. The critical value is decreased down to 1.15 [19] if the contribution of the reflected electrons is taken into account in the secondary electron yield coefficient (SEY). Then, the electron cloud is amplified at each bunch passage and reaches a saturation value determined by the space charge repulsion.

The electrons inside the beam pipe can be generated via photoemission due to the synchrotron radiation, by beam-gas scattering or via secondary emission due to electron, proton or ion impacts. Recent observations indicate that the beam-induced multipacting can also occur far from the resonance condition proposed by O. Gröbner [5]. This is the case when the electrons can interact with several passing bunches (bunch trains) or when the low-energetic secondary electrons can survive an extended gap [14-16].

In August 1999, the first high bunch intensity LHC-type beams were injected in the SPS machine resulting in a dramatic pressure rise by a factor of 50 to 60 in the arcs and in the long straight sections. The maximum pressure measured was  $10^{-5}$  Pa (static pressure i.e. without beam:  $10^{-7}$  Pa) for a proton bunch intensity of  $6 \times 10^{10}$  p/b (half of the LHC nominal bunch intensity) and a duty cycle close to 60%. At the same time, strong perturbations on the electrostatic pick-ups and beam instabilities were observed. The transverse feedback system (“damper”) used in the SPS to damp injection oscillations and to stabilize the beam against transverse coupled bunch instabilities was strongly perturbed [20]. The vertical position signal

---

\* 3 or 4 batches of 72 bunches separated by 225 ns, 25 ns bunch spacing,  $1.1-1.7 \times 10^{11}$  p/bunch (81 bunches per batch in 1999), 4 ns bunch length at injection.

induced by a single batch showed a drift of the signal starting half through the 2  $\mu$ s batch. This drift was due to electrons hitting the pick-up electrode and the threshold intensity of this phenomenon, around  $4 \times 10^{10}$  p/bunch, was increased up to  $7 \times 10^{10}$  p/bunch by applying a longitudinal solenoid magnet field of 100 Gauss ( $10^{-2}$  T) giving a clear indication that electrons, in the vacuum chamber, were at the origin of the effect. The pressure rises, beam instabilities and emittance growth showed also evidences of the electron cloud phenomenon as the mechanism responsible for these instabilities.

In the LHC, electron multipacting is expected to take place in the cold and warm beam pipe due to the presence of the high intensities bunched beams, creating an electron cloud [17,18,21-27]. The additional heat load induced by the electron cloud onto the LHC beam screens of the cold magnets of the LHC bending sections (the arcs represent  $\sim 21$  km in length) was, and is still, considered as one of the main possible limitation of LHC performances. Since 1997 and in parallel with the SPS studies, measurements in other machines or in the laboratory have been made to provide the input parameters required by the simulations.

Among the various experiments, the more relevant are the photoelectron yield measurements in the CERN Electron Positron Accumulator (EPA) ring on different materials [28-30], the studies on the molecular desorption and sticking coefficients at cryogenic temperature [31-34] by the synchrotron radiation and the electron stimulated desorption [35]. In the laboratory, the secondary electron yield of technical materials and its variations with the surface treatment [36-38], the dose effect [39] and the electron stimulated desorption [40] have also been studied.

For the SPS which will serve as the LHC injector, the objective was to be able to inject 3 or 4 batches of 72 bunches ( $1.1 \times 10^{11}$  p/bunch) and to accelerate them up to 450 GeV without loosing in intensity as a consequence of the beam losses induced by the beam-gas scattering and keeping the emittance of the beam constant, since this emittance will be preserved in the LHC [41,42]. Any emittance increase will result in a reduction of the LHC luminosity.

In normal operating conditions (beam lifetime  $> 100$  h), the LHC should not be limited by the pressure rise in the cold parts due to the huge cryogenic pumping speed. If operated at lower beam lifetime, the cold magnets quench limit could be reached due to the radiations generated by the beam-gas scattering. In the long straight section (field free regions), the use of NEG coated copper chambers will provide the adequate distributed pumping speed and a reduced secondary electron yield [43]. Ion pumps spaced by 28 metres maximum will pump the gasses not pumped by the NEG coatings. The expected limitations should be linked to the additional heat losses on the cryogenic system or to the emittance growth and beam losses induced by the e-p instabilities [44].

Since 1999, the experimental program at CERN was based simultaneously on the different SPS and LHC requirements regarding the electron cloud induced limitations. SPS priorities were oriented towards the beam conditioning and vacuum cleaning of room temperature beam pipes in field free and dipole field conditions, as the LHC priorities aimed to provide the input parameters required to refine the simulations mainly for the beam pipes at cryogenic temperature and in dipole field conditions.

This paper presents the CERN experimental program and the associated experimental set-up in the SPS machine or in the laboratory to study the electron cloud effects on the proton beams and on the gas pressures in the vacuum chambers at room temperature, at 4.5 K and in a NEG coated chambers.

## 2.17.2 Set up description - Specific results

### 2.17.2.1 Strip Detectors: Spatial and Energy Distributions

The measurements made in 1999 using the pressure gauges and the shielded pick-ups indicate different behaviours for the electron cloud build up in presence or not of a dipole magnetic field. Simulations predicted the appearance of two lateral strips above a bunch intensity of  $5 \times 10^{10}$  p/bunch, a 3<sup>rd</sup> central strip at higher bunch intensities and the increase of the distance between the two lateral strips with the bunch intensity. This later effect is independent from the magnetic field strength.

To confirm these simulations and study the spatial distribution of the electrons in the cloud, a 16 channels strip-detector [15,16] was installed in the SPS in 2000 in a dipole magnet. This type of detector measures the electron flux to the wall and its dependence with the magnetic field. The copper strips, deposited on a MACOR™ substrate in the longitudinal plane, allow the collection of a fraction of the electrons from the cloud. The strips, which remain under vacuum, were separated from the beam by the vacuum chamber wall in which hundreds of holes ( $\phi$  2mm) were drilled with a total transparency of 7.5 % to avoid the extinction of the multipacting by an excessive collection of electrons. The distribution of the holes was calculated to minimize the interference with the strips arrangement. The signal collected by each channel was measured individually using a current integrator with a minimum integrating time of 2 ms ( $\sim$ 100 turns in the SPS). The detection limit of the current integrator was about  $10^{-8}$  A for each individual channel. In 2002, a new version with 36 channels was installed to improve the spatial resolution by a factor 2 i.e. 1.25 mm in resolution [45]. Two filtering grids were added to the 2001 version to allow a simultaneous measurement of the spatial and energy distributions [45,46] of the electrons in the cloud.

In 2003, two new strip detectors were installed in the SPS with an identical design, one operating at room temperature and the second one at 30 K [46,47]. The cooling of the cold strip detector (CSD) was obtained using a cold head connected to the beam vacuum chamber; the collecting strips were also at 30 K. The measurements at 30 K can be compared to the room temperature measurements obtained by a variable aperture strip detector (VASD). The latter detector measures also the dependence of the electron cloud density with the vacuum chamber height in the  $\pm 17$  mm to  $\pm 40$  mm range with respect to the beam trajectory. This measurement allows studying the variations of the electron cloud intensity with the vacuum chamber height. Both strip detectors were installed in dipole magnets.

The design of the collecting strips (48 channels to provide a wider detection area: 84 mm transverse) and the acquisition electronics were identical to the one used in 2002 for the 36 channels strip detector [15]. Special RF shielding has been used to maintain the electrical continuity along the beam pipe and avoid possible space charge effects.

In 2004, these detectors are being reinforced by a strip detector installed in a quadrupole magnet to study the spatial distribution of the electrons in a quadrupole field [47] and by an updated layout for the cold strip detector which will now be protected against the parasitic effects of the water coming from the upstream and downstream unbaked chambers of the SPS by two 1 meter long cryogenic traps [47]. These cold traps will be operated between 30 and 50 K. The cold strip was also modified and equipped with a retarding field detector.

The spatial distributions of the electrons in the cloud measured with the strip detector in 2001 in dipole and field free conditions have been confirmed using the higher resolution 2002

version. Recent simulations fit fairly well the measurements [19], i.e. the position of the two lateral strips is displaced towards the edges when increasing the bunch intensity. Above  $8 \times 10^{11}$  p/bunch and as predicted by the simulations, a 3<sup>rd</sup> central strip was observed.

The simultaneous energy and spatial distributions studies showed that most of the high-energy electrons i.e. above 200 eV, are located in the central strip, the two lateral strips having electrons with energies below 180 eV. This last observation could explain why the central strip disappears prematurely since the higher electron densities and electron energies will create a faster decrease of the secondary electron yield thus causing the extinction of the cloud in the central area. The strip-detectors confirmed that above the bunch intensity threshold measured in a dipole field condition, only a weak dipole field strength of 20 to 30 Gauss is required to trigger the electron cloud.

The measurements showed that, in the LHC, with bunch intensities between  $1.1 \times 10^{11}$  and  $1.3 \times 10^{11}$  p/bunch, the two vertical lateral strips of the cloud will face the beam screen pumping slots (9 and 11.5 mm respectively from the centre) inducing additional heat load to the cold bore. This effect has been suppressed by additional pumping slot shields [48] introduced in the LHC baseline to intercept the electrons passing through the pumping slots.

#### *2.17.2.2 Retarding Field Detectors: Energy Distributions*

The energy distribution of the electrons in the cloud is an important parameter since it allows the estimation of the electron-induced heat loads and gives indication on the expected efficiency of the electrons for the conditioning of the surfaces. The higher the electron energy, the faster will be the conditioning, the variations being non-linear.

The energy distribution of the electrons was measured in 2002, at room temperature, with the strip and retarding field detectors [49] in dipole and field free conditions. The voltage on the grid is swept from 0 to 1 kV while the beam is present. The energy spectrum of the electrons can be deduced from the derivative of the collected current versus time. Due to the design of the detectors, the electrons with energies below 20 eV could not be measured. In 2003, a new retarding field detector [50,51] with a better shielding against parasitic effects provided the distribution of the low energy electrons [5 - 30 eV] with an expected cut of the very low energy electrons (<5 eV) which could not travel through the grids to the collector. The recent measurements confirmed the distributions obtained in 2002 [45], the mean energies of the electrons are respectively  $300 \pm 10$  eV and  $180 \pm 10$  eV [45] for the dipole and field-free conditions, peak energies being at 180 and 80 eV respectively.

Electrons with energies as high as 900 eV could clearly be observed at RT at the end of the scrubbing period, which account for a shift of the average energy of the electron spectrum towards higher values during the conditioning process since they were not visible at the beginning of the run.

#### *2.17.2.3 NEG test bench: Efficiency of NEG Coatings*

The use of non evaporable getter (NEG) coatings (TiZrV) [52] has been approved as the vacuum baseline for the vacuum chambers of the LHC room temperature long straight sections. It was expected that the low secondary electron yield of the NEG surface after activation ( $\delta=1.1$ ) [43] which is kept after saturation,  $\delta=1.2$  with a CO saturation [53], should prevent the electron cloud build up.

To validate the NEG behaviour, a test bench was installed in the SPS with a symmetrical layout allowing a direct comparison between NEG coated and stainless steel chambers with identical shapes [54].

With the non-activated NEG, an electron current is measured by the shielded pick-ups and the NEG coated chamber behaves like the reference stainless steel chamber. After activation and even when fully saturated by the water coming from the non-baked adjacent vacuum chambers, the results confirmed that NEG coating suppresses the electron cloud at nominal bunch intensity ( $1.1 \times 10^{11}$  p/bunch) with 4 batches injected, confirming the measurements made in the laboratory with H<sub>2</sub>O contamination [55]. In presence of beam, the predominant gases are as expected: H<sub>2</sub>, CO, CO<sub>2</sub> and CH<sub>4</sub>.

No electron activity was observed even after 8 opening to air and reactivation of the NEG which could potentially increase its secondary emission yield or when injecting electrons into the vacuum chambers to form an “electron seed” ( $\sim 10^{16}$  electrons/m).

The NEG coating proved also its efficiency to suppress completely the electron-induced background to a luminescence beam monitor even in a dipole field. The aluminium plates were NEG coated and in situ baked at 200°C during 2 hours in the unbaked SPS environment.

#### 2.17.2.4 Coaxial resonator 100 MHz

As an alternative to an experiment installed in the SPS, a 100 MHz coaxial resonant cavity was developed, tested [56,57] and used in the laboratory to study the multipacting behaviour of different materials and surface treatments. The onset of multipactor is detected by the observation of several changes in the cavity behaviour, which happen when the input power reaches the multipactor threshold. These following changes constitute the cavity multipactor signature: collection of electrons by the pickup, a corresponding increase of the vacuum pressure, a stabilization of the output signal, an increase of the reflected signal, a detuning of the cavity and the generation of harmonics.

The cavity was used to make comparative measurement on the behaviour of stainless steel surfaces as compared to copper and NEG coated copper. The behaviour of a non activated NEG coated surface was as expected similar to the one of an unbaked stainless steel [49,58]. With an activated NEG coating, the multipacting threshold increased and the amount of electrons collected by the pick-up consistently decreased. Similar measurements were made at liquid nitrogen temperature (77 K) and no electron multipacting was measured, even several monolayers of cryosorbed gases (CO, CO<sub>2</sub> and air) onto the inner wall of the cavity did not change the picture.

In 2003, this multipacting cavity was used to validate the design of the last version of the retarding field detector installed in the SPS.

#### 2.17.2.5 COLDEX Experiment

The COLDEX (Cold Experiment) experiment was initially installed in the CERN Electron Positron Accumulator (EPA) in the PS Complex to measure the photon stimulated desorption [31,34]. In 2002, this experiment was installed in a field-free region of the SPS, the aim being to study the dynamic pressure evolutions in presence of LHC-type beams with a cold bore operated between 3 to 5 K and a beam screen operated between 5 and 100 K.

UHV pressure gauges and residual gas analyser allow following the total and partial pressures. The heat load is measured on the cryogenic cooling circuit and with temperature

probes. A gas injection line allows studying the effect of physisorbed gas in the range of a fraction of monolayer to several tenths of monolayers.

During the 2002-2003 SPS shutdown, the COLDEX was upgraded with the installation of a circular beam screen with pumping slots equipped, as in the LHC baseline, with pumping slot shields to protect the cold bore from the direct bombardment by the electrons from the cloud. An electrically isolated shield allows measuring the electron current. The improvement of the cold-warm transition and an in-situ calibration of the COLDEX decrease the heat resolution of the system down to 100 mW/m.

The Cold bore is, in normal conditions, at 3 K and the temperature of the cold copper beam screen (2.2 m in length and 67 mm inner diameter) can be regulated between 5 and 100K. As for the LHC, the pumping slots represent 1% of the beam screen area. The COLDEX is in a field free region.

As mentioned earlier, the COLDEX has been used to simulate and study the behaviour of the LHC cryogenic vacuum system (1.9 K) in presence of beam. The introduction of a beam screen with the appropriate number of pumping slots in the vacuum chambers of the cryogenics magnets resulted from several iterations [59-61] to prevent possible vacuum instabilities in presence of beams.

In fact, in a cryogenic machine, the desorbed gas remains within the vacuum chamber. In presence of an electron cloud, all the condensed gases having low desorption yield will accumulate onto the inner surface of the beam screens during LHC operation and only the H<sub>2</sub> will have a high probability to be physisorbed onto the 1.9 K cold bore [62] or onto the cryosorbers [63] located in the long straight sections. If required, the gases with potential detrimental effects to the beam can be transferred to the cold bore through the pumping slots by a controlled warming up / cool down sequence. Three cases have been studied in details [62]: after a magnet quench, during an operation of the beam screens around 24 K or above and during the regeneration of cryosorbers. This limitation should be suppressed by doing the beam conditioning before the shutdowns.

### 2.17.3 Beam related effects

#### 2.17.3.1 *Electron cloud threshold and build up*

The electron cloud build is a threshold phenomenon, i.e. the build up start only above a given bunch density or beam potential. In the SPS, below a given threshold, no pressure rise was observed and a biased pick-up collector shielded from the beam by a metallic grid [16] detected no signal. Above the threshold, the pressures rose and the shielded pick-ups detected peaks of current separated by 23 microseconds, which corresponds to the revolution time in the SPS [15]. This behaviour was confirmed by KEK observations [7] and by the simulations.

The observed threshold bunch intensity has a weak dependence on the residual gas pressure and is in agreement with electron cloud simulations. Measurements showed that for bunch intensities above  $7 \times 10^{10}$  p/bunch, the weak longitudinal solenoid field becomes insufficient to suppress the electron cloud in view of the keV energies acquired by the electrons near the beam axis.

### 2.17.3.2 *Bunch intensity - bunch length – Ramp in Energy*

Assuming that the transverse emittance remains stable which uses to be the case, the bunch intensity and bunch length determine the beam potential and therefore are the predominant factors for the electron cloud build up. Above the multipacting thresholds and for both field free and dipole field conditions, the electron cloud intensity increases linearly with the bunch intensity ( $\sim$  beam potential). Similarly, a decrease of the bunch length by 30% which induces an increase of the beam potential doubles the electron cloud intensity and the 3<sup>rd</sup> central strip appears prematurely. Conversely, if the bunch length is increased by 30%, the electron cloud disappeared.

The bunch length reduction can also be an explanation for the increase of the electron cloud intensity and pressure rises during the ramp in energy. A squeezing of the bunch during the ramp implies an increase of the beam potential, and therefore an increase of the kick in energy received by the electrons resulting in an enhancement of the electron cloud intensity. The pressure rises were explained both by the increase of the amount of electrons and by the orbit displacement observed with the strip detectors, which involved new “less scrubbed” surfaces with higher desorption yields. This hypothesis was verified by introducing a 4 mm orbit displacement (i.e.  $\sim$ 8 mm peak to peak), which produced an equivalent pressure rise. During the ramp, the bunch length in the SPS decreases from 4 ns down to 1.7 ns. Consistently, the electron cloud intensity was enhanced until the flat top was reached. Right after reaching the flat top, an RF adjustment is required and causes a significant decrease of the bunch length resulting this time in a reduction of the electron cloud. This last observation need to be confirmed in 2004 since an inversion in the enhancement process when decreasing the bunch length could change the behaviour in the LHC where the bunch length will decrease down to 0.25 ns.

### 2.17.3.3 *Filling pattern: Batch length - Batch trains - Batch spacing – Bunch spacing - Missing bunches*

At  $1.1 \times 10^{11}$  p/bunch, the electron cloud build up starts only after 20 bunches [15]. The number of bunches in the batch (called batch length) required to trigger the electron build up increases when the bunch intensity decreases. Above the threshold, the dependence of the electron cloud intensity with the number of bunches is linear, the same observation being made with the number of batches (called batch trains).

The measurements confirmed that the electron cloud build up will decrease by increasing the bunch spacing. Preliminary measurements with 50 ns and 75 ns showed a decrease of the electron cloud intensity by more than a factor of 10 as compared to the nominal 25 ns bunch spacing, the 75 ns spacing being more efficient. These observations were reproduced by the simulations

Another solution to decrease the electron cloud intensity is the introduction of missing bunches or the increase of the batch spacing. However, both solutions will lead to a decrease of the luminosity.

The introduction of 12 missing bunches in a batch made out of 72 bunches showed pressure decrease by a factor 8. The shielded pick-ups showed that missing bunches in the second half of the train are more efficient in decreasing the electron intensity. These results were reproduced by the simulations.

In the SPS, 3 or 4 batches of 72 bunches will be injected and ramped from 26 GeV to 450 GeV before being injected into the LHC. The standard LHC 8 bucket spacing [225ns] showed that the electron cloud did not disappear between two successive batches. The pick-ups even

showed that the build up of the 2<sup>nd</sup>, 3<sup>rd</sup> or 4<sup>th</sup> batch profits from the electron cloud created left behind by the previous batch resulting in a faster build up [15]. But after the 4<sup>th</sup> batch passage and due to the revolution time in the SPS, i.e. 23 microseconds, the 1<sup>st</sup> batch will pass once again after 14.6 microseconds, a delay long enough to loose all the surviving electrons. Other batch spacing have been studied to reduce the electron cloud effect, i.e. 21 bucket [550 ns] and  $\frac{1}{4}$  of the SPS revolution time [5.25  $\mu$ s] showing that a batch spacing bigger than 550 ns is required to decouple the effect of two successive batches on the electron cloud build up [15].

In the LHC [64], the ring will be full of batches and the maximum batch spacing will not exceed 3  $\mu$ s corresponding to the rise time of the LHC dump kickers. According to the SPS observations which will be confirmed in 2004, this delay should be long enough to loose all the surviving electrons.

#### 2.17.3.4 *Beam Conditioning - Vacuum Scrubbing*

In presence of beams, two mechanisms could place simultaneously: the vacuum scrubbing (cleaning) characterised by a pressure decrease and the beam conditioning characterized by a decrease of the secondary electron yield of the beam pipe surface. For the systems operated at ambient temperature, these two processes use to be coupled. At cryogenic temperature and due to the gas physisorbed on the beam pipe walls, recent observations in short systems are showing a different behaviour [47].

#### 2.17.4 **Room temperature observations**

In the SPS (ambient temperature), the photon and ion-stimulated desorption being negligible, the pressure rises ( $\Delta P/P$ ) are a direct signature of the electron bombardment. The pressure decrease results from both a surface cleaning (gas desorbed by the electron bombardment and pumped) and a reduction of the electron cloud intensity.

The beam conditioning and vacuum scrubbing were first studied using the evolution of the pressure gauges all around the ring. The decrease of the pressure rises by 3 or 4 orders of magnitude during the 3 “scrubbing runs” (in 2002 and 2003) in both the field free and dipole field gave evidence of a vacuum scrubbing. The increase of the multipacting thresholds in both dipole field and field free conditions, from  $3 \times 10^{10}$  p/bunch up to  $10^{11}$  p/bunch and from  $5 \times 10^{10}$  p/bunch up to  $1.3 \times 10^{11}$  p/bunch respectively, are an indication of the beam conditioning. No signal was detected in field-free conditions after 10 days of “scrubbing run”.

A continuous measurement of the electron flux using the strip detectors confirmed the tendency given by the gauges. The evolution of the electron cloud intensity measured by the strip-detectors throughout the cleaning process showed a decrease of the electron flux by a factor  $10^2$  in 10 days in a field-free region.

#### 2.17.5 **Observations at cryogenic temperatures**

The reduction of the electron current versus cumulated beam time is significantly slower at 30 K than at room temperature, but initial values are close [46]. In dipole field regions, the reduction of electron current versus cumulated beam time seems also slower at 30 K than at room temperature, but there is much less difference. Again, initial values are quite close [46]. The initial electron activities are hence comparable at room and cryogenic temperatures as expected from laboratory measurements.

Despite the large fluctuations of beam intensity and uncertainties in the measurements which resulted in a scatter too large for reliable conclusions, a significant vacuum cleaning was observed in COLDEX, the pressure rise dropped from  $5 \times 10^{-7}$  down to  $7 \times 10^{-9}$  Torr after 12 A.h of LHC-type beams and a slow reduction of the power deposited on the beam screen,  $\sim 15\%$  reduction was observed. During the pressure decrease, a change of gas composition was measured [65].

The measured heat load to beam screen was  $\sim 1.5$  W/m for 4 batches, proportional to the number of batches (after the 2<sup>nd</sup> batch). A decrease by 30% of the electron current was measured on the pumping slot shield.

A shift in the energy spectrum of the electrons towards higher energies during the scrubbing run consistent with the observations with the retarding field detector, could explain why the heat load does not decrease proportionally to the electron current. Finally, a few monolayers of H<sub>2</sub>, CO and CO<sub>2</sub>, did not significantly change the deposited heat load as expected from laboratory measurements.

The beam conditioning was quantified using an in-situ measurement of the secondary electron yield ( $\delta$ ) of a copper sample exposed to the bombardment of the electrons from the cloud. After receiving a controlled dose, the copper sample was rotated towards the electron gun to measure the SEY. When required, the sample was masked from the beam to avoid any exposure with non-optimal beam conditions. The decrease of the SEY ( $\delta_{\max}$  and  $E[\delta_{\max}]$ ) is significant, from 2.3 down to 1.4. Recent analytical calculations [66] fit fairly well to the measurements. The number of “created” electrons, i.e. corresponding to the surface of the SEY curve above a  $\delta$  of 1.3, which is considered as the multipacting threshold [5,18,19] decreased by more than 80% after about 100 hour of LHC beam time.

All measurements confirmed that the beam conditioning is effective up to the bunch intensity used during the conditioning. Higher bunch intensities will enhance the electron cloud and the pressures will increase. In a dipole field, the displacement of the lateral strips will create an additional enhancement.

Finally, several parameters measured: pressures, electron cloud intensity, heat load measured by the calorimeters [67,68] showed that the beam-induced multipacting and thus the scrubbing stopped after 4 days in the field-free regions which is consistent with the in situ measurement of the secondary electron yield (SEY) which remained constant after 4 days. The upward drift of the SEY ( $\delta$ ) observed if the SPS is not operated with LHC-type beams is not an issue since measurements confirmed that the SEY recovered its initial value after 4 hours of operation with LHC-type beams above the electron cloud threshold. The measurements confirmed that a venting to air, the secondary electron yield will recover its initial value (2.3 for copper or stainless steel), however the reconditioning will be 10 times faster [69].

#### *2.17.5.1 Gas discharge - Memory effect*

No difference in the pressure rises, nor in the increase of the scrubbing effect could be seen between the non treated vacuum chambers and the two chambers treated with a N<sub>2</sub> discharge [15]. Nevertheless, the chambers treated with a N<sub>2</sub> discharge and submitted to a beam conditioning showed a faster conditioning compared to the non-treated chambers after an exposure to air and the pressure rises were 4 times smaller with an equivalent beam. Measurements were made to study the effect of an Ar/O<sub>2</sub> discharge and of a N<sub>2</sub> discharge followed by a 300°C bake out [15]. These results confirmed that the N<sub>2</sub> discharge even after the bake out at 300°C during 24h had behaviour identical to the non-treated chambers. On the other hand, the Ar/O<sub>2</sub> discharge gave

satisfactory results. The pressure rise measured was 2.5 times smaller than the one measured on the identical non-treated chambers.

#### 2.17.5.2 Heat Load estimations

The electron cloud-induced heat loads have been measured directly in field free and in dipole field conditions using close geometry calorimeters (warm multipacting calorimeters: WAMPAC) [68,70]. Pick-up calorimeters [67] with a much lower intrinsic time constant have also been used in field free regions. The heat load was also estimated from the electron cloud intensity and energy distributions. The mean energy in dipole field regions being 1.7 times bigger than the mean energy in field free, the heat load induced by the electrons will also be 1.7 times bigger. The SPS measurements indicated a heat load between 1.5 and 2 W/m for nominal bunch intensity ( $1.1 \times 10^{11}$  p/bunch) and 4 batches. The extrapolation to the LHC assumes a linear dependence with the filling factors of the two machines: 4/11 for the SPS with 4 batches injected and  $\sim 0.85$  for the LHC which gives a multiplication factor of 2.3. All the detectors installed in the SPS confirmed the linear dependence with the number of batches up to 4 batches. The heat load at ambient temperature is similar to the one measured at 30 K.

The number of electrons in the cloud extracted from the measurement of the electron flux to the walls using the strip detectors at room temperature and at 30 K as well as the one deduced from the heat load measured by COLDEX experiment at 4.5 K or by the calorimeters at 300 K [31,71], indicated a much stronger electron cloud intensity than the one initially expected [17].

#### 2.17.6 Epilogue: Open questions – Actions required

As being the LHC injector, the scrubbing runs confirmed that after 5 days of scrubbing, the SPS should be able to inject 3 or 4 batches at nominal intensity into the LHC with the required beam characteristics. However, the electron cloud is still “visible” in the arcs of the SPS (dipole field) after about 500 hours of LHC-type beams (4 batch-injections at nominal intensity). In the field-free regions, i.e. in the long straight sections, the electron cloud intensity decreased below the detection level of the strip-detectors ( $< 10^{-9}$  A/m).

Despite the large amount of data collected over the last three years, a number of questions still need to be answered or confirmed for the LHC. The maximum luminosity achievable with the 75 ns and 25 ns bunch spacing shall be confirmed as well as a quantitative estimation of the limitation levels due to the electron-induced heat loads, the emittance growth and the e-p instabilities. The 2003 measurements [46,47] showed that no electron cloud-induced heat load limitation is expected with the 75 ns bunch spacing. With the 25 ns bunch spacing, the extrapolations of the SPS results to the LHC showed that, in case of a slower beam conditioning process, the LHC machine will be able to operate at  $7.0 \times 10^{10}$  p/bunch within the 2 W/m of cooling capacity available for the electron cloud-induced heat load provided that the machines is not limited by the emittance growth or e-p instabilities. Assuming the 15 % beam conditioning efficiency after 72 hours of operation, about 20 days will be required for the conditioning assuming a 100% machine efficiency. The beam conditioning efficiency measured on the cold surfaces in field free and dipole field conditions need confirmation avoiding possible edge effects due to the limited length of the detectors.

Even if the vacuum scrubbing was effective at room temperature and at cryogenic temperature, the vacuum performances under different electron multipacting conditions, in particular in the collimators areas where an enhancement could be introduced by the halo need

clarifications. The transfer lines are also concerned since a build up is observed after 20 bunches only.

The preliminary results on the behaviour of the NEG coatings with a seeding of electrons will be confirmed. The electron cloud build up and heat load in a quadrupole field will be studied and compared to the dipole field case.

Finally, the reliability of the extrapolations from the SPS to the LHC need an evaluation in particular due to the lack of results on the validity of the SPS thresholds in the LHC or on the influence of the reduced bunch length in the LHC (8 times smaller).

The SPS scrubbing'04 run will be used to answer most of these open questions. However simulations will be required for the threshold and bunch length effects. The different filling schemes in the two machines also complicate the extrapolation from the SPS situation to the LHC since the surviving electrons could significantly change the picture.

### 2.17.7 Acknowledgements

Many thanks to my colleagues of the Vacuum Group, in particular V. Baglin, B. Henrist, N. Hilleret, B. Jenninger, J-M. Laurent, A. Rossi, K. Weiss for their contribution to this paper, to the Operation crew of both SPS and PS machines for their collaboration and also to G. Arduini, P. Collier, K. Cornelis, O. Gröbner, F. Ruggiero, P. Strubin and F. Zimmermann for their helpful discussions.

### 2.17.8 References

1. Budker, G and al., "Experiments on Producing Intensive Proton Beams by Means of the Method of Charge-Exchange Injections", Soviet Atomic Energy 22, 5 (1967)
2. Dudnikov, V, "Some Features of Transverse Instability of Partly Compensated Proton Beams", Proceedings PAC 2001
3. Hereward, H G, "Coherent Instability Due to Electrons in a Coasting Proton Beam", CERN 71-15 ISR Division (1971)
4. Keil E and al., "Landau Damping of Coupled Electron-Proton Oscillations", CERN ISR TH/71-58 (1971)
5. Gröbner, O, "*Bunch Induced Multipacting*", 10th Int. Conf. High Energy Acc., Protvino, July (1977)
6. Decker, F J, Proceeding of the E-CLOUD'02 workshop, CERN Geneva - April (2002)
7. Fukuma, H, Proceeding of the E-CLOUD'02 workshop, CERN Geneva - April (2002)
8. Zhang, S Y and al., Proceeding of PAC'03 Conference, Portland (2003)
9. Neuffer, D and al., NIM A 321, pp.1-12 (1992)
10. Macek, R, Int. Workshop on Two Stream instabilities, KEK Tsukuba – September (2001)
11. Arduini, G and al., "*Electron Cloud : Observations with LHC-Type Beams in the SPS*", CERN LHC Project Report 434 (2000) or Proceedings of the Workshop on LEP-SPS Performance, CERN Chamonix X (2000)
12. Arduini, G and al., Proceeding of the PAC'01 Conference, Chicago (2001)
13. Arduini, G and al., "The SPS as a Vacuum Test Bench for the Electron Cloud Studies with LHC Type Beams", CERN LHC Project Report 490 (2001)
14. Zimmermann, F, Proc. PAC 2001, Chicago (2001)

15. Jiménez, J M and al., "Electron Cloud with LHC-type beams in the SPS: a review of three years of measurements", CERN LHC Project Report 632 (2003)
16. Jiménez, J M and al., "*Electron Cloud – Results from SPS and Experiments for 2003*", Proceedings of Chamonix 2003 Workshop, CERN (2003)
17. Gröbner, O, "*Beam Induced Multipacting*", CERN LHC Project Report 127 (1997)
18. Bruning, O S and al., "*Electron Cloud and Beam Scrubbing in the LHC*", CERN LHC Project Report 290 (1998)
19. Zimmerman, F, "*Electron Cloud Simulations*", Proceedings of the LHC Workshop, CERN Chamonix XI (2002)
20. Höfle, W, "*Observations of the electron cloud effect on pick-up signals in the SPS*", Proceedings of the Workshop on LEP-SPS Performance, CERN Chamonix X (2000)
21. Zimmermann, F, "*A simulation study of electron-cloud instability and beam-induced multipacting in the LHC*", CERN LHC Project Report 95 (1997) , SLAC-PUB-7425. Stanford, CA (1997)
22. Stupakov, G., CERN LHC Project Report 141 (1997)
23. Bruning, O S and al., CERN LHC Project Report 158 (1997)
24. Bruning, O S and al., "Numerical Simulations for the Beam-Induced Electron Cloud in the LHC Beam Screen", CERN LHC Project Report 190 (1998)
25. Ruggiero, F, "*Electron Cloud in the LHC*", CERN LHC Project Report 166 (1998)
26. Ruggiero, F and al., "Simulation of the electron-cloud build up and its consequences on heat load, beam stability and diagnostics", Phys. Rev. Spec. Top. Accel. Beams 4 (2001) 012801
27. Furman, M A, CERN LHC Project Report 180 (1998)
28. Baglin, V and al., "VUV photoemission studies of candidate LHC vacuum chamber materials", CERN LHC Project Report 256 (1998)
29. Baglin, V and al. "Photoelectron Yield and Photon Reflectivity from Candidate LHC Vacuum Chamber Materials with Implications to the Vacuum Chamber Design", CERN-LHC-Project-Report-206 (1998)
30. Baglin, V and al., "Measurement of the primary photodesorption yield at 4.2 K, 77 K and room temperature in a quasi-closed geometry", CERN LHC Project Report 9 (1996)
31. Baglin, V and al., "Performance of a Cryogenic Vacuum System (COLDEX) with a LHC Type Proton Beam", CERN LHC Project Report 667 (2003)
32. Baglin, V and al., "Synchrotron radiation studies of the LHC dipole beam screen with COLDEX", CERN LHC Project Report 584 (2002)
33. Baglin, V and al., "Molecular Desorption by Synchrotron Radiation and Sticking Coefficient at Cryogenic Temperatures for H<sub>2</sub>, CH<sub>4</sub>, CO and CO<sub>2</sub> ", CERN LHC Project Report 518 (2002) or Vacuum 67 (2002) 421-428
34. Baglin, V and al., "First Results from COLDEX Applicable to the LHC Cryogenic Vacuum System", CERN LHC Project Report 435 (2000)
35. Hilleret, N and al., "*Electron Stimulated Desorption on Cold Surfaces*", IVC'04 (to be published)
36. Bozho, N and al., "The Influence of Air Exposures and Thermal Treatments on the Secondary Electron Yield of Copper", CERN LHC Project Report 376 (2000)
37. Baglin, V and al., "The Secondary Electron Yield of Technical Materials and its Variation with Surface Treatments", CERN LHC Project Report 433 (2000)
38. Baglin, V and al., "A Summary of Main Experimental Results Concerning the Secondary Electron Emission of Copper", CERN LHC Project Report 472 (2001)

39. Henrist, B and al., "The variation of the secondary electron yield and of the desorption yield of copper under electron bombardment: Origin and impact on the conditioning of the LHC", CERN LHC Project Report 583 (2002)
40. Vorlaufer, G, "*Modification of Ultra-High Vacuum Surfaces Using Free Radicals*", PhD report, Technischen Universitat Wien - Fakultat fur technische Naturwissenschaften und Informatik, Wien (2002)
41. Arduini, G and al., "*The Electron Cloud Instability of the LHC Beam in the CERN SPS*", CERN LHC Project Report 637 (2003)
42. Arduini, G and al. "Transverse Behaviour of the LHC Proton Beam in the SPS: an Update", CERN-SL-2001-050-OP (2001)
43. Scheuerlein, C and al., CERN EST/2000-07 (SM).
44. Arduini, G and al., "Present Understanding of Electron Cloud Effects in the Large Hadron Collider", CERN LHC Project Report 645(2003)
45. Jiménez, J M and al., "*Electron cloud studies and Beam Scrubbing in the SPS*", CERN LHC Project Report 634 (2003)
46. Jiménez, J M and al., "Electron Cloud Heat Load Estimations for the LHC Using Strip and Retarding Field Detectors", CERN LHC Project Report 677 (2003)
47. Jiménez, J M, "*The latest news on Electron Cloud and Vacuum Effects*", Proceedings of the LHC Project Workshop, CERN Chamonix (2004)
48. Kos, N, CERN EDMS 362883
49. Jiménez, J M and al., "*Electron Cloud Studies and Analyses at SPS*", Proceedings of the PAC03 Conference, Portland (2003)
50. Laurent, J M, Minutes of the Accelerator Performance Committee CERN August 2003
51. Laurent, J M and al., "*Electron Cloud Energy and Power Measurements in the SPS*", CERN Vacuum Technical Note TN-04-02 (2004)
52. Benvenuti, C and al., Vacuum 60 (2001) 57-65.
53. Henrist, B and al., CERN Vac. Tech. Note 98-08.
54. Rossi, A, Scrubbing days CERN 2002
55. Hilleret, N and al., EPAC 2000, Vienna
56. Laurent, J M and al., Vacuum Technical Note TN-02-12, CERN (2002)
57. Iriso-Ariz, U and al., "*RF test benches for electron cloud studies*", CERN-LHC-2002-005-VAC; CERN-PS-2002-025-RF (2002)
58. Laurent, J M and al., CERN Vacuum Technical Note TN-03-04 (2003)
59. Gröbner, O, "*The LHC Vacuum System*", CERN LHC Project Report 181 (1998)
60. Gröbner, O, "*LHC vacuum system*", CERN-OPEN-2000-288 (1999)
61. Gröbner, O, "*Overview of the LHC vacuum system*", Vacuum 60 (2001) 25-34
62. Baglin, V and al., "*Vacuum Transients during LHC Operation*", Proceedings of the LHC Project Workshop, CERN Chamonix 2004
63. Baglin, V and al., "*Cryosorber Studies for the LHC Long Straight Section Beam Screens with COLDEX*", CERN LHC Project Report 580 (2002)
64. Brüning, O, Minutes of the 59th Performance LHC Committee 59 (CERN)
65. Baglin, V and al., Minutes of the LHC Technical Committee, November 2003
66. Vos, L, "*Analysis of Electron Cloud*", CERN-AB-2003-074-ABP (2003)
67. Hilleret, N and al., Scrubbing days CERN 2002
68. Baglin, V and al., Proceedings of the Scrubbing days CERN 2002

69. Hilleret, N and al., Int. Workshop on Two Stream instabilities, KEK Tsukuba – September (2001)
70. Baglin, V and al., “*SPS Electron Cloud Heat Load Measurements with WAMPAC and Simulations*”, Proceedings of the Mini Workshop on Electron Cloud Simulations for Proton and Positron Beams ECLOUD'02, CERN (2002)
71. Baglin, V and al., Minutes of the Accelerator Performance Committee CERN August 2003

## 2.18 Electron-Cloud Effects in the LHC

F. Zimmermann, E. Benedetto  
mail to: [frank.zimmermann@cern.ch](mailto:frank.zimmermann@cern.ch)  
[CERN](#), [AB Department](#), [ABP Group](#)  
1211 Geneva 23, Switzerland

### 2.18.1 Introduction

The LHC is the first proton accelerator for which synchrotron radiation becomes noticeable. At a beam energy of 7 TeV, the relativistic  $\gamma$  factor is comparable to that of electron or positron beams in the B factories or at many light sources. This means that the same number of synchrotron-radiation photons are emitted per proton and turn. The critical photon energy of about 44 eV in the LHC is near the energy of maximum photo-emission yield for many materials. Therefore, a significant electron cloud can be expected from synchrotron radiation and photo-emission alone. The possibility that beam-induced multipacting may also occur in the LHC was suggested in 1996 [1]. Since 1997, electron-cloud build up in the LHC arcs due to both photoemission and beam-induced multipacting were predicted and studied in simulations [2.3.4]. Electron cloud effects in the LHC were reviewed previously [5.6].

### 2.18.2 Experiments in the LHC Injectors

Experiments with LHC type beam in the CERN SPS and PS, which serve as LHC injector and pre-injector, respectively, have indeed revealed the rapid build up of an electron cloud by beam-induced multipacting, even without any contribution from synchrotron radiation at the low beam energy of 26 GeV. At the nominal LHC bunch spacing of 25 ns, the multipacting is observed for bunch populations above  $3 \times 10^{10}$  protons per bunch at the start of a run. The threshold increases to  $10^{11}$  protons per bunch after 10 days of ‘scrubbing’ (continuous operation with LHC beam at the maximum possible intensity and duty cycle permitted by electron-induced pressure rise). In the SPS the two main effects of the electron cloud are a pressure increase by several orders of magnitude [7] and beam instabilities that can lead to emittance growth and even beam loss (coupled bunch instability in the horizontal plane and single-bunch instability in the vertical plane) [8.9]. Degradation of BPM signals or feedback pick-ups due to electron bombardment were also observed; these could be partially cured by solenoid windings or by data processing at higher frequencies [10].

Since about 2000, a large number of detectors were installed in the SPS to benchmark the electron-cloud simulations and to explore possible countermeasures. Promising results were achieved. In particular, vacuum chambers coated with the newly developed TiZrV getter material

[11] showed no sign of multipacting, which suggests that the solution adopted for the warm parts of the LHC, about 10% of the circumference, will work fine. Also a fast surface conditioning by scrubbing was demonstrated in the SPS arcs. After 1 or 2 weeks of scrubbing the electron cloud did no longer limit the SPS operation with LHC beam. In situ measurements confirmed a considerable reduction of the maximum secondary emission yield, decreasing from about 2.0 to 1.5 over the same time period. However, measurements with two cold chambers in the SPS have shown a much slower scrubbing; see, e.g., [12]. This could be due to the fact that the cold sections are too short and influenced by gas influx from the adjacent warm vacuum chambers. A large number of gas molecules cryosorbed on the cold surface could lead to an enhanced secondary emission yield. In the laboratory, cold surfaces did show a conditioning similar to that of warm samples [13].

### 2.18.3 Concerns for the LHC

The primary concern for the LHC is the additional heat load deposited by the electron cloud on the beam screen (a Cu-coated stainless steel shield inserted into the arc vacuum chamber, which absorbs the photons from synchrotron radiation). Only a limited cooling capacity is available for the additional heat load due to the electron cloud. If it is surpassed, a quench of the superconducting magnets would result.

Figure 1 shows the heat load per unit length simulated for an LHC arc cell under various conditions. Each heat-load value was computed as a weighted average of three independent simulations for dipoles, field-free regions, and quadrupoles, according to the cell fraction covered by each type of field (for sextupoles we assumed the same heat load as for quadrupoles). The different curves refer to different values of the maximum secondary emission yield, ranging from 1.1 to 1.7, and to different numbers of successive bunch trains. The available cooling capacity for the electron cloud is also indicated. It decreases towards higher intensity, since the cooling required for synchrotron radiation, image currents, and gas scattering increases. The latter process seems to be dominant: It presently appears that, due to the gas scattering, at the ultimate bunch intensity of  $1.67 \times 10^{11}$  almost no cooling capacity might be left for the electron cloud [14]. However, no final conclusion has yet been reached on this point.

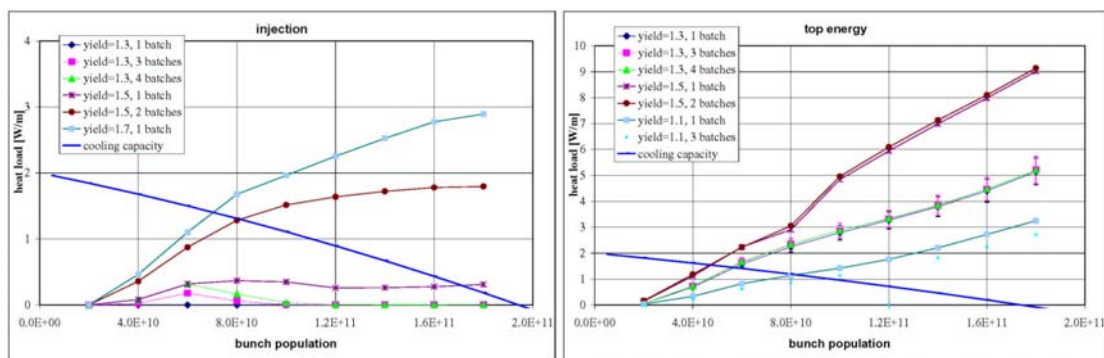


**Fig. 1:** Simulated average arc heat load per unit length as a function of bunch intensity at injection (left) and at top energy (right) for various values of the maximum secondary emission yield and for a variable number of bunch trains, and the available cooling capacity.

The LHC beam consists of batches of 72 bunches with 25-ns bunch spacing, which are separated by gaps of 225 ns. At injection energy, the multipacting process is launched by residual-gas ionization, and the electron build up saturates only at the end of the first or during the second batch. As a result, the simulated heat load depends on the number of batches. At top energy, photoelectrons are abundant and the electron density saturates already after a few bunches of the 1<sup>st</sup> batch, so that in this case the heat load is rather insensitive to the number of batches. The left picture of Fig. 1 suggests a resonance with enhanced heat load for bunch populations around  $6 \times 10^{10}$  protons, visible for the lower values of secondary emission yield. This picture also shows that with a maximum secondary emission yield of 1.3 it is possible to reach or exceed the nominal bunch intensity of  $1.15 \times 10^{11}$  at injection. On the other hand, a maximum emission yield below 1.1 is needed at top energy (right picture).

Before the required low values of the secondary emission yield are achieved by surface scrubbing, the LHC could be operated with a reduced charge per bunch (equal or below  $5 \times 10^{10}$  protons) or with an increased spacing between bunches. Due to the asymmetric arrangement of the collision points, a strict 50-ns bunch spacing (twice the nominal) would yield zero luminosity at one of the collision points (LHCb). Therefore, 75-ns is a more agreeable value. Simulated heat loads for 75-ns bunch spacing are compared with those for 25-ns spacing in Fig. 2, where we consider a single batch and the nominal bunch population of  $1.15 \times 10^{11}$ . The two pictures again refer to injection and to top energy. Figure 2 shows that with 75-ns spacing, any realistic value of  $\delta_{\max}$  can be accommodated, up to  $\delta_{\max} = 2.0$  or beyond. Higher luminosity would be achieved with 50-ns spacing. For example, if nominal bunches at 50-ns spacing were interleaved with low-charge satellites at 25 ns separation, the desired lower luminosity could be delivered to the LHCb experiment, while the heat load would still be under control.

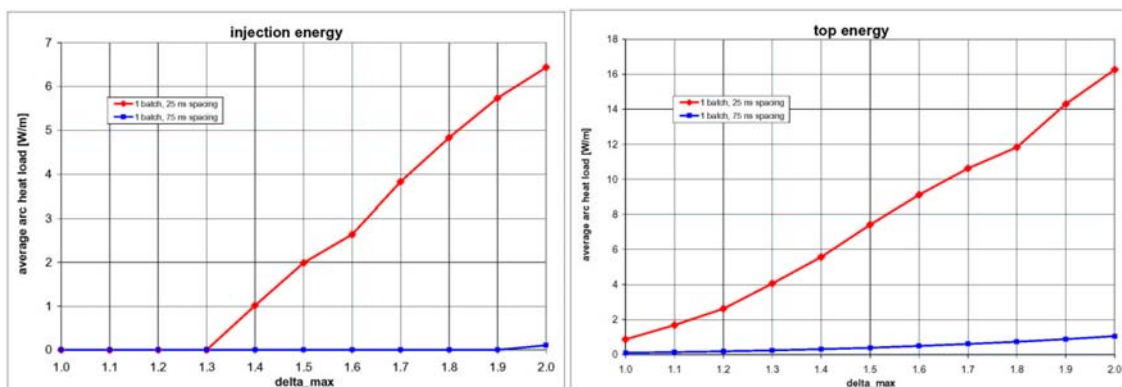


**Fig. 2:** Simulated average arc heat load as a function of the maximum secondary emission yield for bunch spacings of 25 ns and 75 ns at injection (left) and at top energy (right).

In addition to the heat load, the electron cloud could introduce other complications for the LHC operation: instabilities, pressure increase, and emittance growth: Instabilities could be of coupled-bunch or single-bunch type, as in the SPS. The pressure rise might be several orders of magnitude, again as experienced in the SPS. Simulations using the HEADTAIL code indicate the possibility of a long-term emittance growth that could be detrimental for a proton storage ring where the beam is to be stored over tens of hours. As an example, the left picture of Fig. 3 shows the simulated electron volume density as a function of the simulated arc heat load, for various

scenarios. There is no 1-to-1 relation between electron density and heat load, but in general the heat load appears acceptable, if the electron density drops below  $5 \times 10^{11} \text{ m}^{-3}$ . The right picture displays the emittance growth time simulated by HEADTAIL as a function of the electron-cloud density on a double-logarithmic scale. Daringly extrapolating the left five points on this plot linearly to larger rise times and lower densities, we estimate that an emittance rise time larger than 30 minutes is reached for a density of about  $3 \times 10^{10} \text{ m}^{-3}$ . According to these preliminary results, the acceptable limit on the electron cloud density that is imposed by long-term emittance preservation may be one or two orders of magnitude lower than the limit arising from the heat load.

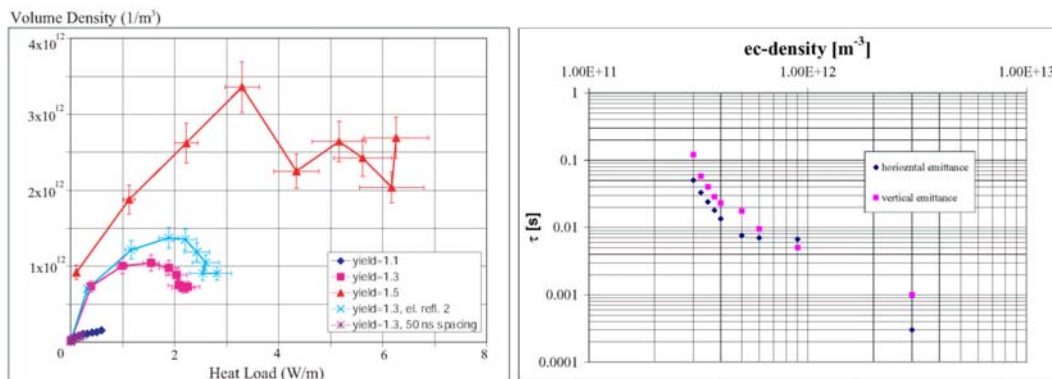


**Fig. 3:** Electron volume density simulated by ECLLOUD as a function of average-arc heat load at top energy (left) and emittance growth rise time simulated by HEADTAIL as a function of electron volume density at injection (right).

#### 2.18.4 Countermeasures

The LHC design adopted a number of countermeasures against the electron cloud. Most vacuum chambers in the warm sections of the LHC are coated by a newly developed getter material, TiZrV [11], which has a low maximum secondary emission yield of about 1.1. In the cold arcs, a sawtooth pattern (steps of 35 micron separated by 500 micron) is impressed on the horizontally outward side of the beam screen that forms the inner layer of the vacuum chamber [15]. The sawtooth pattern results in a locally perpendicular impact of synchrotron-radiation photons yielding both a strongly reduced reflectivity and a lower photoemission yield. The reduced reflectivity is important as, in dipole magnets, photoelectrons emitted at the outer side of the chamber are confined and do little harm to the beam, while photoelectrons emitted at the top and bottom of the chamber, via scattered photons, may approach the beam and contribute to multipacting and heat load.

The LHC beam screen contains pumping slots at its top and bottom. Multipacting electrons which pass through these slots along the magnetic field lines would hit the cold bore of the magnets at 2 K, where the available cooling capacity is much smaller than at the beam-screen temperature of 4-20 K. To prevent this fatal heat load, pumping-slot shields ('baffles') were added on the outer side of the beam screen, so as to intercept such electrons, at the expense of a slightly reduced pumping speed [16.17].

Heat load on the beam screen and vacuum pressure can be confined to tolerable values by reducing either the number of bunches or the bunch charge. As shown above, for a three times

increased bunch spacing of 75 ns, no significant heat load from the electron cloud is expected. Alternatively, bunch populations below  $5 \times 10^{10}$  at the nominal bunch spacing of 25 ns may also yield an acceptable heat load. In addition, low-charge ‘satellite’ bunches, following 5 or 10 ns behind the main bunches, could be employed as a fall back option to suppress the electron-cloud build up and to reduce the heat load during commissioning [18].

The surface of the vacuum chamber will be conditioned by operating near the heat-load limit for extended periods of time (the scrubbing effect is described in [19]). At the LHC this ‘scrubbing’ will be more difficult than in the SPS, since the electron cloud activity will increase during acceleration, due to additional contributions from synchrotron radiation and the reduced beam sizes. If the beam needs to be dumped, when the heat load approaches the magnet quench limits, the time needed to re-iterate is of the order one hour rather than 20 s as in the SPS.

It is expected or hoped, that after several weeks or months of operation, the surface conditioning during commissioning and early operation will reduce the secondary emission yield to a level where operation with nominal LHC beam parameters becomes possible.

### 2.18.5 Uncertainties

The simulated heat load strongly depends on the reflection probability of low-energetic electrons when they hit the chamber wall. Recent measurements and a simple quantum-mechanical calculation suggest that the reflectivity may approach 1 in the limit of zero energy [20]. This conclusion has not yet been generally accepted in the electron-cloud community. The reflectivity has a great influence on the survival of secondary electrons between bunches and, in particular, during the gaps between bunch trains.

The LHC strategy heavily relies on surface conditioning by ‘scrubbing’ (electron bombardment due to the electron cloud itself). In the SPS experiments, some of the cold and also one warm detector showed little scrubbing, while most of the regular warm stainless steel chambers in the arcs did. The apparent lack of scrubbing for the cold detectors could be explained by the peculiarities of the SPS set up, which consists of short (1 or 2 m long) cold sections bordered on either side by warm parts with significant gas influx. This possibility will be explored in the 2004 SPS run, where heat loads will be measured in a cold detector that is isolated by cryogenic barriers from the rest of the ring.

A strong increase in the gas pressure during scrubbing would reduce the beam lifetime and increase the heat load on the cold bore of the magnets due to scattered proton losses. Since already at nominal pressure levels the absorption of scattered-proton energies by the cold bore constitutes a significant load on the LHC cryogenic system, only much lower pressure rises than in the SPS can be tolerated at the LHC. This source of heat load may further complicate the scrubbing process with respect to the SPS, in addition to the reduced duty cycle and to the new effects of synchrotron radiation and photoemission encountered towards top energy.

The LHC requires an exceedingly low value of secondary emission, in order to reach the design parameters for bunch charge and bunch spacing, according to the simulations, one which has not been reached in the SPS experiments. A related concern is that low energy electrons hitting the wall, if there are many, could amount to a significant heat load, without contributing to surface conditioning [21]. For the latter a minimum electron energy of about 30 eV is required [22].

If instabilities occur in the LHC, one could attempt to suppress them by a combination of bunch-to-bunch feedback and increased chromaticity, as is the case in the SPS. The LHC ring

being larger than the SPS, a still higher value of  $Q'$  might be required to suppress instabilities (at the SPS  $Q'$  values up to 30 were needed at the start of a scrubbing run), that could adversely affect the dynamic aperture. The deleterious effect of a large  $Q'$  on the dynamic aperture might also be enhanced by the more complex optics at the LHC, in particular the low-beta insertions.

The long-term emittance growth due to the electron cloud is another open issue [23]. Recent simulation results, already mentioned above, suggest that the emittance growth in the LHC will be acceptable for small, but achievable average electron densities. Further studies of this topic are ongoing. In collaboration with T. Katsouleas' group at USC the continuous interaction of the proton beam and the electron cloud is being modeled by the code QUICKPIC [24]. This provides a valuable benchmark for the HEADTAIL code. The latter code concentrates the beam-electron interaction at a few, typically ten, points around the ring, which speeds up the calculation, and allows for a larger number of turns, but it is less accurate than QUICKPIC. Neither simulation has so far considered the effect of varying beta functions around the ring, which might introduce additional emittance dilution [25,26].

### 2.18.6 References

1. O. Gröbner, "Technological Problems Related to the Cold Vacuum System of the LHC," *Vacuum* **47**, p. 591 (1996).
2. F. Zimmermann, LHC Project Report 95 (1997).
3. O. Gröbner, "Beam Induced Multipacting," PAC 1997 Vancouver (1997).
4. O. Brüning, EPAC98 Stockholm (1998).
5. G. Rumolo, F. Ruggiero, F. Zimmermann, PRST-AB **4**, 012801 (2001).
6. G. Arduini et al., "Present Understanding of Electron Cloud Effects in the Large Hadron Collider," PAC2003 Portland (2003).
7. M. Jiménez et al., CERN-LHC Project-Report-632 (2003).
8. G. Arduini et al., "Transverse Behavior of the LHC Proton Beam in the SPS: An Update," PAC2001 Chicago (2001).
9. K. Cornelis, "The Electron Cloud Instability in the SPS," E-CLOUD02 Geneva (2002).
10. W. Höfle, "Progress with the SPS Damper," Proc. Chamonix01 (2001).
11. C. Benvenuti et al., *Vacuum* **60**, 57 (2001).
12. V. Baglin, LHC Project Report 667 (2003).
13. R. Cimino et al., LHC Project Report 669 (2003).
14. L. Taviani, private communication (2004).
15. V. Baglin, I.R. Collins, O. Gröbner, EPAC98 Stockholm, p. 2169 (1998).
16. N. Kos, "Pumping Slot Shields for LHC Beam Screens," CERN Vacuum Technical Note 03-12 (2003).
17. A. Krasnov, LHC Project Report 671 (2003).
18. F. Ruggiero, X. Zhang, AIP Conf. Proceedings **496**, p. 40 (1999).
19. N. Hilleret et al., Proc. EPAC 2000 Vienna, p. 217 (2000).
20. R. Cimino, I. R. Collins, M. A. Furman, M. Pivi, F. Ruggiero, G. Rumolo, F. Zimmermann, "Can Low-Energy Electrons Affect High-Energy Physics Accelerators?," Submitted to Phys. Rev. Lett. (2004).
21. V. Baglin, private communication (2004).
22. N. Hilleret, private communication (2003).
23. E. Benedetto et al., PAC2003 Portland (2003).

24. G. Rumolo, A.Z. Ghalam, T. Katsouleas et al. PRST-AB **6**, 081002 (2003).
25. K. Ohmi, private communication (2003).
26. G. Rumolo et al., "Single-Bunch Instabilities Induced by Electron Cloud in Short Positron/Proton/Ion Bunches," this ICFA newsletter.

## **3 ADVANCED AND NOVEL ACCELERATORS**

### **3.1 Activity at KEK-ATF**

Junji Urakawa  
KEK  
[junji.urakawa@kek.jp](mailto:junji.urakawa@kek.jp)

#### **3.1.1 Outline of ATF at KEK**

The Accelerator Test Facility (ATF) at KEK consists of three major parts: an S-band injector linac, a damping ring, and a beam diagnostic system (EXT) (see Fig.1). Each part directly contributes to the development of technologies relevant to high luminosity linear colliders(LC). The ATF has been designed to investigate the feasibility of the LC operation scheme and to develop beam-control techniques. The purpose of the ATF is to develop accelerator technology that can stably supply to the main linear accelerator an extremely flat "multi-bunch beam". The multibunch scheme is essential to boost the rf-to-beam transfer power efficiency in the accelerator. The ATF continues to help develop and test many techniques to handle the multibunch beam. One is the beam loading compensation system in the injector linac. A new idea using two rf side-bands was applied to compensate the bunch-by-bunch energy deviation due to beam loading. A newly developed damped cavity suppresses the coupled-bunch instabilities in the damping ring. A new simultaneous injection-extraction system for the damping ring will solve the problem of transient beam loading due to multi-train operation in the damping ring. The small emittance from the damping ring has been achieved by special design of a strong focusing lattice with precise alignment of components and beam orbit control. The nonlinear behavior of the beam has to be well understood to provide enough dynamic aperture under such strong focusing conditions. Table 1 summarizes the achieved accelerator performance of the ATF until the end of 2003.

## ACCELERATOR TEST FACILITY FOR LC

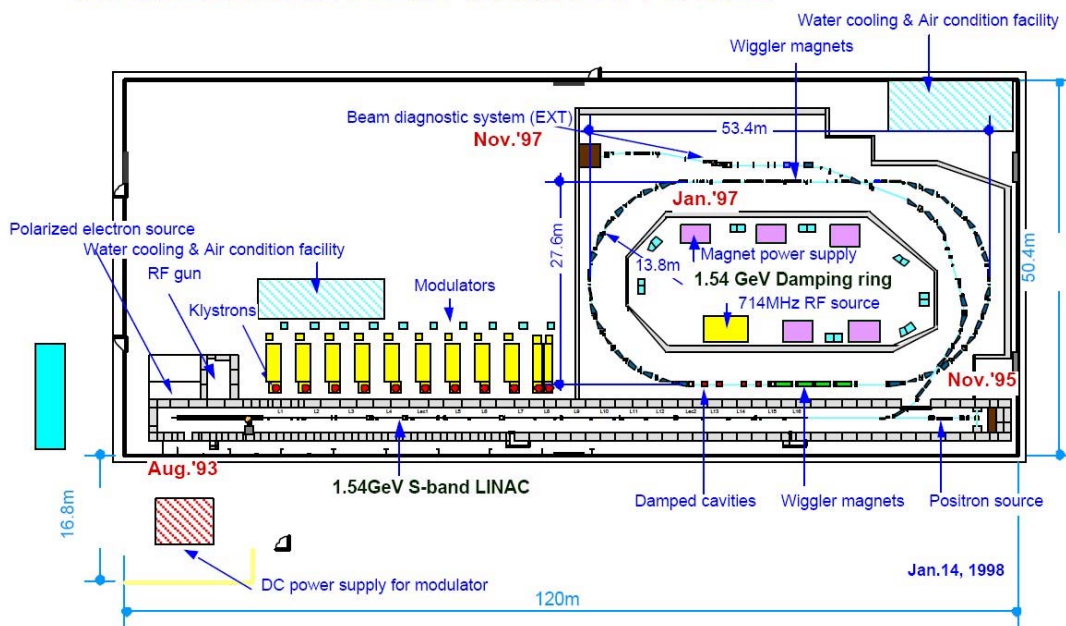


Fig. 1: The Accelerator Test Facility (ATF) at KEK.

Table: Achieved and design parameters at ATF.

Items	Achieved Values	Design
<b>ATF Linac Status</b>		
Maximum Beam Energy	1.42GeV	1.54GeV
Maximum Gradient with Beam	28.7MeV/m	30MeV/m
Single Bunch Population	$2.0 \times 10^{10}$	$2 \times 10^{10}$
20 Multi-bunch Population	$<2.0\%$ (90% beam)	$<1.0\%$ (90% beam)
Energy Spread (Full Width)		
<b>Damping Ring Status</b>		
Maximum Beam Energy	1.28GeV	1.54GeV
Momentum Compaction	0.00214	0.00214
Single Bunch Population	$1.2 \times 10^{10}$	$2 \times 10^{10}$
COD(peak to peak)	$x \sim 2 \text{ mm}, y \sim 1 \text{ mm}$	1 mm
Bunch Length	$\sim 9 \text{ mm}$	5mm
Energy Spread	0.08%	0.08%
Horizontal Emittance	$(2.2 \pm 0.3) \times 10^{-9} \text{ m}$	$1.4 \times 10^{-9} \text{ m}$
Vertical Emittance	$(4.0 \pm 0.5) \times 10^{-12} \text{ m}$	$1.0 \times 10^{-11} \text{ m}$
Multibunch Population	$8 \times 10^{10} \text{ m}$	$20 \times 10^{10} \text{ m}$
Vertical Emittance	$(1 \sim 2) \times 10^{-11} \text{ m}$	$1.0 \times 10^{-11} \text{ m}$

### 3.1.2 Emittance measurements at the EXT

Figure 2 shows the observed dependence of the measured emittance on the bunch intensity, which indicates the effects of intra-beam scattering. The error bar in the figure shows the statistical variation on repeated measurements. Intensive studies on the vertical emittance with the wire scanners in the EXT have been ongoing since March(2000). An important observation we made during this time is that there appears to be a source of x-y cross plane coupling somewhere between the extraction point of the damping ring (DR) and the wire scanner region in the EXT. The measured vertical emittance is approximately  $(1.1 \pm 0.25) \times 10^{-11} \text{m}$  for the beam intensity of  $(2.0 \pm 0.2) \times 10^9$  electrons per bunch. This represents the best result so far obtained at the EXT in a single-bunch mode operation. The emittance is found to grow to  $(2.2 \pm 0.33) \times 10^{-11} \text{m}$  at the beam intensity of  $(8.0 \pm 0.3) \times 10^9$  electrons per bunch, however. This could be partly due to effects of the intra-beam scattering, which according to a simulation can lead to an emittance growth of  $\sim 50\%$  at this bunch intensity. More careful theoretical and experimental studies are needed to fully understand the situation. In these measurements, the x-y beam profile showed a tilting of a few degrees, as observed by using 10 degree wires. The quoted vertical emittance in these plots might be further reduced by re-optimizing the setting of skew magnets. It appears that the following points play an important role.

1. Tuning with skew knobs in ARC sections of DR for reducing the betatron coupling in the ring.
2. Careful corrections for residual dispersion in the EXT.
3. Additional cross-plane coupling correction using a skew quadrupole magnet in the EXT, upstream of the wire scanners.

### 3.1.3 Beam tuning in the DR

We measured the  $R_{12}$  single-pass response matrix of each BPM to excitations of the different dipole correctors, with sextupole magnets turned off. From these data we calculated typical quadrupole field-strength errors of about 1% and upgraded the optics model so as to account for

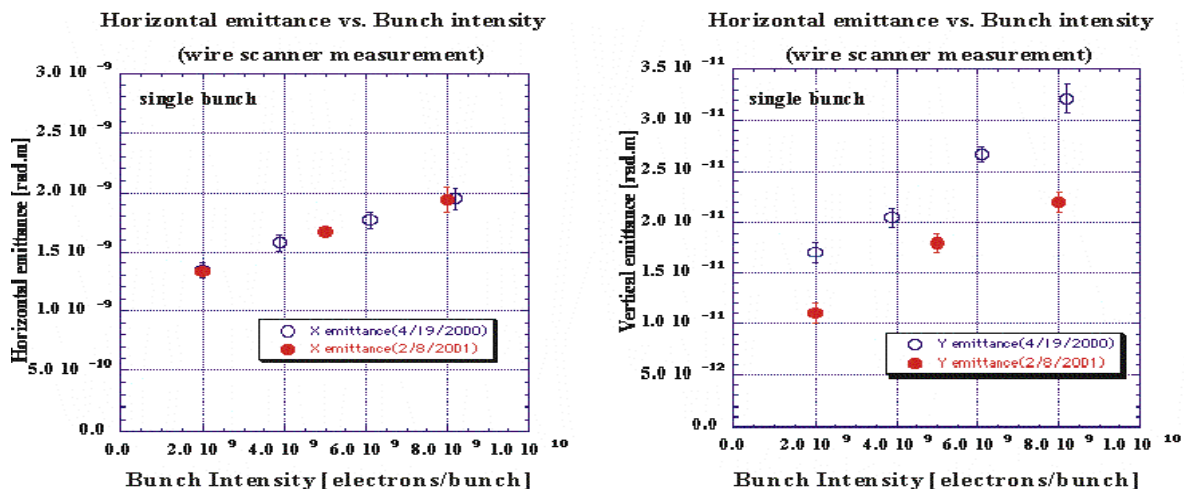


Fig. 2: Recent results of emittance measurements using wire scanners at the EXT.

these errors. The magnetic-field difference between the upgraded model and new beam-based measurements are less than 0.01%. The program SAD is used in orbit and dispersion corrections, for calculating new setting of the steering magnets. The orbit correction in the DR was satisfactory. The dispersion in the DR is measured as difference of the orbits with different RF frequencies. The dispersion correction in the ring worked and typical r.m.s. of the vertical dispersion after the correction was about 3 mm. To correct x-y coupling, trim coils of the all sextupole magnets are connected to produce skew quadrupole field. A global correction of the coupling is essential to achieve the smaller vertical emittance. We tried a global coupling correction minimizing vertical COD response to horizontal steering. The orbit coupling was clearly reduced and some reduction of the vertical emittance was observed after the correction.

Touschek effect causes the beam lifetime to be approximately proportional to the bunch volume at equilibrium. We can take advantage of this fact to infer the beam size in the ring. Since the bunch volume, or equivalently the vertical emittance when horizontal and longitudinal beam sizes are known, can be evaluated from the measurement of the Touschek lifetime, a novel beam diagnostic technique was developed. A beam lifetime model which includes the effects of potential well distortion, intra-beam scattering, photo-desorption and Touschek effect was made. The effect of intrabeam scattering (multiple Touschek scattering) can also be used directly to infer the emittance in the ring via the increase of the energy spread. The measured dependence of the lifetime and the energy spread on the beam intensity recently both indicate an emittance ratio less than  $\sim 0.5\%$ , assuming that the intra-beam scattering effect is the source of the beam-size variation.

### 3.1.4 Future plans

Our goal is to confirm the stable operation with 3 trains in the DR towards the end of JFY2004. Each train should consist of 20 bunches with bunch spacing of 2.8 nsec. There are many study items on the multi-bunch beam physics. For example, transient beam loading, multi-bunch instabilities, fast ion instability and emittance blow-up issues due to the multi-bunch beam which should be overcome. Future plans address the immediate goals of understanding the minimum achievable single bunch emittance and obtaining stable operation with  $3 \times 20$  bunch trains. A program of theoretical and experimental studies has been planned that is focused on understanding the correction and optimization procedures, the stability of the ring component alignment, intra-beam scattering emittance growth and the multi-bunch beam dynamics mentioned before. The RF photocathode source, to be installed in late 2002, provided twice the present stored beam intensity, allowing more precise studies of single bunch intensity dependent phenomena, such as intra-beam scattering and impedance effects. International development studies are as follows:

**1. Photo-Cathode RF Gun;** Since  $\sim 100\%$  beam injection efficiency was dramatically demonstrated during RF gun tests in 2001, we manufactured a photo-cathode RF gun with a  $Cs_2Te$  Cathode. Our photo-cathode RF gun is routinely operated and upgraded for ATF study program.

**2. Beam Based Alignment;** Using new, high-resolution ring BPMs we are developing a quick, accurate beam based alignment procedure that will provide insight into the nature of the optics corrections that are presently used for emittance optimization. We will be able to identify sources

of instability and understand the physical limits on the minimum vertical emittance. This is one of the highest priority beam studies.

**3. Laser Wire;** A laser beam with a very thin waist is generated in an optical cavity formed by nearly concentric mirrors. The laser intensity is amplified by adjusting the cavity length to meet the Fabry-Perot resonance condition. We have already built the cavity which produced a beam waist of  $12\mu\text{m}$  ( $2\sigma$ ) and an effective power of 100 W, with good long-term stability. The laser wire has been installed in the ATF DR at a location with a transverse electron beam size of  $\sim 10\mu\text{m}$ . We can measure the vertical and horizontal emittance of each bunch in the ring with sufficient accuracy.

**4. Optical Transition Radiation;** The linear collider needs a profile monitor that provides images of the low emittance beam with a resolution well below typical beam sizes in order to accurately determine x-y and y-z coupling and other phase space distortions. The required resolution ( $2\mu\text{m}$ ) is well below the state of the art for such monitors ( $20\mu\text{m}$ ) and we have a program to test and perfect such a monitor in the extraction. To date, beam sizes of  $5\mu\text{m}$  have been imaged and tests of transition radiation target durability have been done.

**5. Polarized Positron Generation;** We have proposed a new method of generating highly polarized positrons through Compton scattering of polarized laser light off relativistic electron beams and successive pair creation. A preliminary experiment has been performed in the ATF extraction line. A polarized  $\gamma$ -ray yield of  $3\times 10^6$  photons/pulse has been measured.

**6. Optical Diffraction Radiation Monitor;** A "proof-of-principle" experiment on the use of optical diffraction radiation (ODR) as a single pulse beam profile monitor has been done using the electron beam extracted from the DR. We are measuring the yield and the angular distributions of the optical diffraction radiation from a thin metal target at different wavelengths, impact parameters and beam characteristics. New beam diagnostic tool will be proposed for  $\mu\text{m}$  beam size measurement.

**7. Stable Beam Extraction using Double Kicker Scheme;** We already demonstrated in the single bunch operation that the stability of the beam orbit at the EXT was less than a few  $\mu\text{m}$  with double kicker system using cavity BPM. Regarding the multibunch operation, we need a precise bunch-by-bunch BPM with pulse-by-pulse to check the performance of the double kicker system.

### 3.1.5 References

1. Y.Honda et al., Achievement of Ultra-low Emittance Beam in the ATF Damping Ring, accepted in Phys. Rev. Lett. (2003).
2. M.Fukuda et al., Polarimetry of Short-Pulse Gamma Rays Produced through Inverse Compton Scattering of Circularly Polarized Laser Beams, accepted in Physical Review Letters, 2003.
3. Yosuke Honda et al., Measurements of electron beam emittance in the Accelerator Test Facility damping ring operated in multibunch modes, PRST-AB **6**, 092802 (2003).
4. I.Sakai et al., Production of high brightness g rays through backscattering of laser photons on high-energy electrons, PRST-AB **6**, 091001(2003).
5. T.Muto et al., Observation of Incoherent Diffraction Radiation from a Single-Edge Target in the Visible-Light Region, Physical Review Letters **90**, No.10, 104801-1 (2003).

6. P. Karataev et al., Status of optical diffraction radiation experiment at KEK-ATF extraction line, NIM B **201** (2003), 140-152.
7. H.Sakai et al., PRST-AB **5**, 122801, 2002.
8. H.Sakai et al., Performance studies of a laser wire beam profile monitor, Jpn. J. Appl. Phys. **41**, (2002) pp. 6398-6408.
9. K.L.Bane et al., Intrabeam Scattering Analysis of Measurements at KEK's Accelerator Test Facility Damping Ring, PRST-AB **5** (2002), 084403.
10. K.Kubo et al., Extremely Low Vertical-Emittance Beam in the Accelerator Test Facility at KEK, Physical Review Letters, **88**, No.19, 194801-1(2002).
11. J.Urakawa et al., Feasibility of optical diffraction radiation for a non-invasive low-emittance beam diagnostics, Nuclear Instruments and Methods in Physics Research A **472** (2001) pp. 309-317.
12. H.Sakai et al., Measurement of an electron beam size with a laser wire beam profile monitor, PRST-AB **4**, 022801-6, 2001.
13. Edited by H.Hayano et al., KEK Internal 2000-6 A (2000).
14. T. Okugi et al., Effective Method to Evaluate extremely Small Vertical Emittance ( $\sim 10^{11}m$ ), NIM in Physics Research A **455**, pp. 207-212, 2000.
15. K. Dobashi et al., Generation of Positrons via Pair-Creation of Compton Scattered Gamma-Rays, NIM in Physics Research A **437**, pp. 167-177, 1999.
16. T.Okugi et al., Evaluation of Extremely Small Horizontal Emittances at the KEK Accelerator Test Facility, PRST-AB **2**, 022801-10, 1999.
17. J.Urakawa et al., presented at 17th International Conference on High-Energy Accelerators (HEACC98), Dubna, Russia, 7-12 Sep. 1998. KEK Preprint 98-154.
18. S. Sakanaka et al., Construction of 714 MHz HOM-free accelerating cavities, Journal of Synchrotron Radiation **5**, pp. 386-388, 1998.
19. Junji Urakawa , Beam Dynamics in ATF Damping Ring, ICFA Beam Dynamics Newsletter No.13, edited by K.Hirata, J.Jowett and S.Y.Lee, pp.31-38, 1997.
20. J.Urakawa, KEK/ATF Damping Ring, PAC97, pp.444-448, Vancouver, May, 1997.
21. J.Urakawa et al., Gun trigger system for the ATF, NIM, A **352**, pp. 207-209, 1994.
22. T.O.Raubenheimer et al., The Vertical Emittance in the ATF Damping Ring, NIM A **335**, pp.1-10, 1993.

### 3.2 Laser-Accelerator Research Activity at AIST

K. Koyama  
[k.koyama@aist.go.jp](mailto:k.koyama@aist.go.jp)

National Institute of Advanced Industrial Science & Technology (AIST), Japan

Our research program on a laser accelerator was begun in 1994 at Electrotechnical Laboratory (ETL) and has been continued after the reorganization of our institute, AIST, in 2001. By taking opportunity of rearrangement, we moved our experimental setup to a larger lab and began to improve performance of a TW-laser system.

Recent activities at AIST are focused on studies of particle accelerations by using intense laser pulses, and their applications as well. We are performing experiments on laser interaction with plasma well as theoretical works on laser acceleration.

### 3.2.1 Research

#### 3.2.1.1 *High-energy particle sources produced by an intense laser pulse*

The objective of the program is to study interaction of intense laser pulses with plasmas for developing laser-accelerators, and bright x-ray sources as well. We are performing experiments at higher electron density than the critical value of the relativistic self-focusing of  $2 \times 10^{19} \text{ cm}^{-3}$  for 2 TW laser pulse.

After improvement of a beam quality of the laser system, maximum electron energy of 30 MeV, which was limited by an energy spectrometer, was obtained by focusing a laser pulse with peak power of 2 TW on an edge of a supersonic dense gas jet. An electron density was estimated to be  $1 \times 10^{20} \text{ cm}^{-3}$  from a measured gas density. The vacuum focus intensity was  $5 \times 10^{18} \text{ W/cm}^2$  ( $a_0=1.5$ ). An energy spectrum consisted of two-temperature Boltzman-like distribution. An effective temperature of high-energy component was 4.5 MeV possessing obvious energy humps around 6-MeV. We are now conducting experiment to clarify the origin of energy humps.

Incidentally, the maximum energy of the electron beam was 2 MeV at the laser power of 2 TW of previous system. The energy spectrum of the electron beam was a power-law dependence of  $E^{-3.5}$ . One of the most different parameters is an intensity distribution in a focus. The poor beam quality of the previous laser system gave the vacuum intensity of  $7 \times 10^{17} \text{ W/cm}^2$ .

In order to help understanding physics of acceleration, we are developing a 2-D PIC simulation code.

The program is financially supported by the budget for nuclear research of the Ministry of Education, Culture, Sports, Science and Technology (MEXT), based on the screening and counseling by the Atomic Energy Commission (AEC) of Japan.

#### 3.2.1.2 *Diagnostics of plasma cathode*

The objective is to develop plasma diagnostic techniques to investigate plasma cathodes, which are driven by intense laser pulses. Since optical short pulses are effective diagnostic tools for investigating both density modulations and temperatures of underdense plasmas, we are developing the optical probing technique. A part of laser pulse is divided from an amplifier chain of the TW-laser system and compressed to form the short probe pulse. At first, the shadowgraph technique using the short laser pulse was used to observe the evolution of the plasma channel formed by the relativistic self-focusing, and a complex structure of a density modulation produced by the previous laser system as well. Since the appearance of the complex structure was well coincided with the high-energy electron generation in the previous experimental setup, we supposed that electrons were stochastically accelerated and estimated the contribution of the stochastic acceleration on the observed energy spectrum.

Recently, the probe pulse is amplified to use the laser scattering experiment to diagnose density modulations of the wake field as well as to know a structure of an electron bunch.

The program is a part of the Advanced Compact Accelerator Project under the collaboration with the National Institute of Radiological Sciences (NIRS).

### 3.2.2 Experimental setup

Our laser system was largely reorganized in 2003. A beam quality of an output pulse has been improved by replacing an oscillator, pulse stretcher, regenerative amplifier, preamplifier, relay

optics, and installing a pulse compressor in a vacuum as well. The Schematic layout of the laser is shown in Fig.1. The maximum power of 6-7 TW will be delivered in 2004 by pumping the main amplifier with fully equipped YAG lasers.

Figure 2 is a picture of an interior of a target chamber. The main laser pulse is focused on the gas jet by the off-axis parabolic mirror. The electron beam and the forward scattered laser light are measured on the laser axis. The direction of the probe pulse is changed between normal and collinear to the main pulse.

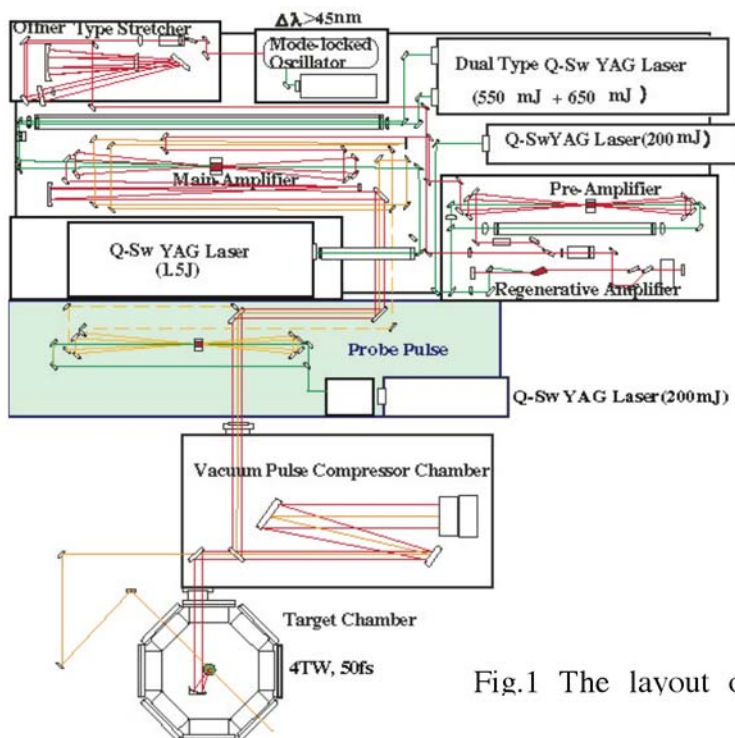


Fig.1 The layout of the laser Ti: sapphire laser

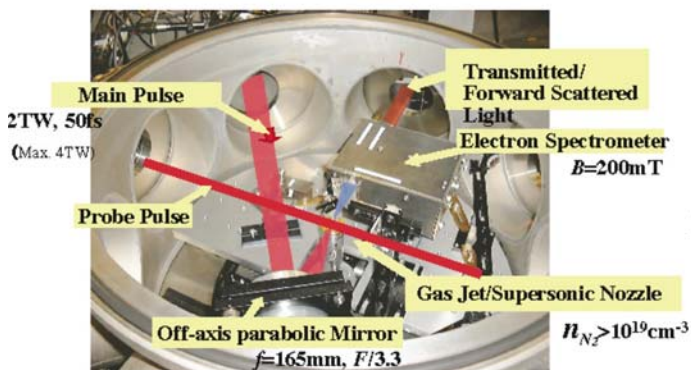


Fig.2 Interior of the target chamber.

### 3.2.3 Publications

1. M.Tanimoto, S.Kato, E.Miura, N.Saito, K.Koyama and J.K.Koga, "Direct electron acceleration by stochastic laser fields in the presence of self-generated magnetic fields", Physical Review E **68** (2003) 026401– 026407.

2. T.Nakamura, S.Kato, J.Koga, M.Tanimoto, K.Koyama and T.Kato, “Acceleration of Injected Electron Beam by Ultra-Intense Laser Pulses with Phase Disturbances”, *Journal of Plasma and Fusion Research* **79** (2003) 318 – 320.
3. Wei Yu, Z.Y.Chen, M.Y.Yu, L.J.Qian, P.X.Lu, R.X.Li, and K. Koyama, “Electron acceleration and high-order harmonic generation by an intense short pulse laser in a magnetic field”, *Physical Review E* **66** (2002) 0364061–0364065.
4. K.Koyama, H.Hazama, N.Saito, and M.Tanimoto, “Emission of High-Energy Electrons from Moderately Underdense Plasmas Produced by TW-fs Laser Pulses”, *International Journal of Applied Electromagnetics and mechanics* **14** (2002) 263–269.
5. K.Koyama, N.Saito, E.Miura, and M.Tanimoto, “Electron Acceleration in the Moderately Underdense Plasmas”, *Science of Superstrong field interactions*, AIP Conf.Proc., No.634, ed. by K.Nakajima and M.Deguchi, (AIP, New York, 2002) 296-302.
6. K.Koyama, N.Saito, M.Tanimoto, and S.Kato, “The High-Energy Electron Beam Emission by the Guided Laser Pulse in the Plasma”, *Inertial fusion Science and applications 2001*, ed. by K.A.Tanaka, D.D.Meyerhofer, and J Meyer-ter-Vehn (Elsevier, Paris,2002), 1144-1147.
7. E.Miura, H.Honda, K.Katsura, E.Takahashi, and K.Kondo, “Enhancement of X-ray emission from a cooled Kr gas jet irradiated by an ultrashort KrF laser pulse”, *Jpn. J. Appl. Phys.* **40** (2001) 7067 – 7071.
8. K.Koyama, N.Saito, and M.Tanimoto, “HIGH-ENERGY ELECTRONS GENERATION IN LASER PRODUCED PLASMAS”, *Proceedings of 13th International Conference on High-power Beams*, Vol.1, ed. by K.Yatsui and W.Jiang, (Nagaoka UT, Nagaoka, 2001), 196-199.
9. E.Miura, H.Honda, K.Katsura, E.Takahashi, and K.Kondo, “Soft x-ray emission from noble gas clusters excited by an ultrashort KrF laser pulse”, *Applied. Physics B* **70** (2000) 783 – 787.
10. H.Honda, E.Miura , K.Katsura, E.Takahashi, and K.Kondo, “Evidence for wavelength dependence Xe M-shell emission from clusters”, *Physical Review A* **61** (2000) 232011–232014.
11. E.Takahashi, H.Honda, E.Miura, N.Yugami, Y.Nishida, K.Katsura, and K.Kondo, “Observation of Spatial asymmetry of THz oscillating electron plasma wave in a laser wakefield”, *Physical Review E* **62** (2000) 7247 – 7250.
12. T.Nakamura, S.Kato, and T.Kato, “Analysis of propagation of an intense and short laser pulse in inhomogeneous plasmas”, *J. Phys. Soc. Jpn* **68** (1999) 2956 –296.
13. K.Koyama, N.Saito, and M.Tanimoto, “Observation of MeV-electrons from Underdense Plasmas Produced by fs-TW-Laser Interaction with Gas-jet Targets”, *Inertial Fusion Science and Applications* 99, ed. by C.Labaune, W.J.Hogan, K.A.Tanaka, (Elsevier,Paris,1999), 1157-1162.
14. K.Koyama, N.Saito, and M.Tanimoto; “Production of MeV electrons in a gas-jet targets”, *Proc. of SPIE*, Vol.3886, ed. by K.Mima, G.L.Kulcinski, W.Hogan, (SPIE, Bellingham,1999), 76-81.
15. J.Koga, S.Kato, Y.Kishimoto, S.P.LeBlanc and M.C.Downer, “Optical Field Ionization Effects on the Generation of Wake Fields with Short Pulse Lasers”, *Nucl. Instrum. Methods A* **410** (1998) 499 –504.
16. S.Kato,Y. Kishimoto, and J.Koga, “Excitation of wake field driven by ionization induced self-modulated intense short pulse laser pulse”, *Physics of Plasmas* **5** (1998) 292 – 299.
17. K.Koyama, M.Tanimoto, A.Yaoita, and H.Hazama, “Experimental Study on Under-Dense Plasma Production with an Ultra-Intense Laser Pulse”, *Laser Interaction and Related Plasma*

Phenomena, AIP Conf. Proc. No.406. ed. by G.M.Miley and E.M.Campbell, (AIP, New York,1998), 435-442.

### People

Kazuyoshi KOYAMA

Eisuke MIURA

Susumu KATO

Masahiro ADACHI (Graduate Student, Hiroshima University)

Yoichi KAWADA (Graduate Student, Tsukuba University)

Tatsufumi NAKAMURA (Postdoctoral Fellow, NIRS)

### Address

National Institute of Advanced Industrial Science and Technology (AIST)

Tsukuba Central-2, Umezono, 1-1-1, Tsukuba, Ibaraki, 305-8568, Japan

## 3.3 Research Activity At Nuclear Engineering Research Laboratory, University Of Tokyo

M. Uesaka

[uesaka@utnl.jp](mailto:uesaka@utnl.jp)

Nuclear Engineering Research Laboratory, University of Tokyo

The research activity of the Laboratory is focused on fundamental studies of ultra-fast beam sciences and their applications, which include experimental and theoretical studies of advanced RF accelerators and particle acceleration by high-intensity laser interactions with matter.

### 3.3.1 Experimental verification of new bunch compression, velocity bunching

The experiment of “velocity bunching” is introduced. The bunching has been performed by the S-band linac and the Mg photocathode RF injector. The velocity bunching was proposed by Prof. L. Serafini in 2000 [1]. The scheme is based on the rectilinear compression, so that magnetic compressors such as chicane are not necessary. The S-band linac with the Mg photocathode injector (18L) has been usually utilized for the radiation chemistry. To realize high time-resolution in order of sub-picosecond, the chicane-type magnetic compressor is used [2,3]. Although the chicane-type compressor is able to generate a bunch less than 1ps, the experimental proof of the velocity bunching is interesting.

Normally, two accelerating tubes are used for the complete scheme of velocity bunching as shown in the SPARC project [4], because the energy of compressed beam in the first tube is low. Unfortunately 18L has one accelerating tube, but Helmholtz coils surround the tube. Thus, we had demonstrated the velocity bunching with concentrating the verification of compression scheme using one accelerating tube and Helmholtz coils. Also shot-by-shot diagnosis had been evaluated to use the femtosecond streak camera.

The tube of 18L is the S-band traveling wave structures operating on the  $2\pi/3$  mode with 2m long. In this experiment, the chicane-type compressor is not used. Therefore, the beam is extracted at the downstream of accelerating tube. Eleven circular coils are located around the

tube. The amplitude of magnetic field is up to 300 Gauss. Aerogel target as a Cherenkov radiator is set at the egress of linac. The Cherenkov light is guided to the femtosecond streak camera to measure the electron bunch width. We have got streak camera images of the compressed bunches by a single shot for several injected RF phase.

In this experiment, we got minimum bunch width of 0.5 ps (FWHM) and 1.3 ps in the average of 30 bunches. Not yet we do not evaluate the emittance, but it is not seen that the beam is expanded extremely at the end of linac. In near future, we are going to measure the emittance.

### 3.3.2 Compact hard X-ray source based on X-band LINAC for medical use

Hard X-rays of 10~50keV are now very useful for medical science, biology, material science etc. For example, Dynamic Intravenous Coronary Arteriography (IVCAG) by a high quality monochromatic hard X-ray via Synchrotron Radiation (SR) is proposed and tested in some institutes. Most of SR sources are too large to apply spread use of IVCAG. Then, we are going to develop a compact hard X-ray (10~50 keV) source based on Laser-electron collision using by X-band (11.525GHz) linac system for dynamic IVCAG. The X-band linac is introduced to realize very compact system.

Compact hard X-ray source based on X-band linac that we propose is shown in Figure 1. Multi-bunch beam generated by thermionic-cathode RF-gun is accelerated by X-band accelerating structure. The beam is bent and focuses at the collision point.

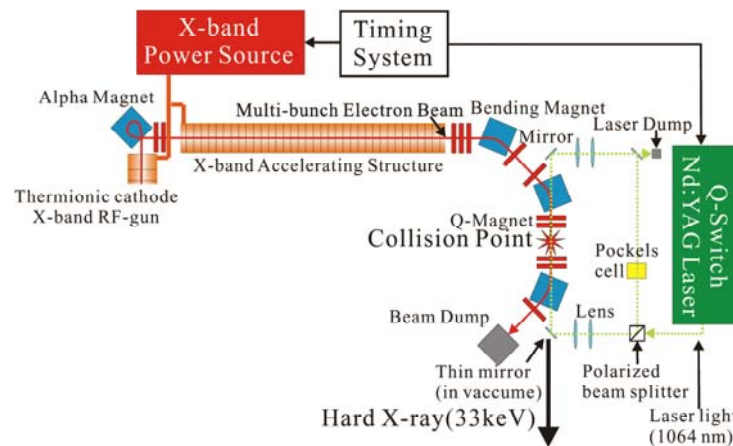


**Fig. 1.** Schematic illustration of Compact Hard X-ray source based on thermionic-cathode X-band RF-gun, X-band accelerating structure and Q-switch Nd:YAG laser with laser light circulation system.

We have performed a fundamental design for the X-band photo-cathode RF-gun using the PARMALA code. Numerical analysis of beam transport for whole system including photo-cathode X-band RF-gun and X-band accelerating structure is already presented [1]. Thermionic-cathode X-band RF-gun is under designing, and we assume beam parameter shown in Table 1.

**Table 1.** Beam parameter.

Beam energy	56 MeV
Charge/bunch	20 pC
Bunch length	1.5ps(FWHM)
Beam Emittance	2.5, 2.5 $\pi$ mm mrad

To concentrate on R&D of the accelerator, we use existing laser system for laser-electron collision. To realize simple and compact system, we apply a Q-switch Nd:YAG laser with intensity 2J/pulse, repetition rate 10pps, pulse length 10ns(FWHM), and wavelength 1064nm, which is commercial product.

We choose a very simple system by focussing on only averaged X-ray flux. We construct the system with the thermionic-cathode RF-gun (20 pC/bunch,  $\sim 10^4$  bunches/RF-pulse, 10paimm mrad) and Q-switch Nd:YAG laser (2J/pulse, pulse length 10ns in FWHM, repetition rate 10pps). We assume head-on collision for calculation of X-ray yield. Figure 13 (left figure) indicates that optimal laser beam size is 82 $\mu$ m (rms) for electron beam size 100 $\mu$ m (rms) at the C.P. Each bunch collides to laser light with some time offset. X-ray yield of each bunch is shown in Figure 13 (right figure). Thus, This system generates X-rays with  $1.7 \times 10^7$  photons/pulse ( $1.7 \times 10^8$  photons/s) that is sum of each bunch.

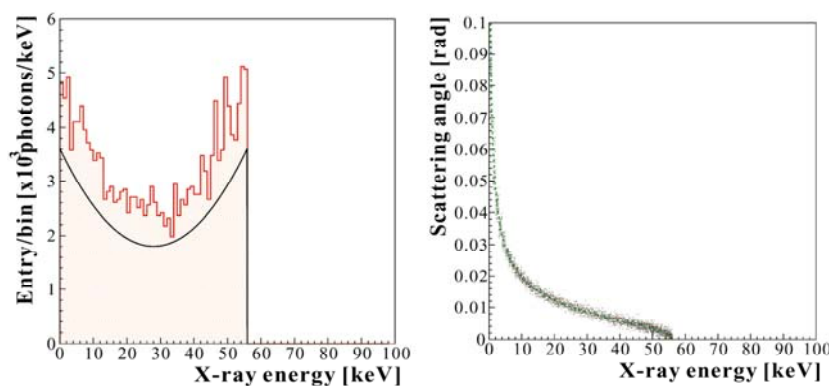


**Fig. 2.** Energy spectrum and energy (left figure ) vs. scattering angle (right figure) of X-ray in single bunch(20pC/bunch) collision with Q-switch Nd:YAG-laser(2J/pulse) . Scattering angle of 0 rad is direction of electron beam.

Energy distribution and angler distribution of generated X-ray is shown in Figure 2. Solid line indicates spectrum calculated by Klein-Nishina's formula [2] and Luminosity calculation, and Histogram shows the result of beam- beam interaction Monte-Carlo simulation code CAIN [2]. X-ray energy reached to 57keV at beam energy 56MeV. The system with Thermionic-cathode and Q-switch laser is not only very simple and compact but also can generate high flux X-ray with intensity  $10^8$  photons/s.

Final target of this study is the integrated system for dynamic IVCAG shown in Figure 3. This system has X-band RF-source and moving arm including X-band linac, Q-switch Laser system with laser circulation system and X-ray detector. We can perform dynamic IVCAG easily and can get clear dynamic image of coronary artery with less distress for patient.

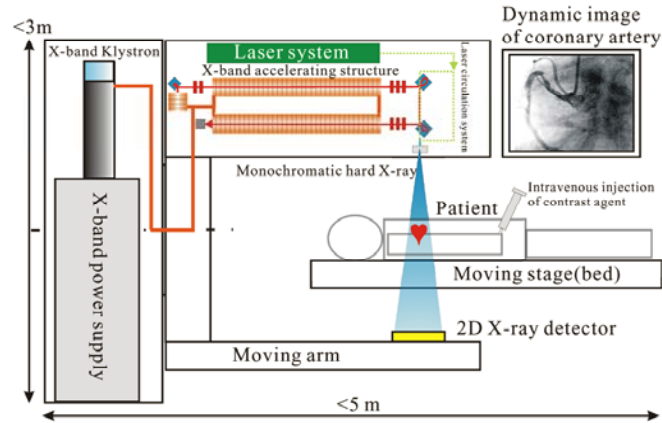


**Fig. 3.** Final target of this work.

### 3.3.3 Electron acceleration via interaction between ultra-short intense laser pulse and gas jet

The particle acceleration via laser-plasma interactions has been studied intensively for many years. Among a number of concepts of the particle acceleration by laser fields, the laser wake-field acceleration (LWFA) in underdense plasma [1] provides one of the most promising approaches to high performance compact electron accelerators.

Until recently, a wake-field of the order of  $100\text{ GeV/m}$  in plasma has been observed in LWFA experiments [2]. Furthermore, since it has a relatively small length of acceleration, the LWFA, particularly, allows the production of an ultra-short electron bunch ( $\sim 10\text{ fs}$ ) for probe-analysis of matter [3]. However, electron injection into the wake-field is a crucial part for LWFA. Since the typical length of the wake-field of plasma wave is the order of  $2\pi c/\omega_{\text{pl}} \sim 10\text{-}100\ \mu\text{m}$ , the length of the injected electron bunch must be  $2\text{-}20\ \mu\text{m}$ . One of the simplest ways to put energetic electrons into the wake-field for their further acceleration is the wave-breaking of plasma waves produced by a single intense laser pulse [4]. However, the wave-breaking requires a steep density plasma interface condition.

Our previous experiment [5] shows that, this condition can be produced via generation of a shock-wave in the gas jet by laser prepulse. Ejection of a narrow-cone MeV electron beam from a gas jet has been shown to depend strongly on the prepulse contrast ratio in a density range up to  $3 \times 10^{19}\ \text{cm}^{-3}$ . In the experiment, spatial and energy distribution of energetic electrons produced by an ultra-short, intense laser pulse with short focal length optical system (Ti:Sapphire,  $12\ \text{TW}$ ,  $50\ \text{fs}$ ,  $\lambda = 790\ \text{nm}$ ,  $f/3.5$ ) in a He gas jet are measured. They are

shown to depend strongly on contrast ratio and shape of the laser pre-pulse. The wave-breaking of the plasma waves at the front of shock wave formed by a proper laser pre-pulse is found to

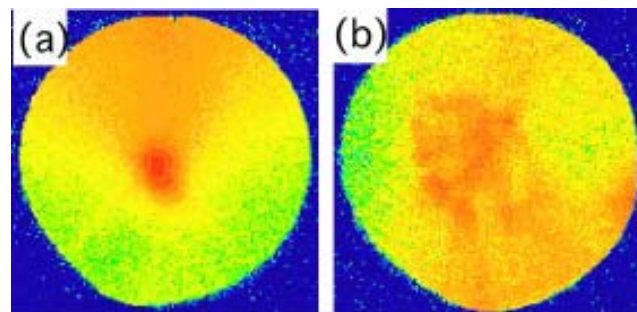


**Fig. 4.** Typical image of electrons on the detector. (a)  $\sim 2.5\text{ ns}$  prepulse (b)  $\sim 5\text{ ns}$  non-monotonic prepulse.

make a narrow-coned ( $0.1\pi$  mm mrad) electron injection. These electrons are further accelerated by plasma wake-field generated by the laser pulse up to tens MeV forming a Maxwell-like energy distribution. In the case of non-monotonic pre-pulse, hydrodynamic instability at the shock front leads to a broader, spotted spatial distribution. The numerical analysis based on a 2D hydrodynamic (for the laser pre-pulse) and 2D particle-in-cell (PIC) simulation justify the mechanism of electron acceleration. The PIC calculation predict that electrons with energy from 10 to 40 MeV form a bunch with pulse duration about 40fs.

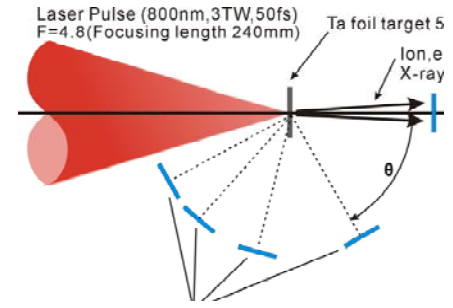


**Fig. 5.** Setup of ion generation

### 3.3.4 Laser plasma ion generation

The prepulse effect is an importance issue for energetic ion generation by means of laser plasma interaction with a ultrashort intense laser pulse. A target foil can be destroyed before the main pulse arrives if the prepulse is too large. We studied nanosecond prepulse effect on ion generation by a laser with the contrast ratio of  $10^5$ . By suppression of the prepulse, the number of ions generated from a metal target was increased.

### 3.3.5 Time-resolved X-ray diffraction

For ultrafast material analyses, we constructed the time-resolved X-ray diffraction system utilizing ultrashort X-rays from laser produced plasma generated by the 12TW-50fs laser. Ultrafast transient changes in laser-irradiated GaAs crystals were observed as X-ray diffraction patterns. Experimental results were compared with numerical analyses as the strain wave described by the equation below.

$$\eta_{33}(z,t) = \Delta T_s \beta \frac{1+v}{1-v} \left\{ e^{-z/\zeta} \left( 1 - \frac{1}{2} e^{-vt/\zeta} \right) - \frac{1}{2} e^{-|z-vt|/\zeta} \text{sgn}(z-vt) \right\}$$

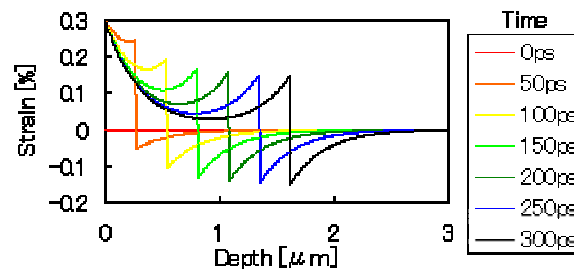


**Fig. 6.** The strain wave propagation into a GaAs crystal.

### 3.3.6 Plasma simulation

In order to study details of electron acceleration in underdense plasmas, we apply a fully relativistic 2D particle-in-cell (PIC) (for  $s$ - and  $p$ -polarized laser pulses) simulation with the

‘moving window’ technique with movable ions. The plasma length is set to a real plasma size, from several mm to several cm, with a real density gradient on either edge. In the 2D simulation, we use typically 16 particles per cell in a  $160\ \mu\text{m} \times 120\ \mu\text{m}$  ( $2800 \times 2048$  cells) window which moves at the speed of light. A FWHM laser pulse is chosen close to an experimental. The difference between the absorbed laser energy and the total plasma energy is controlled to be less than 1%. The numerical error in the group velocity is smaller than the velocity deviation from the speed of light. Typical results of calculation are shown in Figs. 7 and 8.

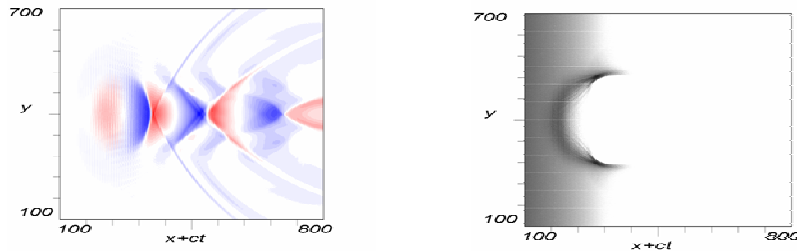


**Fig. 7.** Spatial distribution of the  $x$ -component of the electric field in the moving window;  $p$ -polarized pulse.

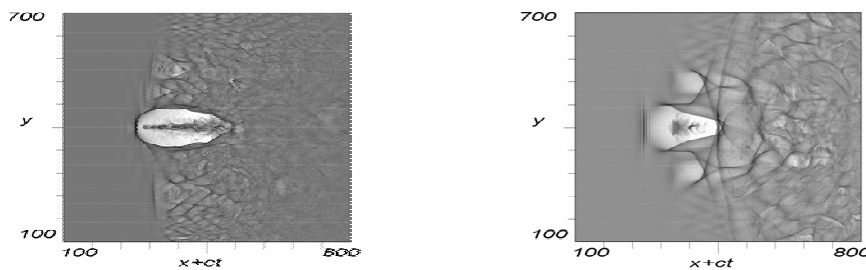


**Fig. 8.** The process of cavity formation in interaction of an relativistic laser pulse with an underdense plasma. The electron density in the plasma.

### 3.3.7 References

- 1-1 L. Serafini and M. Ferrario, Proc. of ICFA Workshop on the Physics of, and Science with, the X-ray Free-Electron Laser, Arcidosso, Italy, Sept. 2000.
- 1-2 M. Uesaka, *et al.*, Rad. Phys. Chem. **60**(2001)303.
- 1-3 Y. Muroya, *et al.*, Nucl. Instrum. & Meth. A **489**(2002)554.
- 1-4 M. Boscolo, *et al.*, Proc. of EPAC, Paris, 2002.
- 1-5 P. Poit, *et al.*, Phys. Rev. ST-AB **6**,033503(2003)
- 2-1 A. Fukasawa, *et al.*, Proceedings of 2<sup>nd</sup> Asian Particle Accelerator Conference, Sep. 17-21, Beijing, China.
- 2-2 V. O. Klein and Y. Nishina, Z. Phys. 52.858,869(1928)

- 2-3 K. Yokoya, CAIN2.1e, contact Kaoru.Yokoya@kek.jp
- 3-1 T. Tajima and J. Dawson, Phys. Rev. Lett. **43**, 267 (1979)
- 3-2 K. Nakajima, D. Fisher, T. Kawakubo, H. Nakanishi, A. Ogata, Y. Kato, Y. Kitagawa, R. Kodama, K. Mima, H. Shiraga, K. Suzuki, K. Yamakawa, T. Zhang, Y. Sakawa, T. Shoji, Y. Nishida, N. Yugami, M. Downer, and T. Tajima, Phys. Rev. Lett. **74**, 4428(1995)
- 3-3 M. Uesaka, K. Tauchi, T. Kozawa, T. Kobayashi, T. Ueda, and K. Miya, Phys. Rev E **50**,3068 (1994)
- 3-4 S.V. Bulanov, N. Naumova, F. Pegoraro, and J. Sakai, Phys. Rev.E **58**, R5257 (1998)
- 3-5 T. Hosokai, K. Kinoshita, A. Zhidkov, K. Nakamura, T. Watanabe, T. Ueda, H. Kotaki, M. Kando, K. Nakajima, M. Uesaka, Phys. Rev. E, **67**, 036407 (2003)

### 3.3.8 Publications

1. H. Iijima. *et al.*, “Mg Cathode S-band RF Gun/Linac for Radiation Chemistry Research”, Proc. of LINAC 2002.
2. H. Iijima, *et al.* “High Charge Mg Photocathode RF Gun in S-band Linac at University of Tokyo”, Proc. of 8th European Particle Accelerator Conference.
3. M. Uesaka, *et al.*, Rad. Phys. Chem. 60(2001)303.
4. Y. Muroya, *et al.*, Nucl. Instrum. & Meth. A 489(2002)554.
5. K. Dobashi, M. Uesaka, M. Akemoto, H. Hayano, T. Higo, J. Urakawa, A. Fukasawa, H. Iijima, ICFA 24th Beam Dynamics Workshop on Future Light Source in SPring-8, Japan, 1-4 March (2002)
6. K. Dobashi, M. Uesaka, M. Akemoto, H. Hayano, T. Higo, J. Urakawa, Fukasawa, H. Iijima 8th European Particle Accelerator Conference in Paris, France, 3-7 June (2002)
7. M. Uesaka, A. Fukasawa, K. Dobashi, H. Iijima, J. Urakawa, T. Higo, M. Akemoto, H. Hayano, The XXI International LINAC Conference in Korea, 19-23 August (2002)
8. H. Iijima, M. Uesaka, T. Ueda, A. Fukasawa, Y. Muroya, K. Yoshii, N. Kumagai, S. Suzuki, M. Kuriki, T. Takatomi, J. Urakawa, S. Kashiwagi, M. Washio, K. Dobashi, ICFA 24th Beam Dynamics Workshop on Future Light Source in SPring-8, Japan, 1-4, May (2002)
9. H. Iijima, M. Uesaka, T. Ueda, K. Yoshii, Y. Muroya, A. Fukasawa, N. Kumagai, S. Suzuki, J. Urakawa, M. Kuriki, T. Takatomi, K. Dobashi, M. Washio, S. Kashiwagi, X. J. Wang 8th European Particle Accelerator Conference in Paris, France, 3-7, June (2002)
10. H. Iijima, K. Dobashi, M. Uesaka, T. Ueda, K. Yoshii, Y. Muroya, A. Fukasawa, N. Kumagai, J. Urakawa, The XXI International LINAC Conference in Korea 19-23, August (2002)
11. M. Uesaka, K. Tauchi, T. Kozawa, T. Kobayashi, T. Ueda, and K. Miya, Phys. Rev E **50**,3068 (1994)
12. M. Uesaka, T. Watanabe, T. Kobayashi, T. Ueda, K. Yoshii, G. Wu, X. Li, Y. Muroya, J. Sugahara, K. Kinoshita, N. Hafs, H. Okuda, T. Nishihara, Y. Terada, K. Nakajima, and Y. Katsumura, Radiation Physics and Chem. 60, 303(2001)
13. T. Hosokai, M. Kando, H. Dewa, H. Kotaki, S. Kondo, N. Hasegawa, K. Horioka, and K. Nakajima Nuclear Instruments and Method in Physics Research A Vol.455(2000) 155-160
14. N. Hafz, M. Uesaka, J. Koga, and K. Nakajima, Nucl. Instr. Meth. Phys. Res. A **455**, 148 (2000)

15. T.Hosokai, M.Kando, H.Dewa, H.Kotaki, S.Kondo, K.Horioka, and K.Nakajima *Optics Letters* vol.25,10 (2000)
16. R.G. Hemker, N.M. Hafz, and M. Uesaka, *Phys. Rev. ST* **5**, 041301 (2002)
17. T.Hosokai, K. Kinoshita, T. Watanabe, K. Yoshii, T. Ueda, A. Zhidkov, and M. Uesaka, *PROC. EPAC2002*, 981 (2002)
18. T. Hosokai, K.Kinoshita, A.Zhidkov, K.Nakamura, H.Kotaki, M.Kando, K.Nakajima, M.Uesaka, "Density effects on the cavity formation and interaction of an intense ultra-short laser pulse with a gas jet" *Phys. Rev. Lett.*, (submitted)
19. A.Zhidkov, J. Koga, T. Esirkepov, T. Hosokai, M. Uesaka, T. Tajima, 'Optical field ionization effects on propagation of an ultra-intense laser pulse in high-Z gas-jets', *Phys. Rev. Lett.* (submitted)
20. Mitsuru Uesaka, A.Zhidkov, T.Hosokai, and K.Kinoshita, 3rd ICFA Workshop on Quantum Aspects in Beam Physics Jan. 7-11, 2003Hiroshima, Japan (in press)
21. Mitsuru Uesaka, T.Hosokai, K.Kinoshita, and A.Zhidkov *AIP PROC* vol.5, P3690-3692 (2003)
22. T.Hosokai, K.Kinoshita, A.Zhidkov, T.Watanabe, M.Kando, H.Kotaki, K.Nakajima, and M.Uesaka
23. Advanced Accelerator Conference , Mandalay Beach California USA *AIP Conference Proceedings* 647 P-628 (2002)
24. K. Matsukado, K. Kinoshita, Z. Li, H. Daido, Y. Hayashi, S. Orimo, M. Uesaka, K. Yoshii, T. Watanabe, T. Hosokai, A. Zhidkov, A. Noda, Y. Iwashita, T. Shirai, S. Nakamura, "Ion Generation via Interaction between Intense Ultra-short Laser Pulse and Solid Target for Application to Cancer Therapy", *Proceedings of Advanced Accelerator Concepts: Tenth Workshop, California, (2002)* pp.265-268.
25. K. Kinoshita, T. Ohkubo, H. Okuda, T. Kobayashi, K. Yoshii, T. Watanabe, T. Ueda, M. Uesaka, "Generation and application of energetic heavy ion and x-ray via 12tw50fs laser-solid interaction", *Proceedings of the 2001 Particle Accelerator Conference, Chicago, (2001)* pp.2138-2140.
26. K. Kinoshita, T. Ohkubo, K. Yoshii, H. Harano, M. Uesaka, "Time-resolved X-ray diffraction for visualization of atomic motion", *International Journal of Applied Electromagnetics and Mechanics* Vo.14 (2002) pp.233-236.
27. K. Kinoshita, H. Harano, K. Yoshii, T. Ohkubo, A. Fukasawa, K. Nakamura, M. Uesaka, "Time-resolved X-ray diffraction at NERL", *Laser Part. Beams* Vol.19 (2001) pp.125-131.
28. A. Zhidkov *Phys. Plasmas* 5, 385 (1998)
29. A. Zhidkov, A. Sasaki *Phys. Rev. E* 59, 7085 (1999)
30. A. Zhidkov and A. Sasaki *Phys. Plasmas* 7, 1341 (2000)
31. A. Zhidkov, A. Sasaki, and T. Tajima *Phys. Rev. E* 61, R2224 (2000)
32. A. Zhidkov, M. Uesaka, A. Sasaki, and H. Daido, *Phys. Rev. Lett.* 89, 215002 (2002)
33. A. A. Andreev, A. G. Zhidkov, M. Uesaka, K. Kinoshita, and K. Yu. Platonov, *Phys. Rev. E* 66, 036405 (2002)
34. A.Zhidkov, J. Koga, A. Sasaki, and M. Uesaka, *Phys. Rev. Lett.* 88, 185002 (2002)
35. A.Zhidkov, J. Koga, K. Kinoshita, M. Uesaka , 'Effect of self-injection on ultra-intense laser wake field acceleration', *Phys. Rev. Lett.*(submitted)
36. A.Zhidkov, J. Koga, T. Esirkepov, T. Hosokai, M. Uesaka, T. Tajima, 'Optical field ionization effects on propagation of an ultra-intense laser pulse in high-Z gas-jets', *Phys. Rev. Lett.* (submitted)

## People

Mitsuru Uesaka (Professor)  
 Hokuto Iijima (Research Associate)  
 Tomonao Hosokai (Research Associate)  
 Alexei Zhidkov (Research Fellow, NIRS)  
 Toru Ueda (Technical Associate)  
 Katsuhiro Dobashi (Post Doctral Fellow, NIRS)  
 Kenich Kinoshita (Post Doctral Fellow, NIRS)  
 Kei Nakamura (Dr course Student)  
 Atsushi Fukasawa (Dr course Student)  
 Takeru Ohkubo (Dr course Student)  
 Fumito Sakamoto (Master's course Student)  
 Futarou Ebina (Master's course Student)  
 Nobuaki Yamaoka (Master's course Student)  
 Haruyuki Ogino (Under graduate Student)

## Address

Nuclear Engineering Research Laboratory Graduate School of Engineering, University of Tokyo  
 2-22,Shirakata-shirane Tokai, Naka, Ibaraki 319-1188, Japan

## 3.4 Activity at Hiroshima University

Kazuyoshi Koyama  
[k.koyama@aist.go.jp](mailto:k.koyama@aist.go.jp)

Hiroshima University

The Beam Physics Group (BPG) at Hiroshima University was organized in October 1998, as a new group belonging to the Graduate School of Advanced Sciences of Matter (AdSM). Since then, efforts have been made to initiate various theoretical and experimental research programs of beam physics.

BPG is also playing an important role in the Japanese beam-physics community [1].

### 3.4.1 Space-Charge-Dominated Beam Physics

Solving the Vlasov-Poisson equations for a one-dimensional beam, we found the coherent resonance condition [2,3]

$$\Omega_m \equiv m(\nu_0 - C_m \Delta \nu) = \frac{n}{2}, \quad (1)$$

where  $\Omega_m$  is the tune of the  $m$ th-order coherent mode,  $\nu_0$  is the bare tune,  $\Delta \nu = \nu_0 - \nu_x$  with  $\nu_x$  being the depressed single-particle tune, and  $C_m$ 's are certain constants. Resonance calculations for circulating two-dimensional beams have also been done numerically. The betatron Hamiltonian, including the effect of momentum dispersion, is given by

$$\begin{aligned} \tilde{H} = & \frac{\tilde{p}_x^2 + \tilde{p}_y^2}{2} + \frac{1}{2}(K_x - K_{sc}\xi_{20})\tilde{x}^2 + \frac{1}{2}(K_y - K_{sc}\xi_{02})\tilde{y}^2 \\ & - \frac{K_{sc}\xi_{40}}{24}[\tilde{x}^4 + 4D_x^{(1)}W\tilde{x}^3 + 6(D_x^{(1)})^2W^2\tilde{x}^2] - \frac{K_{sc}\xi_{04}}{24}\tilde{y}^4 - \frac{K_{sc}\xi_{22}}{4}[\tilde{x}^2 + 2D_x^{(1)}W\tilde{x} + (D_x^{(1)})^2W^2]\tilde{y}^2 + \dots, \end{aligned} \quad (2)$$

where we have assumed the same notation as used in Ref. [4]. Equation (2) strongly suggests the existence of *dispersive resonances*. We have actually confirmed, through particle-in-cell simulations, that such a novel resonance mechanism does affect the beam quality.

In order to improve the quality of a beam, we often introduce some cooling device in a storage ring. Since the tune is gradually depressed as the beam temperature becomes lower, the operating point may cross resonance stopbands. It is thus important to figure out whether a resonance can interrupt the cooling process. Systematic numerical simulations showed that the effective tune is locked at a low-order stopband if the cooling force is weak [5].

For the study of diverse space-charge effects, we proposed a new experimental scheme utilizing non-neutral plasma traps [6,7]. Two types of trap configurations, i.e. a radio-frequency quadrupole trap (Paul trap) and a solenoidal trap, were considered. The reason why these trap systems can be used for the study of charged-particle beams in accelerators is quite simple; a beam seen from the rest frame is almost equivalent to a single-species plasma in a trap. In fact, charged particles in a long Paul trap obey the Hamiltonian

$$H_{trap} = \frac{p_x^2 + p_y^2}{2} + \frac{1}{2}K(\tau)(x^2 - y^2) + \frac{q}{m_0c^2}\phi(x, y, \tau), \quad (3)$$

where  $q$  and  $m_0$  are, respectively, the charge state and rest mass of the particles, the independent variable is  $\tau = ct$  with  $c$  being the speed of light, and  $K(\tau)$  is a periodic function proportional to the radio-frequency voltages applied to the electrodes. Clearly, Eq. (3) has the form identical to the well-known Hamiltonian of betatron motion in a linear transport system, which means that the trap system can reproduce collective phenomena equivalent to those in a beam transport channel.

### 3.4.2 Phase Transition of Ion Beams

At low-temperature limit, a single-species plasma reaches a unique ordered state known as a *Coulomb crystal*. Recalling the dynamical analogy between a trap and a beam transport channel as discussed in the last section, we expect that a similar state may be established even in a cooler storage ring. Molecular dynamic simulations have actually shown that it is possible to crystallize a fast stored beam, at least, in principle. At BPG, the nature of this *crystalline beam* has been extensively studied. In a crystalline ground state, the trajectories of individual particles are strongly correlated; the transverse spatial coordinates of each particle in a coasting crystalline beam can be expressed as  $x = C_x D_x(s)$ ,  $y = C_y D_y(s)$ , where  $D_x$  and  $D_y$  are periodic functions of the path length  $s$  while  $C_x$  and  $C_y$  depend on which particle we see [8]. The orbit functions  $D_x$  and  $D_y$  satisfy coupled differential equations analogous to the envelope equations. It is an easy matter to show that the emittance of a crystalline beam is exactly zero. Provided that a longitudinal

radio-frequency field is present, the motion of a crystalline beam becomes more complex due to the existence of momentum dispersion [9].

To our best knowledge, laser cooling is currently the only means for us to reach a crystalline state, considering the acceptable thermal noise level. However, the dissipative force generated by a laser light has been known to operate only in the longitudinal direction of beam motion. In order to extend the powerful laser-cooling force to the transverse degrees of freedom, we have been testing the *resonant coupling method* [10,11]. It has been verified that the coupling scheme can significantly improve the transverse cooling efficiency [12].

The dispersive effect peculiar to a storage ring imposes a special demand upon the nature of cooling force for stabilizing crystals. Since the revolution frequencies of all particles forming a crystalline beam are identical, a longitudinal laser must provide such a cooling force as to give a greater average velocity to a radially outer particle. This is often referred to as *tapered cooling* [13]. If too powerful a conventional laser is applied, multi-dimensional crystalline structure could be destroyed because the *untapered* friction simply equalizes the longitudinal velocities of all particles. To develop a practical method for generating a tapered light seems to be the most important future issue toward our final goal.

### 3.4.3 Study of Compact Accelerators

It is over fifteen years ago that the idea of using solid structures for particle acceleration was discussed by several researchers. Nevertheless, no proof-of-principle experiments have been performed yet. One primary reason is that the power source appropriate for this purpose is not available. Recently, we have considered the application of artificial macroscopic structures, instead of natural solids, such as a photonic band-gap crystal. The characteristic size of an accelerator structure can then be enlarged to the order of  $1\mu\text{m}$ , much greater than the typical lattice constant of a solid [14].

An alternative, even simpler possibility is the use of a tiny cylindrical hole in a solid. By injecting a laser light into the hole, we can excite *plasmons* along the inner surface if the aperture size is comparable to the laser wavelength. The potential of the plasmons can be utilized to accelerate charged particles [15]. The conversion efficiency of the laser power to the accelerating field is expected to be rather high; e.g., a MW laser should suffice for attaining a gradient of GeV/m level. This scheme is, in some sense, similar to laser wake-field acceleration in a hollow channel and also to a dielectric linac. However, the *plasmon linac* could supply a beam of nanometer in transverse size (though the attainable beam current would be low). Figure 1 shows the dispersion diagram of a typical plasmon linac whose aperture radius is  $a$ .  $\omega_p$  is the plasma frequency and the corresponding wave number has been denoted by  $k_p = \omega_p / c$ . The frequencies of all modes

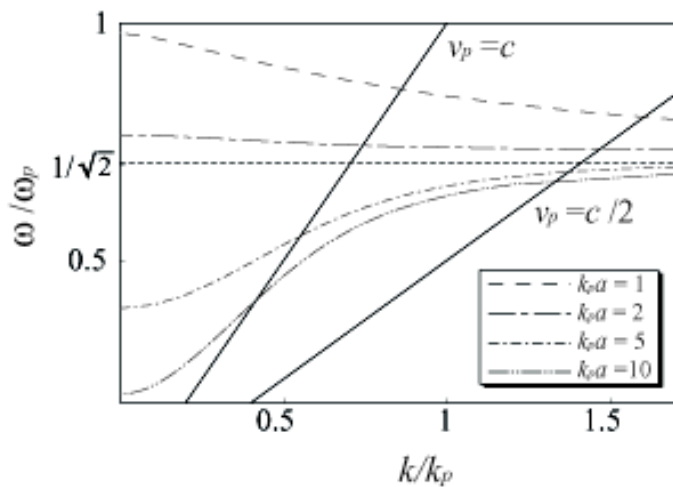


**Fig. 1:** Dispersion diagram of plasmons.

approach the surface plasmon-polariton frequency  $\omega_p / \sqrt{2}$  as the wave number  $k$  increases. The two straight lines in the picture represent the dispersion of the accelerating waves whose phase velocities are  $v_p = c$  and  $c/2$ . To accelerate an electron beam traveling nearly at the speed of light, we simply use a laser that has the frequency at the intersection between the plasmon dispersion curve and the  $v_p = c$  line.

Suppose a plasmon linac made of silver. When  $k_p a = 10$  and  $v_p = c$ , the required aperture radius and laser wavelength are, respectively, 227 nm and 344 nm. In this case, an acceleration gradient of 45.0 GeV/m is achievable with a 1MW laser according to our estimate. The effective acceleration length is, however, only about 4.3  $\mu\text{m}$ , which means that the total energy gain is less than 200 keV. This is basically due to the ohmic loss that raises the temperature of the linac and may eventually destroy the whole structure. One possible way to minimize this heating effect is to operate the linac in an extremely low-temperature atmosphere. At 10 K, for instance, the resistivity of silver becomes 1400 times smaller than that at room temperature. Consequently, the acceleration length and energy gain are increased to 6.1 mm and 273 MeV, respectively. Further, the power loss at  $r = a$  could be kept below the damage threshold of silver unless the repetition rate is too high.

### 3.4.4 Laser-Matter Interactions

For the last several years, there has been growing interest in interactions between high-intensity lasers and matters. In particular, the generation of multi-MeV ions by the irradiation of a high-power ( $> 10$  TW), short-pulse ( $< 1$  ps) laser has attracted worldwide attention. If an analogous effect is realizable by a laser of much lower power, that gives us a possibility of developing a compact ion source for diverse purposes.

The BPG has been performing experiments to irradiate very thin plastic and metal foils by a relatively low-power laser (1 TW) having a pulse width (50 fs) shorter than hitherto experiments [16]. The wavelength and pulse frequency of our laser are 800 nm and 10 Hz. Because the system is not equipped with a pulse cleaner, a main pulse is accompanied by a prepulse with amplitude 1/1000 - 1/100 of the main. It was, however, suggested that the existence of prepulses causes some positive effect in high-energy ion generation [18]. Two types of materials (mylar and aluminum) whose thickness are mostly less than 10  $\mu\text{m}$  have so far been used as a target. It was found that the intensity threshold of ion generation is  $10^{17} \text{ W} \cdot \text{cm}^{-2}$  in the “forward” region (In what follows, we call the laser-illuminated side

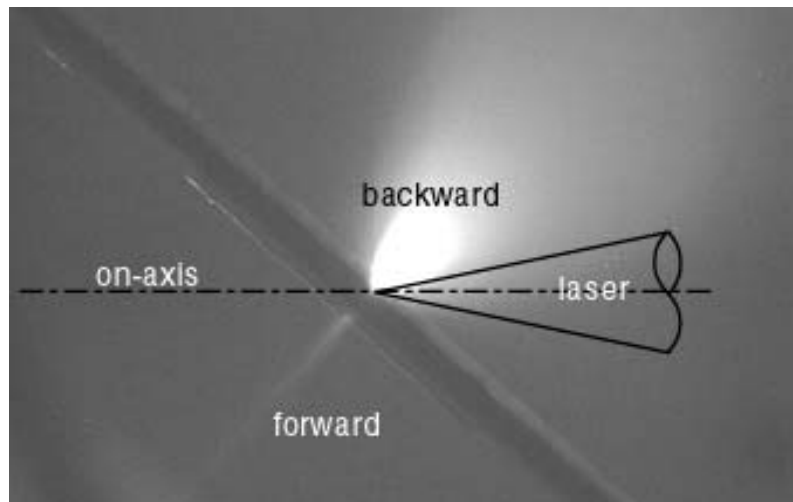


**Fig. 2 :** Photograph taken at the moment of laser irradiation to an Al foil of 3  $\mu\text{m}$  in thickness. A laser is coming from the right side. The target foil is tilted by 45 degrees with respect to the laser axis.

“backward” and the other side “forward”; particles produced below this threshold had no charge. By contrast, no such threshold was observed as to the particle generation toward the backward direction. The most energetic particles were usually protons in both directions, and the highest energy detected at the laser power of  $2 \times 10^{17} \text{ W} \cdot \text{cm}^{-2}$  was about 800 keV. Figure 2 shows a photograph at the moment of the interaction. The visible radiation was spectroscopically analyzed [17].

Energetic neutral particle beams were also observed in addition to ions[16]. They are produced mainly in the forward direction, and the divergence angle is much less than that of ions. According to our spectroscopic data, hydrogen atoms are the most probable candidate; if we assume so, systematic measurements with CR39 track detectors suggest that the maximum energy is beyond 1 MeV. The mechanism of neutral-beam generation has not been understood yet.

### 3.4.5 References

1. The homepage of the Japanese Beam Physics Club can be found at <http://www-acctheory.kek.jp/BP/BPclub.html> (only in Japanese); See also: H. Okamoto, The Japanese beam physics club and its recent activities, *ICFA Beam Dynamics Newsletter* No.12 (1996) p.10.
2. H. Okamoto and K. Yokoya, “Parametric resonances in intense one-dimensional beams propagating through a periodic focusing channel”, *Nucl. Instr. Meth. A*482 (2002) p.51.
3. A. V. Fedotov, I. Hofmann, R. L. Gluckstern and H. Okamoto, “Parametric collective resonances and space-charge limit in high-intensity rings”, *Phys. Rev. STAB* 6 (2003) 094201.
4. H. Okamoto and S. Machida, “Particle beam resonances driven by dispersion and space charge”, *Nucl. Instr. Meth. A*482 (2002) p.65.
5. K. Okabe and H. Okamoto, “Emittance limitation in cooled hadron beams”, Hiroshima University Preprint HUBP-02/02 (2002), *Jpn. J. Appl. Phys.* 42 (2003) 4584.
6. H. Okamoto, “On dynamical analogy between linear beam transport channels and plasma trap systems”, Hiroshima University Preprint HUBP-01/98 (1998); H. Okamoto and H. Tanaka, “Proposed experiments for the study of beam halo formation”, *Nucl. Instr. Meth. A* 437 (1999) p.178.
7. H. Okamoto, Y. Wada and R. Takai, “Radio-frequency quadrupole trap as a tool for experimental beam physics”, *Nucl. Instr. Meth. A* 485 (2002) p.244.
8. H. Okamoto, “Single-particle orbit equation in crystalline beams”, *Phys. Plasmas* 9 (2002) p.322.
9. H. Okamoto, Y. Yuri and K. Okabe, “Oscillating Coulomb chain in a storage ring”, *Phys. Rev. E* 67 (2003) 046501; Y. Yuri and H. Okamoto, “Effect of a longitudinal radio-frequency field on crystalline beams”, *J. Phys. Soc. Jpn.* 71 (2002) p.1003
10. H. Okamoto, A. M. Sessler and D. Möhl, “Three-dimensional laser cooling of stored and circulating ion beams by means of a coupling cavity”, *Phys. Rev. Lett.* 72 (1994) p.3977; H. Okamoto, “Transverse laser cooling induced through dispersion at an rf cavity”, *Phys. Rev. E* 50 (1994) p.4982.
11. H. Okamoto, Y. Yuri and K. Okabe, “Some remarks on beam crystallization”, *Ion Beam Cooling – Toward the Beam Crystallization*, World Scientific Publishing Co., Singapore (2002) p.160.

12. T. Kihara et. al., “Three-dimensional laser cooling method based on resonant linear coupling”, *Phys. Rev. E* 59 (1999) p.3594.
13. J. Wei, H. Okamoto and A. M. Sessler, “Necessary conditions for attaining a crystalline beam”, *Phys. Rev. Lett.* 80 (1998) p.2606; H. Okamoto and J. Wei, “Theory of tapered cooling”, *Phys. Rev. E* 58 (1998) p.3817.
14. A. Ogata, “Use of macroscopic solid structure in accelerators”, to be published in Proc. 3<sup>rd</sup> QABP Workshop.
15. N. Saito and A. Ogata, “Plasmon linac: A laser wake-field accelerator based on a solid-state plasma”, *Phys. Plasmas*, 10 (2003) p.3358.
16. Y. Wada, T. Kubota and A. Ogata, “Neutral beam generation by laser irradiation of thin foils”, in K. Nakajima and M. Deguchi (eds), *Sciences of Superstrong Field Interactions*, no.634 in AIP Conf. Proc. (2002) p.329.
17. T. Kubota, Y. Wada, and A. Ogata, "Visible Spectroscopy in T3 Laser Interaction with Thin Foil Targets", *Jpn. J. Appl. Phys.* 42 (2003) in press.
18. K. Matsukado, T. Esirkepov, K. Kinoshita, H. Daido, T. Utsumi, Z. Li, A. Fukumi, Y. Hayashi, S. Orimo, M. Nishiuchi, S. V. Bulanov, T. Tajima, A. Noda, Y. Iwashita, T. Shirai, T. Takeuchi, S. Nakamura, A. Yamazaki, M. Ikegami, T. Mihara, A. Morita, M. Uesaka, K. Yoshii, T. Watanabe, T. Hosokai, A. Zhidkov, A. Ogata, Y. Wada, and T. Kubota, "Energetic Protons from a Few Micron Metallic Foil Evaporated by Intense Laser Pulse", *Phys. Rev. Lett.* 91 (2003) 215001.

### 3.5 Program of the Particle Beam Physics Laboratory (PBPL)

J. Rosenzweig, UCLA  
[rosen@physics.ucla.edu](mailto:rosen@physics.ucla.edu)

The program of the Particle Beam Physics Laboratory (PBPL) in the UCLA Dept. of Physics and Astronomy contains diverse, yet intertwined, aspects of advanced accelerator, high brightness beam, and light source physics. It is a joint effort between Profs. James Rosenzweig and Claudio Pellegrini; the PBPL in turn has significant collaborations with the other on-campus faculty working in beam physics at UCLA: Chan Joshi (Electrical Engineering), Warren Mori (EE/Physics) and David Cline (Physics). PBPL research covers a wide range of beam dynamics and acceleration methods; beam-radiation interaction and production; beam-plasma interactions; beam-matter interactions and diagnostics. Areas of emphasis include the creation of ultra-fast, high-brightness electron beams; the application of such beams to advanced accelerators using lasers and/or plasmas; the creation of new types of light sources, such as free-electron lasers and inverse-Compton scattering sources based on high brightness electron beams.

The program in advanced accelerators on the UCLA campus is centered on the joint EE/Physics Neptune Laboratory, which combines the capabilities of a state-of-the-art photoinjector and a terawatt, 100 ps pulse-length, two-frequency CO<sub>2</sub> laser. Additional on-campus facilities include the PEGASUS photoinjector/radiation lab, and the Electromagnetics lab for development of advanced magnetostatic and rf devices. The PBPL program contains a strong off-campus experimental component, with a wide array of partners BNL ATF (bunch compression and SASE FEL), FNAL (plasma wakefield acceleration, plasma-based electron sources), INFN-Frascati (high brightness beam physics, FEL) LLNL (inverse-Compton

scattering, high brightness beam physics) and SLAC ORION (high brightness beam physics, plasma-based acceleration).

### 3.5.1 Some of the highlights of recent research include:

- The Neptune photoinjector has been used in next generation plasma beatwave accelerator experiments using Prof. Joshi's MARS laser, a two-frequency CO<sub>2</sub> system. Over 50 MeV electrons were observed, having been accelerated from 12 MeV. The results of these experiments will be published in PRL (publication 12, below).
- Fundamental beam physics studies are a large component of the program at the Neptune photoinjector, especially in sub-picosecond pulse compression. A complete experimental and computational study of transverse phase-space bifurcation during chicane compression of an intense 12 MeV electron beam from 4.5 to 0.65 ps was performed. A UCLA-developed single shot, slit-based phase space reconstruction method allowed direct examination of the phase space distribution; detailed simulations indicated a novel space-charge effect due to configuration space folding of the beam was the dominant mechanism driving this previously unknown effect (publication 3).
- An inverse free-electron laser experiment which utilizes the TW Mars laser and the photoinjector at Neptune is now under way. This ultra-high power laser beam is handled well by small  $f/\#$  focusing, which produces a large Guoy phase shift during the IFEL interaction. A strongly tapered undulator that mitigates these problems has been employed. Over 30 MeV electrons have been observed so far (starting with 14.5 MeV), in experiments where the beam detrap from the ponderomotive bucket halfway through the 50 cm undulator. Eventually, over 50 MeV beam is expected from this IFEL, with already demonstrated 2<sup>nd</sup>-generation advanced accelerator performance: low energy spread, high energy gain, good emittance.
- Neptune was used for initial studies of the velocity bunching (VB) concept, which may help avoid the pitfalls of magnetic compression. Pulses as short as 0.4 ps were observed using coherent transition radiation (CTR). This version of the VB scheme is under study for use at the ORION advanced accelerator facility (see publication 16).
- Two state-of-the-art photoinjector guns (for Neptune and ORION) have been fabricated at UCLA with SLAC collaboration. A new type of photoinjector which is scalable to high frequency and higher beam energy, based on hybrid standing-traveling wave rf structure is now under joint development with industry.
- A new dogleg beamline compressor beamline has been installed at Neptune, which allows generation of a beam with a long ramp and sharp fall. The nonlinear dynamics of this system required novel use of sextupole correctors. This beam is should be useful for a high-transformer ratio plasma wakefield accelerator (PWFA) experiments at Neptune, with a similar system now under study for ORION. Initial measurements using CTR interferometry indicate the sextupole correction works, and under 0.8 ps rms bunches are produced. An rf deflection mode cavity is now under development with INFN-Frascati which will allow below 100 fsec resolution pulse profile measurements on these beamlines.
- Photocathode development has proceeded, with magnesium cathode studies currently underway at Neptune. Diamond film cathode studies have begun at PEGASUS.

- The VISA SASE FEL, a UCLA-led collaboration at the BNL ATF, observed saturation of the 4-m FEL. A novel nonlinear compression mechanism in the ATF dogleg was found to be responsible for anomalously high gain. This experiment was only understood through benchmarking of start-to-end simulations using PARMELA, Elegant, and GENESIS to measurements of emittance, energy spread and pulse length.
- A new chicane compressor system has been developed, and has been installed at the BNL ATF. We will study basic compression-related processes such as coherent edge radiation (CER) using this device, and transverse emittance growth (using phase space tomography). It will also enable a new round of ultra-high gain FEL experiments using the VISA undulator.
- A new round of VISA experiments have begun, in which highly chirped beams are injected into the FEL. Sextupole correctors have been installed at the BNL ATF in order to preserve longitudinal phase space. Initial results have arisen from a regime where an unexpectedly large spectral bandwidth at very high gain is observed due to large angular errors in the electron beam trajectory, showing the robust, yet subtle nature of the FEL amplification process.
- A VB experiment at the LLNL/UCLA PLEIADES inverse-Compton scattering experiment has been performed, with 0.3 psec rms bunch length observed with CTR. These experiments have been extended to show preservation of the beam emittance during compression; compressed beam has been successfully employed in the the inverse-Compton scattering experiment.
- A novel, extremely short focal length final focus system based on very high gradient ( $>500$  T/m) permanent magnet quadrupoles (PMQs) is has been constructed at UCLA and installed at PLEIADES, to enhance the scattering luminosity. This system, which is tuned by longitudinal positioning of the PMQs, is also under study for use in  $\beta$ -matching for beam-plasma experiments, such as plasma wakefield acceleration, and plasma assisted inverse-Compton scattering (for polarized positron sources). Initial results have been obtained; under  $17\ \mu\text{m}$  spot sizes are observed, even with the present 10 mm-mrad emittance of the PLEIADES injector.
- The FNAL/UCLA plasma wakefield acceleration experiments at the FNAL A0 photoinjector were continued. A witness beam was created that allowed sampling of  $>150$  MV/m accelerating fields in the blowout regime.
- A new method of creating phase-locked, fsec beam pulses in plasma waves by trapping background plasma electrons has been developed at UCLA for an experimental demonstration at A0. This scheme uses only a drive beam PWFA that traverses a sharp density gradient in the plasma. By appropriate tailoring of the density profile in simulations, it has been found that a very low emittance, small energy spread electron beam can be “injected” into the plasma wave. Further, it has been shown that this system can be scaled to high plasma density to produce beams of unprecedented brightness. This experiment has now been installed, with initial beam injection into plasma ongoing as of Feb. 2004.
- A dielectric-based resonant laser accelerator, to be operated at either 10 or 340 microns at Neptune, has been studied analytically and computationally; it is now under design evaluation.
- Fundamental analytical and computational studies of plasma wakefields in the extreme blowout regime have been performed. Novel aspects of coherent radiation (CER, near-field CTR, coherent synchrotron radiation instability) and space-charge dominated beam physics

have also been studied through theory and simulation. Computational capabilities in the group have been greatly enhanced by our development of Beowulf parallel computing cluster.

- A senior-level textbook in beams and accelerators, *Fundamentals of Beam Physics*, by J. Rosenzweig, has been published by Oxford. This text is used in training the large student component of the PBPL effort.

### 3.5.2 Contact information:

James B. Rosenzweig, PBPL director

Department of Physics and Astronomy, University of California, Los Angeles

405 Hilgard Ave., Los Angeles, CA, 90095

PHONE: 310/206-4541

FAX: 608/206-5251

E-MAIL: [rosen@physics.ucla.edu](mailto:rosen@physics.ucla.edu)

Website: <http://pbpl.physics.ucla.edu>

#### Selected Figures

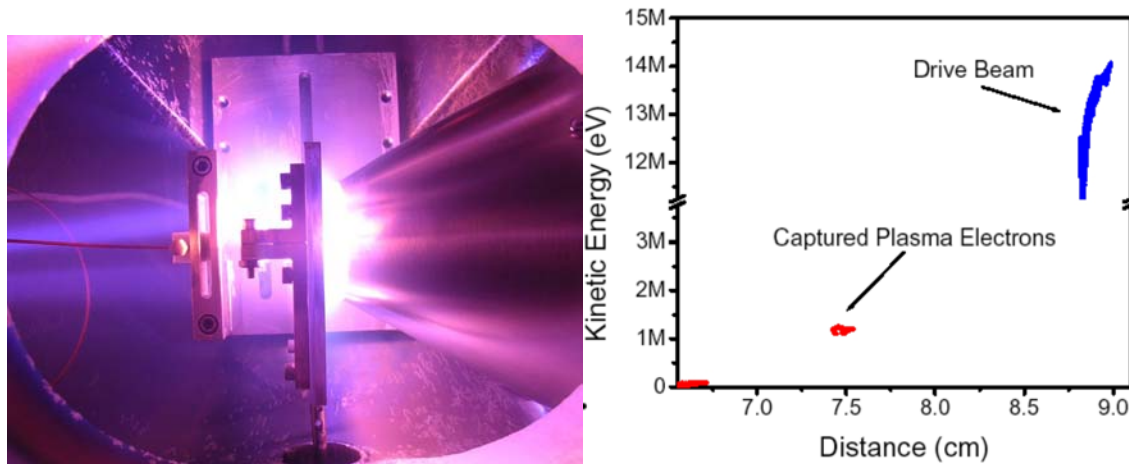


**Fig. 1.** Plasma source for UCLA/NICADD trapping injection experiment at FNAL A0 (left); simulated longitudinal phase space from experiment, from MAGIC code (right).

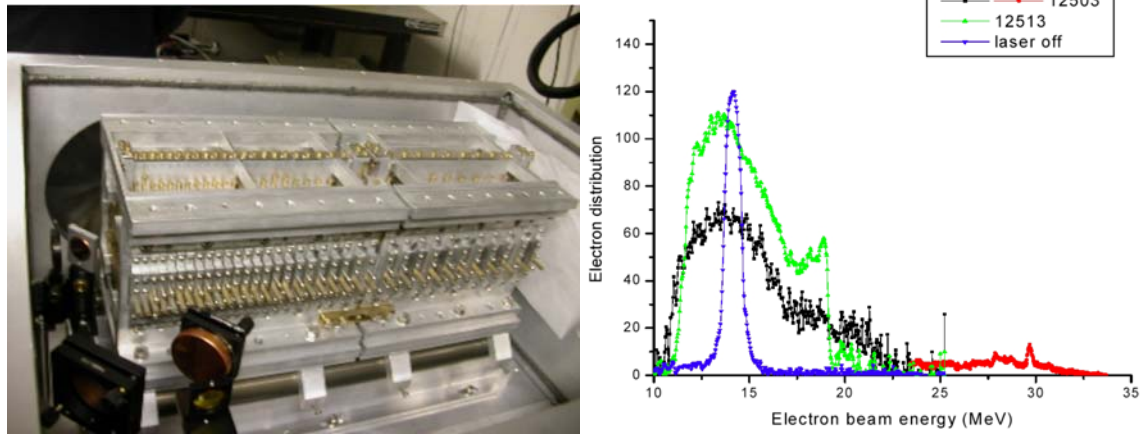


**Fig. 2.** Inverse free-electron laser undulator at Neptune laboratory (left); measured momentum spectra from selected shots, showing no laser, 5 MeV energy gain, up to 15 MeV acceleration (right).

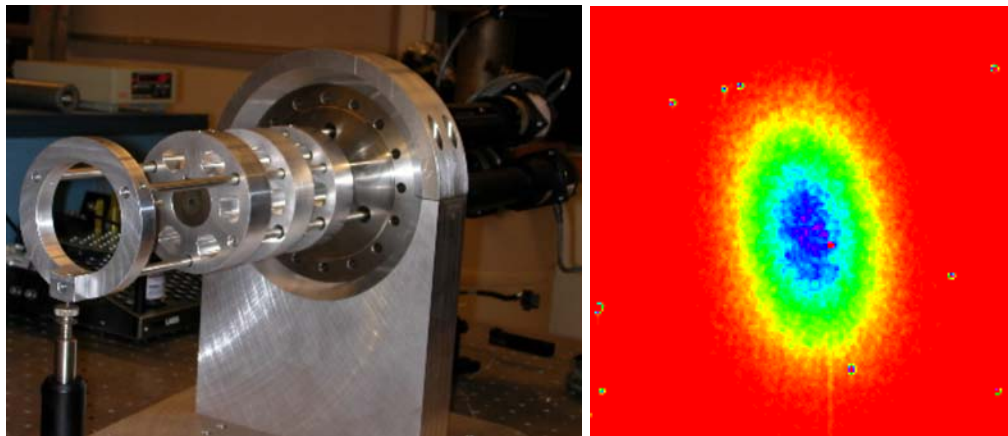


**Fig. 3.** UCLA-built adjustable strength PMQ triplet, with  $>500$  T/m Halbach quads (left); X-ray CCD image of inverse-Compton shot at PLEIADES with  $\sim 2 \times 10^6$  photons — this number is expected to rise by an order of magnitude with the PMQ final focus (right).

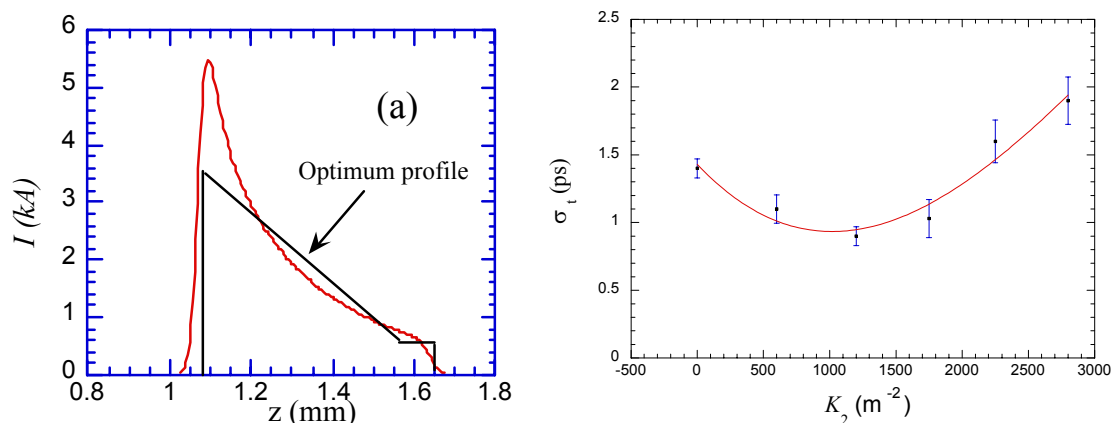


**Fig. 4.** Ramped beam profile expected after sextupole correct in Neptune dogleg compressor, for enhancement of plasma wakefield transformer ratio (left); Sextupole correction giving minimum pulse length, as measured using CTR at Neptune (right).

### 3.5.3 Publications

1. M. C. Thompson, J.B. Rosenzweig and H. Suk "Plasma density transition trapping as a possible high-brightness electron beam source" PRST-AB **7**, 011301 (2004)
2. James Rosenzweig, *Fundamentals of Beam Physics* (text book), Oxford University Press (Oxford, 2003)
3. S.G. Anderson, J. B. Rosenzweig, P. Musumeci, M. C. Thompson, "Horizontal Phase Space Distortions Arising from Magnetic Pulse Compression of an Intense, Relativistic Electron Beam", Phys. Rev. Lett. **91**, 074803 (2003)
4. S.G. Anderson, J.B. Rosenzweig, G.P. LeSage, J.K. Crane, "Space-charge effects in high brightness electron beam emittance measurements", PRST-AB **5**, 014201 (2002).
5. J.B. Rosenzweig, N. Barov, M.C. Thompson, and R. Yoder, "Energy Loss of a High Charge Bunched Electron Beam in Plasma: Nonlinear Plasma Response and Linear Scaling", in *Advanced Accelerator Concepts*, Ed. C. Clayton and P. Muggli, AIP Conference Proceedings **647**, (AIP, 2002).
6. N. Barov, J.B. Rosenzweig, M.C. Thompson, and R. Yoder "Energy loss of a high charge bunched electron beam in plasma: Analysis", in *The Physics and Applications of High Brightness Electron Beams*, Ed. J. Rosenzweig, L. Serafini and G. Travish (World Scientific, 2003)
7. J.B. Rosenzweig, N. Barov, M.C. Thompson, and R. Yoder "Energy loss of a high charge bunched electron beam in plasma: Simulation", in *The Physics and Applications of High Brightness Electron Beams*, Ed. J. Rosenzweig, L. Serafini and G. Travish (World Sci., 2003); also submitted to PRST-AB.
8. R. B. Yoder and J. B. Rosenzweig, "A Resonant, THz Slab-Symmetric Dielectric-Based Accelerator," in *The Physics and Applications of High Brightness Electron Beams*, Ed. J. Rosenzweig, L. Serafini and G. Travish (World Scientific, 2003); also submitted to PRST-AB.

9. R. B. Yoder and J. B. Rosenzweig, "A Resonant, THz Slab-Symmetric Dielectric-Based Accelerator," in *Advanced Accelerator Concepts, Tenth Workshop*, Ed. C. E. Clayton and P. Muggli AIP Conference Proceedings **647**, 331 (AIP, 2002).
10. A. Murokh, *et al*, "Properties of the ultrashort gain length, self-amplified spontaneous emission free-electron laser in the linear regime and saturation" Phys. Rev. E **67**, 066501 (2003). Also in the July 2003 issue of the Virtual Journal of Ultrafast Science <http://www.vjultrafast.org>
11. C. V. Filip *et al.*, "Non-resonant beat-wave excitation of constant phase-velocity, relativistic plasma waves for charged-particle acceleration", accepted for publication by Phys. Rev. E. (2004)
12. S. Ya. Tochitsky, *et al.*, "Enhanced Acceleration of Injected Electrons in a Laser Beatwave Induced Plasma Channel" accepted for publication in Phys. Rev. Lett. (2004).
13. A. Murokh, *et al*, "Results of the VISA SASE FEL experiment at 840 nm", Nuclear Instruments and Methods in Physics Research A **507** (2003) 417–421
14. R.J England, J.B. Rosenzweig, M.C. Thompson, "Longitudinal beam shaping and compression scheme for the UCLA Neptune Laboratory", AIP Conference Proceedings, **647** 884 (AIP, 2002).
15. R. J. England, J. B. Rosenzweig, and N. Barov, "Plasma electron fluid motion and wave breaking near a density transition" Phys. Rev. E **66**, 016501 (2002).
16. S. Reiche and J. B. Rosenzweig "Comparison of the coherent radiation-induced microbunching instability in a free-electron laser and a magnetic chicane" PRST-AB **6**, 040702 (2003). Also in the July 2003 issue of the Virtual Journal of Ultrafast Science <http://www.vjultrafast.org>
17. P. Musumeci, R.J. England, M.C. Thompson, R. Yoder, J.B. Rosenzweig. "Velocity Bunching experiment at the Neptune Laboratory", in *The Physics and Applications of High Brightness Electron Beams*, Ed. J. Rosenzweig, L. Serafini and G. Travish (World Sci., 2003)
18. P. Musumeci, C. Pellegrini, J.B.Rosenzweig, A. Varfolomeev, S. Tolmachev, T. Yarovoi. "Inverse Free Electron Laser Experiment at the Neptune Laboratory", in *Advanced Accelerator Concepts*, Ed. C. Clayton and P. Muggli, AIP Conference Proceedings, No. **647**, (AIP, 2002).
19. A. Tremaine, *et al*, "Measurements of nonlinear harmonic radiation and harmonic microbunching in a visible SASE FEL", Nucl. Instrum. Methods A , **507**, 445 (2003)
20. M.C. Thompson and J.B. Rosenzweig "Plasma Density Transition Trapping as a Possible High-Brightness Electron Beam Source" in *The Physics and Applications of High Brightness Electron Beams*, Ed. J. Rosenzweig, L. Serafini and G. Travish (World Scientific, 2003)
21. M.C. Thompson and J.B. Rosenzweig "Plasma Density Transition Trapping as a Possible High-Brightness Electron Beam Source" Advanced Accelerator Concepts Tenth Workshop Conference Proceedings, AIP Conf. Proc. **647**, 600 (AIP 2002).
22. A. Tremaine, *et al.*, "Experimental Characterization of Nonlinear Harmonic Radiation from a Visible Self-Amplified Spontaneous Emission Free-electron Laser at Saturation", Physical Review Letters, **88**, 204801 (2002).
23. Carl B. Schroeder, *et al.*, "Chirped-beam Two-stage Free-electron Laser for High-power Femtosecond x-Ray Pulse Generation", JOSA B, **19**,1782 (2002). Also in the Aug. 2002 issue of the Virtual Journal of Ultrafast Science - <http://www.vjultrafast.org> .

### 3.6 Laser guiding for high energy plasma accelerators

B. Cros<sup>1,\*</sup>, C. Courtois<sup>1, #</sup>, J. Godiot<sup>1</sup>, G. Matthieussent<sup>1</sup>, G. Maynard<sup>1</sup>, J-R. Marquès<sup>2</sup>, P-G. David<sup>2</sup>, F. Amiranoff<sup>2</sup>, N.E. Andreev<sup>3</sup>, L.M. Gorbunov<sup>4</sup>, P. Mora<sup>5</sup>, and R.R. Ramazashvili<sup>4</sup>

<sup>1</sup> LPGP, CNRS UMR 8578, Bât. 210, Université Paris XI, 91405 Orsay, France

<sup>2</sup> LULI, CNRS-CEA-Ecole Polytechnique, UPVI, France

<sup>3</sup> Institute for High Energy Densities, RAS, Russia

<sup>4</sup> P.N. Lebedev Physics Institute, RAS, Russia

<sup>5</sup> Centre de Physique Théorique, Ecole Polytechnique, France

#### Abstract

The excitation of plasma waves by the laser wakefield mechanism in the resonant, linear regime allows to achieve controllable accelerating electric fields in the 10 GV/m range. Injected electrons will acquire an energy gain in the GeV range provided that the laser pulse is guided over the dephasing length. The structure of the wakefield in a plasma column, created by a monomode laser pulse propagating in a capillary tube, filled with gas is studied numerically. The simulations show that in the central bulk part of a plasma column where the laser intensity exceeds the ionization threshold, the wakefield structure is similar to that of an infinite homogeneous plasma. Monomode guiding over 50 Rayleigh lengths (12 cm) of high intensity ultra-short laser pulses ( $10^{17}$  W/cm<sup>2</sup>, 350 fs) has been experimentally demonstrated in dielectric capillary tubes, in a range of parameters relevant to wakefield excitation.

#### 3.6.1 Introduction

Plasma based accelerators [1] are of great interest because of their ability to sustain accelerating electric fields up to 3 orders of magnitude higher than in conventional vacuum devices. The laser wake-field accelerator (LWFA) [2-4] provides the most promising approach to high-performance compact electron accelerators. In the resonant LWFA scheme a short laser pulse, of the order of the plasma period, excites a trailing plasma wave, or wakefield, that can trap and accelerate electrons to high energy. The present limitation for the energy of accelerated electrons in standard LWFA is due to the small acceleration distance, limited to a few Rayleigh lengths and typically, of the order of 1 mm. Therefore, in spite of high acceleration gradients ( $> 1$  GeV/m), the final energy gain of accelerated electrons is rather small ( $\approx 1$  MeV) [5]. The extended propagation of a laser pulse over many Rayleigh lengths, necessary to create a long acceleration distance and high energy electrons, can be achieved by the use of guiding structures such as plasma channels and capillary tubes.

We have developed the use of capillary tubes as optical wave guides. The laser pulse is guided due to reflection from the inner wall of the capillary tube, while a plasma is created by ionization of a gas filling the capillary tube. Multimode guiding of terawatt laser pulses through wide capillary tubes (with radius  $r_0$  such that  $r_0 > 2\sigma_0$ , where  $\sigma_0$  is the waist of the focal spot at  $1/e^2$  of the maximum intensity) has been observed in experiments [6]. In the multimode regime,

---

\* Email address: brigitte.cros@pgp.u-psud.fr

# presently at University of York, UK

the guided pulse has a complex transverse intensity profile and at high laser intensity the pulse propagation is accompanied by inner wall breakdown [6]. Opposite to multimode, monomode guiding (obtained for  $r_0 \approx 1.5\sigma_0$ ) provides a smooth transverse profile and a small attenuation of the laser pulse which is of essential interest for LWFA. For intense laser pulses ( $10^{16}$  W/cm<sup>2</sup>), monomode guiding over 100 Rayleigh lengths has been demonstrated [7, 8] both in evacuated capillary tubes and in capillary tubes filled with low pressure (2 mbar) He gas.

The radial profile of a plasma in a capillary tube can be mainly homogeneous: the plasma is created by gas ionization and depends on the initial profile of gas density, on the type of gas as well as on the laser intensity [8, 9]. For capillary tubes homogeneously filled with hydrogen gas, which has only one ionization stage, the plasma is formed uniformly inside the region where the laser intensity exceeds the threshold of tunneling ionization. The radial plasma density profile can be well approximated by a flat function with steep edges.

In this letter, we report on the progress towards LWFA inside capillary tubes. In section 3.6.2, numerical simulations show that a linear plasma wave is excited over 20 Rayleigh lengths inside a glass capillary tube filled with hydrogen gas, while in section 3.6.3 experimental results demonstrate the guiding of an intense laser pulse over 50 Rayleigh lengths with an output intensity of the order of  $10^{17}$  W/cm<sup>2</sup>.

### 3.6.2 Laser wakefield in a capillary tube: model and numerical simulations

The self-consistent description of the plasma and laser pulse propagating in a gas-filled capillary tube [10], takes into account both plasma formation via tunneling ionization and boundary conditions at the capillary tube wall. Because of the optical field ionization (OFI), a source term determining the free electrons production rate arises in the continuity equation for a plasma electron density averaged over the laser period,  $n(r,t)$ . The equation for the laser pulse envelope taking into account the effect of ionization may be written in the following form [11, 12]

$$\left\{ 2ik_0 \frac{\partial}{\partial z} + 2 \frac{\partial^2}{\partial z \partial \xi} + \Delta_{\perp} \right\} a = k_0^2 \left[ \left( \frac{n}{n_c \gamma} - \beta_a |a|^2 \right) a - iG^{(ion)} \right], \quad (1)$$

where  $a = eE_0/(mc\omega_0)$  is the dimensionless complex amplitude of the laser field,  $E_0$ , with frequency  $\omega_0$ , and depends not only on the radial variable  $r$  and  $\xi = z - ct$  but also on the axial variable  $z$  characterizing the slow evolution of the pulse in time during the course of its propagation;  $n_c = m\omega_0^2/(4\pi e^2)$  is the critical plasma density,  $\gamma = [1 + (\mathbf{p}/mc)^2 + |a|^2/2]^{1/2}$  is the relativistic factor of plasma electrons where  $\mathbf{p}$  is the electron momentum slowly varying in time [13]. In Eq. (1),  $\beta_a |a|^2$  is the non linear contribution to the dielectric constant coming from the bound atomic electrons. The last term on the right-hand side of Eq. (1) represents the laser energy losses in the process of OFI [14].

For light gases such as helium or hydrogen, considered here, OFI occurs at a relatively low laser intensity,  $|a| < 1$ . In this case, for laser pulses with transverse size,  $L_{\perp}$ , larger than  $1/k_{p0}$ , [ $k_{p0} = (4\pi e^2 N_{0e}/mc^2)^{1/2}$  is the wavenumber corresponding to the maximum electron density  $N_{0e}$  produced by OFI], the equation for the wakefield potential,  $\phi$ , in the quasi-static approximation [15] takes the form [12]:

$$\left\{ (\Delta_{\perp} - k_p^2) \frac{\partial^2}{\partial \xi^2} - \frac{\partial \ln n_0}{\partial r} \frac{\partial^3}{\partial r \partial \xi^2} + k_p^2 \Delta_{\perp} \right\} \phi - \frac{k_p^4}{2} \left[ 1 - \frac{1 + |a|^2/2}{(1 + \phi + \delta \Phi_s)^2} \right] = \frac{k_p^2}{4} \Delta_{\perp} |a|^2, \quad (2)$$

where the wavenumber  $k_p = (4\pi e^2 n_0 / mc^2)^{1/2}$  is determined by the local electron density  $n_0$ , produced by OFI averaged over the laser period, and  $\delta \Phi_s$  takes into account the birth of free electrons due to gas ionization.

In the same quasi-static approximation [15] the relativistic plasma response  $n/\gamma$  in Eq. (1) may be expressed through the potential  $\phi$  [12]:

$$\frac{n}{\gamma} = \frac{k_p^2 + \Delta_{\perp} \phi}{1 + \phi + \delta \Phi_s}. \quad (3)$$

For the numerical modeling of the laser pulse propagation and wakefield generation inside a gas filled capillary tube, Eqs. (1) and (2) have to be supplemented by boundary conditions. For linearly polarized laser pulses, the following boundary condition at the capillary tube wall  $r = r_0$  [12] is used:

$$\frac{\partial a}{\partial r} = ik_{w\perp} \left( 1 - \frac{i}{k_0} \frac{\partial}{\partial \xi} \right) a, \quad k_{w\perp} = \frac{2k_0(\varepsilon_w - 1)^{1/2}}{\varepsilon_w + 1}, \quad (4)$$

where  $\varepsilon_w$  is the dielectric constant of the wall. At the entrance of the capillary tube ( $z = -0$ ) the radial profile of the incident laser pulse  $A(r)$  is assumed to be Gaussian,  $A(r) = \exp(-r^2/\sigma_0^2)$ , where  $\sigma_0$  is the focal spot size. The boundary condition at the capillary tube entrance  $z = 0$  is taken in the form

$$a(\xi, r, z=+0) = a_0 \tilde{A}(r) \exp \left[ -2 \ln 2 \frac{(\xi - \xi_0)^2}{c^2 \tau^2} \right], \quad (5)$$

where  $\tau$  is the pulse duration, measured full width at half maximum (FWHM) of the intensity. The boundary conditions for the wakefield potential imply that  $\phi = 0$  in the unperturbed gas in front of the pulse ( $\xi \rightarrow +\infty$ ) and at the capillary tube wall  $r = r_0$ .

The importance of the nonlinearities during the guided propagation of the laser pulse can be estimated by comparing the propagation with and without gas. For a capillary tube in vacuum, the RHS of Eq. (1) is equal to zero, and the solution of Eq. (1) with the boundary condition (4), where the small terms containing  $\partial/\partial \xi$  and responsible for finite pulse length effects are omitted, gives the eigenmodes [described, in this case, by the zero order Bessel functions  $J_0(k_{s\perp} r)$ ,  $k_{s\perp} = u_s/r_0 - i u_s/(k_{w\perp} r_0^2)$ ] and their attenuation coefficients  $\delta k_{zs}''$  [7,16]:

$$\delta k_{zs}'' = \frac{u_s^2}{2k_0^2 r_0^3} \frac{1 + \varepsilon_w}{\sqrt{\varepsilon_w - 1}}, \quad (6)$$

where  $u_s$  is the  $s$ th root of the equation  $J_0(u_s) = 0$ . The imaginary part of the axial wave vector (6) describes the decrease of the laser pulse energy due to the flux of electromagnetic energy through the capillary tube wall. The propagation inside an evacuated capillary tube is thus determined by approximating (at  $z = +0$ ) the radial profile of the guided pulse  $\tilde{A}(r)$  by a sum of hybrid eigenmodes EH<sub>1s</sub> [16, 17]

$$\tilde{A}(r) = \sum_{s=1}^{S_m} C_s J_0(k_{s\perp} r), \quad (7)$$

where

$$C_s = \frac{2}{[r_0 J_1(u_s)]^2} \int_0^{r_0} A(r) J_0\left(\frac{u_s r}{r_0}\right) r dr . \quad (8)$$

The number of eigenmodes in the expansion (7) is taken to be  $S_m = 5$ .

Numerical simulations have been performed for a capillary tube filled with hydrogen gas with the following, realistic set of parameters: laser wavelength,  $\lambda_0 = 0.8 \mu\text{m}$ , pulse duration 50 fs, power  $P_L = 10 \text{ TW}$ , and maximum intensity  $I_L = 1.1 \times 10^{18} \text{ W/cm}^2$  for a laser spot size  $\sigma_0 = 24 \mu\text{m}$  at the capillary entrance. The radius of the glass capillary tube ( $\varepsilon_w = 2.25$ ) is chosen as  $r_0 = 37.5 \mu\text{m}$ , so that  $\sigma_0/r_0 = 0.645$ . In accordance with Eq. (8) this ratio provides a coupling of the order of 98 % of the incident energy of Gaussian pulse in the fundamental mode  $\text{EH}_{11}$ .

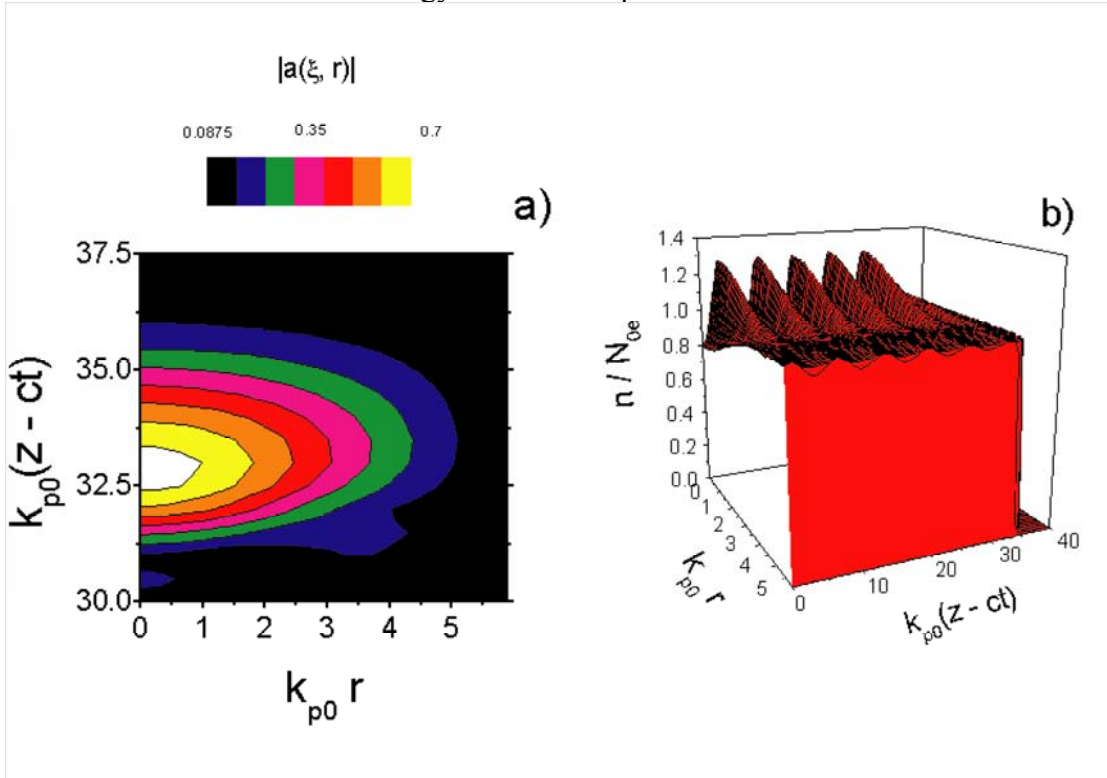


**Fig. 1:** a) Contour plots of the laser pulse envelope  $|a(\xi, r)|$  in the  $(\xi, r)$  plane and b) normalized electron plasma density  $n(\xi, r)/N_{0e}$  at the propagation distance from the entrance of the capillary tube  $z = 4.61 \text{ cm}$  for a hydrogen filled capillary tube.

The wakefield generation inside a capillary tube ( $\varepsilon_w = 2.25$ ,  $r_0 = 37.5 \mu\text{m}$ ) filled with hydrogen gas is illustrated in Fig. 1. The hydrogen gas density,  $N_0 = 0.69 \times 10^{18} \text{ cm}^{-3}$  was chosen so that the maximum electron density produced by OFI  $N_{0e} = N_0$  is the resonant one for the wakefield generation by a 50 fs Gaussian laser pulse. With these parameters, the guiding of the laser pulse is mainly monomode (i.e. the coupling between higher order modes and the fundamental through non linearities is small) and the generation of the wakefield is efficient over many Rayleigh lengths,  $z_R = k_0 \sigma_0^2/2$ . Figure 1 shows a) the contour plots in the  $(\xi, r)$  plane of the normalized laser field envelope,  $|a(\xi, r)|$ , and b) the dimensionless electron density,  $n/N_{0e}$ , taken at the position, or propagation distance,  $z = 4.61 \text{ cm}$ . It can be seen that the pulse shape

as well as the wakefield structure do not undergo essential variations on a sufficiently long distance. In this case, the pulse shape of the laser is preserved while a regular electron density oscillation is created for a distance of the order of 20 Rayleigh lengths.

### 3.6.3 Laser guiding in a capillary tube: experimental results

An experiment was performed at the Laboratoire pour l'Utilisation des Lasers Intenses (LULI) with 20 J,  $\tau = 350$  fs (FWHM) linearly polarized, compressed laser pulses of central wavelength  $\lambda = 1.057$   $\mu\text{m}$ . After compression, the laser pulse is frequency doubled in vacuum by a 2.5 mm thick KDP crystal with a conversion efficiency of the order of 50 % at maximum energy. For each shot, the incident energy is measured before and after frequency doubling, and the pulse duration at the fundamental frequency is measured with a single shot autocorrelator. The frequency doubled beam reflects off 3 mirrors and a focusing parabola coated for high reflectivity at 0.528  $\mu\text{m}$  in order to increase the green/infrared contrast ratio to a value larger than  $10^5$ . The beam is focused by the 1.8 m focal length ( $f/20$ ) off-axis parabola to a waist (radius at  $1/e^2$  in intensity)  $\sigma_0 = 20 \pm 3$   $\mu\text{m}$  (2 times the diffraction limit). The capillary tube is mounted on a target support with 5 degrees of freedom (three translations and two rotations) which allow the micro-positioning of the entrance plane of the capillary tube in the focal spot plane and of the tube on the laser beam axis. 10 % of the transmitted beam is reflected by a rejection plate and sent to diagnostics. A  $f/10$  doublet images the output plane of the capillary tube on a 16-bits CCD camera equipped with a microscope objective (magnification  $\times 20$ ).

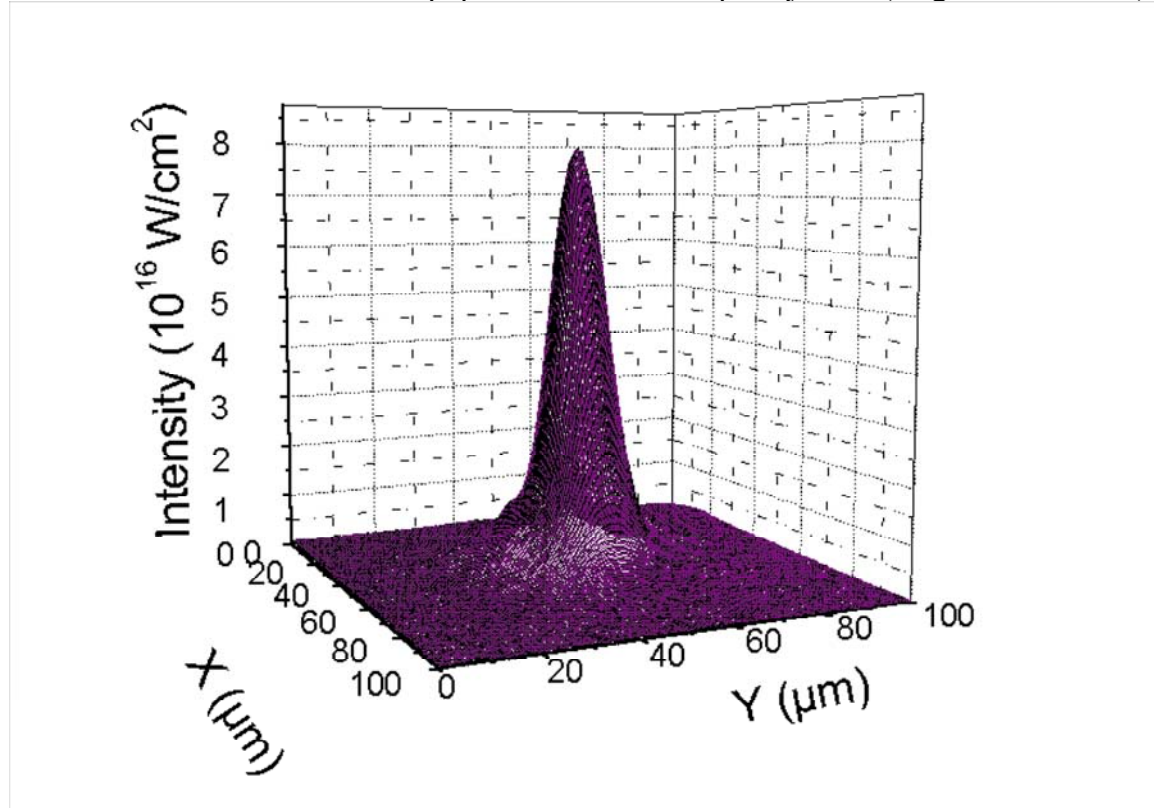


**Fig. 2:** Energy repartition at the output of a 25  $\mu\text{m}$  radius, 12 cm long evacuated capillary tube for an incident energy in the focal plane of 4.3 J.

The energy repartition at the output of a 25  $\mu\text{m}$  radius, 12 cm long capillary tube is shown in Fig. 2 for an incident energy in the focal plane of 4.3 J. The measured energy repartition is very close to the one of the fundamental eigen mode of the tube,  $\text{EH}_{11}$ . The energy transmission on this shot was of the order of 30 %, which corresponds to the theoretical value for the  $\text{EH}_{11}$  mode when the energy repartition at the entrance of the tube is taken into account.

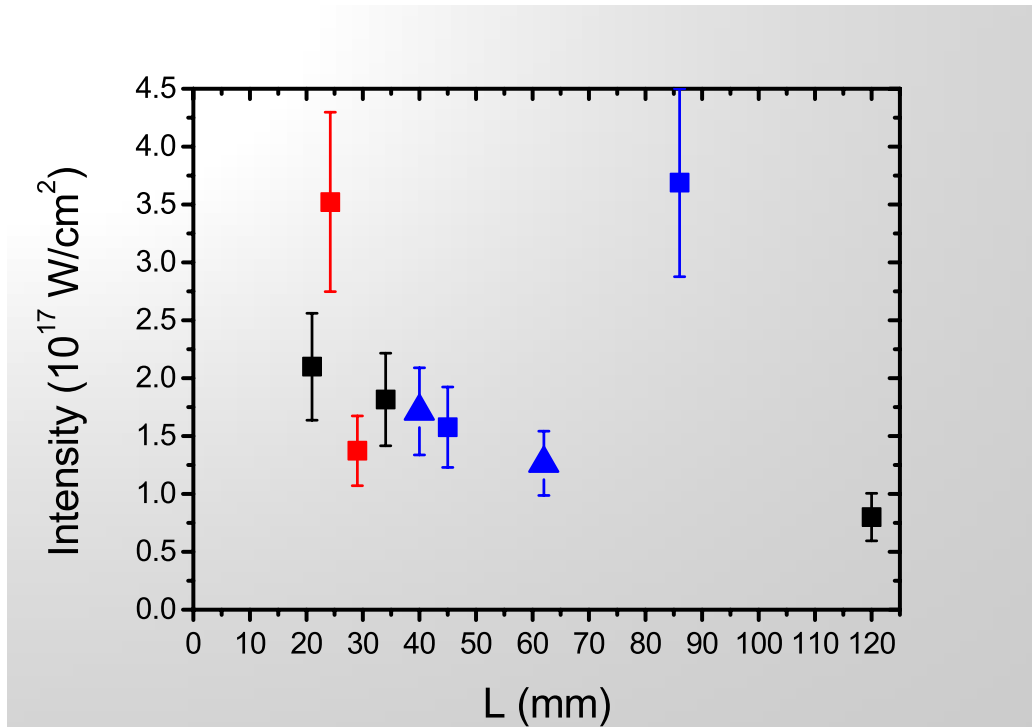


**Fig. 3:** Intensity as a function of the capillary tube length for different capillary tube radii: 25  $\mu\text{m}$  (black squares), 35  $\mu\text{m}$  (red squares) and 38  $\mu\text{m}$  (blue squares) in vacuum; on some shots the capillary tubes were filled with 2.2 mbar of helium gas (38  $\mu\text{m}$  radius, blue triangles).

Peak intensities are determined from calibration shots: the focal plane is imaged on the CCD chip so that the total number of CCD counts is proportional to the energy in the focal plane; the peak intensity is then calculated from the number of counts per pixel on each shot. The output intensity is plotted in Fig. 3 as a function of the tube length, for different tube radii in vacuum or helium gas. Figure 3 shows that an intensity larger than  $10^{17} \text{ W/cm}^2$  is guided over capillary tube lengths up to 12 cm ( $50 z_R$ ). The intensity at  $L = 12 \text{ cm}$  is more than two orders of magnitude larger than it would be in the free propagation case.

For gas filled capillary tubes, the output intensity is larger than  $10^{17} \text{ W/cm}^2$ , about 10 times higher than the second ionization threshold of helium. From this measurement, it is inferred that up to 6 cm long plasma columns have been created, with an on axis electron density of the order of  $4.9 \times 10^{16} \text{ cm}^{-3}$ .

### 3.6.4 Conclusion

A plasma created by intense laser pulses through tunneling ionization of a gas inside a capillary tube is uniform in the region where the laser intensity exceeds the ionization threshold.

The plasma density falls down to zero only close to the capillary tube wall where the laser intensity becomes sub-threshold [10]. Inside the homogeneous bulk part of the column the wakefield has a regular structure which is similar to the one in infinite plasmas.

Monomode guiding over  $50 z_R$  (12 cm) of an ultra-short pulse with output intensity of the order of  $10^{17}$  W/cm<sup>2</sup> has been demonstrated in glass capillary tubes. In He gas, output intensities of the order of  $10^{17}$  W/cm<sup>2</sup> have been measured, indicating that a plasma is created over the whole length of the capillary tube ( $26 z_R$ ). Laser intensity and gas pressure conditions in this experiment are close to linear resonant wakefield conditions; the measurement of the plasma waves excited by resonant wakefield inside a capillary tube will be the subject of future work.

### 3.6.5 Acknowledgements

This work was supported by INTAS project 97-10236, by the Centre National de la Recherche Scientifique (France), by the Russian Foundation for Basic Research by the Grant 01-02-16723, by the NATO Collaborative Linkage Grant PST. 976812, and by grant E 1127 from Région Ile-de-France. The authors gratefully acknowledge the help of the technical staff of the LULI facility.

### 3.6.6 References

1. E. Esarey, P. Sprangle, J. Krall, A. Ting, IEEE Trans. Plasma Sci. **24**, 252-288 (1996).
2. T. Tajima and J. Dawson, Phys. Rev. Lett. **43**, 267 (1979).
3. L.M. Gorbunov and V.I. Kirsanov, Sov. Phys. JETP **66**, 290 (1987).
4. P. Sprangle, E. Esarey, A. Ting, and G. Joyce, Appl. Phys. Lett. **53**, 2146 (1988).
5. F. Amiranoff *et al.*, Phys. Rev. Lett. **81**, 995 (1998); F. Dorchies *et al.*, Phys. Plasmas **6**, 2903 (1999).
6. S. Jackel *et al.*, Opt. Lett. **20**, 1086 (1995); M. Borghesi, A. J. Mackinnon, R. Gaillard, O. Willi, and A. A. Offenberger, Phys. Rev. E **57**, 4899 (1998).
7. F. Dorchies *et al.*, Phys. Rev. Lett. **82**, 4655 (1999).
8. C. Courtois, A. Couairon, B. Cros, J. R. Marquès, and G. Matthieussent, Phys. Plasmas **8**, 3445 (2001).
9. N.E. Andreev *et al.*, IEEE Trans. Pl. Sc. **28** 1090 (2000).
10. N.E. Andreev *et al.*, Phys. Plasmas **9**, 3999 (2002).
11. P. Sprangle, E. Esarey, and B. Hafizi, Phys. Rev. E **56**, 5894 (1997); P. Sprangle, B. Hafizi, and P. Serafim, Phys. Rev. E **59**, 3614 (1999).
12. N.E. Andreev, Y. Nishida, and N. Yugami, Phys. Rev. E **65**, 056407 (2002).
13. P. Mora and T.M. Antonsen Jr., Phys. of Plasmas **4**, 217 (1997).
14. N.E. Andreev, M.E. Veisman, M.G. Cadjan, and M.V. Chegotov, Plasma Physics Reports **26**, 947 (2000); M.V. Chegotov, *ibid.* **26**, 881 (2000); N.E. Andreev, M.V. Chegotov, and M.E. Veisman, IEEE Trans. Plasma Sci. **28**, 1098 (2000).
15. P. Sprangle, E. Esarey, and A. Ting, Phys. Rev. Lett. **64**, 2011 (1990).
16. B. Cros *et al.*, Phys. Rev. E **65**, 026405 (2002).
17. E.A.J. Marcatili and R.A. Schmeltzer, The Bell Syst. Tech. J. **43**, 1783 (1964).

### 3.7 Computational accelerator physics at Tech-X Corporation

D. Abell, D.L. Bruhwiler,\* J.R. Cary,<sup>†</sup> D.A. Dimitrov, P. Messmer, C. Nieter and P. Stoltz  
Tech-X Corporation, 5621 Arapahoe Ave., Suite A, Boulder CO 80303, USA

<sup>†</sup>also Univ. of Colorado, Boulder CO, USA

\* [mailto: bruhwile@txcorp.com](mailto:bruhwile@txcorp.com)

Tech-X Corp. [1] was founded in 1994, with the goal of applying modern software techniques, such as object-oriented computing, distributed computing, parallel computing, graphical user interfaces, interactive scripting and scientific visualization to challenging problems in science and computer science. In the past ten years, Tech-X has grown to over 20 employees – including physicists, computer scientists and software engineers – working on software projects relevant to particle accelerators and other high-power beam devices, various aspects of plasma fusion, and management of scientific data via grid and web service technologies. We present an overview of our most recent research related to advanced concepts for plasma-based particle acceleration and other novel aspects of accelerator physics.

#### 3.7.1 Beam and plasma simulation codes VORPAL and OOPIC

VORPAL [2-5] is a plasma and particle simulation code that takes maximal advantage of object-oriented programming techniques in C++ to provide a greater level of flexibility. Template meta-programming techniques are used to enable simulations in 1, 2 or 3 physical dimensions, with dimensionality specified at run time. Both PIC and fluid representations of various types are available for the plasma. The cold fluid model for electrons can correctly handle vacuum/fluid interfaces and passage of high-power laser pulses through density ramps. The fields can be updated using a fully electromagnetic model based on the Yee mesh [6] or an electrostatic model [7] using the AZTEC libraries. [8] Full source code is available. [9]

The 2-D PIC code OOPIC [10,11] can include the effects of electron-impact excitation, ionization and electron-neutral scattering at relativistic energies, as well as field-induced tunneling ionization. The OOPIC physics kernel can be invoked at the command line in serial or parallel, or it can be used with a GUI on Linux or Windows. Full source code is available. [12]

#### 3.7.2 Field-induced tunneling ionization

We are developing a C library for the calculation of field [13-15] and impact ionization processes. A prototype is available for tunneling ionization of certain atoms and their ions. The library supports direct calls from Fortran 77/90. Integration with VORPAL is underway.

Parallel OOPIC [10,11] simulations of field-induced tunneling ionization by short, intense laser pulses propagating through a He gas jet have shown a blue-shifting of the spectrum that agrees quantitatively [16] with experimental data [17] from the l'OASIS laboratory [18] at LBNL. The leading edge of the pulse fully strips the He atoms via tunneling ionization and the resulting gradient in the plasma density leads to localized blue shifting, in agreement with theory. [19]

OOPIC simulations first showed [20] that tunneling ionization is critically important in high-field PWFA concepts like the plasma afterburner. [21] The necessary meter-scale plasmas can only be pre-ionized to the 10% level, and this work showed one must use neutral gas only, but increase electron beam density so it can both ionize the gas and generate a strong wake. This removes the need for pre-ionization, greatly reducing cost and complexity.

We showed the ADK [14] ionization probability rate could be cast in the following form:

$$W[s^{-1}] \approx 1.52 \times 10^{15} \frac{4^{n^*} \xi_i [eV]}{n^* \Gamma(2n^*)} \left( 20.5 \frac{\xi_i^{3/2} [eV]}{E [GV/m]} \right)^{2n^*-1} \exp \left( -6.83 \frac{\xi_i^{3/2} [eV]}{E [GV/m]} \right) \quad (1)$$

where  $E$  is the local electric field and  $\xi_i$  is the ionization threshold energy. The effective principal quantum number is  $n^* \approx 3.69Z/\xi_i^{1/2}$ , where  $Z$  is the charge number for the ion after ionization.

### 3.7.3 Simulating LWFA channels, in support of P'OASIS experiments

Comparisons between OOPIC and a 2-D relativistic fluid code at LBNL [22,23] has been made in an effort to benchmark the codes. Fig. 1 shows PIC (left) and fluid (right) results of the excited wake field after two Rayleigh lengths of propagation in a pre-ionized plasma channel. The fluid code shows higher, narrower density peaks. This could be due to temperature effects in the PIC code.

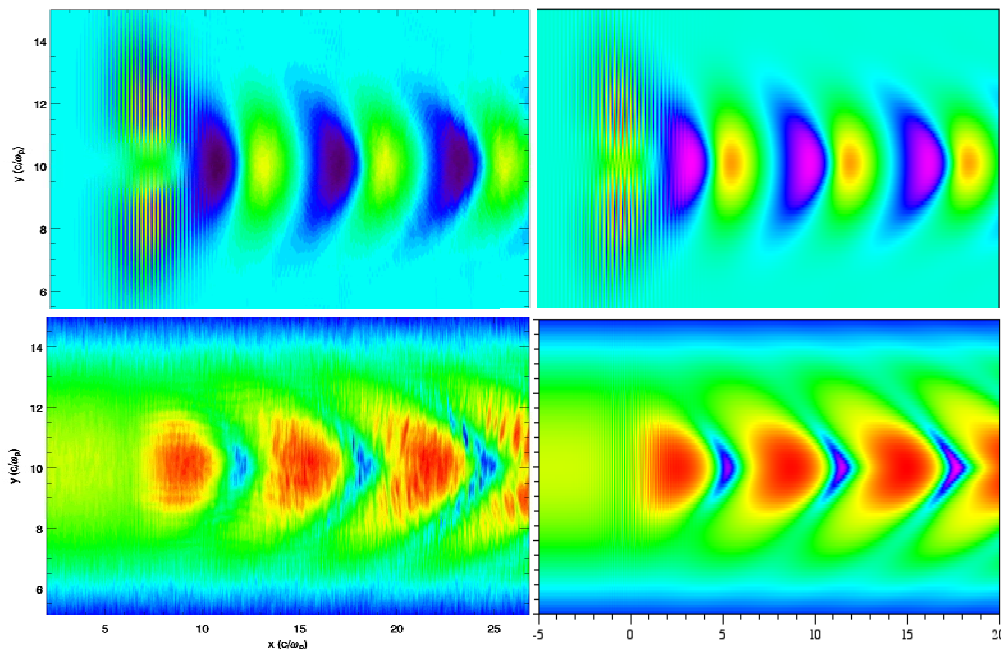


**Fig. 1.** Contours of the longitudinal electric field (top row) and electron plasma density (bottom row), as simulated by OOPIC (left side) and the LBNL fluid code (24) (right side). The laser pulse can be seen at left, having propagated from the right. The wavebreaking field is  $E_0 = 130$  GV/m; the peak wake field is 41 GV/m.

### 3.7.4 Simulating high-power laser-pulses in overdense plasmas

Both 1-D and 2-D VORPAL simulations of ultra-short (<100fs) high-power ( $>10^{18} \text{ Wm}^{-2}$ ) laser pulses striking overdense plasmas are being used to assess the potential for particle acceleration or radiation emission from solid targets. Initial results are consistent with previous work, such as sheath formation and electron recirculation in thin foils [25] and the formation of a collisionless shock front that accelerates ions up to MeV energies [26]. Diagnostics show unambiguously that this shockwave is an ion-acoustic wavepacket or soliton.

### 3.7.5 Simulating positron-driven PWFA experiments

Parameter studies of e- and e+ driven PWFA scenarios with parameters relevant to the E-164 and E-164x experiments at SLAC show [27] that high-field positron beams can ionize neutral Cs and drive a strong wake. Further, the gas density can be varied to control the optimal distance between the drive bunch and a witness beam, with only modest changes to the accelerating field, as seen in Fig. 2. The linear resonance condition [28] between RMS drive bunch length  $\sigma_z$  and plasma wave number  $k_p$  (effectively gas density) was used to obtain the matching condition:

$$2k_p^2\sigma_r^2 = \sqrt{1 + 8\sigma_r^2/\sigma_z^2} - 1 \quad (2)$$

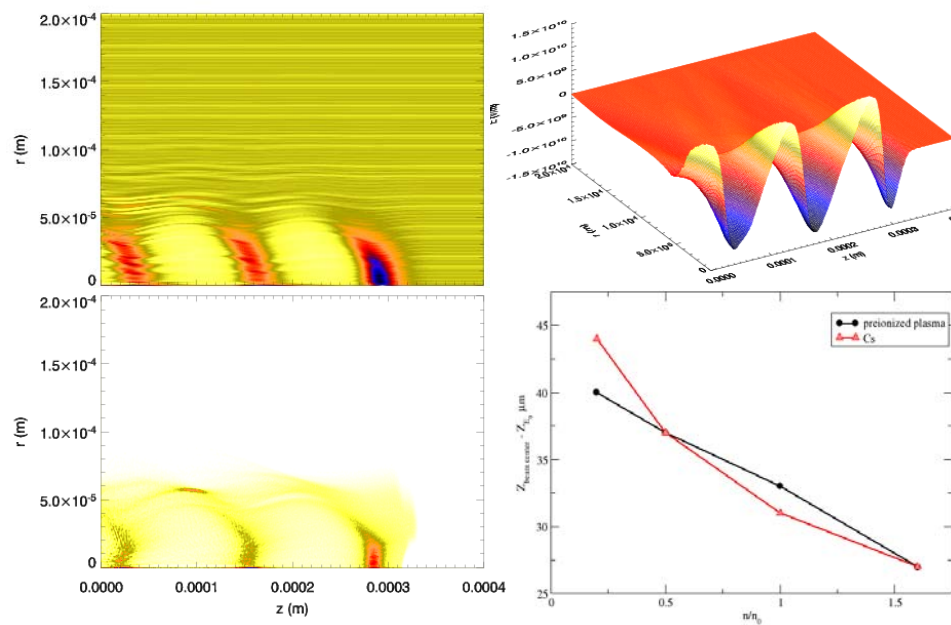


**Fig. 2.** Electron density contours for the case of 100% pre-ionized plasma (top left) and tunneling ionization of Cs by the e+ beam (bottom left), which yield amazingly similar wakefields (top right). The optimal distance from e+ drive beam to witness beam [ $\mu\text{m}$ ] is shown (bottom right) vs Cs gas density, normalized to the prediction of Eq. (2).

### 3.7.6 Simulating electron cooling physics at relativistic energies for RHIC

A key component of the proposed luminosity upgrade for the Relativistic Heavy Ion Collider will be an electron cooling section [29,30] that is novel in three ways: relativistic electrons, bunched electron and ion beams, and use within a collider. In collaboration with Brookhaven physicists, we are using VORPAL to determine the friction force and diffusion coefficients for parameters relevant to RHIC. [31] This project is using molecular dynamics techniques to resolve close binary collisions and capture the transfer of thermal energy with a bare minimum of physical assumptions. This work will resolve ambiguities in theoretical calculations for idealized conditions, and will show the effect of complicating factors, like bulk space charge fields, variable electron density, nearby and crossing ion trajectories, and solenoidal field errors.

### 3.7.7 Simulating electron emission from structures and related physics

Future accelerators like the Next Linear Collider will require higher-gradient structures to reduce size and cost, but breakdown poses a key obstacle. The physical mechanisms leading to breakdown are not fully understood, but surface structures and stray electrons are two important elements. We are generalizing VORPAL to model rf waveguides, including field emission and secondary emission of electrons from the wall. [32]

Many present day circular ion accelerators are limited by the electron-cloud effect. [33] One electron source is those released when halo ions strike the walls. The problem is more acute for future ion accelerators, which will operate with higher peak currents and higher fill factors. We are developing a state-of-the-art suite of numerical routines for modeling secondary electron yield, neutral gas desorption and ion-impact ionization rates, with both Fortran and C bindings. The secondary electron yield modules come from the LBNL code POSINST [34], and an early version of the software has been used to help model the High Current Experiment. [35]

### 3.7.8 Particle tracking

Space charge is a likely source of emittance growth seen during injection in the Booster ring at Fermilab. [36] The Synergia project [37] is using the Python scripting language to combine the parallel 3-D space charge algorithms of the Impact code [38] together with other standard codes. We are working with Fermilab researchers to improve the user interface by enabling direct access to Impact subroutines and modules from Python.

Electrons for the proposed RHIC cooler must be magnetized upon creation and then transported without significant loss of magnetization [29,39]. Present simulations of this electron transport [40,41] rely on the serial Parmela [42]. We have begun simulating this system using MaryLie/IMPACT [38,43]. The parallel 3-D space charge algorithms of IMPACT will enable tracking of order  $10^7$  electrons. We are implementing in MaryLie a novel nonlinear rf cavity model, generalizing previous magnetostatic work [44], by computing high-order maps for very general fields from data given on the surface of a cylinder around the design trajectory. In essence, inward interpolation allows one to obtain high-order derivatives.

We previously developed a novel integration technique for particle tracking [45], which modifies the time-based Boris algorithm, often used in PIC codes, to use spatial steps. Many tracking codes use spatial steps. We implemented this algorithm in the ICOOL code [46], where it was used to model muon cooling.

### 3.7.9 Acknowledgements

Much of this work was collaborative – in particular, we acknowledge J. Amundson, I. Ben-Zvi, S. Berg, A. Burov, X. Chang, R. Cohen, A. Dragt, E. Esarey, A. Fedotov, A. Friedman, M. Furman, C. Geddes, R. Giacone, D. Grote, J. Kewisch, W. Leemans, V. Litvinenko, A. Molvik, R. Ryne, B. Shadwick, P. Spentzouris, R. Trines, J.-L. Vay and J. Verboncoeur. This work was funded in part by the SciDAC Accelerator project, under grant no. DE-FC02-01ER41178; in part by the DoE Office of High Energy Physics, under grant no.'s DE-FG02-03ER83857, DE-FG03-00ER83105 and DE-FG02-03ER83800; in part by the DoE Office of Nuclear Physics, under grant no.'s DE-FG03-01ER83313 and DE-FG02-03ER83796; in part by the DoE Office of Fusion Energy Sciences, under grant no.'s DE-FG02-03ER83840, DE-FG02-03ER83797 and DE-FG02-03ER83841; and in part by Tech-X Corp. We used computing resources at NERSC.

### 3.7.10 References

1. The Tech-X Corporation home page <http://www.txcorp.com>
2. C. Nieter and J.R. Cary, "VORPAL: a versatile plasma simulation code", J. Comp. Phys. (2004), accepted.
3. C. Nieter and J.R. Cary, Proc. 2003 Part. Accel. Conf. (AIP, New York, 2003), p. 1918.
4. J.R. Cary, R.E. Giacone, C. Nieter, D.L. Bruhwiler, E. Esarey, G. Fubiani and W.P. Leemans, Proc. 2003 Part. Accel. Conf. (AIP, New York, 2003), p. 719.
5. R.E. Giacone J.R. Cary, C. Nieter, E. Esarey, W.P. Leemans, G. Fubiani and C. Schroeder, Proc. 2003 Part. Accel. Conf. (AIP, New York, 2003), p. 1885.
6. K.S. Yee, IEEE Trans. Anten. Prop. **14** (1966), p. 302.
7. P. Messmer and D.L. Bruhwiler, Comp. Phys. Comm. (2004), accepted.
8. R.S. Tuminaro, M. Heroux, S.A. Hutchinson and J.N. Shadid, Report SAND99-8801J (1999), unpublished.
9. The VORPAL home page – <http://beams.colorado.edu/vorpal/>
10. J. P. Verboncoeur, A. B. Langdon and N. T. Gladd, Comp. Phys. Comm. **87** (1995), p. 199.
11. D.L. Bruhwiler, R.E. Giacone, J.R. Cary, J. Verboncoeur, P. Mardahl, E. Esarey, W.P. Leemans and B. Shadwick, PRST-AB, 101302 (2001).
12. The OOPIC home page – [http://www.txcorp.com/products/OOPIC\\_Pro/](http://www.txcorp.com/products/OOPIC_Pro/)
13. L.V. Keldish, Sov. Phys. JETP **20**, 1307 (1965).
14. M.V. Ammosov, N.B. Delone and V.P. Krainov, Sov. Phys. JETP **64**, 1191 (1986).
15. V.S. Popov, Usp. Fiz. Nauk **169**, 819 (1999) [Phys. Uspekhi **42**, 733 (1999)].
16. D.A. Dimitrov, D.L. Bruhwiler, W.P. Leemans, E. Esarey, P. Catravas, C. Toth, B. Shadwick, J.R. Cary and R.E. Giacone, Proc. Advanced Accel. Concepts Workshop (AIP, New York, 2002), Vol. **647**, p. 192.
17. W.P. Leemans, D. Rodgers, P.E. Catravas, C.G.R. Geddes, G. Fubiani, E. Esarey, B.A. Shadwick, R. Donahue and A. Smith, Phys. Plasmas **8** (2001), p. 2510.
18. The l'OASIS lab home page – [http://bc1.lbl.gov/CBP\\_pages/EBP/loasis.html](http://bc1.lbl.gov/CBP_pages/EBP/loasis.html)
19. E. Esarey, G. Joyce and P. Sprangle, Phys. Rev. A **44** (1993), p. 3908.
20. D. Bruhwiler, D. Dimitrov, J. Cary, E. Esarey, W. Leemans and R. Giacone, Phys. Plasmas **10** (2003), p. 2022.
21. S. Lee, T. Katsouleas, P. Muggli, W. Mori, C. Joshi *et al.*, PRST-AB **5**, 011001 (2002).
22. B.A. Shadwick, G.M. Tarkenton, E.H. Esarey and W.P. Leemans, "Fluid simulations of intense laser-plasma interactions," IEEE Trans. Plasma Sci. **30** (2002), p. 38.

23. B.A. Shadwick, G.M. Tarkenton, E.H. Esarey and W.P. Leemans, AIP Conf. Proc. **569** (2001), p. 154.
24. G. Tarkenton, B. Shadwick, E. Esarey, C. Schroeder and W. Leemans, Bull. Am. Phys. Soc. **47** (2002), p. 281.
25. Mackinnon, Y. Sentoku, P. Patel, D. Price, S. Hatchett, M. Key *et al.*, Phys. Rev. Lett. **88**, 215006 (2002).
26. L. Silva, M. Marti, J. Davies, R. Fonseca, C. Ren, F. Tsung and W. Mori, Phys. Rev. Lett. **92**, 015002 (2004).
27. D. Bruhwiler, D.A. Dimitrov, J.R. Cary, E. Esarey and W.P. Leemans, Proc. Part. Accel. Conf. (2003), p. 734.
28. S. Lee, T. Katsouleas, R.G. Hemker, E.S. Dodd and W.B. Mori, Phys. Rev. E **64**, R045501/1-4 (2001).
29. Ben-Zvi *et al.*, Proc. 2003 Part. Accel. Conf. (AIP, New York, 2003), p. 39.
30. The RHIC electron cooling home page – <http://www.agsrhichome.bnl.gov/eCool/>
31. R. Busby, D.L. Bruhwiler, P. Stoltz, D.T. Abell, J.R. Cary, P. Messmer, I. Ben-Zvi and A. Burov, Bull. Am. Phys. Soc. **48**, no. 7 (2003), p. 117.
32. S. Hendrickson, J.R. Cary, P. Messmer and P. Stoltz, Bull. Am. Phys. Soc. **48**, no. 7 (2003), p. 314.
33. K. Ohmi, T. Toyama, and C. Ohmori, PRST-AB **5**, 114402 (2002).
34. M.A. Furman and M. Pivi, PRST-AB **5**, 124404 (2002).
35. P.H. Stoltz, M.A. Furman, J.-L. Vay, A. Molvik and R. Cohen, PRST-AB **6**, 054701 (2003).
36. P. Spentzouris and J. Amundson, Proc. 2003 Part. Accel. Conf., (AIP, NY, 2003), p. 2939.
37. J. Amundson and P. Spentzouris, Proc. 2003 Part. Accel. Conf., (AIP, NY, 2003), p. 3195
38. J. Qiang, R.D. Ryne, S. Habib and V. Decyk, J. Comput. Phys. **163** (2000), p. 434.
39. Burov *et al.*, PRST-AB **3**, 094002 (2000).
40. J. Kewisch *et al.*, Proc. 2003 Part. Accel. Conf. (AIP, New York, 2003), p. 2005.
41. D. Wang *et al.*, Proc. 2003 Part. Accel. Conf. (AIP, New York, 2003), p. 3186.
42. L.M. Young, J. H. Billen. LA-UR-96-1835, LANL (rev. 2002).
43. R.D. Ryne, J. Qiang, A.J. Dragt *et al.*, MaryLie/IMPACT Manual (2003).
44. M. Venturini and A.J. Dragt. Nucl. Instr. Meth. Phys. Res. A **427** (1999), p. 387.
45. P.H. Stoltz, J.R. Cary, G. Penn and J. Wurtele, PRST-AB **5**, 094001 (2002).
46. R.C. Fernow, Proc. 1999 Part. Accel. Conf. (AIP, New York, 1999), p. 3020.

## 4 Recent Doctoral Theses

### 4.1 Analytical and Numerical Studies of Stochastic Effects in Beam Dynamics

Gabriele Bassi

Mail to: [gbassi@math.unm.edu](mailto:gbassi@math.unm.edu)

**Affiliation:** DESY and University of Bologna

(present affiliation: University of New Mexico)

**Title:** Analytical and Numerical Studies of Stochastic Effects in Beam Dynamics

**Name:** Gabriele Bassi ([gbassi@math.unm.edu](mailto:gbassi@math.unm.edu))

**Graduation date:** May of 2003.

**Supervisor1:** H. Mais, [mais@mail.desy.de](mailto:mais@mail.desy.de), DESY-Hamburg

**Supervisor2:** A. Bazzani, [Armando.Bazzani@bo.infn.it](mailto:Armando.Bazzani@bo.infn.it), Department of Physics University of Bologna, INFN sezione di Bologna

**Supervisor3:** G. Turchetti, [Giorgio.Turchetti@bo.infn.it](mailto:Giorgio.Turchetti@bo.infn.it), Department of Physics University of Bologna, INFN sezione di Bologna

#### Abstract:

The aim of this thesis is to study the influence of stochastic perturbations on beam dynamics. In particular the single-particle longitudinal dynamics in storage rings is investigated under the influence of additive and multiplicative noise in the RF-cavities. As it is known, the longitudinal dynamics (synchrotron motion) of a particle in a circular accelerator can be described by the equation of a pendulum in the limit of cavities homogeneously distributed along the ring. One important question is to understand the particle losses out of the stable RF-bucket and more generally the diffusive degradation of the beam quality induced by random perturbations. Besides Gaussian white-noise processes, which are a good approximation if one is interested in very short time correlations of the random effects, we also study the more realistic case of finite correlation times (colored noise).

In order to study this problem analytical and numerical tools such as solvers for stochastic differential equations and the corresponding partial differential equations (the Fokker-Planck equation) have been developed.

In the white-noise case a method based on the Dyson series expansion for deriving the Fokker-Planck equation from the stochastic continuity equation has been applied. In the colored noise case closed Fokker-Planck like equations and corrections to the Fokker-Planck equation have been derived.

We have applied various algorithms for the numerical solution of the Fokker-Planck equation for Hamiltonian systems perturbed stochastically. We have performed an error analysis of these schemes which has been checked and compared with Monte Carlo particle simulations and with direct simulations of the stochastic continuity equation. The stochastic continuity equation, or in the Hamiltonian case, the stochastic Liouville equation is important, if one wants

to investigate the influence of noise on the time evolution of particle distributions under the influence of stochastic fields. This is the case in accelerator physics where the particles of a bunch are subject to the same external fluctuating fields (same realization of the noise).

The structure of the thesis is the following. In the first chapter a short introduction to stochastic beam dynamics is given. In the second chapter the theoretical framework is set up. In the third chapter algorithms for the numerical solution of the Fokker-Planck equation are analyzed. In particular, we investigate Hamiltonian systems with weak noise. Because of the interplay between phase space volume conserving dynamics, the symplectic properties of the phase flow and the effects of stochastic perturbations a numerical treatment of these systems is highly non trivial. As a sensitive benchmark problem the longitudinal beam echo in proton storage rings is considered.

The relevance of the analytical tools proposed in this thesis to study colored noise problems is discussed next. In particular, higher order correction terms to the Fokker-Planck equation for systems driven by an Ornstein-Uhlenbeck noise are analyzed and compared with the numerical solution of the Fokker-Planck equation in the extended space, where one treats the system as a Markovian vector process with an increased number of variables.

## 5 Workshop and Conference Reports

### 5.1 13<sup>th</sup> ICFA Beam Dynamics Mini-Workshop on Beam Induced Pressure Rise in Rings.

#### 5.1.1 Summary of Pressure Rise Workshop

T. Roser and S.Y. Zhang  
mail to: [roser@bnl.gov](mailto:roser@bnl.gov) and [syzhang@bnl.gov](mailto:syzhang@bnl.gov)

Brookhaven National Laboratory  
911B, Upton, NY 11973, USA

The Workshop of Beam Induced Pressure Rise in Rings, the 13th ICFA Beam Dynamics Mini-Workshop, was held at BNL, Dec. 9 to 12, 2003.

##### *5.1.1.1 Background of the Workshop*

Beam induced pressure rise was an intensity limit at CERN ISR during the early 1970's. The beam gas ionization created pressure rise caused more gas ionization, resulting in pressure run-away at high beam intensity. Extensive baking, chamber treatment, and perhaps more importantly, a lot of added pumps helped raise the intensity threshold.

Due to the large charge exchange cross sections low energy heavy ion machines such as the AGS Booster, CERN LEAR, and GSI SIS require very high vacuum to obtain good beam lifetime. Nevertheless, the beam loss/gas ionization created pressure rise increases with beam intensity, limiting the maximum attainable intensity.

Pressure rise can also be created by electron stimulated desorption if an electron cloud has been formed by the beam. For most machines, electron cloud induced beam instability and/or beam emittance growth limit the beam intensity before pressure rise does. A special case is the RHIC, where electron clouds occur only in part of the warm sections (the total warm section is less than 1/4 of the ring). The beam intensity can be increased without inducing beam instability and emittance growth until the pressure rise impacts operation.

The beam induced pressure rise is of concern, therefore, for several machines in operation. These include the AGS Booster, the GSI SIS, and the RHIC heavy ion and proton operations.

The beam induced pressure rise is also an important issue for machines under construction or being planning. These include the LHC, SNS, LEIR, GSI upgrade, RHICII, eRHIC, and heavy ion fusion accelerators.

The Workshop focused on three aspects relevant to the beam induced pressure rise: electron and ion desorption, vacuum chamber coating and treatment, and electron cloud effects.

#### 5.1.1.2 *Electron and Ion Desorption*

The main sources of beam induced pressure rise are electron stimulated gas desorption, ion desorption, and beam loss/halo scraping.

For electron multipacting and ISR type ion desorption, the incident angles are typically perpendicular. Given surface conditions, electron and ion desorption rates can be obtained with reasonable accuracy.

There are, however, large uncertainties for non-perpendicular incident angle, and its importance has become apparent only recently. For example, during the design stage of the AGS Booster, the heavy ion desorption rate was believed to be between 1 and 10, and the Booster gold beam injection efficiency was designed to be higher than 98%. In fact, under grazing angle the gold ion desorption rate can be larger than  $10^5$ , and the gold beam injection loss created a pressure rise that was more than 4 decades higher than the residual gas pressure of  $5 \times 10^{-9}$  Torr. After more than a decade of improvements, the Booster gold beam injection efficiency is about 60% for high beam intensity.

For low energy heavy ion machines, the beam charge exchange incidents are with the angles in mrad range, but other beam losses may happen at even smaller angles. For high energy machine, it is suspected that the beam loss/halo scraping may dump significant amount of energy on the chamber surface and may cause large desorption.

In recent several years, the ion desorption rate of around  $10^5$  or higher has been observed at AGS Booster, LEAR, SIS, SPS, and RHIC. Similar results also have been obtained at several test stands. The existing data are, however, not complete and sometimes not consistent. It is not unusual that the data under similar conditions differ by orders of magnitude.

The progress and plans were discussed during this workshop. It is believed that the surface chemistry/physics and the theoretical understanding of desorption are important. For example, it is not clear yet if the bulk is involved in the desorption mechanism. It was also proposed to undertake systematic measurements with respect to projectile energy, species, charge state, and incident angle. Considering the limitations of facilities and the importance of the problem, extensive collaboration between laboratories is required.

The reduction of the ion desorption rate through beam scrubbing, i.e., heavy ion sputtering, was observed at the CERN LINAC3 test stand, and it is planned for the commissioning of LEIR. The same effect was observed at the AGS Booster over a longer time period. The other countermeasure is chamber treatment, which is the subject of next section.

#### 5.1.1.3 Chamber Coating and Treatment

The chamber coating and treatment are aimed at the reduction of the yields of secondary electron (SEY), secondary ion, and neutral particle from electron or ion impact.

TiN coating has received much attention in the past. A general improvement of the secondary electron yield, and therefore suppression of electron multipacting, was observed, but not all times. The installation of three TiN coated chambers at the LANL PSR has yet to reach a conclusion. One of the factors might be the coating condition. For the SNS chamber coating at BNL, an improvement was recently achieved using higher sputtering pressure. The SEY was improved from 2 - 2.5 to 1.5 - 1.9. It has also been found that the better coated TiN surface is rougher.

The newly developed NEG (non-evaporable getter) coating has been intensively discussed in this workshop. The NEG coating turns the chamber walls from an outgassing source to a getter pump, and important improvements relevant to pressure rise have been confirmed. These include the SEY reduction and electron desorption reduction. For the ion desorption, only limited measurements were done, and the results are not very consistent. One problem in measuring NEG coating ion desorption rate is that it needs to be separated from the NEG pumping. Using a saturated surface may exclude the pumping effect, but the desorption rate of non-saturated surface could be different.

An activated NEG surface has a SEY of 1.1 - 1.3 and, even after saturation, remains below 1.4. Some data shows higher SEY after storage, 1.3 - 1.6, but it is still comparable to a beam scrubbed stainless steel surface and a well conditioned TiN coating. A beam measurement at the SPS has confirmed that electron clouds are eliminated where the vacuum chambers are NEG coated.

It has been found that the roughness of the activated NEG surface improves the pumping. The SEY reduction might be also related to the roughness of the NEG surface. Test at CERN indicated that the coating surface is rougher if the chamber itself is rougher. Also, the coating process is likely to affect the roughness of the surface.

Issues relevant to the NEG coating, such as the activation, aging, possible dust, impedance, venting effect, etc. are collaboratively studied at Cornell, ESRF, GSI, KEKB, LHC, LEIR, PEP-II, and RHIC.

#### 5.1.1.4 Electron Cloud Effect

The mechanism of electron multipacting is in general understood, thanks to theoretical and experimental studies on electron cloud in the past years. When electron multipacting occurred in RHIC, it wasn't much of a surprise to observe the "classical" features of the electron cloud. These include the effects of bunch intensity, bunch spacing, bunch gap, solenoid field, and beam scrubbing. Also, the electron cloud induced pressure rise approaches saturation - rather different from the ISR type pressure rise, which rises exponentially.

However, many questions remain to be answered. The agreement on the electron density and distribution is yet to be reached. The relation between the electron signal and pressure rise at RHIC is not well understood. The effect of a solenoid field was not clearly identified. There are

also other issues, such as dose stripes in dipole field, trapped electrons in quadrupoles, and electron bursts at the PSR.

Cures for electron clouds have been intensively pursued in recent years. Beam scrubbing has been confirmed to be beneficial at SPS and RHIC. It was found that the pressure rise induced by electron multipacting can be used as a measure for the effectiveness of the beam scrubbing. At RHIC, for example, the pressure rise was kept as high as possible to make best use of the scrubbing time.

On the other hand, it was observed at SPS that the SEY recovers after only 4 hours without running beam. The beam scrubbing study at the PSR did reduce the electron activity, but the effect on the beam instability threshold was not clearly identified.

A challenge for LHC and eRHIC is that the recent measurement at the SPS shows that in terms of electron activity and heat load the beam scrubbing is less effective at the cold regions. The beam instabilities and the tolerable heat load during scrubbing also need to be considered.

The outlook for the application of NEG coating is generally encouraging with respect to pumping and SEY reduction. In addition to measurements in test chambers, the machine experiences at SPS, ESRF, Cornell, and recently the RHIC are mostly positive.

Several other techniques to prevent the electron clouds are also effective depending on the machine operations and limitations. Solenoids play a key role in raising luminosity at the B-factories. Colliders can adopt flexible bunch injection pattern to maximize the luminosity. For example, the bunch filling pattern is adjustable during RHIC operation, depending on pressure rise limits. In general, it is better to extend the bunch spacing and to raise bunch intensity. At RHIC, the 56 bunch pattern yielded less background and higher luminosity than the 112 bunch pattern used in the past. The electron multipacting threshold at SPS shows that for 25 ns, 50 ns, and 75 ns bunch spacing, the bunch intensity thresholds are  $0.3 \times 10^{11}$ ,  $0.6 \times 10^{11}$ , and  $1.2 \times 10^{11}$ , respectively. The corresponding luminosity ratio would be 1, 2, and 5.3, given that the luminosity is proportional to square of bunch intensity.

#### 5.1.1.5 Conclusion

Many new results reported at this workshop were obtained during recent months, not years, indicating the interest and need of existing and planned machines.

With the constant improvement in accelerator technology and pursuit of high intensity and luminosity, many machines are now facing limits caused by particles other than the beam. Electron clouds are a typical example, but ions are also relevant, especially in hadron machines. The direct and indirect effect of these ions may not be negligible.

Ions involved in RHIC pressure rise include: beam gas ionization generated ions, beam loss generated ions, secondary ions due to these two kinds of ions, and secondary ions generated from electron multipacting. Electrons in the beam pipe are promptly kicked to the wall by each passing bunch. Ions are also pushed to the wall by the circulating beam. The lifetime of secondary electrons in the gap between bunches could be affected by these slow moving ions.

It is very important to identify and understand the dominant mechanism in each type of pressure rise. This goal is served by the several fronts pushed forward during this workshop, i.e., the understanding of the electron and ion desorption, the chamber coating and treatment, and the comprehensive strategy to prevent electron clouds during the accelerator and collider operations.

### 5.1.1.6 References

1. E. Mahner, “Electron and ion desorption working group summary”, <http://www.c-ad.bnl.gov/icfa/agenda.html>
2. H.C. Hseuh, “Report of the working group II on chamber coating and treatment”, <http://www.c-ad.bnl.gov/icfa/agenda.html>
3. R. Macek, “Report of the working group of electron cloud effect”, <http://www.c-ad.bnl.gov/icfa/agenda.html>

## 5.1.2 Report of the Working Group on Electron Cloud Effects

R.J. Macek  
mail to: [macek@lanl.gov](mailto:macek@lanl.gov)

LANSCE Division, LANL, Los Alamos, NM, 87544

The Working Group (3) on Electron Cloud Effects (ECE) was organized for the 13<sup>th</sup> ICFA Beam Dynamics Mini-Workshop on Beam Induced Pressure Rise at BNL. Participants are listed in the Appendix. During this group’s meeting on Thursday afternoon, Dec 11, 2004, several topics were discussed including:

- Definition of electron cloud or electron cloud effect and related terms
- Clarification of points raised at the BNL workshop
- Status of our present understanding
- Unresolved issues
- Future plans and work that needs to be done
  - Needed experiments
  - Comparison of codes and comparison of simulations to experiments
- Recommendations for RHIC

A summary of the discussions follows.

### 5.1.2.1 Definitions

K. Harkay requested a definition of the electron cloud or electron cloud effect since the term is used by various speakers to cover a number of different situations. In the ensuing discussion it became clear that the terms had different meanings for various groups. While individual research groups or localized communities can share a common understanding of the terms, the meanings are not universal and it behooves speakers to define their meaning for wider audiences. For many machines, the term implies creation of a significant electron density in the beam chamber through amplification of the initial or primary electrons by some form of beam-induced multipactor process. However, there are machines where a large number of photo-electrons create a troublesome electron density without the need for further amplification by beam induced multipactor. Similarly, heavy ions scraping the chamber can also release copious numbers of electrons without further amplification by multipactor processes. At the end of the discussion it was generally accepted that an electron cloud is a collection of sufficient low energy electrons in the beam chamber to cause a noticeable effect on the beam or the accelerator performance.

There is no single electron cloud effect to associate with the term. An electron cloud of sufficient density can produce a variety of effects, whose importance varies with the particular situation. A list of electron cloud effects observed to date at one or more accelerators includes:

- Gas desorption (pressure rise), the subject of this workshop
- Betatron tune shifts along a bunch train
- Coupled-bunch instabilities
- Space charge neutralization
- Single-bunch instabilities, often referred to as two-stream instabilities in plasma physics
- Emittance growth along a bunch train
- Heat load on cryogenic walls
- Interference with diagnostics

In the course of the discussion other terms came up that needed a context dependent definition including “saturation”, “neutralization” or “equilibrium” value of the electron cloud spatial or line density. In multi-bunch machines the electron cloud builds up along the bunch train until it reaches a constant value, which is loosely and variously referred to by any one of these terms, but is perhaps best described by the equilibrium value where the electron loss rate equals the electron generation rate. In the Los Alamos PSR, the electron density surviving the gap between bunch passages “saturates” i.e., reaches a maximum value nearly independent of beam intensity, beam losses and other parameters that influence the line density of electrons generated during trailing edge multipactor. Even the term “beam scraping” admitted to more than one meaning. The lesson here is that speakers and authors should be careful to define their use of these terms, especially for wider audiences.

#### 5.1.2.2 *Clarification of certain points raised at this workshop*

This working group discussed a number of issues that came up during the workshop. One of the ongoing puzzles has been the absence of any observed electron cloud effects at ISIS. The working group leader asked Giulia Bellodi (RAL) to give an impromptu summary of the work on this subject carried out at RAL. She reported on her comparison of POSINST and E-CLOUD simulations of PSR, ISIS and ESS. The difficulties of putting in the geometry of the ISIS vacuum chamber whose aperture varies continuously to keep a more or less constant ratio of aperture to beam size were noted. In addition, the RF shields (array small rods parallel to the beam) in the ceramic chambers are difficult to model. She reported that it took 4000-5000 slices of the PSR beam pulse to get convergence in the answers, especially for a Gaussian longitudinal beam profile.

Dr. Bellodi also discussed preliminary results of an experimental search for an electron cloud at ISIS. They used channel plates to amplify the electron signal. This set up did have some time resolution but was not fast enough for turn-by-turn resolution. In general, they saw a weak signal early in the ramp ( $\sim 0.1 \text{ nA/cm}^2$ ) and at the end of acceleration saw a number of electrons more or less consistent with residual gas ionization by the beam.

J. M. Jiménez (CERN) noted that the saturation (equilibrium) density cloud density at SPS does not differ between Cu and Stainless Steel but the POSINST simulations showed a factor of 5-10 difference. M. Furman suggested that it may be due to conditioning (beam scrubbing) in the experiments whereas the simulations use secondary emission yields (SEY) for unconditioned materials.

J. M. Jiménez and F. Ruggiero pointed out that the evidence for or against electron cloud effects in the arcs at RHIC has very important implications for the LHC project. D. Trbojevic (BNL) noted that they can not, at the present, directly measure pressure rise in the RHIC arcs. An upper bound from the increase in heat load can be estimated but it has large uncertainties. It was agreed that an electron detector in the RHIC arcs would be most informative and the Working Group recommends that such a detector be installed.

The potential of non-evaporable getter coatings (NEG) to reduce the SEY of beam chambers is a relatively new development attracting considerable attention as a possible cure for ECE. Needless to say, accelerator personnel are very interested in any observations and operating experience with these materials. In this regard, we should mention the positive operating experience at ESRF, reported by Roberto Kersevan at this workshop where NEG coatings were used to avoid a pressure bump in the middle of a straight section and the radiation safety problem (bremsstrahlung) such a bump can cause. A cautionary note was reported by Yulin Li in studies at Cornell where a powdery substance developed on a NEG coated surface after extensive pumping tests. It was suggested this may be due to excessive H<sub>2</sub> sorption. There was some discussion and considerable confusion during this meeting over second and third hand reports that the SEY curve for a NEG sample went from  $\sim 1.3$  to  $\sim 1.6$  in 22 days of exposure to vacuum of  $\sim 3 \times 10^{-10}$  Torr during offline tests at SLAC, which were ultimately clarified and confirmed by reference to the published results [1].

### 5.1.2.3 *The present understanding of electron cloud effects*

R. Macek led a discussion of the present understanding of electron cloud effects which is summarized below. For more information, see the informative recent review of theoretical investigations on the electron cloud by Frank Zimmermann in the August 2003 issue (No. 31) of the ICFA Beam Dynamics Newsletter.

It was noted that the important basic features are understood at varying levels of detail and sophistication. For example, the SEY and emission spectrum curves in the POSINST code are quite detailed and validated against a significant body of data. In another example, according to Francesco Ruggiero, the existence and positions of two electron stripes (high-density spots) in the electron cloud density in a dipole magnet was predicted by Frank Zimmermann's simulations before it was observed experimentally at the CERN SPS, as was the dependence of stripe position on bunch spacing.

While there have been some notable successes as mentioned above, the overall understanding of electron cloud effects is not complete. Some simplification of the physics models is generally needed to produce a tractable code. However, depending on the accelerator and the beam being modeled, the missing physics may or may not have a significant impact on the results. This is not always easy to judge beforehand. For a variety of reasons, it is useful to identify and be aware of the missing physics. For example, the electrons stripped at the injection foil and those from secondary emission of the stored beam striking the foil, and even thermionic emission from the foil, are not in the models for PSR, SNS, ESS and ISIS. Typically, the electrons born at the wall (which are important for trailing edge multipactor) from residual gas ions created by beam ionization and driven to the wall are not included. The extra residual gas ionization from the electron cloud is also not included in some codes. In a related subject, the issue of whether the gas ions liberated by residual gas ionization can affect the electron dynamics was studied by F. Zimmermann and G. Rumolo [2] and found to be negligible for SPS/LHC conditions.

Clearing fields are being considered for mitigation in certain applications, e.g. at the stripper foil for SNS, but have not yet been included in the SNS simulations. At this time, L. Wang (BNL) is incorporating clearing fields in the CLOUDLAND code for electron buildup. Simulations with clearing fields included have been done earlier for LHC and KEKB [3,4].

Perhaps the most important and difficult code development task remaining is the coupling of a good model for electron build-up with the complete dynamics of the beam motion in a fully dynamical simulation. The problem is being addressed but is very computer intensive. As a result considerable approximation has been invoked by various authors to obtain results with present day computing capabilities.

Another problem with the simulations is the number of poorly determined input parameters. For example, the SEY for technical surfaces in particular machines can vary greatly depending upon the history of beam scrubbing, venting, etc. The peak SEY can have a large effect on the gain from beam induced multipactor especially in situations such as the long bunch beam at the LANL PSR, where the trailing edge multipactor gain has not yet reached “saturation”. The absolute value of the source term for seed electrons from beam losses is very uncertain because the details of the beam losses - their location, angle of incidence and distribution of scattered and secondary hadrons are very difficult to determine with the required accuracy. When the build up reaches an equilibrium level, as is the case for certain machines with a long train of short bunches, the source term has little influence on the equilibrium value but can affect the time to reach equilibrium. However, for a machine such as the LANL PSR, where equilibrium is not reached, the electrons from trailing edge multipactor are observed to depend linearly on the losses.

At this time, the confidence in the predictions of electron cloud effects for the new machines is not high enough for the risks involved. To a considerable extent this is because the consequences of being wrong can be very costly. More benchmarking and successful comparisons with experiments are needed. Successful predictions made before the experimental results are obtained are especially valuable in building confidence. When experimental results are known in advance the natural tendency is stop the code development when agreement is reached or adjust parameters within uncertainties to get agreement with the data.

#### 5.1.2.4 *Some unresolved issues*

A number of unresolved issues were touched on by the working group.

As noted in the last section, detailed estimates of seed electrons from beam losses for long bunch machines such as the LANL PSR, SNS ring and the ISIS ring are poorly determined and almost impossible to measure. One approach that was mentioned by R. Macek, is to use one set of experimental data on electron signals to fix the source term by varying the input parameters until the simulations agree with the data set. Then, with the source term fixed, one can vary other beam parameters e.g. beam intensity, to obtain tests of the simulations. Another approach, not yet undertaken, is to do detailed simulations of losses using particle tracking codes such as ORBIT along with simulations of the scattered beam using a code such as MCNPX or LAHET to see where the scattered beam goes. This would be followed by estimates of the secondary electrons from the grazing angle encounters with beam chambers using the semi-empirical models described in the Thieberger et al paper [5].

The measurements of microwave transmission at CERN made by F. Caspers et al and reported at this workshop by F. Ruggiero are rather surprising and not well understood but could

be compatible with the effect of dust particle stirred by the beam. A new test involving mechanical shaking of the beam pipe will be performed at the SPS in a few months.

There are still significant discrepancies between experiments and simulations that ought to be resolved regarding the flux and spectrum of electrons hitting the wall for SPS. At the LANL PSR, the observed electron bursts are not understood and the same is true of the so called “1<sup>st</sup> pulse instability.”

#### 5.1.2.5 *Worked needed or planned for the future*

There was general agreement that more detailed benchmarking of codes was a high priority need. This includes code-to-code comparisons, and more definitive comparisons with experiments, which explore a number of parameter variations. Macek noted that there is a large amount of experimental data at PSR that has not been compared with simulations.

Francesco Ruggiero outlined a number of needs and plans for the LHC/SPS facilities. These included:

- Efforts to further simulate heat load on cryogenic walls and compare with warm/cold measurements
- Explore the dependence of the energy spectrum on bunch dimensions
- Simulate spectrum of multi-bunch instabilities including the conventional impedance
- Calculate growth rates and scaling of single bunch instability and emittance growth with damper and  $Q' \neq 0$
- Simulate LHC scrubbing scenarios, heat load, collimator regions, and emittance preservation
- Compare simulations for field-free region, dipoles and quadrupoles at  $\delta_{\max} = 1.5$  (value achieved by beam scrubbing) and bunch intensity,  $N_b \cong 1.2 \times 10^{11}$ . This task is motivated by SPS observations which indicate that, for typical LHC bunch intensities up to  $N_b \sim 1.2 \times 10^{11}$ , multipacting (and beam scrubbing) stops in the field-free regions when  $\delta_{\max}$  is reduced below  $\sim 1.5$  (by beam scrubbing), while there is still multipacting in the arcs.

To date there has been little experimental work on the electron cloud in quadrupoles. However, a number of simulations show that significant numbers of electrons can be trapped for a long time in the mirror-like magnet field of quadrupoles [6,7]. J. M. Jiménez mentioned that studies using a strip detector in a quadrupole are planned at CERN. R. Macek described some simulations of the electron cloud by M. Pivi for a PSR quadrupole and a proposal for a detector to observe the cloud, especially that due to the trapped electrons. See Figures 1-3 below.

Pivi’s simulations used the POSINST code and a constant source term independent of location for seed electrons from beam losses. The simulations show a maximum electron density (averaged over the chamber cross-section) in quadrupoles that was about a factor of 6 below those for a drift space. If one takes account of the fact that beam losses at grazing angle are expected to be significantly larger in quadrupoles than in drift spaces, then the electron density in quadrupoles could make the largest contribution to the ring average of the electron line density. The other noteworthy feature of Pivi’s simulations is the significant fraction ( $\sim 10\%$  of the peak) of electrons trapped in the quadrupole fields.

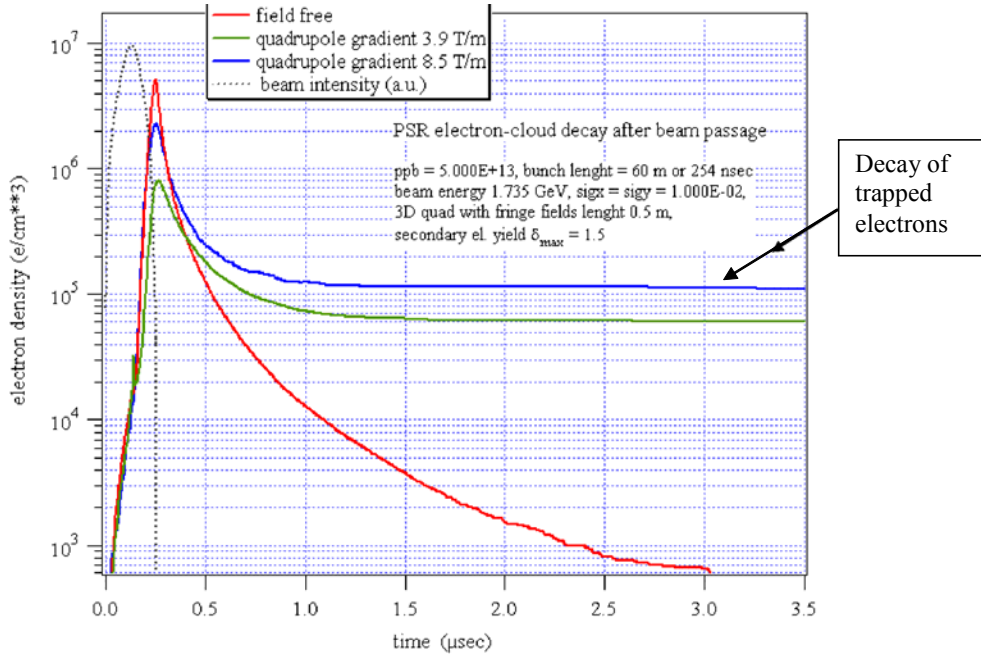


**Fig. 1.** Simulations of electrons in a PSR quadrupole. (Courtesy M. Pivi). The red curve is the simulated electron density in a field free region, the green curve is the electron density for the standard-gradient quadrupole (3.9 T/m) in the PSR and the blue curve for a gradient of 8.5 T/m. Note the very slow decay of electrons trapped in the quadrupole long after the beam pulse has passed.

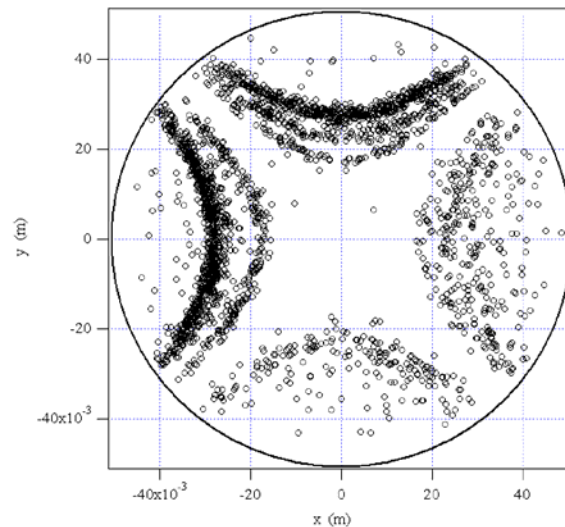


**Fig. 2.** Snapshot of trapped electrons in a PSR quadrupole 5  $\mu$ s after passage of the beam pulse. (Courtesy M. Pivi). As it might be expected, the trapped electrons follow the magnetic field lines.

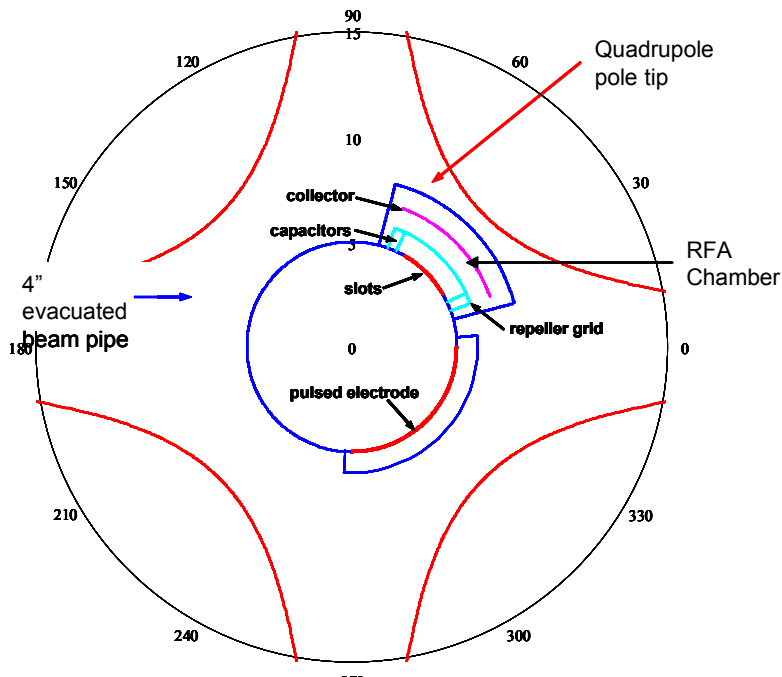


**Fig. 3.** Schematic cross section of a proposed electron sweeping detector for a PSR quadrupole.

The proposed detector (Figure 3) is an adaptation of the electron sweeping detector developed at PSR for use in a drift space. A pulsed electrode would be used to sweep trapped electrons into the chamber of the retarding field analyzer (RFA). The proposed detector makes use of the fact that the aperture of the PSR quadrupoles is significantly larger (7 inch diameter) than the aperture of other beam chambers (4 inch) in PSR. Thus, the 4 inch aperture of the beam chamber in the quad is not a limiting aperture.

#### 5.1.2.6 Recommendation from the Working Group

The question of possible electron clouds in the cold arcs of RHIC was discussed in the working group meeting and afterwards by email. Francesco Ruggiero noted that the existence or absence of electron clouds in the RHIC arcs has important implications for LHC. Thomas Roser and S.Y. Zhang mentioned that the absence of cryogenic heat load (within significant errors) and electron cloud induced instability or emittance growth support the case that they do not have electron clouds in RHIC arcs. The evidence on the change in total heat load (when operating at conditions that might lead to multipacting) was briefly discussed but level of uncertainty on the measurements was reported to be large. The issue of electron clouds in the RHIC arcs does not seem to be resolved at this juncture.

It was the consensus of the working group during the meeting to recommend that the RHIC operation try to find a way to detect any electron cloud in the RHIC arcs. This would help clarify the situation at RHIC and the information would be of great value to the community, especially for LHC. That said, it should be noted that installations in the cold parts of the machine are very expensive and any single detector could only sample a very limited part of the

RHIC circumference. The working group made no attempt to do a careful cost-benefit analysis of such a program.

The working group meeting ended with mention of the E-CLOUD'04 workshop scheduled for April 19-23, 2004 at Napa, CA.

#### 5.1.2.7 Acknowledgements

I would like to thank all of the participants for a most interesting meeting. I would especially thank those (including Frank Zimmerman, who was not present) who read over this report and supplied invaluable comments and corrections.

#### 5.1.2.8 References

1. F. Le Pimpec et al, SLAC-TN-03-052, <http://www.slac.stanford.edu/pubs/slactns/slac-tn-03-052.html>
2. F. Zimmermann and G. Rumolo, "Interplay of Ionization and Sputtering with the Electron Cloud", CERN-SL-2001-014-AP.
3. O. Brüning, "Simulations for the Beam-Induced Electron Cloud in the LHC beam screen with Magnetic Field and Image Charges", CERN LHC Project Report 158 (November 1997).
4. F. Zimmermann, "Beam Sizes in Collision and Electron-Cloud Suppression by Clearing Electrodes for KEKB," CERN-SL-Note-2001-022.
5. P. Thieberger et al, "Secondary-electron yields and their dependence on the angle of incidence on stainless-steel surfaces for three energetic ion beams", Physical Review A **61**, 042901 (2000).
6. O. Brüning, "Numerical simulations for the beam-induced electron cloud in the LHC," CERN LHC Project Report 190 (1998), presented at the Sixth European Particle Accelerator Conference (EPAC98, session MOP02C), Stockholm, 22-26 June 1998.
7. F. Zimmermann, "Electron Cloud at the KEKB Low Energy Ring: Simulations of Central Cloud Density, Bunch Filling Patterns, Magnetic Fields, and Lost Electrons," CERN-SL-2000-017 (AP) (June, 2000).

## Appendix

### List of Working Group Participants

- R. Macek, LANL, Group Leader, macek@lanl.gov
- G. Bellodi, RAL, g.bellodi@rl.ac.uk
- M. Blaskiewicz, BNL, mmb@bnl.gov
- V. Dudnikov, BTG, vadim@btg.cc
- M. Furman, LBNL, mafurman@lbl.gov
- K. Harkay, ANL, harkay@aps.anl.gov
- M. Hoffman, DESY, markus.hoffmann@desy.de
- J. M. Jimenez, CERN, jose.miguel.jimenez@cern.ch
- C. Prior, RAL, c.prior@rl.ac.uk
- F. Ruggiero, CERN, Francesco.Ruggiero@cern.ch
- P. Seidel, DESY, PASEidl@lbl.gov
- L. Smart, BNL, lsmart@bnl.gov

- P. Stoltz, Tech-X, pstoltz@txcorp.com
- D. Trbojevic, BNL, dejan@bnl.gov
- L. Wang, BNL, wangl@bnl.gov
- D. Wang, MIT, dongwang@rocko.mit.edu
- J. Wei, BNL, jwei@bnl.gov
- U. Wienands, SLAC, uli@slac.stanford.edu
- SY Zhang, BNL, syzhang@bnl.gov

### 5.1.3 Electron and ion desorption working group summary

E. Mahner

Mail to [edgar.mahner@cern.ch](mailto:edgar.mahner@cern.ch)

European Organization for Nuclear Research – CERN  
CH-1211 Geneva 23-Switzerland

#### 5.1.3.1 Introduction

The working group was created during the 13<sup>th</sup> ICFA Beam Dynamics Mini-Workshop about *Beam Induced Pressure Rise in Rings*, held in December 2003 at Brookhaven National Laboratory. This note briefly summarizes the discussion about electron and ion desorption phenomenon currently observed at different accelerator laboratories.

#### 5.1.3.2 Summary

A starting point for discussion was the overview of available data for heavy-ion induced desorption yields measured as a function of the ion energy. The plot, which was presented during the workshop, is displayed in Fig.1. Effective molecular desorption yields, derived from machine experiments (AGS: Au<sup>31+</sup>, SIS 18: U<sup>28+</sup>, RHIC: Au<sup>79+</sup>), are compared with dedicated “test-stand” experiments (LINAC 3: Pb<sup>53+</sup>, HLI: Pb<sup>27+</sup>, Zn<sup>10+</sup>).

The working group discussed the question of whether test-stand experiments give adequate answers to accelerator questions. We concluded that one has to distinguish between the low energy case (MeV/u) and the high energy case (GeV/u). For low energy machines, like AGS Booster, SIS18, and LEIR, charge exchange processes (capture & loss) lead to beam-losses onto the vacuum chamber with well-defined impact angles in the mrad range. Therefore, dedicated experiments with extracted beam (e.g. at LINAC 3 or HLI) should give the right values for effective molecular desorption yields. The situation is different (no charge exchanges) for high energy machines, like RHIC and LHC, where losses are due to non-linear dynamics and nuclear scattering, and result in very small impact angles in the  $\mu$ rad range or even less. Therefore, corresponding experiments are much more complicated. It was emphasized that a well defined scraper experiment, like the LHC-type collimator material test, recently done with In<sup>49+</sup> ions at the SPS, would be also desirable in a warm section of RHIC in order to verify the estimated yield of  $1.5 \times 10^7$  molecules per Au<sup>79+</sup> ion.

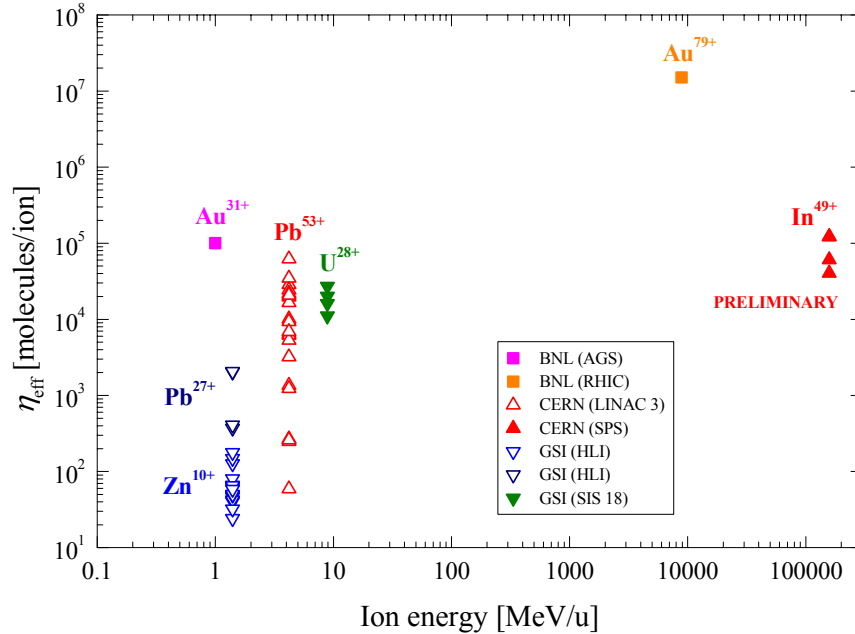


**Fig. 1.** Overview of heavy-ion induced desorption data, obtained at BNL [1, 2], CERN [3, 4, 5], and GSI [6, 7]. The ion impact angles (perpendicular, mrad,  $\mu$ rad) of the experiments are different (see text).

The working group also addressed the question of how possible future machine experiments could evolve. The following proposals were made and discussed:

- BNL is currently installing a test-stand at the Tandem machine in order to measure and verify the low energy desorption yield ( $10^5$  molecules/Au<sup>31+</sup> ion), previously obtained at the AGS Booster. Desorption experiments with NEG coatings (comparison between activated and saturated getter) are planned. One should also think about measurements at higher energies, for example using a slow extraction line from the Booster which could deliver heavy ions with an energy up to 1 GeV/u and intensities between  $10^6$  and  $10^9$  ions/s.
- At GSI, further experiments are under consideration at HLI, UNILAC, and SIS where U<sup>28+</sup> ions up to about 1 GeV/u can be used for desorption yield studies. Measurements of cold surfaces are considered to be very important for the GSI future project, but also for RHIC and LHC.
- At the Svedberg Laboratory (Uppsala), desorption tests with Ne, Ar, and Xe ions are possible at energies up to 46 MeV/u. This option is interesting because of the intermediate energy range which is not covered by other laboratories.
- The working group discussed the possibility of a machine experiment in a warm section of RHIC and elaborated a possible experimental set-up to test different samples either under perpendicular or grazing impact. The advantage of such a test would be to get another high energy data point under well defined conditions (ion energy, ion intensity, impact angle). A potential drawback is that an extreme grazing incidence angle (some  $\mu$ rad) would require a complicated set-up with a precise alignment and measurement of

the number of impacting ions on the target in order to calculate the effective desorption yield. The working group recommended the installation of a simple experiment in a warm section of RHIC and to study the feasibility of a “single-pass experiment” at injection energy. A possible experimental set-up, which would allow dedicated desorption studies on different samples either under perpendicular impact or under grazing angle (some mrad), is sketched in Fig. 2.

The working group collected all pressure rise observations reported so far from different accelerator laboratories world-wide, and identified experimental set-ups that are either currently running, starting up, or are possible in the future. An overview is shown in Table 1.

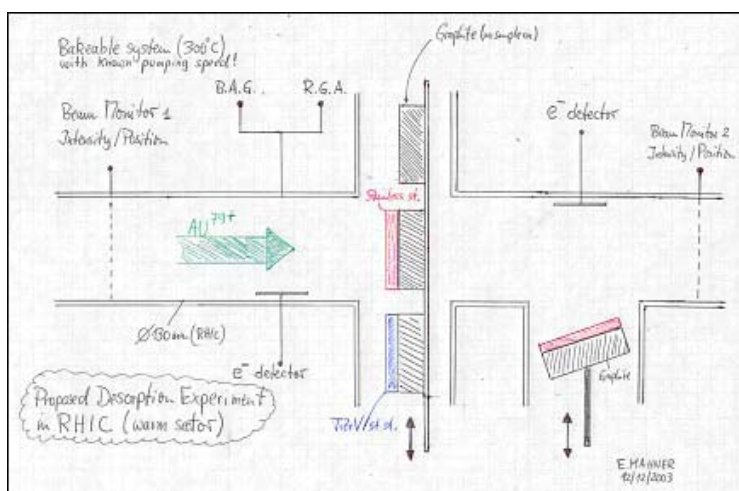


**Fig. 2.** Proposed RHIC single-pass experiment to measure heavy-ion induced molecular desorption of  $\text{Au}^{79+}$  impacting on different targets.

**Table 1.** Overview of pressure rise observations in different accelerators and various experiments, classified as: running, starting, and possible in the future.

Accelerators				Experimental setups			
	E [MeV/u]	Ion	Target		E [MeV/u]	Ion	Target
BNL Booster	1-100	Au31+	valve, chamber wall	BNL Tandem	1	Au31+	chamber wall
BNL RHIC	8900	Au79+	valve, chamber wall, samples				
CERN LEAR	4.2	Pb54+	chamber wall	CERN LINAC3	4.2	Pb27+/53+	chamber wall
				CERN SPS	158000	In49+	collimator
GSI SIS	10 to 100	p to U28+	chamber wall	GSI HLI	1.4	C,Pb,Cr, Zn	samples
	10	U28+	scraper, chamber wall	GSI UNILAC	2 to 11	p to U	to define
				GSI SIS18	10 to 1000	p to U	to define
LBNL					0.025	K+	samples
The Svedberg Lab.				Uppsala	<46	Ne,Ar,Xe	to define
observed	running	starting	possible				

Some other important topics were raised but could only be discussed briefly. Therefore we simply list them as “open questions and what has to be studied in the future”:

- Theoretical aspects of ion-beam induced desorption
  - Applied surface physics: could/would they help?
  - Is the desorption phenomenon a surface or a bulk effect?
  - Measurements should be performed with well defined (characterized) samples.
  - The objective is to understand the physics.
- What has to be considered and carried out in future experiments
  - More NEG desorption experiments with heavy ions.
  - Cold surfaces: mounted samples on a cold head (first step).
  - Electron detection: how do secondary electrons contribute?
- Instrumentation for experiments (seems to be trivial, but it is not)
  - One has to know: pumping speed, number of lost ions, impact angle, chamber volume....
  - Use calibrated instruments: ion gauge, residual gas analyser.
  - The objective is to benchmark experiments for reliable comparison.

#### 5.1.3.3 Conclusion

The working group concluded that it is very important to gain a better understanding of the theoretical aspects of the heavy-ion induced desorption phenomenon, to close the gap of missing data between the MeV/u and GeV/u energy range, and to perform reliable and comparable measurements. No concrete proposals were made how to proceed in detail. The working group proposed and recommended a dedicated desorption experiment with Au<sup>79+</sup> ions in a warm section of RHIC.

#### 5.1.3.4 Acknowledgements

Many thanks to all my colleagues who participated in the electron and ion desorption working group, namely: W. Fischer (BNL), H. Huang (BNL), A. Krämer (GSI), A. Molvik (LLNL), H. Reich-Sprenger (GSI), T. Roser (BNL), D. Trbojevic (BNL), L. Westerberg (The Svedberg Laboratory), and SY Zhang (BNL).

#### 5.1.3.5 References

1. S.Y. Zhang, L.A. Ahrens, “Gold beam losses at the AGS Booster injection”, Proceedings of Particle Accelerator Conference, New York, 1999, p. 3294.
2. S.Y. Zhang et al., “RHIC Pressure Rise and Electron Cloud”, Proceedings of Particle Accelerator Conference, Portland, 2003, p.54.
3. E. Mahner, J. Hansen, J.-M. Laurent, N. Madsen, “Molecular desorption of stainless steel vacuum chambers irradiated with 4.2 MeV/u lead ions”, PRST-AB **6**, 013201 (2003).
4. E. Mahner, J. Hansen, D. Küchler, M. Malabaila, M. Taborelli, ”Ion-stimulated gas desorption yields of coated (Au, Ag, Pd) stainless steel vacuum chambers irradiated with 4.2 MeV/u lead ions”, CERN Divisional Report, CERN AT/2003-6 (VAC).

5. E. Mahner, I. Efthymiopoulos, J. Hansen, E. Page, "Beam-loss induced pressure rise of LHC collimator materials irradiated with 158 GeV/u In<sup>49+</sup> ions at the CERN SPS", to be published.
6. E. Mustafin, O. Boine-Frankenheim, I. Hofmann, H. Reich-Sprenger, P. Spiller, "A theory of the beam loss-induced vacuum instability applied to the heavy-ion synchrotron SIS18", Nucl. Instr. and Methods A **510**, No.3 (2003), p.199.
7. M. Bender, H. Kollmus, A. Krämer, E. Mahner, "Ion-induced desorption yield measurements of bare and coated stainless steel, Nb, Mo, Ta, W, and Re samples irradiated with 1.4 MeV/u Zn<sup>10+</sup> ions at GSI", to be published.

## 5.2 31<sup>st</sup> ICFA Advanced Beam Dynamics Workshop on Electron-Cloud Effects "E-CLOUD04"

### 5.2.1 E-CLOUD04 Workshop (Napa, California, April 19-23, 2004).

*Miguel A. Furman*

mail to: [mafurman@lbl.gov](mailto:mafurman@lbl.gov)

Lawrence Berkeley National Laboratory  
Bldg. 71R0259, 1 Cyclotron Rd., Berkeley, CA 94720-8211, USA

The 31st ICFA Advanced Beam Dynamics Workshop on Electron-Cloud Effects "E-CLOUD04" took place in Napa, California, during April 19-23, 2004. This workshop was co-sponsored by LBNL, CERN, ORNL and SNS, in addition to the ICFA Beam Dynamics Panel. The organization of the program was led by Bob Macek (LANL); the setting up and maintenance of the workshop website was (and still is) managed by Frank Zimmermann (CERN); supplemental funds for unanticipated business expenses were secured by Stuart Henderson (ORNL/SNS); the design of the poster was a collaboration between Mauro Pivi (SLAC) and Juliette Thomashausen (CERN); and the overall oversight of the organization, plus logistics and local arrangements, was led by Miguel Furman (LBNL).

There were 59 attendees from various institutions around the world. Most of the attendees gave presentations. The program was divided into several sessions: Observations at Existing Accelerators and Concerns for Future Machines; Surface Properties, Measurements and Treatments; Simulations of E-Cloud Buildup; Theory and Simulations of Electron-Cloud Instabilities; and Summaries. In addition, there was a Panel Discussion on Future Needs and Future Directions.

As in previous workshops dealing with electron-cloud effects (KEK, July 1997; Santa Fe, February 2000; KEK, September 2001; CERN, April 2002), the focus of this workshop was broad, covering all aspects of the phenomena. The work presented at E-CLOUD04 represented a significant advance relative to E-CLOUD02 (CERN, April 2002). The systematic experimental program being carried out at the SPS for many years now, in preparation for LHC operation, keeps yielding valuable information particularly concerning surface conditioning by the beam. Clear evidence for an electron-cloud effect at RHIC was presented, although direct detection of electrons in the cold regions remains to be achieved. With the clear establishment of electron-cloud effects at the PSR, other high-intensity hadron machines are studying the effect either

experimentally or by simulations, or both. In particular, ORNL personnel are paying special attention to the phenomenon as the fabrication of the SNS storage ring vacuum chamber is being completed. Electron effects are being investigated at ISIS (RAL), and at the HCX experiment for heavy-ion fusion drivers (LBNL). On the simulation front, there has been significant progress towards extending simulation techniques to three dimensions, towards more realistic description of machine lattice elements, and towards self-consistency (in which both the beam and the electrons respond dynamically to each other). The electron-cloud community is thus enriched by the expertise brought in by researchers in intense hadron machines, which includes advanced computational techniques on parallel computers. The two B factories were reported to be running quite well, exceeding their design specifications on beam current and luminosity, after controlling the electron-cloud effect largely by means of weak solenoidal fields. Ambitious plans for future luminosity upgrades were presented for both machines. Multi-lab collaborations were discussed and encouraged; one notable example of such a possibility would be a collaboration between the LARP project in the US and ESGARD in Europe.

In the opinion of many participants, the workshop was valuable and productive, helped define future lines of R&D in the area of electron-cloud effects, and incubated future collaborations. Besides the intense work and long hours of meetings, we had a most pleasant (optional) excursion and banquet in the wine country, which included the unveiling of a brand-new label, "Château Ecloud". A sample bottle, vintage 2004, will be allowed to age appropriately and will be consumed at a future similar meeting. The only disappointment was the inability of three invited participants to attend the workshop as a result of the new US requirements on visas or passports. In addition, a fourth participant declined our invitation citing the new procedures for entry into the US. Several organizers opined that it would be in the US's (and everybody else's) best interests to expedite the visa process for foreign scientists to attend meetings in the US, consistent with security concerns. The excessive delays we have seen in such a process is damaging to our mutual scientific enterprise.

Pursuant to the ICFA requirements for a "full workshop," proceedings are being published. All information on the workshop can be accessed from its home website, <http://www.cern.ch/icfa-ecloud04/>.

## 6 Forthcoming Beam Dynamics Events

### 6.1 ICFA Advanced Beam Dynamics Workshops

#### 6.1.1 32nd ICFA Advanced Beam Dynamics Workshop on Energy Recovering Linacs, "ERL2004"

Swapan Chattopadhyay and Lia Merminga  
mailto: [merminga@jlab.org](mailto:merminga@jlab.org), [swapan@jlab.org](mailto:swapan@jlab.org)

This is the first announcement of the 32nd ICFA Advanced Beam Dynamics Workshop on **Energy Recovering Linacs, "ERL2004"** to be held at **Jefferson Laboratory**, Virginia, USA, October 10-14, 2004. *(Note by the editors: This workshop has been postponed to early 2005!)*

As Energy Recovering Linacs (ERLs) worldwide operate at increasing beam power and more are being contemplated for a variety of applications, including synchrotron radiation sources, free electron lasers, electron cooling devices and electron-ion colliders, it is timely to address questions of scaling the ERL performance from the present state of the art to the parameters of envisioned applications. The focus of this workshop is to address issues related to the generation of high brightness and simultaneously high average current electron beam, and its stability and quality preservation during acceleration and energy recovery. **The workshop is sponsored by the ICFA Panel on Beam Dynamics, Jefferson Laboratory, Brookhaven National Laboratory, Cornell University and Daresbury Laboratory.** Preliminary information can be found at: <http://www.jlab.org/intralab/calendar/archive04/erl/index.html> .

**If visa is required for your travel to the USA, we urge you to initiate the necessary application now, as these procedures may be lengthier than expected. If we can be of any assistance with your visa application, please do not hesitate to let us know.**

If you have any questions, suggestions or feedback on the program please contact Lia Merminga ([merminga@jlab.org](mailto:merminga@jlab.org)) or Swapan Chattopadhyay ([swapan@jlab.org](mailto:swapan@jlab.org)). For administrative questions, please contact the workshop administrators at: [ERL@jlab.org](mailto:ERL@jlab.org) .

#### 6.1.2 33rd ICFA Advanced Beam Dynamics Workshop on High Intensity and High Brightness Hadron Beams "HB2004"

Ingo Hofmann (GSI) and Jean-Michel Lagniel (CEA)  
mail to: [I.Hofmann@gsi.de](mailto:I.Hofmann@gsi.de) and [jean-michel.lagniel@cea.fr](mailto:jean-michel.lagniel@cea.fr)

The 33rd ICFA Advanced Beam Dynamics Workshop on **High Intensity and High Brightness Hadron Beams "HB2004"** will be held during the week of October 18-23, 2004 at the Conference & Culture Center of Bensheim, a romantic town of medieval charm located between Darmstadt and Heidelberg (about 50 km south of the Frankfurt Airport and 30 km south of GSI Darmstadt).

This workshop is sponsored by ICFA, GSI, CEA and FZJ. It will focus on high intensity and high brightness issues of: High Intensity Proton and Ion Facilities & Projects; Linear and Circular Accelerators; Beam Dynamics Experiments & Simulation; Injection, Instabilities & Feedback; Lattices, Loss & Collimation; Beam Diagnostics; Beam Cooling; E-Cloud & Vacuum. The program consists of invited talks in the opening plenary and in the parallel invited sessions. We encourage submission of contributed oral talks to be presented in the working sessions. We intend to publish both the invited and contributed papers as American Institute of Physics (AIP) Proceedings.

Important upcoming dates are: August 15, 2004: deadline for contributed abstract submission. August 31, 2004: deadline for early registration (reduced fee). August 31, 2004: deadline for hotel reservations. For full details, please visit <http://www.gsi.de/ICFA-HB2004> or send email to [HB2004@gsi.de](mailto:HB2004@gsi.de).

## **7 Announcements of the Beam Dynamics Panel**

### **7.1 ICFA Beam Dynamics Newsletter**

#### **7.1.1 Aim of the Newsletter**

The ICFA Beam Dynamics Newsletter is intended as a channel for describing unsolved problems and highlighting important ongoing works, and not as a substitute for journal articles and conference proceedings that usually describe completed work. It is published by the ICFA Beam Dynamics Panel, one of whose missions is to encourage international collaboration in beam dynamics.

Normally it is published every April, August and December. The deadlines are 15 March, 15 July and 15 November, respectively.

#### **7.1.2 Categories of Articles**

The categories of articles in the newsletter are the following:

1. Announcements from the panel.
2. Reports of Beam Dynamics Activity of a group.
3. Reports on workshops, meetings and other events related to Beam Dynamics.
4. Announcements of future Beam Dynamics-related international workshops and meetings.
5. Those who want to use newsletter to announce their workshops are welcome to do so. Articles should typically fit within half a page and include descriptions of the subject, date, place, Web site and other contact information.

6. Review of Beam Dynamics Problems: this is a place to bring attention to unsolved problems and should not be used to report completed work. Clear and short highlights on the problem are encouraged.
7. Letters to the editor: a forum open to everyone. Anybody can express his/her opinion on the beam dynamics and related activities, by sending it to one of the editors. The editors reserve the right to reject contributions they judge to be inappropriate, although they have rarely had cause to do so.
8. Editorial.

The editors may request an article following a recommendation by panel members. However anyone who wishes to submit an article is strongly encouraged to contact any Beam Dynamics Panel member before starting to write.

### 7.1.3 How to Prepare a Manuscript

Before starting to write, authors should download *the latest* model article file, in Microsoft Word format, from the Beam Dynamics Panel home page

<http://wwwslap.cern.ch/icfa/>

It will be much easier to guarantee acceptance of the article if the latest model is used and the instructions included in it are respected. These model files and instructions are expected to evolve with time so please make sure always to use the latest versions.

The final Microsoft Word file should be sent to one of the editors, preferably the issue editor, by email.

The editors regret that LaTeX files can no longer be accepted: a majority of contributors now prefer Word and we simply do not have the resources to make the conversions that would be needed. Contributions received in LaTeX will now be returned to the authors for re-formatting.

In cases where an article is composed entirely of straightforward prose (no equations, figures, tables, special symbols, etc.) contributions received in the form of plain text files may be accepted at the discretion of the issue editor.

Each article should include the title, authors' names, affiliations and e-mail addresses.

### 7.1.4 Distribution

A complete archive of issues of this newsletter from 1995 to the latest issue is available at

<http://wwwslap.cern.ch/icfa/>

This is now intended as the primary method of distribution of the newsletter.

Readers are encouraged to sign-up for to electronic mailing list to ensure that they will hear immediately when a new issue is published.

The Panel's Web site provides access to the Newsletters, information about Future and Past Workshops, and other information useful to accelerator physicists. There are links to pages of information of local interest for each of the three ICFA areas.

Printed copies of the ICFA Beam Dynamics Newsletters are also distributed (generally some time after the Web edition appears) through the following distributors:

Weiren Chou	<a href="mailto:chou@fnal.gov">chou@fnal.gov</a>	North and South Americas
Rainer Wanzenberg	<a href="mailto:rainer.wanzenberg@desy.de">rainer.wanzenberg@desy.de</a>	Europe* and Africa
Susumu Kamada	<a href="mailto:Susumu.Kamada@kek.jp">Susumu.Kamada@kek.jp</a>	Asia** and Pacific

\* Including former Soviet Union.

\*\* For Mainland China, Jiu-Qing Wang ([wangjq@mail.ihep.ac.cn](mailto:wangjq@mail.ihep.ac.cn)) takes care of the distribution with Ms. Su Ping, Secretariat of PASC, P.O. Box 918, Beijing 100039, China.

To keep costs down (remember that the Panel has no budget of its own) readers are encouraged to use the Web as much as possible. In particular, if you receive a paper copy that you no longer require, please inform the appropriate distributor.

### 7.1.5 Regular Correspondents

The Beam Dynamics Newsletter particularly encourages contributions from smaller institutions and countries where the accelerator physics community is small. Since it is impossible for the editors and panel members to survey all beam dynamics activity world-wide, we have some *Regular Correspondents*. They are expected to find interesting activities and appropriate persons to report them and/or report them by themselves. We hope that we will have a "compact and complete" list covering all over the world eventually. The present *Regular Correspondents* are as follows

Liu Lin	<a href="mailto:liu@ns.lnls.br">liu@ns.lnls.br</a>	LNLS Brazil
S. Krishnagopal	<a href="mailto:skrishna@cat.ernet.in">skrishna@cat.ernet.in</a>	CAT India
Ian C. Hsu	<a href="mailto:ichsu@ins.nthu.edu.tw">ichsu@ins.nthu.edu.tw</a>	SRRC Taiwan

We are calling for more volunteers as *Regular Correspondents*.

## 7.2 ICFA Beam Dynamics Panel Members

Caterina Biscari	<a href="mailto:caterina.biscari@lnf.infn.it">caterina.biscari@lnf.infn.it</a>	LNF-INFN, Via E. Fermi 40, C.P. 13, Frascati, Italy
Swapn Chattopadhyay	<a href="mailto:swapan@jlab.org">swapan@jlab.org</a>	Jefferson Lab, 12000 Jefferson Avenue, Newport News, VA 23606, U.S.A.
Pisin Chen	<a href="mailto:chen@slac.stanford.edu">chen@slac.stanford.edu</a>	SLAC, P.O. Box 4349, MS 26, Stanford, CA 94309, U.S.A.
Weiren Chou (Chair)	<a href="mailto:chou@fnal.gov">chou@fnal.gov</a>	Fermilab, MS 220, P.O. Box 500, Batavia, IL 60510, U.S.A.
Yoshihiro Funakoshi	<a href="mailto:yoshihiro.funakoshi@kek.jp">yoshihiro.funakoshi@kek.jp</a>	KEK, 1-1 Oho, Tsukuba-shi, Ibaraki-ken, 305-0801, Japan
Miguel Furman	<a href="mailto:mafurman@lbl.gov">mafurman@lbl.gov</a>	Center for Beam Physics, Lawrence Berkeley National Laboratory, Building 71, R0259, 1 Cyclotron Road, Berkeley, CA 94720-8211, U.S.A.
Jie Gao	<a href="mailto:gao@lal.in2p3.fr">gao@lal.in2p3.fr</a>	Laboratoire de L'Accélérateur Linéaire, B.P. 34, 91898 Orsay cedex, France
Ingo Hofmann	<a href="mailto:i.hofmann@gsi.de">i.hofmann@gsi.de</a>	High Current Beam Physics, GSI Darmstadt, Planckstr. 1, 64291 Darmstadt, Germany
Sergei Ivanov	<a href="mailto:ivanov_s@mx.ihep.su">ivanov_s@mx.ihep.su</a>	Institute for High Energy Physics, Protvino, Moscow Region, 142281 Russia
Kwang-Je Kim	<a href="mailto:kwangje@aps.anl.gov">kwangje@aps.anl.gov</a>	Argonne National Laboratory, Advanced Photon Source, 9700 S. Cass Avenue, Bldg 401/C4265, Argonne, IL 60439, U.S.A.
In Soo Ko	<a href="mailto:isok@postech.ac.kr">isok@postech.ac.kr</a>	Pohang Accelerator Laboratory, San 31, Hyoja-Dong, Pohang 790-784, South Korea
Alessandra Lombardi	<a href="mailto:Alessandra.Lombardi@cern.ch">Alessandra.Lombardi@cern.ch</a>	CERN, CH-1211, Geneva 23, Switzerland
Yoshiharu Mori	<a href="mailto:Yoshiharu.mori@kek.jp">Yoshiharu.mori@kek.jp</a>	KEK, 1-1 Oho, Tsukuba-shi, Ibaraki-ken, 305-0801, Japan
David Rice	<a href="mailto:dhr1@cornell.edu">dhr1@cornell.edu</a>	Cornell University, 271 Wilson Laboratory, Ithaca, NY 14853-8001, U.S.A.
Yuri Shatunov	<a href="mailto:Yu.M.Shatunov@inp.nsk.su">Yu.M.Shatunov@inp.nsk.su</a>	Acad. Lavrentiev, prospect 11, 630090 Novosibirsk, Russia
Junji Urakawa	<a href="mailto:junji.urakawa@kek.jp">junji.urakawa@kek.jp</a>	KEK, 1-1 Oho, Tsukuba-shi, Ibaraki-ken, 305-0801, Japan
Jie Wei	<a href="mailto:wei1@bnl.gov">wei1@bnl.gov</a>	BNL, Bldg. 911, Upton, NY 11973- 5000, U.S.A.
Jiu-Qing Wang	<a href="mailto:wangjq@mail.ihep.ac.cn">wangjq@mail.ihep.ac.cn</a>	Institute for High Energy Physics, P.O. Box 918, 9-1, Beijing 100039, China
Rainer Wanzenberg	<a href="mailto:Rainer.wanzenberg@desy.de">Rainer.wanzenberg@desy.de</a>	DESY, Notkestrasse 85, 22603 Hamburg, Germany

*The views expressed in this newsletter do not necessarily coincide with those of the editors.  
The individual authors are responsible for their text.*